

Malaga [Spain] · March 23>26

# NANOSPAIN CONF2010

**PHANTOMS**  
foundation



Fundación Progreso y Salud  
CONSEJERÍA DE SALUD



Institute for Bioengineering  
of Catalonia

**UAM**

UNIVERSIDAD AUTÓNOMA  
DE MADRID

DONOSTIA INTERNATIONAL  
PHYSICS CENTER



INSTITUTO UNIVERSITARIO  
DE INVESTIGACIÓN EN  
NANOCIENCIA DE ARAGÓN



DLPC

NanoSciences  
GRAND SUD - OUEST

**CSIC**  
CONSEJO SUPERIOR DE INVESTIGACIONES CIENTÍFICAS

**FCT** Fundação para a Ciência e a Tecnologia

MINISTÉRIO DA CIÊNCIA, TECNOLOGIA E ENSINO SUPERIOR Portugal



**CEM**

Centro Español de Metrología

## Cyclodextrin-bioadhesive nanoparticles for oral delivery of paclitaxel

*M. Agüeros<sup>1</sup>, M.A. Campanero<sup>2</sup>, J.M. Irache<sup>1\*</sup>*

<sup>1</sup> *Centro Galénico. University of Navarra. Irunlarrea s/n. 31008 Pamplona (Spain)*

<sup>2</sup> *Departamento de Farmacología Clínica. Clínica Universitaria. Irunlarrea s/n. 31008 Pamplona (Spain)*  
*jmirache@unav.es*

### INTRODUCTION

Oral delivery is the most convenient and desired way for drug delivery. The major factor determinant for bioavailability of orally administered drug is the membrane permeability and drug solubility in the intestinal lumen. Many drugs show bioavailability problems due to their low water solubility, slow dissolution rate and instability in the gastrointestinal tract.

One possibility to enhance drug absorption may be the use of biodegradable nanoparticulate systems with bioadhesive properties.

Recently, Gantrez<sup>®</sup> AN (PVM/MA) has been proposed as a new polymer to prepare bioadhesive nanoparticles for oral drug delivery (1). In the other hand, cyclodextrins (CDs) can improve drug solubility, and also increase the loading capacity of nanoparticles (2). Thus, the association between CDs and Gantrez nanoparticles would be a good strategy to increase the loading capacity of lipophilic drugs and modulate their release from these pharmaceutical forms.

The objective of this study was to evaluate the feasibility of CD-Gantrez nanoparticles and their behaviour within the gut.

### EXPERIMENTAL METHODS

#### Materials

Gantrez<sup>®</sup> AN 119 [poly (methyl vinyl ether-co-maleic anhydride)] was gifted by ISP (Spain).  $\beta$ -cyclodextrin ( $\beta$ -CD) was provided by Sigma-Aldrich (Steinheim, Germany) and 2-hydroxypropyl- $\beta$ -cyclodextrin (OH-CD) by RBI (Massachusetts, USA). Rhodamine B isothiocyanate (RBITC) was purchased from Sigma (Spain).

#### Nanoparticles preparation

Nanoparticles were prepared as previously described (1). Briefly,  $\beta$ -CD or 2-HP- $\beta$ -CD were sonicated in 2 ml of acetone containing 100 mg Gantrez. Then, the nanoparticles were formed by the addition of an ethanol/water mixture (1:1) and the organic solvents were eliminated by evaporation under reduced pressure. For bioadhesion studies, nanoparticles were fluorescently labelled by incubation with 1.25 mg of Rhodamine B isothiocyanate (RBITC). Finally the different CDs – Gantrez nanoparticle formulations were purified by centrifugation and lyophilized using sucrose (5%) as cryoprotector.

#### Characterization of nanoparticles

Size and zeta potential were determined by photon correlation spectroscopy (PSC) and electrophoretic laser Doppler anemometry, respectively, using a Zetamaster analyser system.

The amount of CDs associated to the nanoparticles was determined by HPLC coupled with Evaporative Light Scattering Detector (ELSD) (3). These results were confirmed by elemental analysis.

The quantity of loaded RBITC was estimated after total hydrolysis of certain amount of nanoparticles in 0.1 N NaOH medium (24 h, 37 °C). RBITC was determined by colorimetry at wavelength 540 nm.

### In vivo bioadhesion studies

The bioadhesion study was carried out using a protocol previously described (4). An aqueous suspension containing 10 mg nanoparticles-RBITC was administered perorally to male Wistar rats fasted overnight. At 0.5, 1, 3 and 8 hours post administration, animals were sacrificed, the entire gastrointestinal tract removed and cut in six anatomical regions: stomach, intestine (I1, I2, I3 and I4) and caecum. RBITC was extracted with methanol and determined by spectrofluorimetry, to estimate the fraction of adhered particles to the mucosa. The kinetic parameters of bioadhesion ( $Q_{max}$ ,  $AUC_{adh}$ ,  $K_{adh}$  and  $MRT_{adh}$ ) were estimated using the WinNonline 1.5 software.

## RESULTS AND DISCUSSION

### Nanoparticles characterization

CD-Gantrez nanoparticles displayed a spherical- shape and a typical size of about 150 nm (Table 1). Interestingly, the association between CDs and Gantrez enabled us to obtain nanoparticles with a smaller size than conventional ones. In addition, this decrease in the size was associated with a high yield of the process (about 90% by HPLC). The amount of CDs associated to nanoparticles was found to be dependent on the type of the oligosaccharide used (about 90  $\mu$ g/mg for beta-CD and 70  $\mu$ g/mg for OH-CD). The presence of CD was also confirmed by elemental analysis.

Table 1. Physico – chemical characteristics of PMV/MA nanoparticles (mean $\pm$ SD, n=10).

	Size (nm)	Zeta pot. (mV)	CD loading ( $\mu$ g/mg NP)	RBITC content ( $\mu$ g/mg NP)
<b>NP</b>	179 $\pm$ 2	-48.1 $\pm$ 0.8	-	10.9 $\pm$ 0.3
<b><math>\beta</math>CD-NP</b>	144 $\pm$ 6	-51.1 $\pm$ 8.8	88.4 $\pm$ 9.9	13.3 $\pm$ 2.1
<b>OH-CD-NP</b>	140 $\pm$ 7	-52.1 $\pm$ 3.7	68.4 $\pm$ 4.3	12.4 $\pm$ 1.1

### Bioadhesive profile of NP in the GI tract

Figure 1 shows the bioadhesive profiles of the formulations tested by representing the amount of NP adhered to the different GIT segments (stomach, small intestine and caecum) at different times post-administration.

OH-CD-NP displayed a significantly higher ability to develop adhesive interactions within the gut that  $\beta$ CD-NP and NP. On the other hand,  $\beta$ CD-NP displayed a quite homogeneous distribution within the whole gut, whereas OH-CD-NP displayed a significant tropism for the upper regions of the gut. Formulations displayed a homogeneous distribution along the gastrointestinal tract.

Table 2. Bioadhesion parameters for the different formulations tested.

	$Q_{max}$ (mg)	$AUC_{adh}$ (mg h)	$K_{adh}$ ( $h^{-1}$ )	MRT (h)
<b>NP</b>	2.3 $\pm$ 0.3	9.90	0.19 $\pm$ 0.03	3.19
<b><math>\beta</math>CD-NP</b>	2.3 $\pm$ 0.3	13.86	0.07 $\pm$ 0.01	3.53
<b>OH-CD-NP</b>	3.5 $\pm$ 0.5	18.16	0.09 $\pm$ 0.08	3.41

Table 2 summarises the parameters used to quantify the in vivo bioadhesive characteristics of the different formulations tested. OH-CD-NP showed the highest initial capability to develop adhesive interactions within the gut ( $Q_{max}$ ). Similarly, the intensity of these interactions ( $AUC_{adh}$ ) was found 2-times higher than for NP. On the other hand, CD-NP did not show a special ability to interact with the gut mucosa; although the  $AUC_{adh}$  was found to be 1.5-times higher than for CD. In any case, both CDs nanoparticles displayed 2-times lower elimination rates ( $K_{adh}$ ) than conventional nanoparticles.

These results enable us to hypothesise that the presence of CDs (mainly OH-CD) may facilitate the interaction with the mucosa and the development of stronger adhesive interactions with components of the mucosa than NP.

In summary, the combination between CDs and Gantrez nanoparticles may be of interest for the oral delivery of lipophilic drugs. The rationale selection of the cyclodextrin can, not only modify the drug loading and modulate its release, improve the residence of the drug delivery system in intimate contact with the gut mucosa.

### ACKNOWLEDGEMENTS

“Asociación de Amigos”, “Fundación Universitaria de Navarra”, “Gobierno de Navarra” (Dpto. Educación), Proyecto “Tu eliges, tu decides” de Caja Navarra, ISP Corp., “Ministerio de Ciencia y Tecnología” (SAF2001-0690-C03) and Instituto de Salud Carlos III (Grant RITC Cancer C1/03) in Spain.

### REFERENCES

- [1] P. Arbós et al. *J Control Release*. 88(2); (2003) p.345.
- [2] F. Kihara et al. *Bioconjugate Chem*.14; (2003) p.342.
- [3] M. Agüeros et al. *J Pharm and Biomed Anal*. 39; (2005) p.495.
- [4] P. Arbós et al. *Int J Pharm*. 242(1-2); (2002) p. 129.

### Figures:

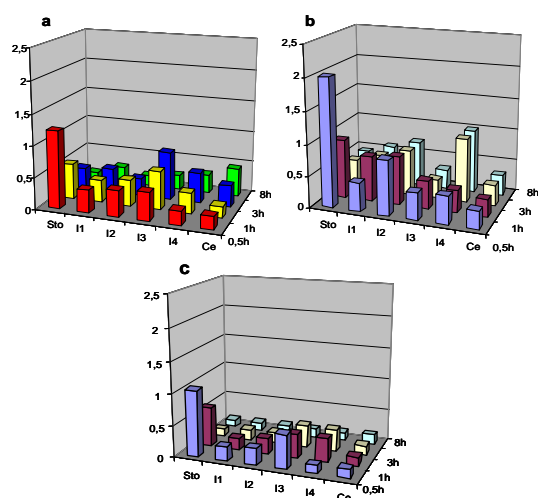


Fig. 1. Distribution of nanoparticles in the GIT after the oral administration of 10 mg nanoparticles. Each value represents the mean of the results of four experiments. (a)  $\beta$ CD-NP, (b) OH-CD-NP, (c) NP. Plot: x-axis represents the adhered fraction (mg); y-axis represents the different gut segments (Sto: stomach; I1, I2, I3, I4: intestinal portions; Ce: caecum); z-axis represent the time post-administration (in hours).

**Recent trends in the use of nanotechnology for the control of tumor markers**

*M.P. Aguilar-Caballos, A. Gómez-Hens, J.M. Fernández-Romero*

*Department of Analytical Chemistry. University of Cordoba, Annex to “Marie Curie”  
building, 14071-Córdoba, Spain*

[galgohea@uco.es](mailto:galgohea@uco.es)

Cancer diagnosis and therapy have experienced notable advances as a consequence of using Nanotechnology. In one hand, nanostructures are useful tools in cell proliferation and tumor marker assays to detect the presence and/or activity of tumor cells at relatively low percentages in biological fluids and/or tissues. On the second, modern therapies are based on drug delivery systems involving the use of nano-carriers, which decrease the side effects to patients and provide a higher effectiveness in the treatment of the disease.

Cancer diagnostics combines the use of imaging techniques and the detection of tumor markers in fluids and/or tissues. These markers are characterized by a glycoprotein structure and are mainly determined by using immunological methods, which have traditionally involved the use of enzymes or fluorophores as labels. Nanoparticles (NPs) can be used in tumor marker assays as labels, nanoscaffolds and separation media. Carbon nanotubes, quantum dots, and noble metal, organic polymer, silica and magnetic NPs are the main nanomaterials that have shown their usefulness for these purposes up to date. Generally, the use of nanotechnology in tumor marker assays has provided them with shorter analysis times and higher sensitivity compared to the conventional methods. These assays can be miniaturized using microarray or microfluidic systems and allow the individual or multiplexed determination of tumor markers using direct, competitive or sandwich schemes.

It can be concluded that innovations in this field should be directed towards the development of multiplexed assays with application to real samples, which has been very scarcely reported up to date.

## Monodisperse superparamagnetic Fe@C nanoparticles for biomedical applications obtained by a modified arc discharge method

*Noemí Aguiló-Aguayo, Enric Bertran*

*FEMAN Group, IN<sup>2</sup>UB, Martí i Franquès 1, Barcelona, Catalonia, Spain*

[noemiaguilo@ub.edu](mailto:noemiaguilo@ub.edu)

A wide range of nanoparticles (NPs) is used for several biomedical applications. Metal nanoparticles made of Au, Ag or Pd presenting surface plasmon resonance provide a method for biosensing detection [1], such as DNA analysis [2], virus-induced diseases [3] or enzyme-substrate interaction. Magnetic nanoparticles based on Fe, Co or Ni elements are used for Magnetic Resonance Imaging (MRI) [4], cancer therapy [5] or drug delivery purposes [6].

For such applications, some properties are required. Nanoparticles have to be biocompatible, easily functionalized, chemical and temporary stable (in acidic or basic solutions and under air atmosphere), monodisperse with sizes less than 50 nm and not aggregated [7]. For this reason, some surface coatings (silica, carbon or some polymers) are used in the synthesis of nanoparticles [8, 9].

In this report, we present carbon-coated monodisperse Fe NPs of about 6.6 nm, prepared using a modified arc discharge method. Carbon coating provides a huge amount of properties over the other coatings above mentioned, such as protection against oxidation, acidic solutions, thermal treatments and high-pressure conditions [10]. In addition, carbon presents suitable electrical, thermal and mechanical properties for biomedical uses and near-infrared absorption.

The arc discharge technique has been modified to use a precursor of iron under helium atmospheric plasma. The system allows an accurate control of the core sizes due to a better stability of plasma. The current applied is about 25A and graphite electrodes are faced to form an arc and to ionize the helium. The graphite from the electrodes supplies the carbon coating for the nanoparticles.

Morphological and structural characterization of the nanoparticles has been studied by high-resolution and transmission electron microscopy (HRTEM, TEM), selected area electron diffraction (SAED) and X-ray diffraction (XRD). Magnetic properties have been investigated using a superconducting quantum interference device (SQUID) magnetometer.

Results from the techniques above mentioned reveal that nanoparticles present monodisperse (23% of dispersion) pure  $\alpha$ -Fe cores of 6.6 nm (figure 1). The monodispersity and very small sizes (lower than 10 nm) of the nanoparticles guarantee their superparamagnetic behaviour at room temperature, suitable for the biomedical applications. In addition, the purity of the cores ensures a higher magnetic response of the samples and an improved stability.

Zero-Field-Cooled (ZFC) plot (figure 2) shows a very narrow peak at the blocking temperature ( $T_B = 25$  K), which supports the monodispersity of the samples. Field-Cooled (FC) measurements (figure 2) at lower temperatures (below  $T_B$ ) exhibit an increasing of the magnetization, pointing a non-interaction among nanoparticles. This fact confirms that nanoparticles are in a non-aggregate state, behaving each one as an individual magnetic entity.

To conclude, the modified arc discharge technique developed allows the production of Fe@C nanoparticles overcoming, for the first time, the disadvantages that this kind of nanoparticles presented for biomedical applications. Although, carbon-coated magnetic nanoparticles had a lot of advantageous properties, their disperse sizes and aggregated clusters made them very difficult to use for biomedical purposes. However, samples presented in this report open the

way to their applications, as well as the better understanding of the formation mechanism of carbon nanostructures.

This study was supported by projects CSD2006-12 and DPI2006-03070 of MEDU of Spain. The authors thank Serveis Científico-tècnics of the Universitat de Barcelona (SCT-UB) for measurements facilities.

## References:

- [1] Liao H., Nehl C. L., Hafner J. H., *Nanomedicine*, **1** (2006) 201-208.
- [2] Willner I., Baron R., Willner B., *Biosensors and Bioelectronics*, **22** (2007) 1841-1852.
- [3] Elechiguerra J. L., Burt J. L., Morones J. R., Camacho-Bragado A., Gao X., Lara H. H., Yacaman M. J., *Journal of Nanobiotechnology*, **3** (2005) 1-10.
- [4] Mornet S., Vasseur S., Grasset F., Duguet E., *Journal of Materials Chemistry*, **14** (2004) 2161-2175.
- [5] B. Thiesen, A. Jordan, *International Journal of Hyperthermia*, **24** (2008), 467-474.
- [6] Li F. R., Yan W. H., Guo Y. H., Qi H., Zhou H. X., *International Journal of Hyperthermia* **25** (2009) 383-391.
- [7] Grainger D. W., Castner D. G., *Advanced Materials*, **20** (2008) 867-877.
- [8] Win K. Y., Feng S. S., *Biomaterials* **26** (2005) 2713-2722.
- [9] Lu A. H., Salabas E. L., Schüth F., *Angewandte Chemie International Edition*, **46** (2007) 1222-1244.
- [10] Ostrovskaya L. Y., Perevertailo V. M., Matveeva L. A. Milani P., Ralchenko V. G., Shpilevsky E. M., *Powder Metallurgy and Metal Ceramics*, **42** (2003) 1-8.

## Figures:

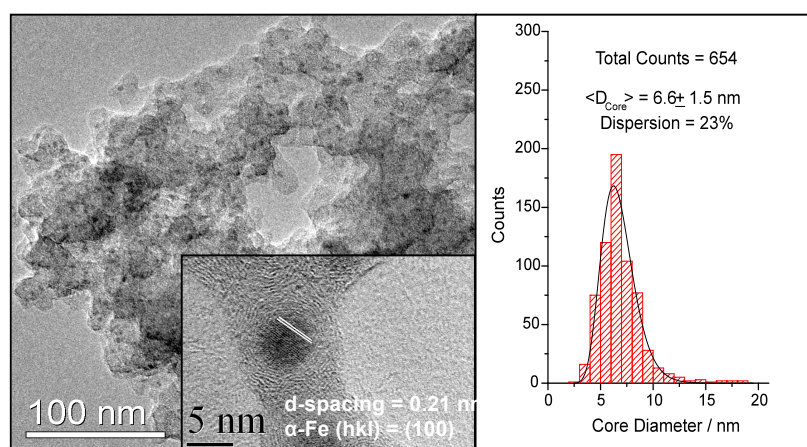


**Figure 1.** TEM and HRTEM images of the Fe@C NPs. Iron cores show a very narrow dispersion (23%) of their sizes, samples are considered to be monodisperse. Carbon coating completely seals  $\alpha$ -Fe cores.

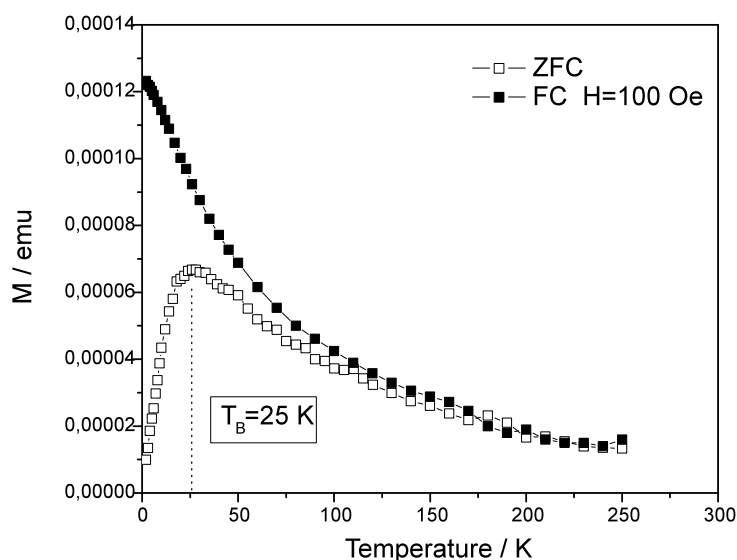


**Figure 2.** ZFC-FC curves for Fe@C NPs. Peak from ZFC measurements shows a blocking temperature of about 25 K. At room temperature the total magnetization tends to zero, which reflects a superparamagnetic behavior for the samples.

## Boundary conditions for nanoscale electron devices with realistic lead-sample Coulomb correlations in small simulating boxes

G. Albareda, H. López, X. Cartoixà, J. Suñé and X. Oriols  
 Universitat Autònoma de Barcelona, Bellaterra, Spain  
[guillem.albareda@uab.cat](mailto:guillem.albareda@uab.cat)

Most quantum electron transport simulators use small simulation boxes implying a reduction of the degrees of freedom that are explicitly simulated. Nevertheless, the separation between the simulated degrees of freedom (electrons inside the simulation box) and those that are not simulated is always traumatic because there are correlations (interchange of energy and particles) between the active region and the leads. The importance of such correlations in electron transport was discussed in dc and ac regimes some years ago [1,2] but it has been ignored in most of the powerful quantum simulators, which have to use very small simulation boxes [3]. In this conference, we will present an accurate model of such lead-sample coulomb correlations valid for small simulating box by properly modelling the boundary conditions (BC). Instead of assuming the standard Neumann (i.e. a fixed external bias) or Dirichlet (i.e. a fixed zero electric field) BC [4], we propose an original model that does not fix the value of the scalar potential, neither the electric field nor the charge density, but just a time-dependent and self-consistent relationship between them.

As seen in figure 1, our whole BC model differentiates three regions: the two leads which are treated analytically (dotted blue), and the active region which is simulated numerically (solid yellow). Based on screening arguments, the main ingredient of our BC algorithm is imposing that the total charge in the whole system (active region, leads and reservoirs) tends (exponentially) to neutrality within the dielectric relaxation time,  $\tau_c$ . This condition is equivalent to force that the (analytical) electric fields deep inside the leads (white region in figure 1) tend to its drift value,  $E_{Drift} = J_x / \sigma$ , within a time  $\tau_c$ . Appealing to the screening theory, an exponential charge density shape between the leads and the sample can be reasonably argued. Then, the Poisson equation together with the appropriate values of the charge,  $\rho(\vec{r}, t)$ , electric field,  $\vec{E}(\vec{r}, t)$ , and the scalar potential,  $V(\vec{r}, t)$ , deep inside the contacts (white region in figure 1), and in the interface of the analytic-simulated regions, are sufficient to relate this three magnitudes. In particular the scalar potential at the borders of the simulated region,  $V_{SD}$  at the source side, and  $V_{DD}$  at the drain side, can be finally written as (see figure 1),

$$V_{SD/DD}(t) = V_{SL/DL}(t) - E_{SL/DL}(t) \cdot (L_{Contact}) - \frac{\rho_{SD/DD}(t) \cdot (L_{CS/CD}(t))^2}{\epsilon}, \quad (1)$$

The definition of time-dependent screening lengths,  $L_{CS/CD}(t)$  at source and drain sides respectively, give rise to formations of depletion regions at high bias that could not been described within an equilibrium screening theory. Even more, our model couples the scalar potential values at the borders of our sample with the injection model [5] through the self-consistent movement of the pseudo-fermi levels, in order to obtain the desired over-all charge neutrality.

In order to test our BC algorithm, in figure 2, we compare the potential energy profiles given by (i) a semi-classical many-particle Monte Carlo (MC) simulator [6] with a large 45 nm simulating box (LBMC) that includes both the leads and the active region, and (ii) the same simulator, provided with the described BC model, with a much smaller 8 nm simulating box (SBMC) that only encloses the active region. While the LBMC simulating times are around 1 day per bias point, the simulation times related to the SBMC decrease until 3 hours. The results of the SBMC are in excellent agreement with those obtained with LBMC even at high applied bias, where exists wide depletion regions. In the quantum regime, the implementation

of our BC model in a quantum trajectory simulator [6,7] is extremely important because it allows us to use small simulating boxes that make a many-particle quantum transport simulation with realistic (far from equilibrium) conditions viable. In figure 3 we compare the characteristic I-V curves for a Resonant Tunneling Diode (RTD) computed with (i) simple fixed Neumann BC and (ii) overall charge neutrality with the BC approach described here that includes the Coulomb correlations between the leads and the active region. As can be observed such correlations play an important role in the relevant parameters of the RTD even at dc regime.

As far we know, our BC approach represents the first model that allows the (computationally desirable) use of small simulating box with the (physically desirable) consideration of the meaningful Coulomb correlations between the active region and the leads. Instead of assuming standard fixed Neumann or Dirichlet BC, the model provides a time-dependent and self-consistent relationship between the value of the scalar potential, electric field and the charge density. The results are excellent without fitting parameters (See fig. 2). Our BC approach is valid for dealing with lead-sample correlations in static and also time-dependent scenarios up to times related to  $\tau_c$  (i.e.  $f \sim 100THz$  for highly doped contacts).

**References:**

[1] M.Büttiker, Y.Imry, R.Landauer, and S.Pinhas, Phys. Rev. B, 31 (1985) 6207.  
 [2] Ya.M.Blanter and M.Buttiker, Physics Reports, 336 (2000) 1.  
 [3] R. Baer and D. Neuhauser, Int. J. Quantum Chem., 91 (2003) 524.  
 [4] A.Rahman, J.Guo, S.Datta and M.Lundstrom, IEEE Trans Electron Dev, 50 (2003) 1853.  
 [5] X.Oriols, E.Fernández-Díaz, A.Alvarez and A.Alarcon, Solid-State Elect. 51 (2007) 306.  
 [6] G.Albareda, J.Suñé and X.Oriols, Phys. Rev. B, 79 (2009) 075315.  
 [7] X.Oriols, Phys. Rev. Lett., 98 (2007) 066803.

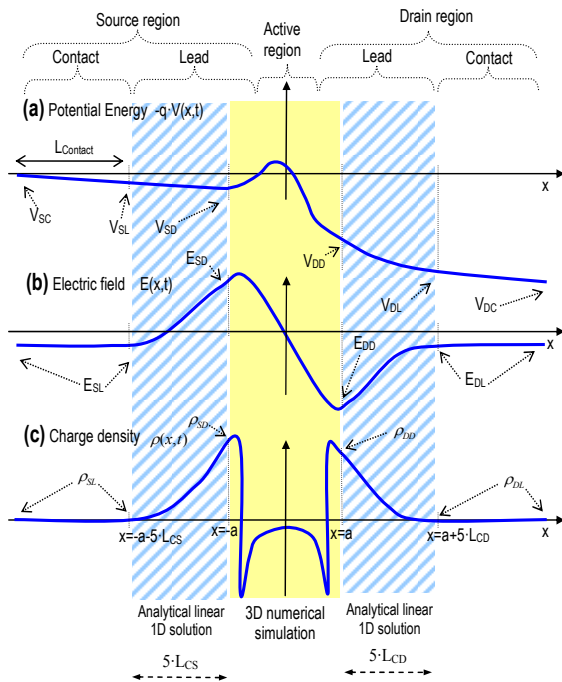


Fig. 1. Schematic description of the model. The whole system is divided into contacts (white), leads (dotted blue) and active region (yellow).

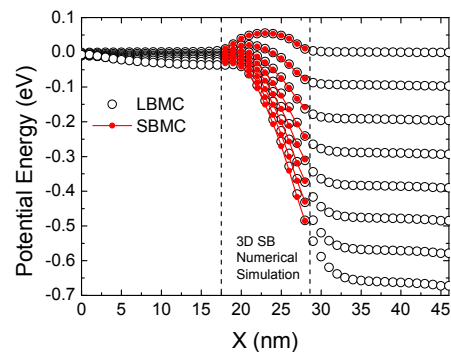


Fig. 2. Potential energy curves at different bias simulated with a LBMC that includes the whole system and a SBMC including only the active region.

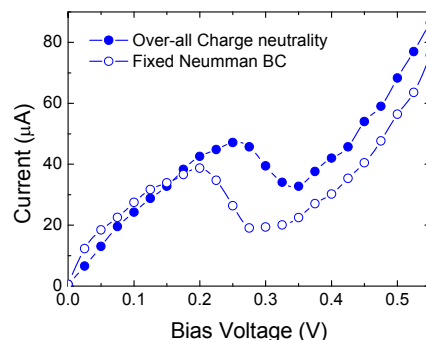


Fig. 3. I-V characteristic for a RTD, with/without including Coulomb correlations between the leads and the active region.

## Consolidating stone materials by means of nanoparticles

*Luz Gomez Villalba, Paula Lopez-Arce, Monica Alvarez de Buergo, Rafael Fort*  
*Instituto de Geologia Economica (CSIC-UCM), c/ Jose Antonio Novais 2, 28040 Madrid,*  
*Spain*  
[alvarezm@geo.ucm.es](mailto:alvarezm@geo.ucm.es)

Petrology has turned into a fundamental discipline for the step forward in research and conservation of architectural and monumental heritage, in the causes generating its decay, as well as in the most adequate conservation and protection techniques according to materials' petrophysical characteristics and the type of environment in which materials are located [1]. Most of the materials deterioration is directly related to intrinsic aspects of them, such as textural and compositional properties, porosity, and the alteration degree of the existing minerals constituting the rock. Besides, there are some extrinsic factors related to the environment in which they are placed (climatic, environmental, biological and antropic, etc), which contribute in a different way to the degradation of monuments.

The development in the last years of nanotechnology and nanoscience, and the interest they arise, is due to the fact that at nanometric scale, materials behaviour changes as a result of the size decrease. Lately, nanotechnology is being considered as an opportunity to be applied in the field of rocks and stone conservation. Among the consolidants used to restore the lost cohesion of the stone materials employed in architectural heritage, calcium hydroxide has been extensively used and is well known. The existence of different methods of nanoparticle synthesis to be applied for stone materials conservation [2], has increased the possibility of assess the effect of consolidants as the nano-calcium hydroxide applied to carbonatic rocks, in different environmental conditions; this compound helps the carbonation processes and improve physical and hydric properties.

The synthesized products exhibit different morphological, structural and chemical characteristics according to the synthesis method that has been used, being susceptible to factors such as relative humidity [3], time of exposure to the product, temperature and textural and mineralogical aspects of the stone materials on which it has been applied. The study of the effect of the nanoparticles-based consolidant products obtained by different synthesis methods, will allow to assess their behaviour at a nanometric scale, their morphological-crystalline evolution, and also to analyse their reaction with different surfaces to which they have been exposed. At the same time, it will be possible to evaluate the behaviour of these consolidants at different environmental conditions with the aim of improving the physico-chemical properties of the stone materials.

*Acknowledgements: to both programmes CONSOLIDER (CSD2007-0058) and GEOMATERIALES (S2009/MAT-1629).*

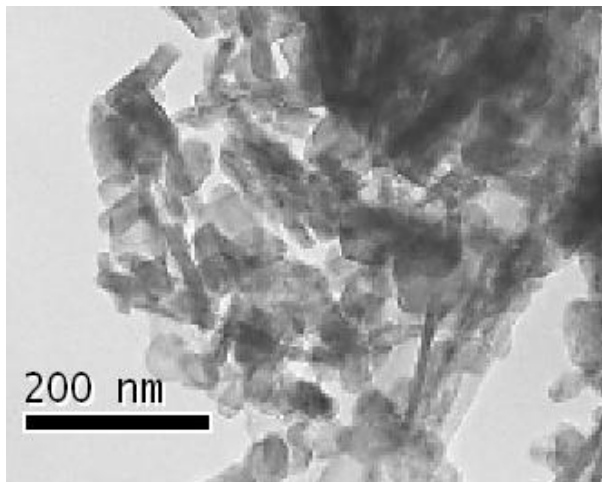
### References:

[1] Fort, R., García del Cura, M.A., Varas, M.J., Bernabeu, A., Álvarez de Buergo, M., Benavente, D., Vázquez-Calvo, C., Martínez-Martínez, J. y Pérez-Monserrat, E. "La Petrología: una disciplina básica para el avance en la investigación y conservación del Patrimonio". En C. Saiz Jiménez y M.A. Rogerio-Candelera (eds.) La investigación sobre Patrimonio Cultural: 217-239. Sevilla: Red Temática del CSIC de Patrimonio Histórico y Cultural. (2008).

[2] Ziegenbald, G. Colloidal calcium hydroxide- a new material for consolidation and conservation of carbonate stone, Proceedings of 11th International congress on deterioration and conservation of stone, (2008). vol. III 1109p.

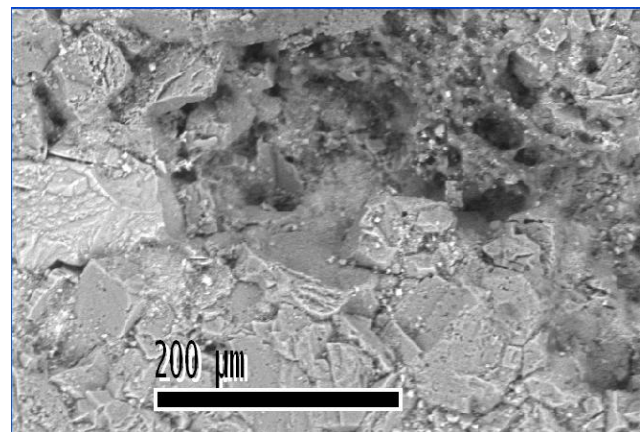
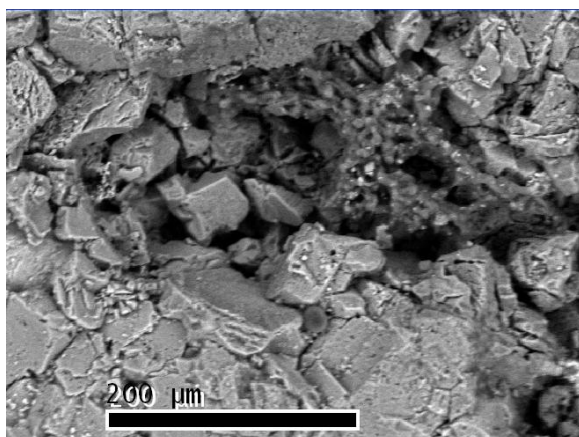
[3] López-Arce, P., Gomez-Villalba, L.S., Pinho, L., Fernández-Valle, ME. Álvarez de Buergo M., Fort R. 2010. Influence of porosity and relative humidity in the consolidation of dolostone with calcium hydroxide nanoparticles: assessment of consolidation effectiveness with non destructive techniques. Materials Characterization, 61 (2): 2010, pp.168-184  
DOI: 10.1016/j.matchar.2009.11.007.

**Figures:**



TEM image of a comercial consolidant product based on colloidal calcium hydroxide nanoparticles (a).

**a)**



**b)**

**c)**

ESEM images of dolostone treated with the consolidant before (b) and after 20 days treatment at 33% relative humidity (c). Porosity and roughness are modified.

## XPS and STM study of Metal-organic nanostructures

*L. Álvarez, R. Caillard, M.F. López, J.A. Martín-Gago and J. Méndez*  
*Instituto de Ciencia de Materiales de Madrid (CSIC), Cantoblanco 28049 Madrid.*  
[lualpima@icmm.csic.es](mailto:lualpima@icmm.csic.es), [jmendez@icmm.csic.es](mailto:jmendez@icmm.csic.es)

Nanotechnology is a new and very promising field of science. Nanomaterials are studied looking for new properties derived from the dimensionality reduction. Hybrid materials [1] obtained by a combination of inorganic and organic units, as metal-organic nanostructures [2], present new properties and applications, derived from a combined nature.

In this work, we have performed photoemission spectroscopy (XPS) at the Elettra Synchrotron and scanning tunneling microscopy (STM) on the structures resulting from the combination of iron atoms and organic molecules of PTCDA on a gold substrate. We have deposited iron on Au(111) in quantities below 1 monolayer (ML) and PTCDA organic molecules at low rates. By choosing the adequate growth conditions different systems can be generated: previously reported nanostructures [2], molecular chains and organic nanodots, and extended 2-D structures.

The XPS analysis of the C-1s (see figure 1) and O-1s spectra revealed some changes in the binding energies as well as in the peaks distribution for the case of the formed nanostructures as compared to the PTCDA organic monolayer. On the other hand, the comparison of the Fe-2p spectrum corresponding to 1ML Fe deposited on Au(111) and the nanostructures exhibited no significant changes, even in the oxidation state, which indicates a coordination bond between the iron atoms and the carboxylic group of the organic molecules in the nanostructures formed.

By means of STM, we have focus in the extended structures resulting from two chains connected by perpendicular PTCDA molecules like the rungs of a ladder. These ladder structures can be extended over the entire surface, forming domains. Analysing the images, we can propose models to the structures, some of which have been corroborated by theoretical calculations.

### References:

- [1] For a review on hybrid materials see for example the special issue: *Journal of Materials Chemistry* **15** (2005).
- [2] J. Méndez, R. Caillard, R. Otero, N. Nicoara, and J.A. Martín-Gago, *Advanced Materials* **18** (2005) 2048-2052.

## Figures:

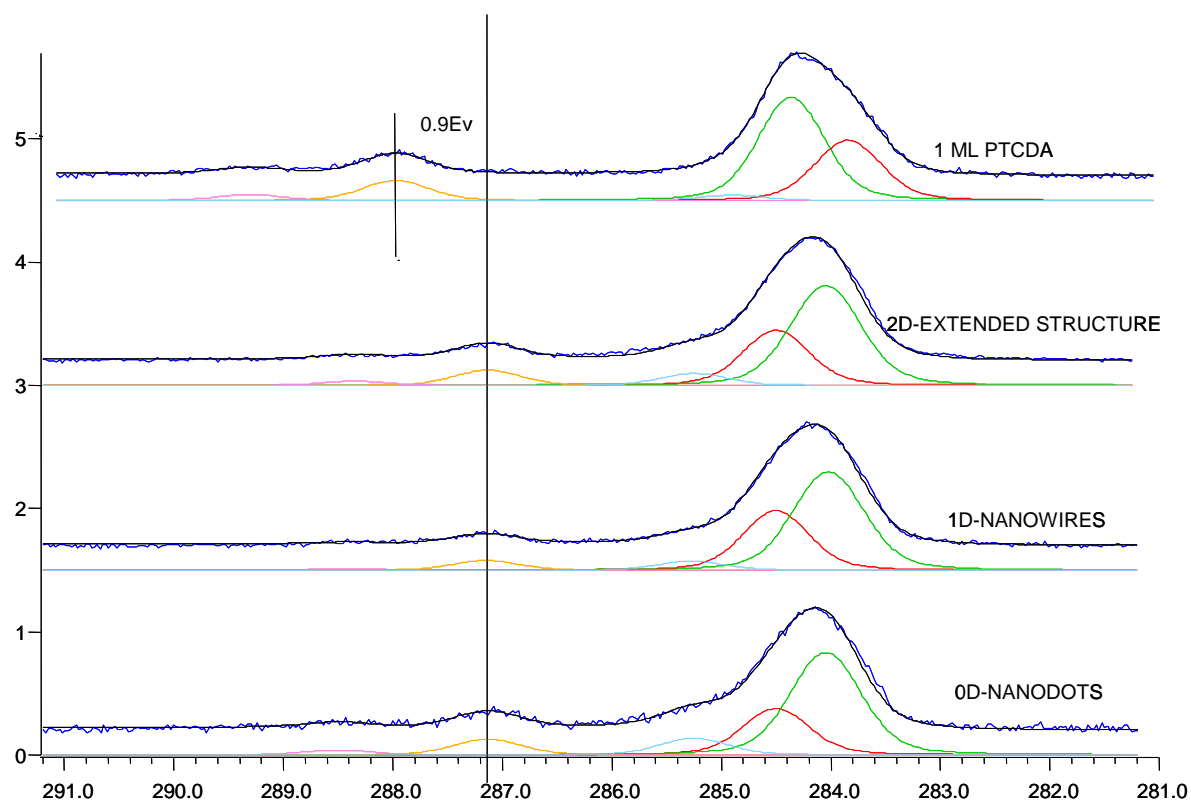


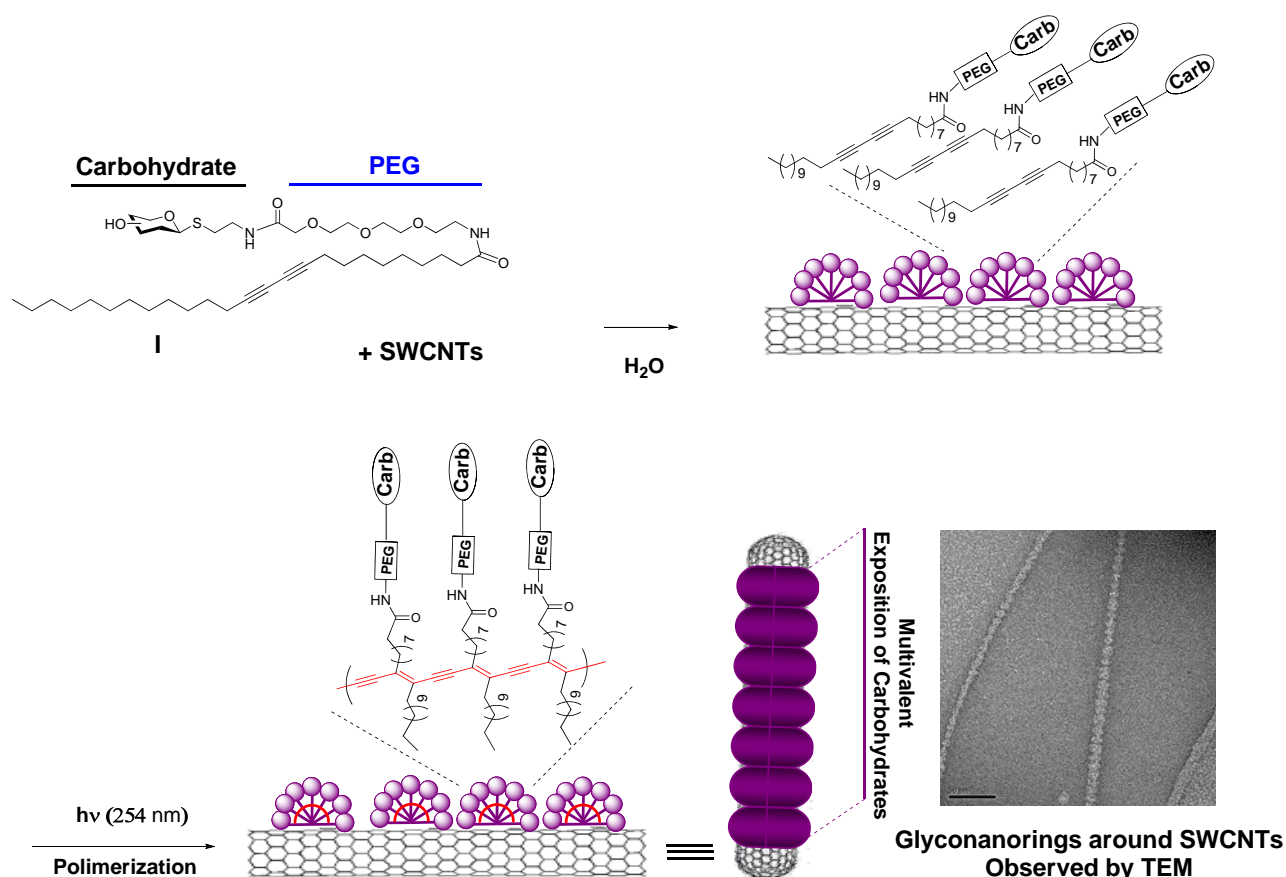
**Figure 1.** XPS spectra of the C-1s region. Comparison of the C-1s spectra of the metal-organic nanostructures with the spectrum of 1ML of PTCDA, both on a Au(111) substrate. We observe a shift in energy of the functional groups of the nanostructures and a peak redistribution of the perylene components.

## Bioengineering of Carbon Nanotubes: Glyconanoabacus with Biomimetic Display of Carbohydrates

N. Khlar,<sup>\*1</sup> M. Assali,<sup>1</sup> M. Pernía,<sup>1</sup> R. Baati,<sup>2</sup> R. Recio,<sup>3</sup> I. Fernández,<sup>3</sup> and C. Mioskowski.<sup>2</sup>

<sup>1</sup> Instituto de Investigaciones Químicas, CSIC, c/. Américo Vespucio, 49, Isla de la Cartuja, 41092- Seville. Spain. <sup>2</sup> Laboratoire de Synthèse Bio-Organique, Faculté de Pharmacie, 74, route du Rhin BP 60024. 67401 Illkirch-Graffenstaden, Strasbourg. France. <sup>3</sup> Dpto. Química Orgánica y Farmacéutica, Facultad de Farmacia, Universidad de Sevilla, 41012-Seville. Spain. e-mail: [Khiar@iiq.csic.es](mailto:Khiar@iiq.csic.es)

Single-walled carbon nanotubes (SWCNTs) are interesting 1D nanomaterials endowed with unique size shape and physical properties that make them promising candidates for biomedical applications.<sup>1</sup> Nevertheless, advances in these directions have been very slow as SWCNTs are insoluble in most organic solvents, specifically in water. In the present work, we present our results on the utilisation of carbon nanotubes as molecular jig or platform for a multivalent presentation of saccharide epitopes, and for the generation of new biologically relevant nano-objects.<sup>2</sup> Our approximation is based on the supramolecular self-organization of neoglycolipids such as **I**, on the nanotube surface giving rise to rings made of rolled-up half cylinders, Scheme 1.<sup>3</sup> As a consequence, water soluble, highly stable aggregates were obtained, where the physical and electronic characteristics of SWCNTs are preserved.



Scheme 1

Photopolymerisation of the diacetylene function upon ultraviolet irradiation (254 nm) affords a conjugated polydiacetylene backbone of alternating enyne groups, a known colorimetric biosensor, which rigidifies the rings around the SWCNT. In the present communication, the following points will be discussed: (i) the modular synthetic strategies developed for the synthesis of tailored amphiphilic neoglycoconjugates, (ii) the determination of the neoglycolipid structural requirements for an efficient interaction and solubilization of SWCNTs, (iii) the determination of the type and shape of the supramolecular self-organization of the neoglycolipids on the SWCNTs surface, and (iv) the preliminary studies of the selective binding of SWCNT-neoglycoconjugate with specific biological receptors.

1) Liu, Z. ; Davis, C. ; Cai, W. ; Chen, X. ; Dai, H.J. *Proc. Natl. Acad. Sci. U.S.A.* **2008**, *105*, 1410.

2) Assali, M.; Pernía Leal, M.; Fernández, I.; Baati, R., Mioskowski, C.; Khiar, N. *Soft Matter*, **2009**, *5*, 948.

3) Khiar, N.; Pernia Leal, M.; Baati, R.; Ruhlmann, C.; Mioskowski, C., Schultz, P.; Fernández, I. *Chem. Commun.* **2009**, 4121.

**Precise probing spin wave dynamics in circular magnetic dots: influence of dots aspect ratio, magnetic field and direction of microwave field pumping**

*A.A. Awad<sup>1</sup>, J. F. Sierra<sup>1</sup>, G. N. Kakazei<sup>2</sup>, D.-S. Han<sup>3</sup>, S.-K. Kim<sup>3</sup>, V. Metlushko<sup>4</sup>, K.Y. Guslienko<sup>5</sup>, and F.G. Aliev<sup>1</sup>*

<sup>1</sup> *Dpto. Física de la Materia Condensada, CIII, Universidad Autónoma de Madrid, 28049 Madrid, Spain*

<sup>2</sup> *Depto. Física da Faculdade de Ciências, Universidade do Porto, 4169-007 Porto, Portugal*

<sup>3</sup> *Research Center for Spin Dynamics and Spin-Wave Devices, Seoul National University, Seoul, 1510744 South Korea* <sup>4</sup> *Dept. of Electrical and Computer Engineering, University of Illinois at Chicago, Chicago, Illinois, 60607 USA*

<sup>5</sup> *Dpto. Física de Materiales, Universidad del País Vasco, 20018 Donostia-San Sebastian, Spain*

[ahmad.awad@uam.es](mailto:ahmad.awad@uam.es)

Vortices are encountered many natural systems ranging from galaxies to superconductors and superfluids. Knowledge of vortex dynamics in stratified conditions is of special importance. Spin wave dynamics in Permalloy dots with magnetic vortex and situated in the applied external in-plane magnetic field could be considered as a simple toy model to investigate dynamics of single vortex state in the confined stratified media.

First we discuss dependence of spin wave modes (Fig.1a) excited by in-plane magnetic field on dots aspect ratio [1]. The frequency splitting of two lowest azimuthal modes was observed (Fig. 1b) and described by dynamic splitting model accounting the spin waves and vortex gyrotropic mode interaction [2].

Secondly, we describe precise measurements of spin dynamics in the vortex state of the circular magnetic dots by exciting spins in different in-plane directions (Fig. 2b,c) with respect to applied in-plane bias magnetic field [3]. Spin wave dynamics was measured using FMR-VNA technique [4,5]. We unambiguously demonstrate experimentally and by micromagnetic simulations the existence of two distinct dynamic vortex (stable and metastable) regimes. Dynamic response in the metastable state strongly depends on relative orientation of the external rf pumping and bias magnetic fields. Parallel rf pumping (Fig. 2c) is shown to be unique tool to observe spin excitation modes localized near the strongly shifted vortex core for the bias field between the vortex nucleation and annihilation fields. Meanwhile, the perpendicular rf pumping (Fig. 2b) which excites the spin waves throughout the entire dot, reveals crossover between two dynamic vortex regimes near the nucleation field. Our findings open new possibilities for development of magnetic devices with precise control over the magnetization switching process. They also underscore importance of understanding of dynamic response in different nanostructured materials with vortices in confined and stratified conditions.

This work was supported by Spanish MICINN (MAT2009-10139), Consolider (CSD2007-00010) and CAM (P2009/MAT-1726).

**References:**

- [1] A. Awad, et al., Appl. Phys. Lett., 96, 012503 (2010).
- [2] K.Guslienko, et al., Phys. Rev. Lett., 101, 247203 (2008).
- [3] F.G. Aliev, et al., Phys. Rev. B 79, 174433 (2009).
- [4] J. F. Sierra, et al., Appl. Phys. Lett., 93, 172510, (2008).
- [5] J. F. Sierra, et al., Appl. Phys. Lett., 94, 012506 (2009).

Figures:

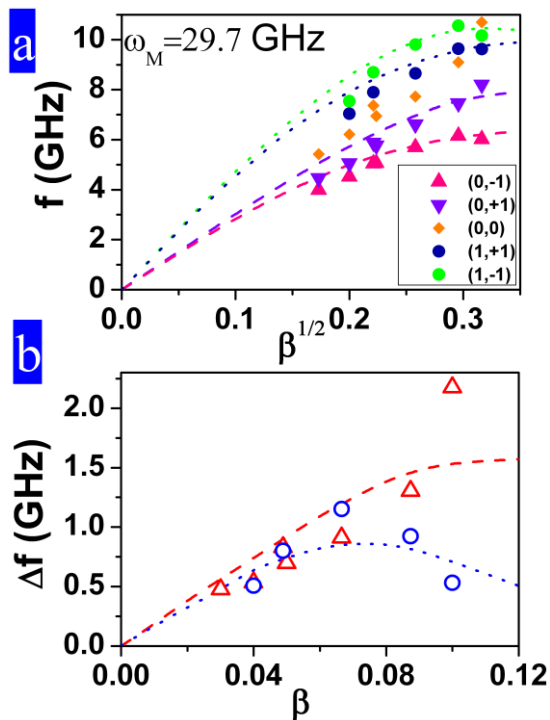


Fig. 1. (a) Measured spin wave mode frequencies vs. square root of the dot aspect ratio  $\beta$ . The dashed line and the dotted lines represents theoretical values for first azimuthal mode and second azimuthal mode respectively. (b) splitting open triangles of the first azimuthal mode, open circles second azimuthal mode both as function of the dot aspect ratio  $\beta$ . The dashed line and dotted lines represents theoretical values [2] for the first and second azimuthal modes splitting respectively.

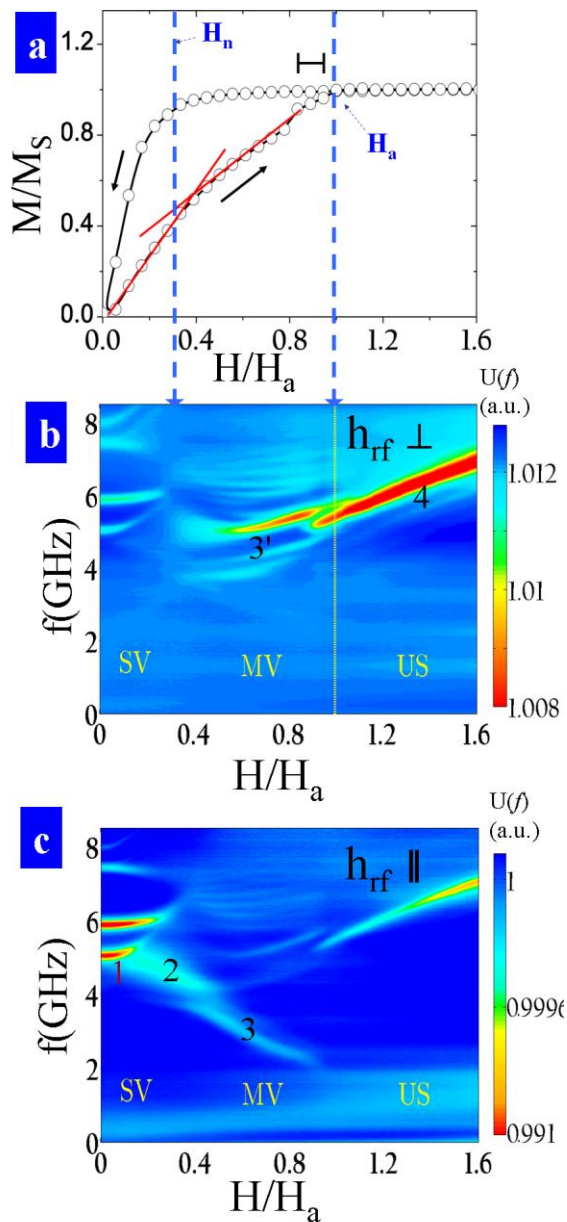


Fig. 2. (a) Magnetization vs. magnetic field normalized by the vortex annihilation field. Vertical dashed lines indicate the vortex nucleation and annihilations fields, while the error bar evaluates uncertainty in vortex annihilation field. Red lines indicate change in the slope in  $M(H)$  near  $H_n$ . (b,c) Intensity ( $U$ ) plots of the measured spectra for the Py dot arrays with thickness 25 nm and 1035 nm diameter for rf field perpendicular (b) and parallel (c) to the increasing bias magnetic field. Numbers 1, 2, 3, 3' and 4 label the spin wave modes.

**Magnetic particles for biotechnology**

*Paul Balint<sup>1</sup>, Hélène Joisten<sup>1</sup>, Philippe Sabon<sup>1</sup>, Stéphane Aufret<sup>1</sup>, Jérôme Faure Vincent<sup>2</sup>,  
Bernard Dieny<sup>1</sup>*

*<sup>1</sup>SPINTEC, UMR-8191, CEA-INAC/ CNRS/UJF-Grenoble 1/Grenoble-INP, 17 rue des Martyrs, 38054  
GRENOBLE cedex 9, France*

*<sup>2</sup>SPrAM, UMR-5819, CEA-INAC/ CNRS/UJF-Grenoble 1/Grenoble-INP, 17 rue des Martyrs, 38054  
GRENOBLE cedex 9, France*

*[paul.balint@cea.fr](mailto:paul.balint@cea.fr)*

This study aims at developing a new type of magnetic particles for biotechnological applications (in particular in-vitro diagnostics). The standard magnetic particles, currently used in biological applications, are chemically obtained and usually spherical. They are superparamagnetic. They have limitations due to their low magnetic susceptibility, their low magnetic moment, the lack of choice of shape, and a poor control of monodispersity. In contrast, our fabrication process is based on a top-down approach taking advantage of all the know-how in magnetic thin films engineering and microelectronic technology. The magnetic nanoparticles that we prepare exhibit magnetization curve having a superparamagnetic-like behaviour (i.e. no remanent magnetization and reversible magnetization variation under field up to saturation). However, their susceptibility are 2 to 3 orders of magnitude larger than conventional particles and their shape and size can be perfectly controlled (see Figure 1).

Our "top down" approach of fabrication comprises several steps: 1) the patterning of the substrates by nanoimprint and optical lithography, 2) the deposition of original magnetic stacks, 3) biological functionalization, 4) lift-off to release the functionalized particles in a solution (see Figure 2). After release, the functionalized particles are studied in solution. The particles motion under gradient of magnetic field is observed by microscopy imaging.

As a preferred magnetic material, we used sets of multilayered synthetic antiferromagnets with the composition NiFe/Ru0.6nm having different susceptibilities. These stacks present zero remanence and a high isotropic magnetic susceptibility. They imitate very well superparamagnetic particles (see Figure 3). We report, for our particles, magnetic susceptibilities two order of magnitude higher than those of conventional iron oxide based magnetic particles in fields of the order of 10mT. This gives us the possibility of using weaker magnetic fields and/or to apply larger forces on the particles.

Phenomena of self-organization of the particles in suspension were observed related to the magnetostatic interactions between the particles. These phenomena can be controlled and suppressed by changing the magnetic susceptibility of the particles which influences their self-polarization (see Figure 4).

Besides, the intrinsic "flat" shape of the particles yields a weaker viscosity force in the solution as compared to spherical particles.

This approach can yield lot of biological applications in particular related to in-vitro diagnostics.

Figures:

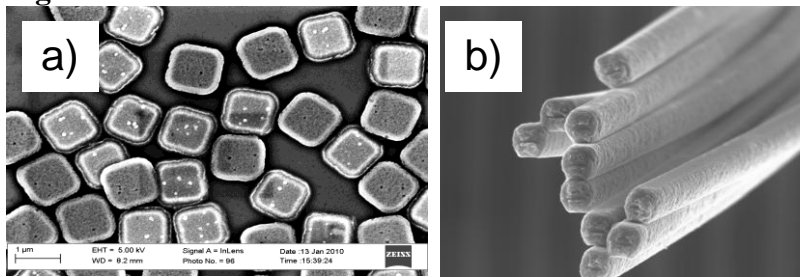


Figure 1. Photos SEM: a) square 1x1μm synthetic antiferromagnetic particles; b) magneto-elastic nanowires 100 nm in diameter

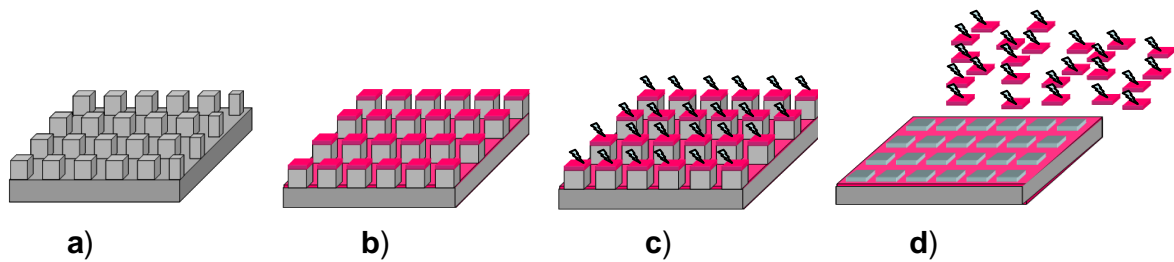


Figure 2. Preparation of micro and nanoparticles; a) Substrate patterning; b) Magnetic stack deposition; c) Biological functionalization; d) Lift-off of the particles

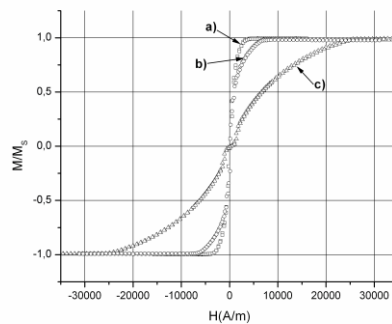


Figure 3. Hysteresis loop for 3 different stacks: a)  $NiFe_{60nm}/Ru_{0.6nm}/NiFe_{60nm}$ ; b)  $(NiFe_{30nm}/Ru_{0.6nm})_3/NiFe_{30nm}$ ; c)  $(NiFe_{15nm}/Ru_{0.6nm})_7/NiFe_{15nm}$

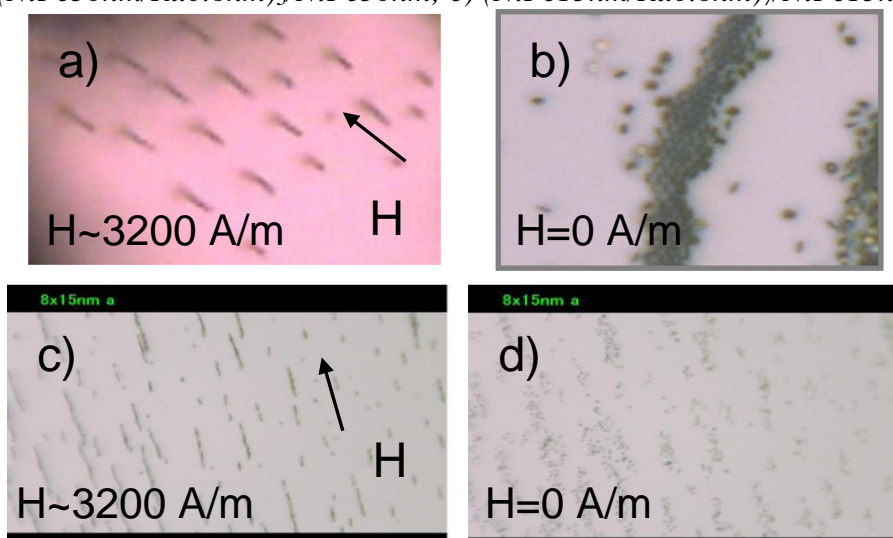


Figure 4. Suppression of self-polarization of super-paramagnetic-like particles; a) and b) particles with high susceptibility; c) and d) low susceptibility particles

## Electrospun cellulose-based membranes for bioelectrochemical devices

*A.C. Baptista, E. Fortunato, R. Martins, J.P. Borges and I. Ferreira*  
CENIMAT/I3N, Departamento de Ciência dos Materiais, Faculdade de Ciências e  
Tecnologia (FCT), Universidade Nova de Lisboa, and CEMOP/UNINOVA,  
2829-515 Caparica, Portugal.  
[baptista.anna@gmail.com](mailto:baptista.anna@gmail.com)

Research applications in biomedical science and technology usually require various portable, wearable and implantable devices that can be used in biological and biomedical systems. The development of portable micropower sources has become a demanding and a challenging goal [1]. The decreasing of power requirements for portable electronics and nanodevices has improved the design of flexible energy-storage devices. If integrated structures containing the three essential components (electrodes, separator, and electrolyte) of the electrochemical device can be made mechanically flexible, it would enable these to be embedded into various innovative and functional devices [2]. In order to power electronic medical implant, power-supply systems must be capable of operating independently over a prolonged period of time, without the need of external recharging or refueling [3].

The present work aims the production of thin and flexible bioelectrochemical devices able to generate electrical energy from physiological fluids to supply small biomedical implants and biosensors for health care diagnostics.

Common energy-storage devices such as batteries and capacitors rely on large-surface-area electrodes to function. Due to that a cellulose-based membrane was produced by electrospinning. The electrospun matrix is highly porous, flexible and has a high surface area which are important properties for the present application. The electrospun membrane works both as the separator and as the support of the electrochemical device.

The membrane's electrochemical behavior was analysed by cyclic voltammetry. In pristine membranes the current density obtained is low, in the range of  $20 \text{ nA.cm}^{-2}$ . However, when impregnated with a salt solution a change of the electronic behavior is observed (Figure 1) as a consequence of the incorporation of ions and solvent molecules into the polymer matrix. Reversible redox reactions were detected and the current density obtained range from  $20 \text{ nA.cm}^{-2}$  to  $0.6 \text{ mA.cm}^{-2}$ . The salt solution added (less than 0.1ml of NaCl 0.9% (w/w) in water) intends to simulate a body fluid, such as blood plasma or sweat.

After membrane's electrochemical characterization, thin films were deposited on both sides of membrane to form the electrodes (Figure 2). The power generated by these devices depends not only on the materials used as electrodes but also on the membrane thickness.

To demonstrate the great potential of these bioelectrochemical devices, some of them were tested, and promising results were found. For instance, using silver and aluminium as electrodes in a thin film form, the device with  $1 \text{ cm}^2$  showed a voltage of 0.62V and a current of  $54 \mu\text{A}$  when in contact with sweated skin (Figure 3).

### References:

- [1] P. Xian Gao, J. Song, J. Liu, and Z. Lin Wang, *Adv. Mater.*, **19** (2007), 67–72.
- [2] V. Pushparaj, MM. Shaijumon, A. Kumar, S. Murugesan, L. Ci et al., *PNAS*, **104** (2007), 13574-13577.
- [3] S. Kerzenmacher, J. Ducreé, R. Zengerle and F. von Stetten, *Journal of Power Sources*, **182** (2008), 1-17.

## Figures:

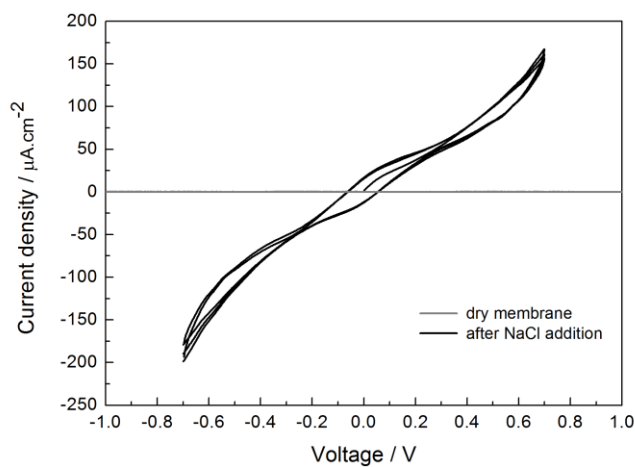


Figure 1 – Cyclic voltammogram obtained for a dry pristine membrane (grey line) and after salt solution addition (dark line). This measurement was processed at a voltage scan rate of 40 mV/s. The membrane used has 26.7 $\mu\text{m}$  of thickness.

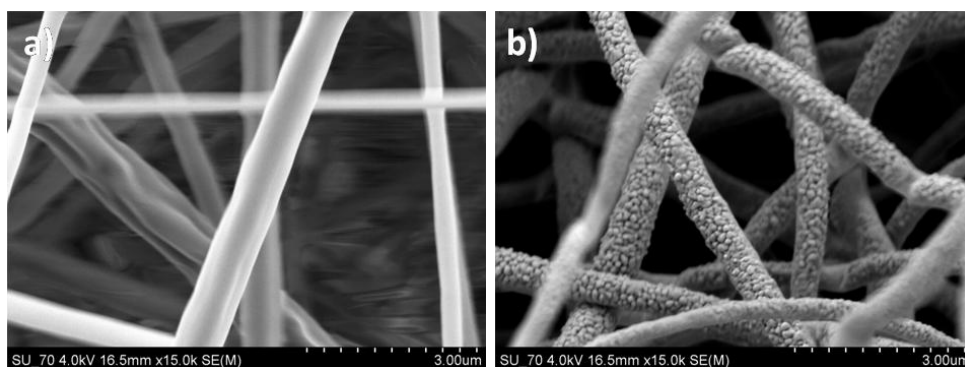


Figure 2 – SEM image of membrane's superficial fibres a) uncoated and b) after thin film deposition.

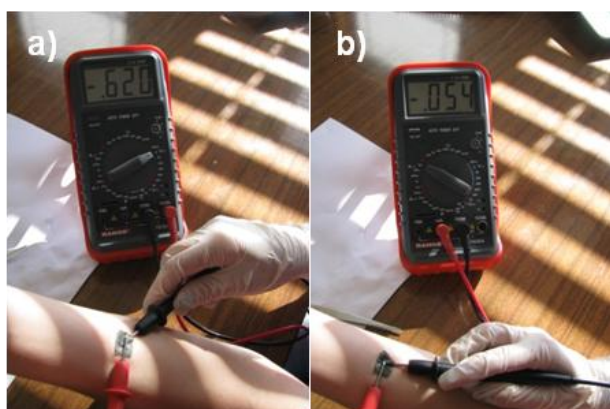


Figure 3 – Demonstration of the bioelectrochemical device's performance in sweated skin: a) voltage value (V) and b) current value (mA).

## Conformal Growth of Organic Luminescent Planar Defects within Artificial Opals

<sup>†</sup>Francisco J. Aparicio, <sup>†</sup>Gabriel Lozano, Iwona Blaszczyk-Lezak, Angel Barranco, and Hernán Mínguez

*Instituto de Ciencia de Materiales de Sevilla CSIC-Universidad de Sevilla, c/Américo Vespucio 49 41092 Sevilla Spain*

<sup>†</sup>F.J.A. and G.L. contributed equally to this work.

[hernan@icmse.csic.es](mailto:hernan@icmse.csic.es)  
[angelbar@icmse.csic.es](mailto:angelbar@icmse.csic.es)

Herein, we present the result of combining, for the first time, the techniques of colloidal selfassembly and plasma-enhanced chemical vapor deposition to create a novel, high-quality, purely organic active photonic crystal structure of controlled optical properties. We show a fast, reliable, and accurate procedure to introduce two-dimensional luminescent organic defect layers within artificial polystyrene opals via a versatile room-temperature remote plasma deposition process. This method is gentle enough to allow highly conformal growth on polystyrene microspheres without altering their morphology or the ordered arrangement that they form. The luminescent organic layer behaves both as an optical dopant, causing the opening of transmission windows within the forbidden frequency interval of the lattice, and as an optically active material, whose emission can be tailored by the photonic environment.

### References:

[1] F.J. Aparicio, G. Lozano, et al., Chem. Mater., **2** (2010) 379.

**Analysis of cellular and molecular interactions using Atomic Force Microscopy**

*Gerd Behme, Christian Loebbe, Carmen Pettersson  
JPK Instruments, Bouchestr. 12, Berlin, Germany  
behme@jpk.com*

Recent advances in AFM-based techniques for force spectroscopy are generally centered mostly about two major application areas. For single molecule force spectroscopy (SMFS) most of the relevant information is in the first several hundred nm of extension, whereas for cell-cell and cell-substrate interactions, the force extension can extend to 80 microns or more. The optimization of AFM equipment for these two techniques has some similarities but many significant differences. Which features and parameters need to be optimized for cell-cell and SMFS investigations will be discussed.

## Nanostructured electrochemical aptasensors for ochratoxin A (OTA) determination

*Bonel. L, Duato. P, Vidal. J. C, Castillo. J. R.*

Analytical Spectroscopy and Sensors Group (GEAS)

Institute of Environmental Sciences (IUCA) University of Zaragoza

C/ Pedro Cerbuna 12. 50009 ZARAGOZA. Spain

E-mail: [lbonel@unizar.es](mailto:lbonel@unizar.es)

Ochratoxin A is a naturally occurring mycotoxin produced primarily by *Aspergillus ochraceus* and *Penicillium verrucosum* usually present in a variety of foods. It is mainly found as a contaminant of cereals, cereal products and coffee beans. Previously, we have developed a device based on Quartz Crystal Microbalance sensor for OTA determination.

In the literature has been reported the combination of electrochemical immunosensor using gold nanoparticles (AuNPs), carbon nanotubes (CNTs) or magnetic beads (MBs). Nanostructured materials have proven as one of the most powerful tool in new technologies and research, due to their absolutely peculiar properties at nanometer size scale.

The interesting approach of this work is related to the using of a selective aptamer to OTA. Aptamers are nucleic acids (DNA or RNA) that selectively bind to low molecular weight organic or inorganic substrates or to macromolecules such as proteins.

Anyway, this work is the first step in the realization of an assay for OTA based on the use of the specific aptamer exploiting the known advantages of these biomimetic receptors. In literature only two papers report the development of an assay for OTA detection using specific aptamer.

A disposable electrochemical assay involving MBs and carbon-based screen-printed electrodes (SPCEs) was developed for the detection of OTA. The Streptavidin Paramagnetic Particles consist of a magnetite core coated with streptavidin. Thus, these particles combine convenient magnetic separation technology with the versatility and high affinity of the biotin-streptavidin interaction. The assay was based on a direct competitive format in which a DNA aptamer biotinylated was used as biorecognition element, and horse-radish-peroxidase (HRP) was used as enzymatic label.

All steps of the assay were carried out onto MBs; only the electrochemical detection was performed transferring the functionalized MBs onto the working electrode of a SPCE. In this assay there is a competition step between OTA and OTA-HRP, finally hydroquinone (HQ) and H<sub>2</sub>O<sub>2</sub> were added as co-substrate and substrate. The enzymatic product was determined by DPV.

The performance of the assay in terms of sensitivity, reproducibility and selectivity were studied. The calibration curve carried out shows a LOD and LOQ 0.2 and 6 µg/l respectively and the average coefficient of variation (ACV) resulted 8 %.

Finally, this approach will be applied to the analysis of some OTA samples to determine the concentration of OTA and predict the risk of a possible contamination with OTA.

## Electrospinning of PVP-calcium phosphates sol precursors for the production of hydroxyapatite nanofibres

*J.P. Borges<sup>(1)</sup>, P.Q. Franco<sup>(1)</sup>, J.C. Silva<sup>(2)</sup>*

*(1) CENIMAT/I3N, Departamento de Ciência dos Materiais,  
Faculdade de Ciências e Tecnologia, FCT, Universidade Nova de Lisboa,  
2829-516 Caparica, Portugal*

*(2) CEFITEC, Departamento de Física,  
Faculdade de Ciências e Tecnologia, FCT, Universidade Nova de Lisboa,  
2829-516 Caparica, Portugal*

[jpb@fct.unl.pt](mailto:jpb@fct.unl.pt)

Natural bone consists of nanometer-sized needlelike crystals of hydroxyapatite (HA) growing in intimate contact with collagen. These hydroxyapatite nanofibres are about 5–20 nm wide and 60 nm long and act as tiny reinforcements to enhance the hardness and strength by many orders of magnitude. In this work, we investigated the production of HA nanofibres by the combination of sol-gel, a versatile technique frequently used to produce ceramic nanoparticles [1], and electrospinning, a technique that permits the fabrication of nanometer-sized fibres from polymeric solutions in an electric field-assisted spinning process [2].

A new method of producing HA fibres combining electrospinning and a non-alkoxide sol-gel system, using cheap precursors, was used. Phosphorus pentoxide ( $P_2O_5$ ) and calcium nitrate tetrahydrate ( $Ca(NO_3)_2 \cdot 4H_2O$ ) were used as precursors of phosphorus and calcium, respectively. Fibrous membranes were electrospun from a mixture of the gel obtained from the system  $Ca(NO_3)_2 \cdot 4H_2O/P_2O_5$  with polymeric solutions of polyvinylpyrrolidone (PVP) in water and ethanol/water mixtures. Polymeric solutions were prepared with 15 % (w/w) and 18 % (w/w) of PVP. After sintering the as-spun membranes, at 500 °C, 600 °C and 700 °C, nano and microfibres were obtained. The fibres were analyzed for their morphology (Scanning Electron Microscopy, SEM), chemical composition (Fourier Transform Infrared Spectroscopy, FTIR) and structure (X-ray diffraction, XRD). XRD analysis revealed that the fibres were composed mainly by type B carbonated HA with traces of calcium oxide (CaO) and  $\beta$ -tricalcium phosphate ( $\beta$ -TCP). Figures 1 and 2 present the typical morphology of the HA sintered fibres and the XRD pattern of the fibres after sintering at 700 °C, respectively. From SEM analysis it was found that higher concentration of PVP in the electrospinning solutions leads to the formation of cylindrical fibres and that a larger amount of water allows for smaller diameter fibres and narrow diameters' distribution.

These HA nanofibres can have important applications in the field of bone tissue engineering.

### References:

- [1] Wang F, Li MS, Lu YP, Qi YX *Materials Letters* (2005), 48, 5742
- [2] Li D, Xia Y., *Advanced Materials* (2004), 16, 1151-1170

## Figures:

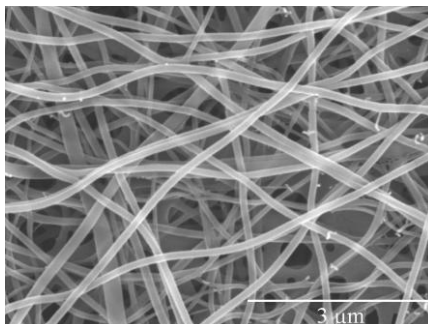


Figure 1. HAp fibres obtained after sintering, at 700 °C, precursor electrospun nanofibres (from a mixture of sol and 18% water solution of PVP).

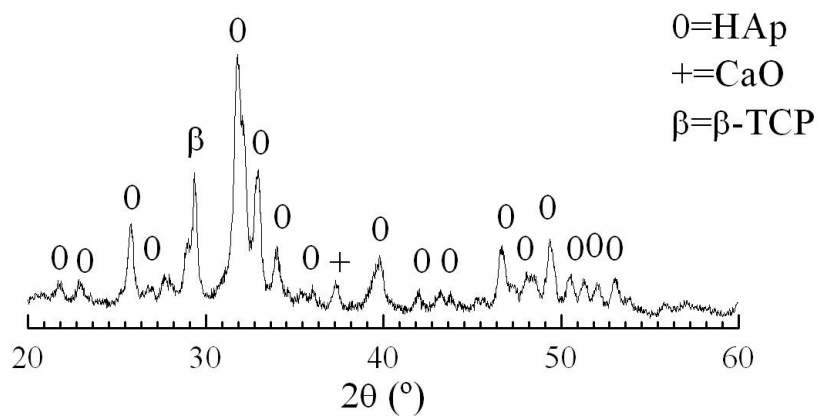


Figure 2. XRD pattern of the fibres sintered at 700 °C.

**Generation of Calcium Phosphate Nanoparticles by Laser Ablation in Ambient Conditions.**

*M. Boutinguiza, R. Comesaña, F. Lusquiños, A. Riveiro, J. Pou*

*Dpto. Física Aplicada, Universidad de Vigo, ETSI Industriales, c/ Maxwell, 36310 Vigo, Spain*

*mohamed@uvigo.es*

Calcium phosphate-based bioceramics have been used in medicine for decades due to their excellent biocompatibility, bioactivity and osteoconductive characteristics [1]. Hydroxyapatite (HA) and related calcium phosphate ceramic materials have been widely used as implant materials because of their close similarity in composition and high biocompatibility with natural bone. In terms of biocompatibility, hydroxyapatite with the stoichiometric formula  $\text{Ca}_{10}(\text{PO}_4)_6(\text{OH}_2)$  and a Ca/P molar ratio = 1.67 is an important bioceramic material, present in the inorganic part of the bones and teeth as nano-crystals. It seems to be a suitable ceramic material for hard tissue replacement implants and tends to form a direct bonding with the neighbouring bones [2]. It has been reported that nanocrystalline HA compared to coarse present greater biological efficacy in terms of osteoblast adhesion, proliferation and the formation of new bone on its surface [3]. On the other hand, tricalcium phosphate ( $\beta$ -TCP), with the formula  $\text{Ca}_3(\text{PO}_4)_2$  and calcium to phosphorous ratio of 1.5 dissolves more rapidly in the body fluid than crystalline hydroxyapatite, therefore, the empty space leaved by the dissolved material can be replaced by bond tissue [4,5]. It has been reported that the use of low crystalline TCP and nanosized TCP particles improve the performance of apatitic cements [6,7] and increase the bioactivity when used in scaffolds [8].

In this work calcined fish bones, which consisted mainly of hydroxyapatite (figure 1) were used as precursor material to produce calcium phosphate nanoparticles by means of laser ablation method combined with a gas jet. As laser source, a Nd:YAG laser was employed. Morphology and composition of the obtained particles were characterized by scanning electron microscopy (SEM), energy dispersive X-ray spectroscopy (EDX) and conventional and high resolution transmission electron microscopy (TEM, HRTEM).

When the laser beam impinges on fish bones, its surface is exposed to thousands of high energy pulses, which cause a rapid increase of temperature, leading to material fracturing, melting and/or evaporation [9]. According to collected material, there are particles exhibiting approximately a rounded shape, which can suggest the condensation of the material in reduced fragment tending to be spherical, as can be seen in figure 2. Its shape reveals that the formation mechanism is based on a melting process. The EDX analysis showed that its composition is similar to that of calcined fish bones. The rest of the obtained particles present a reduced size, showing rounded shape, and its length is about only few nanometers, as shown in figure 3. The crystalline particles are thin enough to enable obtaining lattice fringe images. A considerable quantity of these fringes have been used to quantify the interplanar spacing by means of the fast Fourier transform, in order to compare it with those of the well known calcium phosphates (see figure 4). Results show good agreement with hydroxyapatite and  $\beta$ -TCP with substitutions of Mg,  $(\text{Ca}, \text{Mg})_3(\text{PO}_4)_2$ . The presence of Mg substituting Ca is usual in biological apatites [10]. The formation of  $\beta$ -TCP is promoted by the high temperature reached at the surface target [11].

In summary, the results show that nanometric particles of hydroxyapatite and  $\beta$ -TCP can be obtained from fish bones by combining laser ablation technique in ambient conditions and a perpendicular gas jet. The presence of  $\beta$ -TCP is due to the high temperature which causes the transformation of hydroxyapatite into  $\beta$ -TCP.

**Acknowledgements**

This work was partially funded by the European Union program POCTEP (Project 0330\_IBEROMARE\_1\_P), FPU program AP2006-03500 grant and by Xunta de Galicia (PR405A2002/11-0, INCITE081R303002ES, INCITE08PXIB303225PR and INCITE09E2R303103ES).

**References:**

[1] L.L. Hench, Bioceramics, J. Am. Ceram. Soc. 81 (1998) 1705.  
 [2] W. Suchanek, M. Yoshimura, J. Mater. Res. 13 (1998) 94.  
 [3] T.J. Webster, C. Ergun, R.H. Doremus, R.W. Siegel, R. Bizios, Biomaterials 21 (2000) 1803.  
 [4] K. Fujihara, M. Kotakib, S. Ramakrishna, Biomaterials 26 (2005) 4139.  
 [5] O. Adamopoulos, T. Papadopoulos, J. Mater. Sci: Mater. Med. 18 (2007) 1587.  
 [6] T.J. Brunner, M. Bohner, C. Dora, C. Gerber, W.J. Stark, J. Biomed. Mater. Res. B (2007) 400.  
 [7] T.J. Brunner, R.N. Grass, M. Bohnerb, W.J. Stark, J. Mater. Chem. 17 (2007) 4072.  
 [8] O.D. Schneider, S. Loher, T.J. Brunner, L. Uebersax, M. Simonet, R.N. Grass, H.P., Merkle, W.J. Stark, J. Biomed. Mater. Res. B: Appl. Biomater. (2007) 350.  
 [9] Chen, Y., Bulatov, V., Singer, L., Stricker, J. and Schechter I. Anal. Bioanal. Chem. 383, (2005), 1090–1097.  
 [10] A. Bigi, E. Foresti, R. Gregorini, A. Ripamonti, N. Roveri and J. S. Shah. Calcif. Tissue Int. (1992) 439-444.  
 [11] Linc, C., Lee, B., Lin, F., Kork, S. and Lan W. J. Endodont. 27, 2001, 389-393.

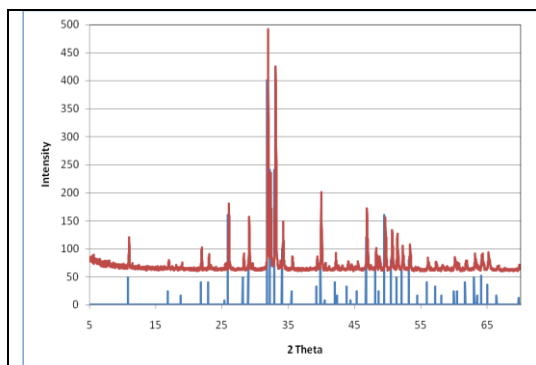


**Fig. 1:** XRD pattern of the used fish bones compared with stoichiometric hydroxylapatite.

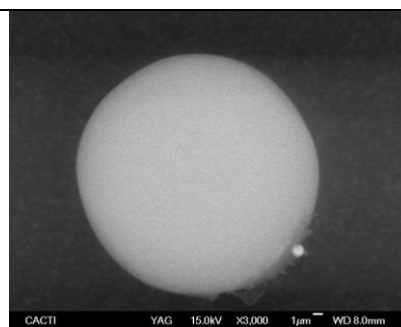


**Fig. 2:** particle from the interaction zone with spherical shape

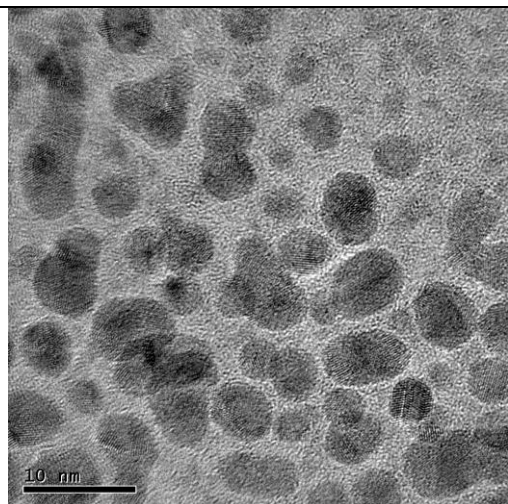


**Fig. 3:** HRTEM image of nanoparticles obtained from fish bones.

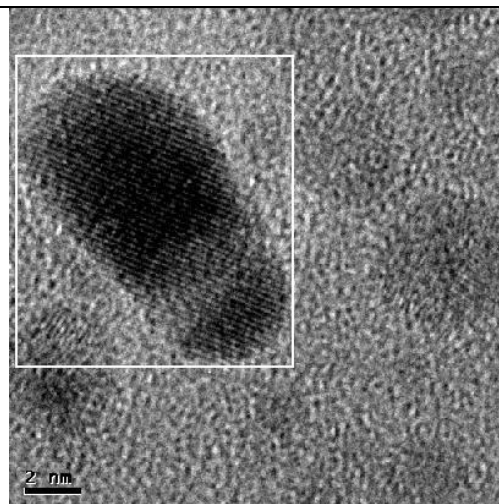


**Fig. 4:** HRTEM image showing the crystalline structure of a calcium phosphate nanoparticle.

## High frequency resonant tunneling behavior: Testing an analytical small signal equivalent circuit with time dependent many-particle quantum simulations

*E. Buccafurri*<sup>(1)</sup>, *F.L.Traversa*<sup>(2)</sup>, *X.Oriols*<sup>(2)</sup>, *A.Alarçòn*<sup>(2)</sup>, *G.Albareda*<sup>(2)</sup>, *R.Clerc*<sup>(3)</sup>,  
*F.Calmon*<sup>(1)</sup> *A.Poncet*<sup>(1)</sup>

(1)INL-INSA-Lyon, 7 av. Jean Capelle, 69621 Lyon, Villeurbanne Cedex, France

(2)Departament d'Enginyeria Electrònica, Universitat Autònoma de Barcelona 08193 Bellaterra SPAIN

(3) IMEP-LAHC, 3 rue Parvis Louis Néel, BP 257 Grenoble Cedex, France

[emanuela.buccafurri@insa-lyon.fr](mailto:emanuela.buccafurri@insa-lyon.fr)

Since the pioneering work by Tsu and Esaki [1], resonant Tunneling Diodes (RTDs) have attracted a lot of attention. Their peculiar properties like Terahertz maximum operating frequency and Negative Differential Resistance (NDR), offer a wide range of applications, in either analog (frequency divider or multiplier, oscillator [2]) or digital (“multi-value” logic [3]) circuits. Recently, there is renewed interest in such devices because the progress of Silicon On Insulator (SOI) technology made it possible to build RTD devices on ultra-thin crystalline silicon with thickness lower than 10nm [4] (rather than the common III-V materials).

This work is devoted to an accurate analysis of the frequency behavior of RTDs. Such accurate analysis is a really very difficult task because one has to take into account the Coulomb correlation among electrons to assure (i) **current conservation** (the total current is the sum of the conduction plus the displacement currents due to time-dependent variations of the electric field) and (ii) **overall charge neutrality** (screening deep inside the leads assures that the total charge tends to zero). To the best of our knowledge, this is the first time that a detailed analysis of how conditions (i) and (ii) affects the relevant cut-off frequency of RTD.

We apply two different approaches. The first is a time-dependent Quantum Monte Carlo (QMC) based on many-particle Bohm trajectories [5]. This powerful simulator can include Coulomb correlations self-consistently and it has been used to extract the RTD intrinsic frequency limitation directly from the current response to a small step voltage signal. Such a rigorous approach it is used to understand the RTD behavior and to test an analytical Small Signal Equivalent Circuit (SSEC) [6] (see fig. 1) derived from a DC physics based model [7] following Liu’s approach [8].

To extract information about the different time constants associated to the several processes characterizing the electron dynamics in the RTDs, we accounted for three different conditions employed in NDR regime.

**a) Without conditions (i) and (ii):** we remove self-consistency of the Coulomb interaction in the QMC. The current in the RTD follows the voltage step with an intrinsic delay of about 0,035 ps (see fig. 2). In absence of coulomb interactions, this time is assumed to be equal to the RTD dwell time  $\tau_d$ . In the analytical model  $\tau_d = \hbar/\Gamma$  where  $\Gamma$  is the total width of the resonant level [9]. The value extracted for this structure is 0,03 ps in excellent agreement with QMC. In this case, the SSEC can be simplified by connecting in series a negative conductance  $G$  and a negative inductance  $L$  (see fig. 1 solid blue line). The resulting cutoff frequency of this simple filter is  $2\pi\tau_d = 5$  THz.

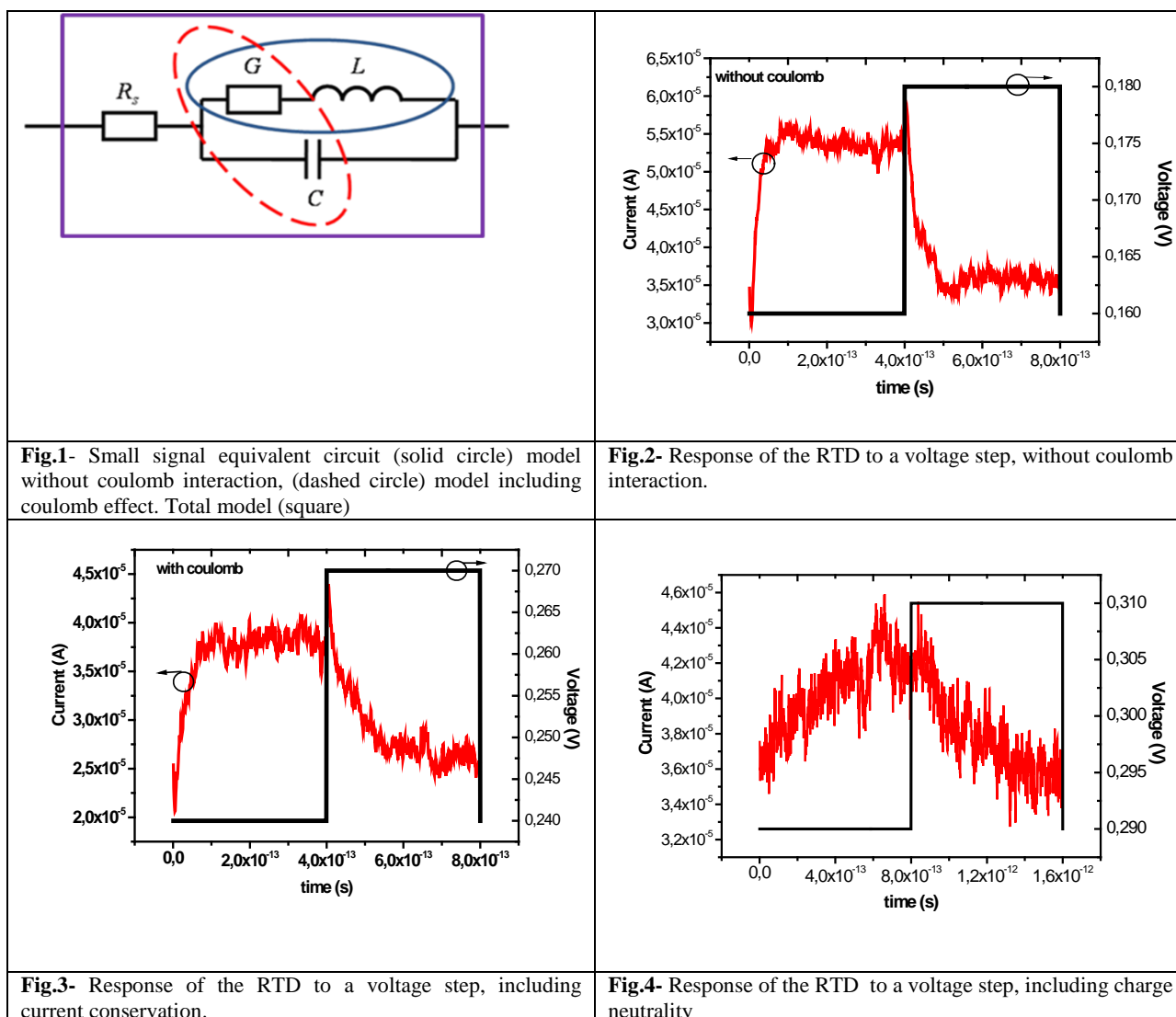
**b) With condition (i):** The potential is computed by solving the Poisson equation self-consistently with QMC. In this condition the “simulation box” is very small, thus leads are neglected. The Coulomb interaction can be modeled by a capacitance  $C$  in parallel to  $G$  (see fig. 1 dashed red line). The total capacitance  $C$  account for two contributions, the geometrical capacitance  $C_0$  and the quantum capacitance defined as  $C_q = -G\tau$ . In this case the cutoff frequency of SSEC results of 3.6 THz and it is consistent with the characteristic time (0,25 ps see fig. 3) found with QMC.

**c) With conditions (i) and (ii):** In order to ensure charge neutrality in whole device, the leads have been introduced in QMC consistently with the Poisson equation. Conversely in the small signal circuit, contacts have been included by means of a series resistance (see fig. 1 squared solid line). Thus the cut off frequency of SSEC is now  $1,4$  THz. This value is in very good agreement with cutoff frequency reduction obtained with QMC (see fig. 4).

We can conclude that several limitations come into play in the frequency response of an RTD, namely the intrinsic tunneling process, the transit time across the non-tunneling regions and time constant associated to the total capacitance of the structure. On the one hand the full time-dependent simulation provides a rigorous picture of the physics that governs the frequency behavior of RTD. On the other hand, our study shows that the equivalent small signal circuit is able to catch characteristic times, resulting a useful tool to design RTD.

### References:

- [1] R. Tsu, L. Esaki, Appl. Phys. Lett. **22** (1973) 562-564
- [2] H. J. De Los Santos, et al., IEEE Microwave Wireless Compon. Lett. **1** (2001) 193-195
- [3] H.C. Lin, Proc. IEEE Int. Symp. Multiple Valued Logic (1994) 188-195
- [4] M. Vinet, et al., IEEE Electron Device Lett. **26** 5 (2005) 317-319
- [5] X. Oriols, Phys. Rev. Lett. **98** (2007) 066803
- [6] E. Buccafurri et al., Phys. Status solidi c, **6** 6 (2009) 1408-1411
- [7] E. Buccafurri et al., IEEE ULIS proc. (2009) 91-94
- [8] Q. Liu et. al. IEEE Trans. Elec. Dev. **51** (2004) 653 - 657
- [9] E.R. Brown, C.D. Parker, L.G. Sollner Appl. Phys. Lett. **54** (1989) 2291-2293



## Synthesis and antimicrobial study of silver-kaolinite nanocomposites

*B. Cabal<sup>1</sup>, M. Miranda<sup>2</sup>, R. Torrecillas<sup>2</sup>, F. Malpartida<sup>3</sup>, J.S. Moya<sup>1</sup>*

<sup>1</sup>*Instituto de Ciencia de Materiales de Madrid (ICMM-CSIC), 28049, Cantoblanco, Madrid, Spain*

<sup>2</sup>*Centro de Investigación en Nanomateriales y Nanotecnología (CINN), Consejo Superior de Investigaciones Científicas (CSIC) – Universidad de Oviedo (UO) – Principado de Asturias, Parque Tecnológico de Asturias, 33428, Llanera, Spain*

<sup>3</sup>*Centro Nacional de Biotecnología (CNB-CSIC), 28049, Cantoblanco, Madrid, Spain*

[bcabal@icmm.csic.es](mailto:bcabal@icmm.csic.es)

Microorganism produce a wide range of diseases and they are responsible of contamination of drinking water and the decay of fruits and vegetables [1, 2]. Pathogenic microorganisms with resistance to various antimicrobial agents have risen over the last several years, resulting in increase in morbidity and mortality and overall treatment cost. In this regard, inorganic bactericides have attracted special interest due to their chemical stability, long life and heat resistance [3, 4]. Silver, known as a disinfectant for many years, has a broad spectrum of antibacterial activity. Silver nanoparticles show efficient antimicrobial properties compared to other silver salts due to their extremely large surface area and low solubility, which provides better contact with micro-organisms. Silver nanoparticles in most studies are suggested to be non-toxic in low concentrations, but in high concentration could have toxic effects.

In the present work, a nanocomposite of kaolinite with a low content (1 wt% Ag) of silver nanoparticles is presented. Two different methods were followed to deposited Ag nanoparticles in a controlled way on the kaolinite surface. In the first procedure, the precursor is reduced thermally, while in the second there is a chemical reduction employing in this case sodium borohydride as a reductor agent. In both cases, the first step is the preparation of a kaolin dispersion (9 wt% of solids loading) in the best possible conditions in terms of stability and homogeneity. A dispersant is used (Dolapix CE-64) to improve the suspension stability. All the steps in both procedures to add the silver were carried out in a dark room to avoid the spontaneous reduction of silver cations due to the presence of light. The samples were characterized by TEM, SEM and UV-Visible spectroscopy. Figure 1 and Figure 2 show some TEM images for the samples thermally and chemically reduced. In both cases, in the samples obtained by both reduction procedures, the silver nanoparticles appear perfectly isolated and attached onto the surface of the kaolin particles. The kaolin matrix acts an effective scaffold where the nanoparticles are dispersed, avoiding their agglomeration.

Dehydroxylation of kaolinite it was also studied. The effect of the thermal treatment of kaolinite before and after the incorporation of Ag nanoparticles was evaluated.

The antimicrobial benefits of the composite were evaluated as antibacterial against Gram-negative and Gram positive bacteria, and the antifungal activity against yeast. *Escherichia coli* JM 110, *Micrococcus luteus* and *Issatchenkia orientalis* were selected as models of the Gram-negative bacteria, Gram-positive bacteria and yeast, respectively.

### References:

[1] Tian, S.P., Fan, Q., Xu, Y., Jiang, A.L., *Plant Pathology*, **51** (2002), 352-358

- [2] Chang, Q., He, H., Zhao, J., Yang, M., Qu, Journal of Environment Science and Technology, **42** (2008), 1699-1704  
[3] Trapalis, C.C., Kokkoris, M., Perdikakis, G., Kordas, G., Journal of Sol-Gel Science and Technology, **26** (2003), 1213-1218  
[4] Pal, S., Tak, Y.K., Song, J.M., Applied and Environmental Microbiology, **73** (2007), 1712-1720

**Figures:**

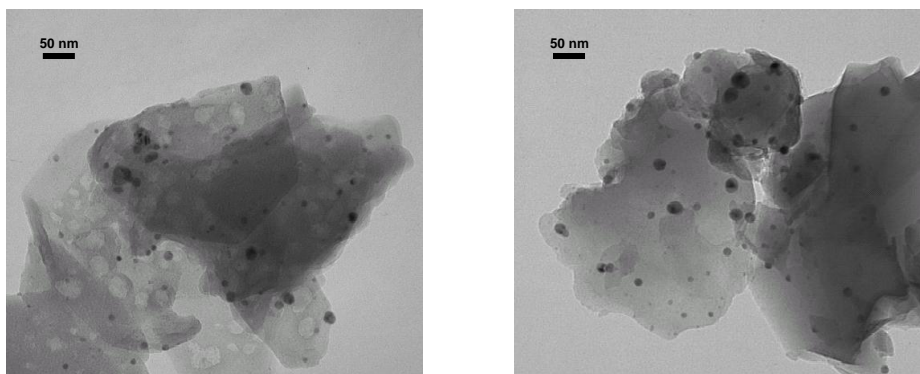


**Figure 1.** TEM micrographs of the sample thermally reduced

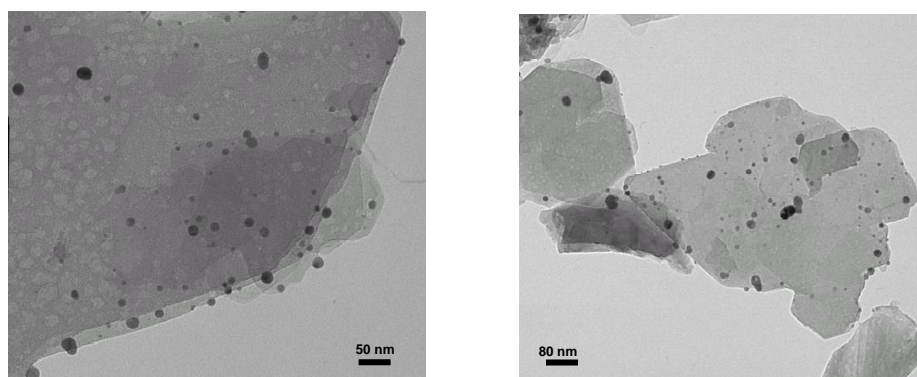


**Figure 2.** TEM micrographs of the sample chemically reduced

## Pd Nanoparticles Functionalized with alkylamines: Structural and Magnetic Characterization

I. Castellanos-Rubio, L. Lezama, M. Insausti, I. Gil de Muro, T. Rojo

Zientzia eta Teknologia Fakultatea, Euskal Herriko Unibertsitatea, P.O. Box 644, E-48080 Bilbao, Spain.

[icastellanos001@ikasle.ehu.es](mailto:icastellanos001@ikasle.ehu.es)

Palladium nanoparticles are candidate materials for controllable magnetism because of the density of states at Fermi energy for Pd is close to fulfilling the Stoner criterion of magnetism [1]. The change in the electronic structure due to size effects or to a surface environment could enhance the density of states at the Fermi level and modify the magnetic behavior of palladium [2]. Therefore, Pd magnetic nanoparticles could play an important role not only in the understanding magnetism at nanoscale but also in the applications to magnetic devices or in biomedical fields [3]. In this sense, Pd nanoparticles stabilized with two alkylamines have been synthesized and characterized by x-ray diffraction, thermogravimetry and transmission electron microscopy (TEM). The magnetic behaviour has been studied by magnetization measurements (SQUID) and Electron Magnetic Resonance (EMR).

Pd nanoparticles have been obtained by liquid-liquid phase reduction, based on Brust method [4]. In these method the transfer of  $\text{Pd}^{+2}$  ions from an aqueous solution of  $\text{Na}_2\text{PdCl}_4$  (aq) to toluene occurs using tetraoctylammonium bromide (TOAB) as the phase-transfer reagent in the presence of butylamine. If this alkylamine is not present, TOAB can also acts as stabilizer preventing the nanoparticles from aggregating. As a result, two kind of Pd nanoparticles have been obtained, Pd-NR (NR = butylamine) and Pd-TOAB, respectively. Changes in the preparation conditions yield samples with different magnetic behaviour.

Colloidal solutions of the nanoparticles were analyzed by means of TEM microscopy and homogeneous distributions of NPs with mean sizes around 4 nm were observed. In solid samples, Pd (fcc) structure was corroborated by the maxima observed by X ray diffraction. In order to know the content of organic matter thermogravimetric measurements were performed in Ar atmosphere and different contents (from 20% to 60%), depending on the sample preparation and the type of surfactant, have been obtained.

Magnetic measurements, at 5 and 300 K, have revealed a ferromagnetic nature in only some of samples in which magnetic hysteresis loops with low coercitive fields can be observed. The maximum value for saturation is achieved at 0.16 emu/g at 300 K for some of the preparations of the Pd-TOAB system. This magnetic behaviour has also been corroborated by EMR measurements where an intense resonance signal with a peak to peak linewidth ( $\Delta H_{pp}$ ) greater than 1000G appears. Further experiments are being performed in order to know the relation between the appearance of magnetic behaviour and characteristics of the nanoparticles.

### References:

- [1] Janak, J. F. *Phys. Rev. B.* **16** 255 (1977).
- [2] Litrán, R; Sanpedro, B; Rojas, T.C.; Multigner, M; Sánchez-López, J.C.; Crespo, P; López-Castes,C; García, M.A; Hernando, A; Fernández, A. *Phys. Rev. B.* **73**, 054404 (2004).
- [3] David, I. Gittins; Frank, Caruso. *ChemPhysChem.* **3**(1), 110-113 (2002),
- [4] Brust, M.; Walker, M.; Bethell, D; Schiffrin, D.J; Whyman, R. *J. Chem. Soc., Chem. Commun.* 801 (1994).

## Development of superparamagnetic nanocomposite: The effect of nanoparticles dispersion and matrix structure on magnetic properties.

*M. Castrillon<sup>1</sup>, J.G. Meier<sup>1</sup>, S. Irusta<sup>2</sup>*

*Instituto Tecnológico de Aragón (ITA,) C/ María de Luna, nº 7. 50018, Zaragoza, Spain 1.*

*Instituto de Nanociencia de Aragón, (INA) C/Pedro Cerbuna 12, 50009, Zaragoza, Spain 2.*

[mcastrillon@ita.es](mailto:mcastrillon@ita.es)

Polymer nanocomposites with response under magnetic field application were obtained by dispersion of magnetic nanoparticles in polymer matrices by extrusion, which is the preferred industrial method for polymer compounding and processing [1]. These nanostructured materials are expected to have a wide application range since the polymer technology allows components fabrications with diverse forms and mechanical properties. Applications in fields of sensors [2], magnetic storage [3], electromagnetic absorption and magnetic yielding [4] are usual. Ferromagnetic nanoparticles are very difficult to process, suffering from problems such as sticking of the particles at metallic components of the mixing machine, and to disperse due to their permanent magnetic moment causing strong particle-particle interactions. Superparamagnetic nanoparticles were used instead having the advantage that the thermal energy and the associated thermal fluctuations of the particles at process conditions supersedes the magnetic interparticle interaction but maintaining closely the high magnetic moment of their ferromagnetic counterparts. The superparamagnetic particles were magnetite, synthesised in a wet-chemical process and concentrated to a slurry to be used in the extrusion process. Two different types of polymer matrices were used: 1) an amorphous thermoplastic elastomer SEBS characterised by cylindrical phase morphology of the polystyrene blocks in the ethylene-co butylene phase and 2) a semicrystalline engineering thermoplastic PPS. The nanocomposites were prepared by melt-extrusion of Fe<sub>3</sub>O<sub>4</sub> superparamagnetic nanoparticles with the polymer matrices using a twin-screw microextruder [5].

The nanocomposites were characterized by transmission electron microscopy (TEM) and thermal gravimetric analysis (TGA). Magnetic properties were evaluated by means of hysteresis curves, ZFC/FC curves and AC magnetic susceptibility measurements in superconducting quantum interference device (SQUID) and quantum design physical properties measurement system (PPMS) magnetometer. Results showed that with a small content of nanoparticles (<1,5wt%) a global magnetic response from the composite is achieved. The dispersion of nanoparticles was found to be affected by the matrix used. Contrary to the expectations, the lowest blocking temperature was obtained with the rigid matrix (PPS, having a T<sub>g</sub> of 90°C) instead of the flexible one (SEBS with a T<sub>g</sub> of the soft phase of -55°C). This effect is attributed to the cylindrical/micellar structure of SEBS that induces "depletion interaction" between superparamagnetic nanoparticles causing aggregation [6] and will be discussed in more detail. Our findings have general implication on the design of nanoparticles polymer composites and its processing for dedicated purposes.

### References:

- [1] MR Bockstaller, RA Mickiewicz, EL Thomas, Adv Mater. 17 (2005) 1331-1349.
- [2] K Singh, A Ohlan, RK Kotnala, AK Bakhshi, SK Dhawan, Mater.Chem.Phys. 112 (2008) 651-658.
- [3] J Jeong, S Shin, S Lee, J Kim, J Magn Magn Mater. 286 (2005) 5-9.

- [4] NA Buznikov, IT Iakubov, AL Rakhmanov, AO Sboychakov, J Magn Mater. 293 (2005) 938-946.
- [5] G Kickelbick, Progress in Polymer Science. 28 (2003) 83-114.
- [6] B Heck, P Arends, M Ganter, J Kressler, B Stuhn, Macromolecules. 30 (1997) 4559-4566.

### Figures:

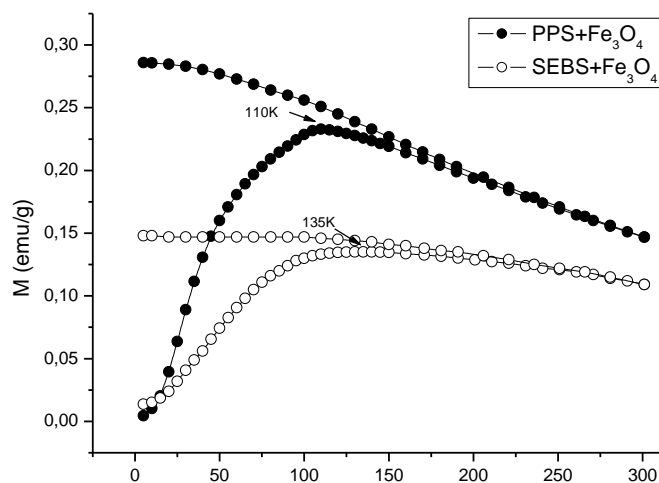


Figure 1. Comparison between the ZFC/FC curves for SEBS+Fe<sub>3</sub>O<sub>4</sub> nanocomposite and PPS+Fe<sub>3</sub>O<sub>4</sub> nanocomposite.

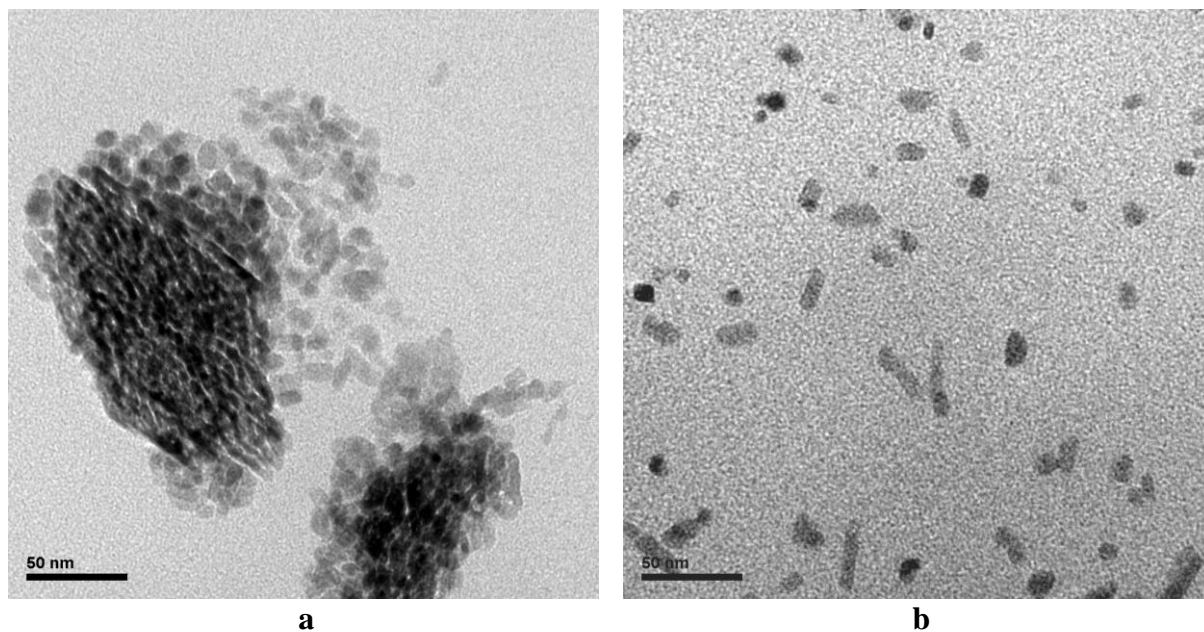


Figure 2. Dispersion analysis by TEM images. a) SEBS+Fe<sub>3</sub>O<sub>4</sub> nanocomposite. b) PPS+Fe<sub>3</sub>O<sub>4</sub> nanocomposite.

**Embedding 1-Mercapto-(triethylene glycol) methyl ether functionalized gold nanoparticles into poly(1,2-butadiene)-block-poly(ethylene oxide) polymersomes for bioimaging**

*E. Castro*<sup>a,b</sup>, *S. Lecommandoux*<sup>a</sup>, *P. Taboada*<sup>b</sup>, *V. Mosquera*<sup>b</sup>.

<sup>a</sup>*University of Bordeaux, Laboratoire de Chimie des Polymères Organiques, CNRS UMR 5629, 16 Av. Pey Berland, 33607 Pessac, France.*

<sup>b</sup>*University of Santiago de Compostela, Department of Condensed Matter Physics, Faculty of Physics, 15782 Santiago de Compostela, Spain.*

Polymersomes are useful in nanomedicine because of their subcellular size and ability to encapsulate diagnostic and therapeutic molecules. We report the selective incorporation of commercial gold nanoparticles into the interface of polymersomes *via* TEM and DLS investigations. Polymersomes were fabricated from the diblock copolymer poly-(butadiene-block-ethylene oxide) using a double emulsion process.

Results shows that whereas hydrophobic Au-NPs can be successfully embedded into the polymersome, we found evenly hydrophobic nanoparticles distributed in the inner- and outer compartments of the polymersomes. We can conclude from TEM images of the polymersome suspensions that gold nanoparticles smaller than the bilayer thickness were primarily embedded within the vesicle membrane, while larger nanoparticles were primarily centered inside the vesicle

The process of the incorporation of the nanoparticles into the polymersome bilayer is important because allows a fine control over these new polymersome-embedded nanoparticle nanostructures that has potential application in drug delivery coupled with localization studies.

## Functionalization and Characterization of Carbon Nanotubes solubles in physiological media

*Daniel Collado,<sup>1</sup> Ezequiel Perez-Inestrosa,<sup>1</sup> Rafael Suau,<sup>1</sup> Juan Casado,<sup>2</sup> Pedro Nieto<sup>3</sup>*

<sup>1</sup>*Department of Organic Chemistry, University of Málaga, Málaga, Spain*

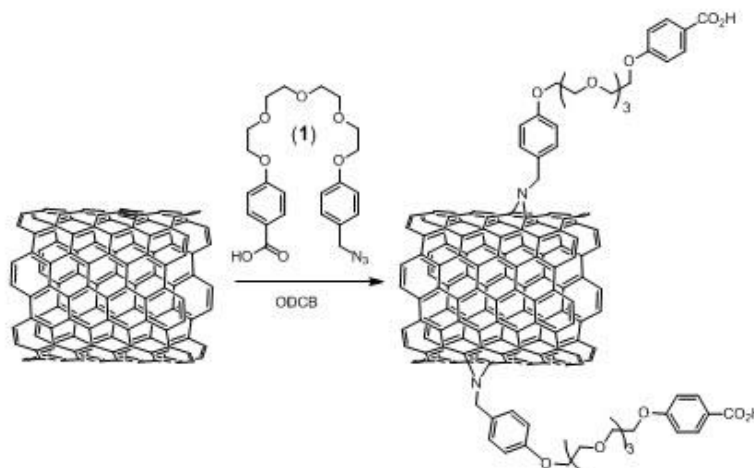
<sup>2</sup>*Department of Physical Chemistry, University of Málaga, Málaga, Spain*

<sup>3</sup>*Instituto de Investigaciones Químicas, CSIC, Sevilla, Spain*

[dcollado@uma.es](mailto:dcollado@uma.es)

Over the last few years, single-walled carbon nanotubes (SWNTs) have triggered intensive study towards numerous applications. In nanomedicine SWNTs have been used as substrates for detecting antibodies associated with human autoimmune diseases with high specificity and carriers of contrast agent. When covalently or noncovalently attached by nucleic acids, vaccines, and proteins, SWNTs have been shown as effective gene and drug transporters.[1] Considerable efforts have therefore been made to make carbon nanotubes stably dispersed or soluble in water and in organic solvents.[2]

In this communication we describe a covalent functionalization of SWNT to obtain water-soluble nanotubes. The reaction of purified SWNTs with excess azide (**1**) in *o*-dichlorobenzene under thermal condition involved a [2+3] cycloaddition of azide to a double bond of nanotube with formation of intermediate triazole, followed by thermal cleavage of N<sub>2</sub>. [3].



Functionalized SWNT were characterized by analytical, spectroscopic such Raman, UV/Vis, XPS and NMR techniques. The Raman spectra taken both in aqueous dispersion and in the solid phase indicated modification of the SWNT backbone. These simple functionalized SWNTs are promising for attaching other functional groups, amino acids, and DNA to nanotube for chemical and biological applications.

### References:

- [1] Q. Lu, J. M. More, G. Huang, A. S. Mount, A. M. Rao, L. L. Larcom, P. C. Ke, *Nano Lett.* **4** (2004), 2473-2477. S. Lin, A. S. Mount, Y. Wu, J. Moore, *Appl. Phys. Lett.* **89** (2006), 143118.
- [2] Y. Wang, Z. Iqbal, S. Mitra, *J. Am. Chem. Soc.* **128**, (2006), 95–99; K. C. Etika, F. D. Jochum, P. Theato, J. C. Grunlan, *J. Am. Chem. Soc.* **131** (2009), 13598–13599.
- [3] R. Wu, X. Lu, Y. Zhang, J. Zhang, W. Xiong, S. Zhu, *Tetrahedron*, **64** (2008), 10694-10698.

**Tyrosinase bioconjugates with gold nanoparticles for use as nanoprob**A. Pascoal<sup>1</sup>, D. Ribeiro<sup>1</sup>, F. Pereira<sup>1</sup>, S. Aparício<sup>1</sup>, I. Osório<sup>1</sup>, R. Franco<sup>1</sup>, J. Cortez<sup>1\*</sup><sup>1</sup> *REQUIMTE, Dept Química, Faculdade de Ciências e Tecnologia, Universidade Nova de Lisboa, 2829-516 Caparica, Portugal,*\* [j.cortez@dq.fct.unl.pt](mailto:j.cortez@dq.fct.unl.pt)

Keywords: Gold nanoparticle, tyrosinase, biosensor, bionanoconjugate, bionanoprobe.

Tyrosinase (EC 1.14.18.1) is a copper containing oxidoreductase which catalyzes two different reactions via separate active sites: (i) the o-hydroxylation of monophenols (cresolase activity) and (ii) the oxidoreduction of o-diphenols to o-quinones (catecholase activity). It is commonly found in fungi, yeast, apples, and potatoes.

Tyrosinase offers great potential for the development of biosensors [1-3] for the detection of phenolic compounds (pollutants, pesticides) in e.g. wastewaters. The enzyme has been reported for use in electrochemical sensors with success, in particular when applied on top of a layer of gold nanoparticles [4,5].

Our goal was to prepare active bionanoconjugates of the enzyme tyrosinase (TYR, from *Agaricus bisporus*) and spherical gold nanoparticles (AuNPs) with different surface functionalities. The bionanoconjugates (BNC) were prepared at different conditions (buffer, pH) and for a range of ratios AuNP:TYR (1:5 up to 1:500). The conjugation yielded BNCs with equivalent or superior enzymatic activity compared to the free enzyme, with increased stability for lower pH levels. The bionanoconjugates were further characterised using Dynamic Light Scattering spectroscopy and  $\zeta$ -potential measurements, confirming the attachment of the enzyme to the AuNPs.

The interaction of AuNPs with tyrosinase afforded bionanoconjugates that present properties that are useful for their employment as novel bionanoprobes for use in biosensors or in biocatalysis.

## References:

- [1] Kim, G., Shim, J., Kang, M., Moon, S., J. Environ. Monit., 2008, 10, 632–637
- [2] Abdullah, J., Ahmada, M., Karuppiah, N., Henga, L., Sidek H. Sensors and Actuators B 114, 2006, 604–609
- [3] Hedenmo, M., Narviez, A., Domínguez, E., Katakis, I. Journal of Electroanalytical Chemistry, 1997, 425, 1-11.
- [4] Kim, G., Shim, J., Kang, M., Moon, S., Journal of Hazardous Materials, 2008, 156, 141–147
- [5] Kim, G., Kang, M., Shim, J., Moon, S. Sensors and Actuators B, 2008, 133, 1-4.

## Insulin-loaded poly(D,L-lactide-co-glycolide) micro- and nanoparticles obtained by Flow Focusing technology

*Cózar-Bernal M.J.<sup>1</sup>, Arias J.L.<sup>2</sup>, Muñoz-Rubio, I.<sup>1</sup>, Alvarez-Fuentes J.<sup>1</sup>, Martín-Banderas L.<sup>1</sup>, Holgado M.A.<sup>1</sup>, Fernández-Arévalo M.<sup>1</sup>*

<sup>1</sup>Department of Pharmacy and Pharmaceutical Technology, Faculty of Pharmacy, University of Seville, Spain.

<sup>2</sup>Department of Pharmacy and Pharmaceutical Technology, Faculty of Pharmacy, University of Granada, Spain.  
cozar@us.es

### Introduction

The subcutaneous injection of insulin typically results in an inappropriate control of glycaemia, and poor treatment compliance. Despite oral administration could be much advantageous, many difficulties must be faced, e.g., the protection of the biomolecule against self-aggregation, and enzymatic degradation. Intense research is undergoing to develop oral delivery systems for the enhancement of the efficacy and safety of insulin [1, 2]. In this work, we describe the preparation of insulin-loaded poly(D,L-lactide-co-glycolide) (PLGA) particles using two methods: the flow focusing (FF) technology, and the traditional solvent evaporation method (SEV). It is compared the effect of both methodologies on the: *i*) geometry and physicochemical properties of the particles; *ii*) chemical structure of insulin inside PLGA; and *iii*) insulin loading and release properties.

### Materials and Methods

*Preparation of the insulin-loaded PLGA particles:* a water-in-oil emulsion was prepared by mixing a 10 % (v/v) acetic solution containing insulin (10 mg/mL) with 1 mL of a 1 % (w/v) solution of PLGA in ethyl acetate. When PLGA particles were prepared by SEV [3], this emulsion was added to a 0.3 % (w/v) PVA solution and homogenized. Then, PLGA particles were spontaneously formed when the double emulsion was diluted with 20 mL of a 2 % (w/v) PVA solution. Following the FF procedure [4], the previously prepared emulsion was used as focused fluid in a simple flow focusing nozzle [Avant 2 (D = 50 µm), Ingeniaticas Tecnologías S.L., Spain]. Distilled water was used as focusing fluid. PLGA particles were formed into a 0.3 % (w/v) PVA solution.

*Characterization methods:* the mean particle size and particle size distributions were measured at room temperature by laser scattering (Partica LA-950V2, Horiba). Insulin loading was determined by reverse phase-high performance liquid chromatography (RP-HPLC) (Hitachi LaChrom® (D-7000) Series HPLC system). Insulin content was expressed in terms of insulin entrapment efficiency (EE, %) and insulin loading (%) [5]. The zeta potential (ζ)-pH trend and ζ-ionic strength dependence were investigated in order to characterize surfaces of particles [4]. Fluorescence spectroscopy (maximum excitation λ = 311 nm) was carried out to establish if the tertiary structure of insulin is kept unmodified after encapsulation process and, additionally, to qualitatively check the efficacy of the protein loading [6]. Insulin release from PLGA was performed *in vitro* at 37.0 ± 0.5 °C by following the dialysis bag method, and using PBS (pH 7.4 ± 0.1) as the release medium [5].

### Results and Discussion

SEV method allows obtaining smaller particles than the FF technology: 0.49 ± 0.32 µm and 1.26 ± 0.12 µm, respectively. On the opposite, a more narrow size distribution was defined by FF (figure 1). The morphology and surface of the particles were not affected by the preparation method. Regarding to formulations electrokinetic, similar results were obtained for non-loaded and insulin-loaded PLGA, independently of the formulation method (data not shown for brevity). This point out that the protein was not surface adsorbed and, thus, a very efficient entrapment have led to insulin-loaded PLGA particles which, from an electrokinetic point of view, are indistinguishable from non-loaded PLGA.

Greater insulin EE (%) and loading (%) were obtained by following the FF technology: 98.95 ± 0.21 (SEV: 61.27 ± 0.64) and 4.74 ± 0.01 % (SEV: 2.92 ± 0.04 %), respectively. These high values for both methods could be due to a stronger electrostatic interaction between the positively charged insulin (-NH<sub>2</sub> groups protonated) and the negative polymer. In addition, as PLGA particles are obtained in just one step by FF, the possibility of drug loss during the synthesis is negligible [3]. Insulin absorption into PLGA was also qualitatively checked by fluorescence spectroscopy (figure 2a): the characteristic band of insulin is present in the spectrum of the protein-loaded PLGA particles. Interestingly, a significant reduction in the intensity of the insulin band is observed when the protein-loaded PLGA particles are prepared by SEV. This is the consequence of the lower protein content obtained by SEV.

Insulin release follows a biphasic profile (figure 2b) due to diffusion-cum-degradation mediated processes. During the rapid early phase, protein release could occur by the loss of the surface-associated insulin and by protein diffusion from the core. During the slower phase, the release may result from polymer degradation, from insulin diffusion through the polymeric core, or both [3]. At this point, we should also take into account that particle size is an important parameter that could affect the polymer degradation: an increase in particle size reduces the surface area/volume ratio of the polymer, leading to decreased buffer penetration into PLGA and slower protein release. This may define the slower insulin release from PLGA obtained by FF [3].

### Conclusions

We have analyzed two formulation procedures, the classic SEVM and the novel FF technique, for the preparation of spherical PLGA particles loaded with insulin. Compared to SEVM, it was found that FF allowed obtaining microparticles with a clear more narrow size distribution. Importantly, the microparticles

obtained by FF showed a higher loading and a much slower insulin release. This demonstrating the potential use of FF for the engineering of PLGA micromedicines based on proteins (or peptides).

### Acknowledgements

Financial support from Junta de Andalucía, Spain, under Project P06-CTS-01688 is gratefully acknowledged.

### References

- [1] Shelma R, Paul W, Sharma CP. *Carbohydr Polym* **80** (2010) 285.
- [2] Hamishehkar H, Emami J, Najafabadi AR, Gilani K, Minaiyan M, Mahdavi H, Nokhodchi A. *Colloids Surf B: Biointerfaces* **74** (2009) 340.
- [3] Holgado MA, Arias JL, Cózar MJ, Álvarez-Fuentes J, Gañán-Calvo AM, Fernández-Arévalo M. *Int J Pharm* **358** (2008) 27.
- [4] Holgado MA, Cózar-Bernal MJ, Salas S, Arias JL, Álvarez-Fuentes J, Fernández-Arévalo M. *Int J Pharm* **380** (2009) 147.
- [5] Arias JL, Reddy LH, Couvreur P. *J Drug Target* **17** (2009) 586.
- [6] Yong Z, Yingjie D, Xueli W, Jinghua X, Zhengqiang L. *Colloids Surf B: Biointerfaces* **371** (2009) 71.

**Figure 1.** Scanning electron microphotographs of insulin-loaded PLGA particles formulated by SEV (a), and by FF (b). (c) Size histograms of insulin-loaded PLGA particles prepared by both methods.

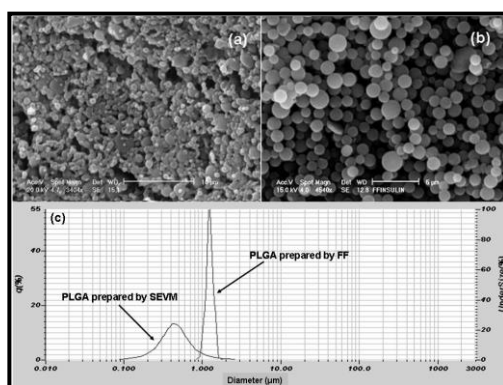
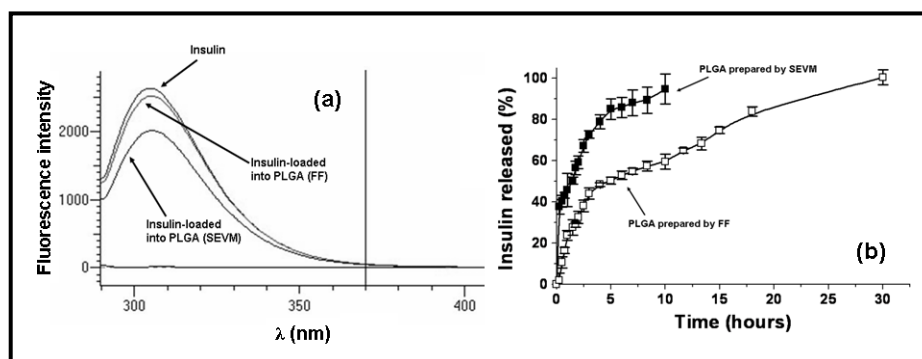


**Figure 2.** (a) Fluorescence spectra of insulin, and insulin-loaded particles obtained by SEV, and FF. (b) Release of insulin from PLGA prepared by SEV (■) or FF (□), as a function of the incubation time in PBS.



### YF<sub>3</sub>:Tm,Yb nanocrystals: enhanced up-conversion blue and UV emitters

*M. Quintanilla<sup>1</sup>, N.O. Núñez<sup>2</sup>, E. Cantelar<sup>1</sup>, M. Ocaña<sup>2</sup> and F. Cussó<sup>1</sup>*

<sup>1</sup> *Depto. Física de Materiales, C-IV, Universidad Autónoma de Madrid, Spain*

<sup>2</sup> *Instituto de Ciencia de Materiales, CSIC, Isla de la Cartuja, Sevilla, Spain*

[fernando.cusso@uam.es](mailto:fernando.cusso@uam.es)

Fluorides doped with rare earth (RE) ions have been used in a wide range of photonic applications along the last decades. At present, the importance of nanoscale optically functional materials to be used as medical and biological tags has increased the potentiality of fluorides. To exploit those possibilities new methods to obtain several nanostructures based on fluorides are being developed, and several doping possibilities are being tried to obtain visible emissions using biologically innocuous excitation [1,2]. Recently, a novel synthesis method, providing a straightforward and versatile procedure for the synthesis of uniform lanthanide fluoride nanophosphors has been proposed [3].

At present, there is a renewed interest in YF<sub>3</sub> nanophosphors directed to obtain high energy luminescent emissions. Along this line, doping with Tm<sup>3+</sup> & Yb<sup>3+</sup> has been reported to produce enhanced blue and ultraviolet emissions [4-5]. In the present work, synthesis and optical characterization of the Tm<sup>3+</sup>/Yb<sup>3+</sup> co-doped YF<sub>3</sub> nanophosphors is reported. The dominant Tm<sup>3+</sup> up-converted emission bands have been investigated by exciting the Yb<sup>3+</sup> ions at around 980 nm.

The RE-doped fluoride nanoparticles were prepared by a homogeneous precipitation reaction in ethylene glycol solutions containing the rare earth precursors and [BMIM]BF<sub>4</sub> as a source of fluoride ions [3]. In order to investigate the effects of the doping level on the optical properties of the nanophosphors, the Yb<sup>3+</sup> content was varied in the range 10-20% molar while the Tm<sup>3+</sup> concentration was kept constant (2% molar).

The morphology of the nanoparticles was examined by transmission electron microscopy using a TEM Philips 200CM system. Qualitative composition of the particles was assessed by energy dispersive X-ray analysis using an EDX system (Philips DX4) coupled to an electron microscope. The crystalline structure of the particles was assessed by X-ray diffraction. The optical characterization has been performed using a Ti:Za laser pumped with an Ar-laser to excite Yb<sup>3+</sup> ions. The visible Tm<sup>3+</sup> luminescence was dispersed by using an ARC Spectrapro 500-I monochromator and then detected with a photomultiplier tube.

In Figure 1 a TEM image of the Tm<sup>3+</sup>/Yb<sup>3+</sup>-doped nanophosphors can be seen, illustrating the morphology and uniformity of the obtained nanocrystals.

Figure 2 shows the visible emissions in the wavelength range 300 nm < λ < 810 nm, arising from Tm<sup>3+</sup> ions after Yb<sup>3+</sup> excitation at λ = 980 nm. These results demonstrate that effective co-doping has been achieved, providing the adequate conditions for effective energy transfer between Yb<sup>3+</sup> and Tm<sup>3+</sup> ions, with effective blue and UV up-conversion.

#### References:

- [1] L. Wang and Y. Li, Chem. Mater. **19** (2007), 727.
- [2] G.S. Yi, G.M. Chow, Adv. Funct. Mater. **16** (2006), 2324.
- [3] N.O. Núñez, M. Quintanilla, E. Cantelar, F. Cussó, M. Ocaña, J. Nanopar. Res. DOI 10.1007/s11051-009-9824-6

- [4] Guanshi Qin, Weiping Qin, Changfeng Wu, Shihua Huang, Dan Zhao, Jisen Zhang, Shaozhe Lu, *Optics Communications* **242** (2004) 215–219
- [5] Chunyan Cao, Weiping Qin, Jisen Zhang, Yan Wang, Peifen Zhu, Guofeng Wang, Guodong Wei, Lili Wang, Longzhen Jin, *J. Fluorine Chemistry* **129** (2008) 204–209

**Figures:**

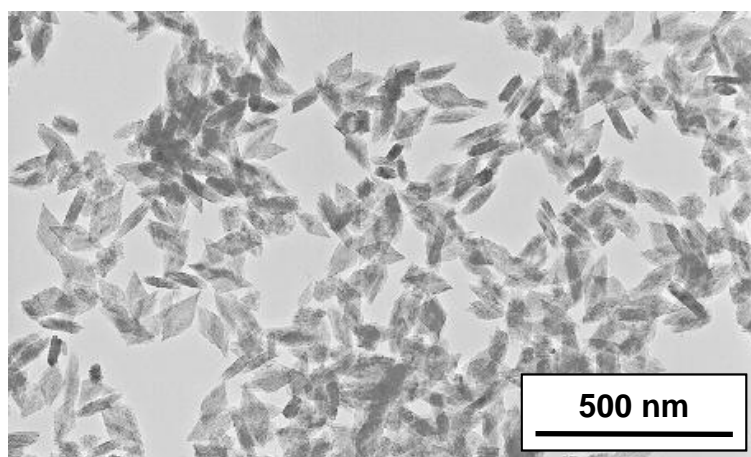


**Figure 1.** TEM image of the  $\text{Tm}^{3+}/\text{Yb}^{3+}$ -doped nanophosphors.

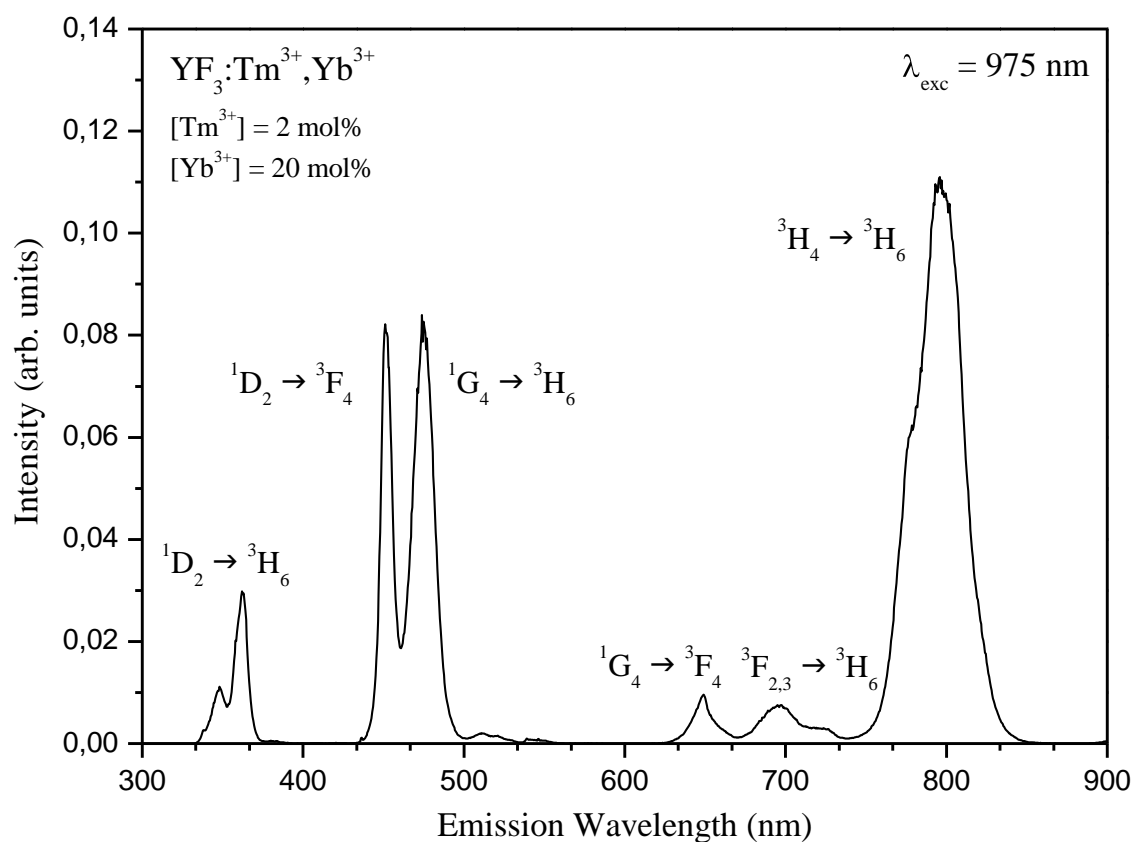


**Figure 2.** Emission spectra of  $[\text{Tm}^{3+}] = 2 \text{ mol\%}$  and  $[\text{Yb}^{3+}] = 20 \text{ mol\%}$  co-doped samples by pumping at 975 nm.

**Effect of nano-irregularities in the work function and field emission properties of metallic surfaces.**

T. Albuquerque<sup>1,3</sup>, F. Borondo<sup>2</sup>, C.M.C de Castilho<sup>4</sup>, R. F. S. Andrade<sup>4</sup>, R. M. Benito<sup>3</sup>

<sup>1</sup> *Departamento de Química Universidad Autónoma de Madrid, Cantoblanco, 28049 Madrid, Spain.*

<sup>2</sup> *Departamento de Química and Instituto Mixto de Ciencias Matemáticas CSIC-UAM-UC3M--UCM, Universidad Autónoma de Madrid, Cantoblanco, 28049 Madrid, Spain.*

<sup>3</sup> *Grupo de Sistemas Complejos, Departamento de Física y Mecánica, ETSI Agrónomos, Universidad Politécnica de Madrid, Ciudad Universitaria, 28040 Madrid, Spain.*

<sup>4</sup> *Instituto de Física, Universidade Federal da Bahia, Campus Universitário da Federação, 40210--340, Salvador, BA, Brazil.*

[t.albuquerque@uam.es](mailto:t.albuquerque@uam.es)

An important property that significantly affects the emitting properties of a metal film is the work function (WF). This concept is related to the total energy variation of the metal sample when an electron in the Fermi level is completely removed. Accordingly, the WF can be determined as the electronic energy difference between the associated initial and final state, this one being the condition after complete removal of the electron previously at the Fermi level. The WF is strongly affected by the conditions of the metal surface [1]. These conditions include the presence of contaminants (in quantities lower than one monolayer), the occurrence of oxidation and other chemical reactions, unequal distribution of adsorbates, crystallographic orientation, etc

As a matter of fact, the micro-geometry of the surfaces of practical electron emitters is far from being smooth. Even in the best cases, when the use of crystalline materials results in a smoother surface, it is important to keep in mind that the surface results from a combination of several facets, leading to an irregular surface in a micrometric scale. In a previous paper [2], in a tentative of reproducing geometrical defects associated to real metallic surfaces by computational simulation, it was studied how the surface roughness and fractal dimension affect their emitting properties. The results lead to the conclusion that, while the roughness exhibits a significant influence in the electronic current density, the fractal dimension would be related to the electric field amplification factor – an information which is embedded in the Fowler-Nordheim (FN) plots.

The aim of this work is to analyze how the nano-irregular geometry of the surface of a metallic profile affects the corresponding WF and, as result of this, the effect on the emitting properties. In doing this, it was considered a simplified model of rectangular fractures, using a classical formalism for the WF determination. Within this formalism, the WF of a solid is defined as the minimum energy required for removing an electron at the surface of the solid, with an initial energy equal to the one of the Fermi level, till a point situated far away from the solid. By using the classical method of images, it was possible to determine how the WF is related to the fracture size. It were also analyzed the properties of the emission current density when the solid is under the influence of an applied external electric field. In order to compute the electronic current density, it was used the model recently proposed by Forbes [3,4] where it was considered a reasonable approximation for the elliptical functions which characterize the potential barrier to which the electron is subjected.

**References:**

- [1] N. A. Burnhama, R. J. Colton, H. M. Pollock, Phys.: Rev. Lett., **69**, 144 (1992) .
- [2] T. A. de Assis, F. Borondo, R. M. Benito, R. F. S. Andrade, Phys.: Rev. B, **78**, 235427 (2008).
- [3] R. G. Forbes, Appl. Phys. Lett., **89**, 113122 (2006).
- [4] R. G. Forbes, J. H. B. Deane, Proc. R. Soc. Lond. A, **463**, 2907 (2007).

## Fabrication of optical gratings coated with Si<sub>3</sub>N<sub>4</sub> for efficient immunosensing monitored by Optical Waveguide Spectroscopy

*L. Diéguez*<sup>a,b</sup>, *D. Caballero*<sup>b\*</sup>, *J. Calderer*<sup>c</sup>, *M. Moreno*<sup>a</sup>, *E. Martínez*<sup>b,d</sup>, *J. Samitier*<sup>a,b,d</sup>

*a) Department of Electronics, University of Barcelona, Barcelona (E)*

*b) Nanobioengineering group, Institute for Bioengineering of Catalonia (IBEC), Baldori Reixac 10-12, Barcelona (E)*

*c) Electronic Engineering Department, Universitat Politècnica de Catalunya, Campus Nord, Barcelona (E)*

*d) Networking Research Center on Bioengineering, Biomaterials and Nanomedicine (CIBER-BBN), Barcelona (E)*

*\* Present address: Institut de Science et d'Ingénierie Supramoléculaires (ISIS), CNRS UMR 7006 et Université de Strasbourg, 8 allée Gaspard Monge - BP 70028, 67083 Strasbourg Cedex (F)*

[ldieguez@el.ub.es](mailto:ldieguez@el.ub.es)

Biosensors are nowadays a powerful tool to enable the detection of biological interactions. The novel Electrochemical Optical Waveguide Spectroscopy technique (see figure 1) incorporates an electrochemical cell to a grating coupler optical biosensor [1]. In this way, this system allows obtaining electrochemical measurements such as cyclic voltammetry or impedance spectroscopy while monitoring the immobilization kinetics through optical measurements with similar accuracy than Surface Plasmon Resonance based techniques. Moreover, by numerical methods, it is possible to simulate both the refractive index change and the thickness of the adsorbed film and its mass, exhibiting a very high sensitivity of 1 ng/cm<sup>2</sup>. The system keeps this sensitivity measuring changes at the sensor surface closer than 200 nm [2].

In the field of optical label-free biosensing, the most used transducer is a sensor chip with gold surface which presents an easy functionalization and provides information about the success of the biomolecular adsorption on the surface. Depending on the application, the possibility of choosing a surface would remain a challenge. In the case of the grating couplers, the substrate must be a transparent material to allow the light coupling in the waveguide. There are only a few materials commercially available covering the sensor chip: insulators such as SiO<sub>2</sub>, TiO<sub>2</sub>, Ta<sub>2</sub>O<sub>5</sub>, or transparent conductive materials like the Indium Tin Oxide (ITO), which allow electrical measurements to be coupled with the optical sensing.

Silicon nitride is one of the most important materials for electronic-based biosensors [3]. Several widely available methods for the immobilization of biological elements on this substrate rely on silanization procedures. But for immunosensing applications, a fast-to-functionalize and efficient procedure for the immobilization of antibodies onto the surface by covalent binding is required. In figure 2, a new approach for the direct immobilization of CHO groups onto silicon nitride substrates has been described previously [4]

To test the functionality of such an approach, commercial optical grating chips were covered with a Si<sub>3</sub>N<sub>4</sub> layer by Low Pressure Chemical Vapor Deposition. Silicon nitride offers a number of advantages compared to other coating materials, such as the absence of undesirable impurities and the good control of the film composition and thickness. This is especially important for ultrathin layers used in optical spectroscopy measurements. The silicon nitride surfaces were chemically oxidized and subsequently silanized with an aldehyde organosilane self-assembled monolayer by using the vapour phase method leading to the direct and covalent binding of anti-human serum albumin (anti-HSA) antibodies and used for the specific detection of different concentrations of HSA proteins with a sensitivity of 1 ng/cm<sup>2</sup> and detection limit of 10<sup>-8</sup>M (Figure 3).

## References:

- [1] L. Diéguez et al., *Soft Matter*, **5** (2009) 2415-2421.  
 [2] J. Vörös et al., *Biomaterials* **23** (2002) 3699-3710.  
 [3] A. Tliti et al., **25** (2005) 490-495.  
 [4] D. Caballero et al., *Small* **5** (2009) 1531-1534.

## Figures:

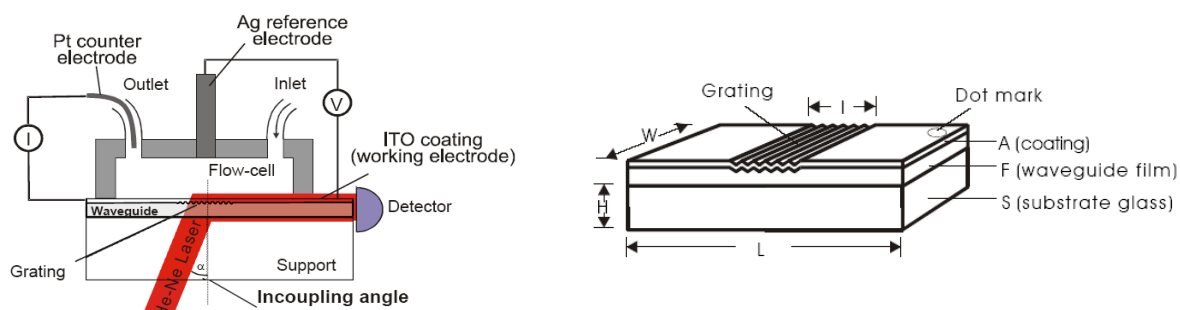


Figure 1: (left) Electrochemical Optical Waveguide Spectroscopy set-up.  
 (right) Optical grating coated chip.

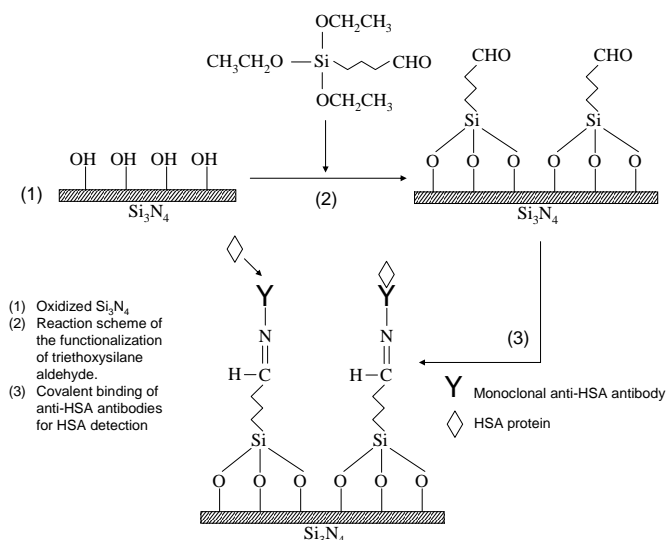


Figure 2: Direct immobilization of CHO groups onto silicon nitride or the binding of anti-HSA antibodies.

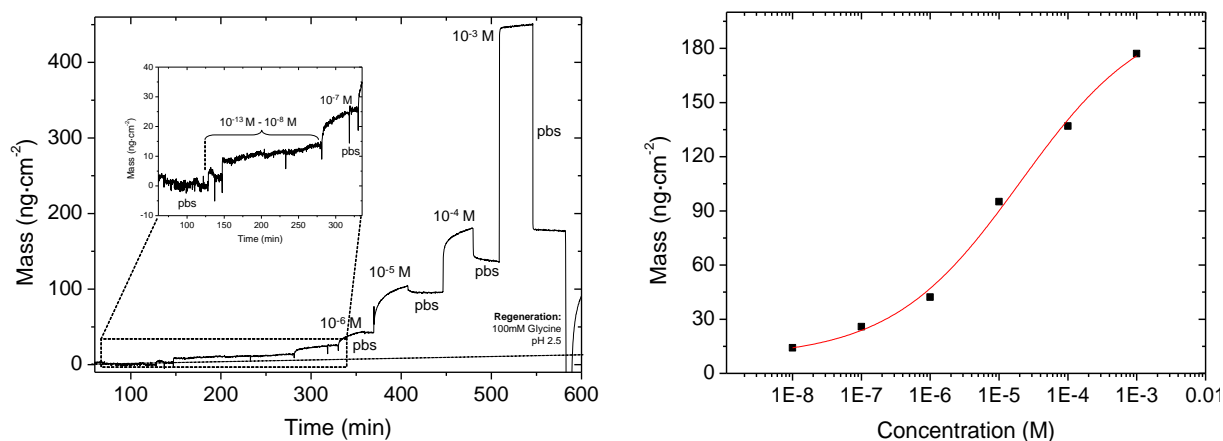


Figure 3: (left) HSA immunosensing reaction monitored by Optical Waveguide Spectroscopy.  
 (right) Relationship between the adsorbed mass and the concentration.

## Micromagnetic simulations of metastable states in circular magnetic dots

*D. Dieleman, F.G. Aliev*

*Dpto. Física de la Materia Condensada, CIII, Universidad Autónoma de Madrid, 28049 Madrid, Spain*

*(\*) presenting author: [Dennis.Dieleman@student.ru.nl](mailto:Dennis.Dieleman@student.ru.nl)*

Magnetic confinement in nanomagnets leads to a variety of topological anomalies which can be decomposed into two topologically different basic types: domain walls and vortices. The simplest ground states of the circular magnetic dot are the state with uniform magnetization (present in thin dots or in any dots in a high magnetic field) and magnetic vortex state with single vortex with about 10 nm vortex core situated in the dot center. Transition from the uniform to the vortex type ground states, when controlled by the magnetic field, involves two well defined intermediate metastable states: namely the so called S-type and double vortex states [1,2]. Here, by using micromagnetic simulations, we present the first detailed study of transition between different metastable states of circular magnetic dots. The simulations were performed using an extension [3] on the original OOMMF code [4] that augments to the LLG equation a highly irregular fluctuating field, so the resulting equation is a stochastic differential equation of the Langevin type [5]. The micromagnetic simulations were carried out for a circular Py dot having a thickness of 25 nm and a diameter of 1035nm.

We first saturated the dot at 1000 Oe, subsequently we released this field in one step and tracked the energy and total magnetization of the system every ns and took a snapshot of the local magnetization every 10ns, see figure 1. To break the deterministic characteristic of OOMMF, we used a different set of random fluctuation for each run that we made as can be seen in figure 2. By using this method we could identify different energy steps in the relaxation from saturation to zero field as can be seen in figure 1. These steps correlate with different metastable (MS) states. The 4 typical topologies that arise are first the saturated state, then the MS\_1 S-State, the MS\_2 double-vortex (DV) state and finally the one- vortex ground state. Typically a dot needed about 20~40ns to reach the one-vortex state. Although in some runs this state was never reached and the system remained in a MS state for at least the duration of our simulations ( ~ 200ns). For both the MS\_1 S-state and the MS\_2 DV-state, there were runs where this state remained stable in this period. For the MS S-state these stable so called 'hard' states are characterized by a more symmetric magnetization than their 'soft' unstable counterparts, see figure 1 on the right.

Also we saw instances where the double vortex state remained the stable state at zero field. This is in accordance with [1], where the authors reported the formation of double vortices during the reversal of the magnetization for dots of large diameter (1µm). They found experimentally that the double vortex state appears in about 20% of the cases during in-plane reversal of magnetism for Co dots. We propose that that the DV-state always appeared but that just in 20% of the cases it was stable long enough to be measured. In our simulations we saw a range of distribution of core polarities P and positions of the two cores, as can be expected from symmetry arguments. The central part of a DV-vortex is however always diagonally oriented, with the M<sub>x</sub> component anti-parallel to the history field.

Our findings open perspectives of investigation of both static and dynamic properties of different metastable states in nanomagnets.

This work was supported by Spanish MICINN (MAT2009-10139), Consolider (CSD2007-00010) and CAM (P2009/MAT-1726).

## References:

- [1] Prejbeanu, I. L.; Natali, M.; Buda, L. D.; Ebels, U.; Lebib, A.; Chen, Y.; Ounadjela, K., *Journal of Applied Physics*, **91** (2002) 7343.
- [2] M. Rahm, M. Schneider, J. Biberger, R. Pulwey, J. Zweck, D. Weiss, V. Umansky, *Applied Physics Letters*, **82** (2003) 4110.
- [3] O. Lemcke, University of Hamburg, [http://www.nanoscience.de/group\\_r/stm-spstm/projects/temperature/download.shtml](http://www.nanoscience.de/group_r/stm-spstm/projects/temperature/download.shtml)
- [4] M.J. Donahue and D.G. Porter, *OOMMF User's Guide, Version 1.0*, Interagency Report NISTIR 6376 (NIST, Gaithersburg, MD, 1999).
- [5] J.L. Garcia-Palacios and F.J. Lazaro, *Phys. Rev. B*, **58** (1998) 14937.

## Figures:

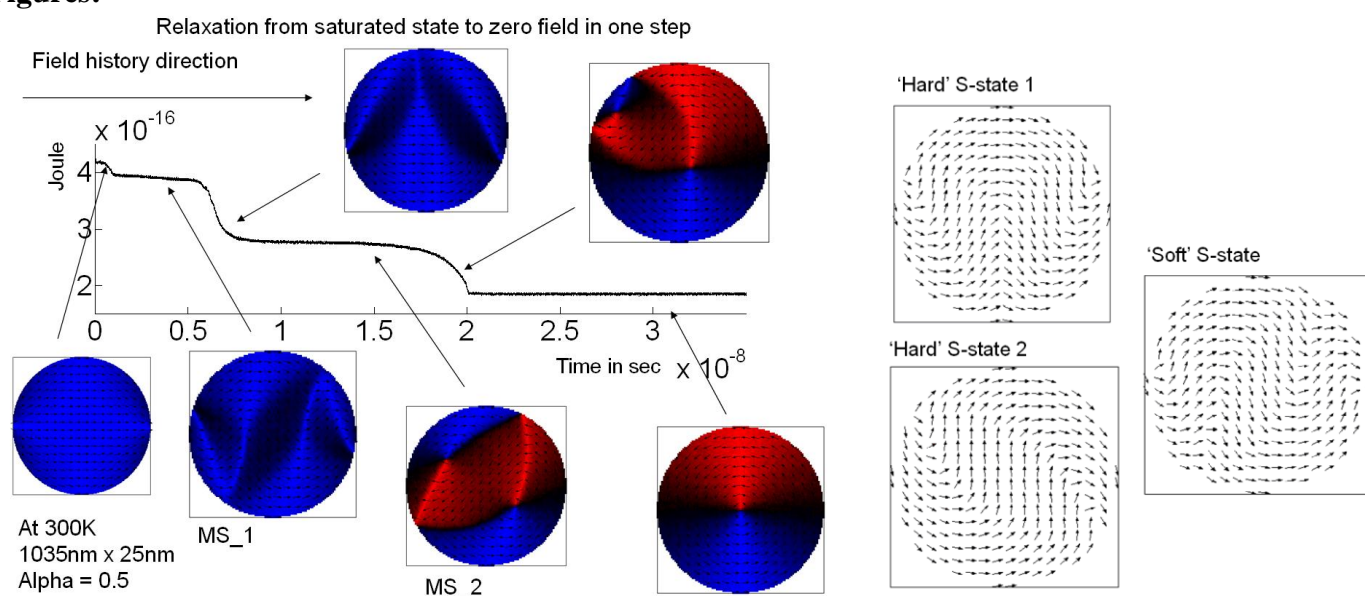


**Fig 1:** Left: Total energy as a function of time after the 1000Oe saturation field is turned up abruptly. Three different levels can clearly be distinguished. The insets show the snapshots of the magnetization at the indicated time, with a colour coding for  $M_x$ . MS\_1 and MS\_2 signify the MS S-state and the MS DV-state respectively. Right: Several MS S-states. The stable hard states and a unstable soft state. (dot: 1035x25nm)

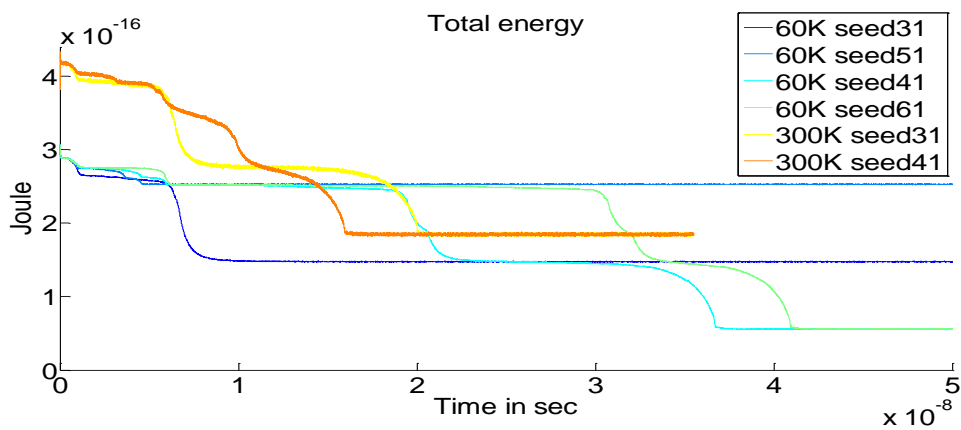


**Fig 2: Total energy as function of time for several different runs with different random fluctuations (seeds) at 60K and 300K. For 60K two runs don't lead to the one-vortex ground state but remain in either an hard S-state or MS DV-state.**

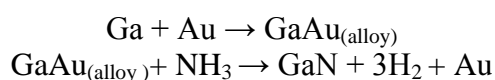
## Application of gold nanocolloidal system to obtain gallium nitride nanowires by Sublimation Sandwich Method

*Paweł Dominik<sup>1</sup>, Dariusz Smolen<sup>1</sup>, Sławomir Podsiadło<sup>1</sup>,  
Kamil Sobczak<sup>2</sup> Piotr Dłużewski<sup>2</sup>, Wojciech Paszkowicz<sup>2</sup>*

<sup>1</sup>Warsaw University of Technology Faculty of Chemistry, Noakowskiego 3, 00-664 Warsaw, Poland

<sup>2</sup>Institute of Physics Polish Academy of Science, Al. Lotników 32/46, 02-668 Warsaw, Poland  
[pdominik@ch.pw.edu.pl](mailto:pdominik@ch.pw.edu.pl)

Among bottom up techniques the vapour-liquid-solid mechanism is the most universal to obtain gallium nitride nanowires. There are many transition metals which are potential candidates to be a catalysts in the process e.g.: nickel[1], iron[2], cobalt[3] and gold[4]. Based on literature, the most popular method to obtain a catalyst nanodroplets on the surface of the single crystalline substrate is physical vapour deposition or magnetron deposition of thin films of transition metals (the average thickness is 1-10 nm). Herein we present results from experiments concerning obtaining gallium nitride nanowires by using gold nanocolloidal system. The Sublimation Sandwich Method which was previously applied at Warsaw University of Technology to obtain gallium nitride layers [5,6] was used as a growth technique. As starting materials mixture of gallium and gallium nitride powder, and gaseous ammonia as source of nitrogen were used. The process reactions are as follows:



The obtained gallium nitride nanowires were examined with scanning electron microscopy (SEM), transition electron microscopy (TEM) and powder X-ray diffraction (PXRD).

This work was funded by the State Committee for Scientific Research (Grant No. N N209 117737) and has been supported by the European Union in the framework of European Social Fund through the Warsaw University of Technology Development Programme.

### References:

- [1] G.Seryogin, I. Shalish, W. Moderlychan, V. Narayanamurti, *Nanotechnol.*, **16** (2005) 2342
- [2] J. Zhang, L. Zhang, *J. Vac. Sci. Technol. B*, **21** (2003) 2415
- [3] L. Qin, C.Xue, Y. Duan, L. Shi, *Nanoscale Res. Lett.* **4** (2009) 584
- [4] Z. Yu, Z. Yang, S. Wang, Y. Jin, J. G. Liu, X. Sun, *Chem. Vap. Deposition* **11** (2005) 433
- [5] M. Kaminski, S. Podsiadło, K. Wozniak, L. Dobrzycki, R. Jakiela, A. Barcz, M. Psoda, J. Mizera, *J. Cryst. Growth*, **303** (2007) 395
- [6] M. Kaminski, P. Dominik, S. Podsiadło, K. Wozniak, L. Dobrzycki, R. Jakiela, A. Barcz, M. Psoda, J. Mizera, *Chem. Mater.* **19** (2007) 3139

## INFLUENCE OF BORON ON THE NANOCRYSTALLINE SILICON FILMS GROWN BY PLASMA ENHANCED CVD

**A. Dussan**

Group Nanostructured Materials and their Applications  
Dpto. Física – Universidad Nacional de Colombia – Bogotá

### Abstract

In this work, a series of boron doped nanocrystalline silicon films (nc-Si) were deposited by plasma-enhanced chemical vapor deposition (PECVD), using silane ( $\text{SiH}_4$ ) diluted in hydrogen, and diborane ( $\text{B}_2\text{H}_6$ ) as a dopant gas. The concentration of  $\text{B}_2\text{H}_6$  was varied in the range of 0 – 100 ppm. The nucleation and the growth process of nc-Si were investigated by using AFM, SEM, TEM and XRD measurements. It is observed, that an increase of Boron in the material produces a raise in the size of the crystals, but no significant change in surface roughness. Existence of a substructure dominated by regions of much smaller crystals growing in between grains that stand out on the surface was observed. The doped nanocrystalline silicon films presented a crystallographic preferential orientation in the plane (220). Correlations between structural and morphological properties were also studied.

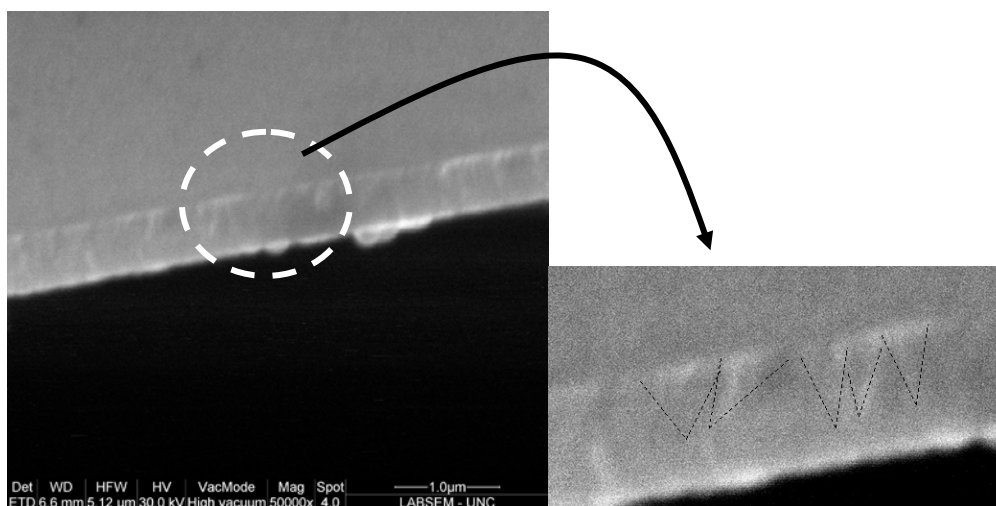


Figure 1. Cross-sectional Scanning Electron Micrographs nc-Si:H thin film. The concentration in this sample was 0ppm.

## Magnetic immunosensors for the determination of cortisol

*Marcos Eguílaz, María Moreno-Guzmán, Araceli González-Cortés, Paloma Yáñez-Sedeño, José M. Pingarrón*

*Department of Analytical Chemistry, Faculty of Chemistry, University Complutense of Madrid, 28040-Madrid. Spain*

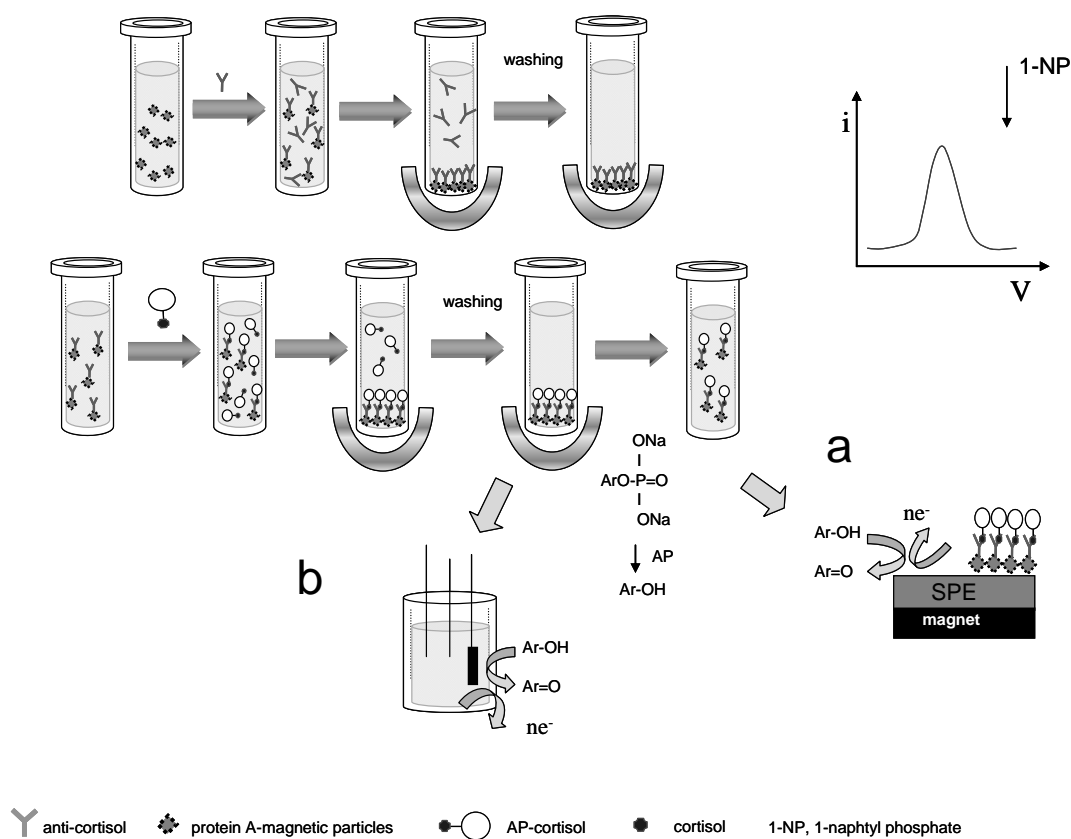
[yseo@quim.ucm.es](mailto:yseo@quim.ucm.es)

Belonging to the glucocorticoid hormones family, cortisol is an important bio-marker of stress and its detection is important in sports medicine [1]. It is well known that athletes use corticoids to improve their performance. Since 1975, the International Olympic Committee Medical Commission restricted the use of these compounds to legitimate medical purposes. However, the existing methods for detecting cortisol are limited with respect to their sensitivity, time of analysis and cost. In this context, the use of electrochemical immunosensors, because of their excellent analytical capabilities as sensitivity, reproducibility, simplicity of construction and use, and feasible miniaturization, could offer alternative advantages for doping control. Furthermore, these important advantages become more evident insofar as the immobilization of immunoreagents and the transduction event are more efficient. Thus, the preparation of bioelectrodes combining immobilization methods capable of improving stability with no significant loss of the biological activity of biomolecules, with electrochemical transducers that enhance electron transfer, constitutes a challenge in modern bioanalytical chemistry. Related to this goal, electrochemical biosensors involving the use of nanoparticles have demonstrated to possess interesting features [2].

In this work, we present two configurations of electrochemical immunosensors for cortisol based on magnetic particles and / or gold nanoparticles. In the first design (Figure 1a) a disposable voltammetric immunosensor was developed using screen printed electrodes prepared with different materials (carbon SPE, gold nanoparticles-modified carbon SPE, and gold SPE). Competitive immunoassay involving cortisol antigen labeled with alkaline phosphatase (AP) was employed. Anti-cortisol antibody was immobilized onto protein A-magnetic particles, and the resulting conjugate was trapped with a small magnet on the surface of the screen-printed electrode. Cortisol determination was made by 1-naphtylphosphate additions, and detection of 1-naphtol using differential pulse voltammetry in the -0.15 to +0.25 V vs Ag/AgCl.

A second design, based on the preparation of an electrode surface consisted of a composite of gold nanoparticles and carbon nanotubes, using 1-n-octylpyridinium hexafluorophosphate (OPPF<sub>6</sub>) or Teflon as the binding material, was also developed. The same immunoassay configuration than that described above was used. However, as shows Figure 1b, the product of the alkaline phosphatase enzyme reaction, 1-naphtol, was measured in the supernatant solution by differential pulse voltammetry at the composite electrode.

All the experimental variables involved in the assays, i.e. the amount of anticortisol immobilized or the time of incubation, and those affecting the electrochemical response (pH, cortisol-AP/cortisol ratio and composition of the electrode surface) were optimized. Calibration plots obtained for cortisol have linear ranges between 0.1 and 100 ng/mL, which cover the concentration levels required for the analysis of biological samples. Other analytical characteristics such as the limits of detection, reproducibility, and stability tests, have been evaluated.



## References:

- [1] A. Kumar, S. Aravamudhan, M. Gordic, S. Bhansali, S.S. Mohapatra, *Biosens. Bioelectron.*, **22** (2007) 2138.  
 [2] V. Carralero, A. González-Cortés, P. Yáñez-Sedeño, José M. Pingarrón, *Anal. Chim. Acta* 596 (2007) 86

## Figures:

Scheme of the immunoassay procedure for the determination of cortisol based on the voltammetric detection of 1-naphtol: a) after immobilization of immunoconjugate onto SPE; b) by measuring in the supernatant solution at the composite electrode.

## Gold nanoparticles capped with mannose glycans block HIV-1 gp120 binding to antibody 2G12 as studied by means of NMR and SPR techniques.

P.M. Enriquez-Navas<sup>1</sup>, P. Di Gianvincenzo<sup>1</sup>, M. Marradi<sup>1</sup>, O. Martínez-Avila<sup>1</sup>, J. Angulo<sup>2</sup>, S. Penadés<sup>1</sup>

<sup>1</sup>CIC-biomaGUNE/CIBER-BBN, Paseo Miramón 182, Parque Tecnológico, E-20009 San Sebastián, Spain.

<sup>2</sup>Instituto de Investigaciones Químicas (IIQ-CSIC) C/Américo Vespucio 49, E-41092 Sevilla, Spain.  
[spenades@cicbiomagune.es](mailto:spenades@cicbiomagune.es)

The human immunodeficiency virus (HIV) uses its envelope glycoprotein gp120 in the initial steps of infection. The immune system raises antibodies against it as a defensive mechanism. Human antibody 2G12 neutralizes a broad range of human immunodeficiency virus type 1 (HIV-1) isolates by binding an unusually dense cluster of carbohydrate moieties (*high-mannose* glycans) on the “silent” face of the virus envelope glycoprotein gp120.[1] Crystallographic studies revealed that 2G12 is highly specific for terminal Man $\alpha$ 1 $\rightarrow$ 2Man of the glycans present in the gp120 [1,2]. 2G12 is one of the few monoclonal antibodies (mAb) able to neutralize a broad range of HIV-1 primary isolates. Understanding the atomic contacts that the antibody 2G12 makes to neutralize the virus is essential for the correct design of vaccines against HIV.

To understand better the molecular mechanism of HIV interactions, we have prepared gold glyconanoparticles that present oligomannosides (*manno*-GNPs) in a multivalent way in order to mimic the *high-mannose* clusters on gp120. [3] Previously, we have characterized the interactions between 2G12 and synthetic oligomannosides, which are structural motifs of the natural *high-mannose* of gp120. Using a new STD NMR protocol and theoretical calculations we have determined the minimum structural requirement for maximum affinity to 2G12 to be a trimannoside (Man $\alpha$ 1 $\rightarrow$ 2Man $\alpha$ 1 $\rightarrow$ 2Man). Based on these results, multivalent oligomannoside functionalized gold nanoclusters (glyconanoparticles) have been synthesized pursuing to improve the affinity of these monovalent ligands as multivalent ligands.

In the present work, we study by NMR the affinities of these glyconanoparticles towards 2G12 in solution. Their interactions with the antibody are compared to that of the monovalent ligands by competition STD NMR experiments. The binding of the GNPs to the 2G12 and the potency of *manno*-GNPs to inhibit the binding of gp120 to 2G12 were also studied by using Surface Plasmon Resonance (SPR) technology. NMR and SPR techniques identify the best multivalent *manno*-GNP inhibitor. The enhancement of the affinity observed for the *manno*-GNPs related to the monomeric oligomannosides due to the so-called *cluster effect* will be discussed.

### References:

- [1] Calarese, D. A., *et al.*, Science, **2003**, 300, 2065-2071.
- [2] Calarese, D. A. *et al*, Proc. Natl. Acad. Sci. USA, **2005**, 102, 13372-13372.
- [3] Martínez-Ávila O., *et al*, Chem-Eur J **2009**, 15, 9874-9888

## Challenges on the Characterization of Superparamagnetic Particles as Contrast Agents in MRI

<sup>1, 2, 4</sup> N. Félix González, <sup>1, 2, 4</sup> J. Serrano Olmedo, <sup>1, 3, 4</sup> C. Maestú Unturbe, <sup>1, 3, 4</sup> F. del Pozo Guerrero

<sup>1</sup>Bioengineering and Telemedicine Group. Biomedical Technology Center.

<sup>2</sup>Electronic Technology Department. <sup>3</sup>Photonic Technology Department.

Polytechnic University of Madrid. Av. Complutense 30. "Ciudad Universitaria", 28040.

<sup>4</sup>Bioengineering, Biomaterials and Nanomedicine Network for Biomedical Research. Madrid, Spain.

[nfelix@gbt.tfo.upm.es](mailto:nfelix@gbt.tfo.upm.es), [jserran@etsit.upm.es](mailto:jserran@etsit.upm.es)

Contrast Agents (CA) in MRI enhances the differences between tissues with similar properties by locally modifying the nuclear relaxation rates of water protons. The efficiency of a CA is determined by its longitudinal and transversal relaxivities, defined as the relaxation rate per mol of colloid ( $r_1$ ,  $r_2$  respectively). This data can be expressed as a function of the magnetic field strength in the NMRD profiles (figures 1-3). One of the most important steps in the characterization of a new CA is the study of the NMRD profiles from which it is possible to determine the best application for the CA in a specific field strength, either to enhance images weighed on T1 or on T2, depending on the ratio  $r_1/r_2$ . CA based on superparamagnetic particles significantly reduces the transverse relaxation rate due to the local field created by its large magnetic moment. Those structures consist of an iron oxide core coated with macromolecular materials.

Some theories have been formulated to describe physical phenomena associated with the proton relaxation by superparamagnetic particles. These theories are important not only for the understanding of these phenomena but also to relate the information contained in the NMRD profiles to the morphological and physical properties of the particles like: average radius, specific magnetization or Néel relaxation time. All these parameters are important for the design and fabrication of the CA, along with their ability to predict the behavior and the final target of certain types of particles prior to their manufacture. In this work we present the challenges on the characterization of superparamagnetic particles as CA in MRI.

One of the challenges is the lack of consistence between experimental data and the theoretical model. In our last work we found some discrepancies when evaluated some experimental data against a theoretical model (figures 1-3). Some of these inconsistencies were explained by a low field dispersion caused by the anisotropy of the crystal, or by the aggregation of the particles in solution. It has been shown that the more sensitive parameter in the theoretical model is the particle's radius, so the aggregation can cause that a group of agglomerated particles can be seen as only one particle of bigger size. It is also observed that the experimental measurement of this parameter is very sparse (table 1); this may be due to the aggregation of the particles or lack of consistence in measurement, which also leads to another challenge in the characterization.

Our first measurements of relaxivities in new contrast agents have shown that the lack of an experimental protocol results in a lack of repeatability and consistency in the data, because the parameters involved in making the measurements are too many and depend largely on the equipment used, so that measurements can be not objective enough and depending on the laboratory that performed them. To ensure the reliability of the measurements a protocol is needed. It must specify in detail the equipment, the pulse sequence and the parameters of the sequence used.

Finally, it is necessary to develop or to modify an existing theoretical model in order to understand the relaxation mechanism in biological environments. The last challenge in the research of nanoparticles as CA is the determination of concentrations directly from the MRI data. This is important because for therapy and for diagnosis it is necessary to know if you have the needed amount of drug or of marker for a particular disease or condition.

### References:

[1] Carroll MRJ, Woodward RC, House MJ, Teoh WY, Amal R, Hanley TL, et al. Experimental validation of proton transverse relaxivity models for superparamagnetic nanoparticle MRI contrast agents. *Nanotechnology* 2010; 21:035103

[2] N. Felix Gonzalez, J. Serrano Olmedo, F. del Pozo Guerrero, Noticed Discrepancies when Evaluating Experimental Data against Theoretical Model on the Characterization of Superparamagnetic Particles as Contrast Agents in MRI, In the 6<sup>th</sup> Conference Field Cycling Relaxometry 2009 proceedings. *Stelar* 2009: 64.

[3] Laurent S, Forge D, Port M, Roch A, Robic C, Vander Elst L, et al. Magnetic iron oxide nanoparticles: synthesis, stabilization, vectorization, physicochemical characterizations, and biological applications. *Chem.Rev.* 2008; 108(6):2064-2110.

[4] Muller RN, Roch A, Gillis P, et al. Relaxation by Metal-Containing Nanosystems. *Advances in Inorganic Chemistry: Academic Press*; 2005. p. 239-292.

### Figures:

Dextran Coated SPIO AMI-25 ENDOREM®	
Reference	Particle Diameter (nm)
[3]	58
[4]	120-180 $\langle d \rangle_p^*$
[6]	23(22%) 130(78%)
[7]	4.8-5.6 (core), 80-150 $\langle d \rangle_p^*$
[8]	72 $\langle d \rangle_p^*$
Theoretical Model [9]	12.8

**Table 1.** Experimental values of the measurement of particle diameter of the compound ENDOREM. At the bottom, the value used for the NMRD profiles of the theoretical mode is shown. \*  $\langle d \rangle_p$ : Hydrodynamic diameter derived from the technique of dynamic light scattering, which calculates the average of the particles in solution by monitoring the characteristics of diffusion.

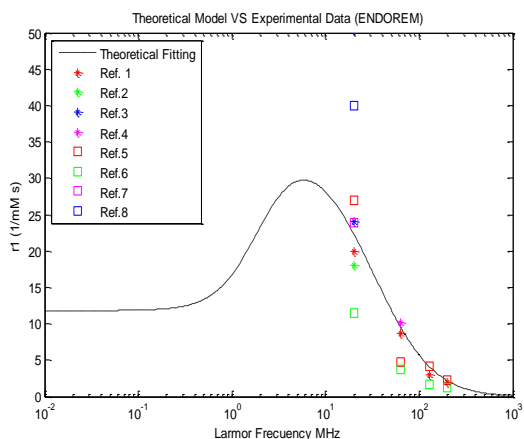


**Figure 1.** T1 NMRD profiles for ENDOREM. The graphic shows the experimental data and the fit with the theoretical model for a diameter of 12.8 nm.

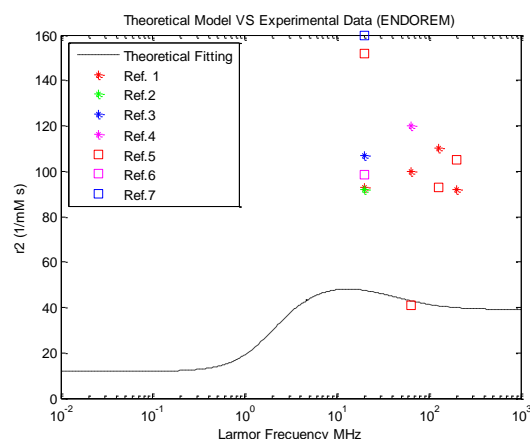


**Figure 2.** T2 NMRD profiles for ENDOREM. The graphic shows the experimental data and the fit with the theoretical model for a diameter of 12.8 nm.

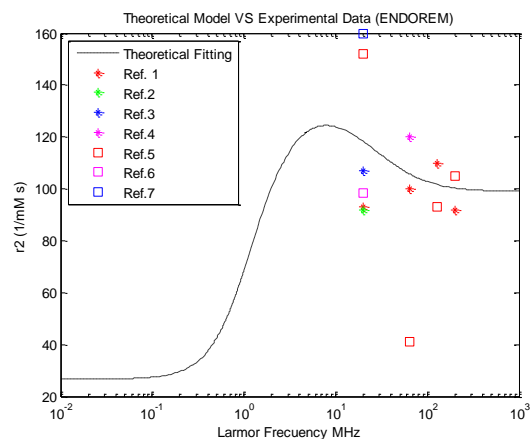


**Figure 3.** T2 NMRD profiles for ENDOREM. The graphic shows the experimental data and the fit with the theoretical model when the diameter is modified from 12.8 nm to 16 nm.

**Striking “Nano-onion” nanoparticles with core ( $\gamma$ -Fe) / double shell ( $\alpha$ -Fe / Fe-oxide): synthesis, microstructure and magnetism.**

*M.P. Fernández-García<sup>a</sup>, P. Gorria<sup>a</sup>, J.A. Blanco<sup>a</sup>, R. Boada<sup>b</sup>, J. Chaboy<sup>b</sup>, M. Sevilla<sup>c</sup>, A.B. Fuertes<sup>c</sup>, J.-M. Greneche<sup>d</sup>.*

<sup>a</sup>*Dpto. de Física, Universidad de Oviedo, Calvo Sotelo s/n, 33007, Oviedo, SPAIN.*

<sup>b</sup>*Instituto de Ciencia de Materiales de Aragón and Dpto. de Física de la Materia Condensada, CSIC-Universidad de Zaragoza, 50009, Zaragoza, SPAIN*

<sup>c</sup>*Instituto Nacional del Carbón, CSIC, Ap. 73, 33080, Oviedo, SPAIN.*

<sup>d</sup>*LPEC, UMR 6087, Université du Maine, 72085 Le Mans Cedex 9, France*

[fernandezpaz.uo@uniovi.es](mailto:fernandezpaz.uo@uniovi.es)

The large variety of magnetic scenarios displayed by nanoparticle (NP) systems is mainly governed by the reduced size and/or miscellaneous morphologies of the particles, because surface, interface or finite-size effects play an important role. Furthermore, the physical-chemical nature of the surrounding medium or matrix (amorphous or crystalline, insulating or conducting, magnetic or non-magnetic...) strongly influences the magnetic properties of the NPs. The complete understanding of the correlation between microstructure, morphology and magnetic behaviour is, at present, an interesting and novel issue that can lead to functionalize NPs for potential applications.

We have followed an inexpensive and easy-to-follow synthesis technique to fabricate massive (several grams) samples. The chemical process consists on a pyrolysis process taking place inside the restricted volume formed by the pores of an activated carbon and leads to the encapsulation of Fe-NPs on the nanoporous of the carbon matrix. The Fe-NPs present a broad particle-size distribution (5-40 nm) (Fig. 1). A combined structural and magnetic study seems to suggest that most of the nanoparticles of mean size  $\sim 15$  nm have exotic “onion-like” core-shell morphology of  $\gamma$ -Fe nucleus surrounded by a concentric double shell of  $\alpha$ -Fe and maghemite-like oxide (Fig. 2). The true nature of Fe-oxide was successfully evidenced through room temperature X-ray absorption spectroscopy. The whole system does not reach a fully superparamagnetic regime even at 750 K, probably due to higher blocking temperatures for the largest nanoparticles. Mössbauer spectrometry indicates that low temperature para-to-antiferromagnetic transition for the  $\gamma$ -Fe phase cannot be discarded. In addition, the external Fe-oxide shell exhibits spin-glass behaviour giving rise to the freezing of its magnetic moments at low-temperatures. Hence, we propose a competing double magnetic coupling: (i) the oxide shell /  $\alpha$ -Fe interaction and, (ii) the possible antiferromagnetic coupling between  $\gamma$ -Fe nucleus and  $\alpha$ -Fe layer; as being both responsible for the observed exchange bias effect at  $T = 5$  K ( $H_{\text{ex}} \approx 150$  Oe).

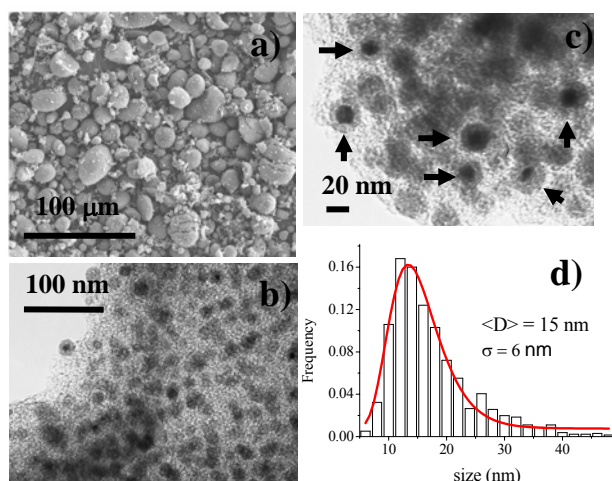
The financial support for this research work provided from FEDER and the Spanish MICINN (MAT2008-06542-C04, MAT2008-00407) is acknowledged. One of us, M.P.F.G thanks MICINN for the award of a FPI grant cofinanced by the European Social Fund.

**References:**

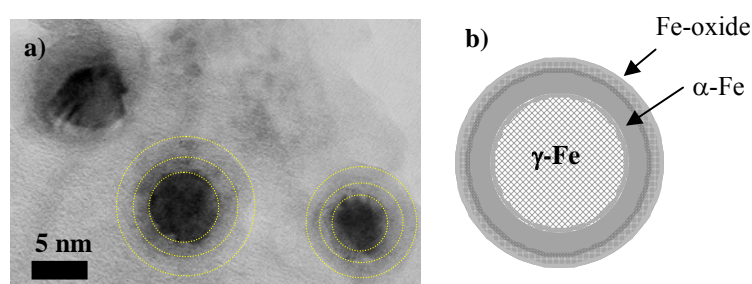
- [1] A. B. Fuertes, and P. Tartaj, *Chem. Mater.*, **18** (2006) 1675
- [2] M. Sevilla, and A. B. Fuertes, *Carbon*, **44** (2006) 468
- [3] P. Gorria, M. Sevilla, J. A. Blanco, and A. B. Fuertes, *Carbon*, **44** (2006) 1954

- [4] M. P. Fernández, D. S. Schmool, A. S. Silva, M. Sevilla, A. B. Fuertes, P. Gorria, and J. A. Blanco, *J. Non-Crystalline Solids*, **354** (2008) 5219
- [5] P. Gorria, M. P. Fernández-García, M. Sevilla, J. A. Blanco, and A. B. Fuertes, *Phys. Status Solidi-RRL*, **3** (2009) 4
- [6] M. P. Fernández, D. S. Schmool, A. S. Silva, M. Sevilla, A. B. Fuertes, P. Gorria, and J. A. Blanco, *J. Magn. Magn. Mater.* DOI: 10.1016/j.jmmm.2009.04.058 (2009)
- [7] M.P. Fernández-García, P. Gorria, J.A. Blanco, A.B. Fuertes, M. Sevilla, R. Boada, J. Chaboy, D. Schmool, J.-M. Greneche, *Phys. Rev. B* *accepted*

### Figures:



(a) SEM image showing almost spherical AC powders with a size in the 10 – 60  $\mu\text{m}$  range. (b) and (c) Different details of TEM images for Fe-NPs. Arrows are pointing out Fe-NPs with different core/shell morphology. (d) Histogram of the NP diameter together with a fit (red solid line) to a log-normal function. The mean particle size obtained is  $\langle \tau(\sigma) \rangle = 15(6)$  nm.



(a) TEM image showing in detail an Fe-NP with three different electronic densities and a well-defined “onion-like” morphology. In the figure, yellow lines are guides to the eye. (b) Schematic drawing of the morphology of Fe-NPs in Fe-AC sample.

## Transverse magneto-optical effects in Fe antidot arrays

J. F. Torrado<sup>1</sup>, E. Th. Papaioannou<sup>2</sup>, G. Ctistis<sup>3</sup>, P. Patoka<sup>4</sup>, M. Giersig<sup>4</sup>, G Armelles<sup>1</sup> and A. Garcia-Martin<sup>1</sup>

<sup>1</sup>*Instituto de Microelectrónica de Madrid (IMM-CNM-CSIC),  
Isaac Newton 8, Tres Cantos, 28770 Madrid, Spain*

<sup>2</sup>*Department of Physics and Astronomy, Uppsala University, 75121 Uppsala, Sweden*

<sup>3</sup>*Complex Photonic Systems (COPS), MESA+ Institute for Nanotechnology, University of Twente, The Netherlands*

<sup>4</sup>*Helmholtz-Zentrum Berlin für Materialien und Energie GmbH, 14109 Berlin, Germany  
[jftorrado@imm.cnm.csic.es](mailto:jftorrado@imm.cnm.csic.es)*

During the last decade, an increasing interest has been devoted to the analysis of the interplay between plasmon resonances and magneto-optical (MO) effects [1], since the plasmon resonances can be used to enhance the MO response [2-4] and the MO effect can be used to control the plasmon propagation [5].

A great number of the studies of the MO enhancement due to plasmon excitation have been carried out in the so-called Polar Kerr configuration for MO active nanostructures (either dots or antidots) [2] or when metal nanostructures have been put into contact with continuous films of MO active material [3]. However, in the Transverse Kerr configuration the studies focus on metallic nanostructures over continuous films [4].

Here we will cover that gap and study the Transverse Kerr Magneto-Optical Effect (TMOKE) of iron hexagonally perforated films (470nm pitch, 100nm thickness and radii of 248nm and 297nm respectively). We observe a large enhancement of the TKOME signal with respect to that of the continuous film, and relate that frequencies to the possibility of surface plasmon excitations. We will also analyze their dependence on the hole radius and compare the results to a continuous iron film of same thickness.

Apart from the orientation of the magnetic field the TMOKE differs from the Polar configuration in the angle of incidence of the light beam: the Polar effect is studied at normal incidence, whereas the TMOKE needs to be off normal, since the signal is zero otherwise. This means that when the nanostructuration is realized in a periodic fashion (see Fig. 1) there is an additional parameter to take into account: the azimuth (in-plane) angle. We will thus also analyze the TMOKE enhancement as a function of the crystal orientation of the sample plane with respect to the incident light beam as shown in the experimental TMOKE spectra in Fig 1.

### References:

- [1] G. Armelles, *et al.*, J. Opt. A: Pure Appl. Opt. **11** (2009) 114023.
- [2] J.B.González-Díaz, *et al.*, Adv.Mater. **19**, (2007) 2643; Small **4**, (2008) 202; G. Ctistis *et al.*, Nano Lett. **9**, (2009) 1; J.B. González-Díaz, *et al.*, Appl. Phys. Lett. **94**, (2009) 263101; E.Th. Papaioannou, *et al.*, Phys. Rev B *in press* (2010).
- [3] A.B. Khanikaev, *et al.*, Opt. Express **15**, (2007) 6612; V. I. Belotelov, *et al.*, Phys. Rev. Lett. **98**, (2007) 077401; G.A. Wurtz, *et al.*, New J. of Phys. **10** (2008) 105012; G.Armelles, *et al.*, Opt. Express **16**, (2008) 16104.
- [4] V.I. Belotelov, *et al.*, J. Opt. Soc. Am. B, **26** (2009) 1594; J.F. Torrado, *et al.*, submitted (2010).

[5] J.B. González-Díaz, *et al.* Phys. Rev. B. **76**, (2007) 153402; E. Ferreiro-Vila, *et al.*, Phys. Rev. B **80**, (2009) 125132; V.V. Temnov, *et al.* Nature Photonics **4**, (2010) 107.

**Figures:**

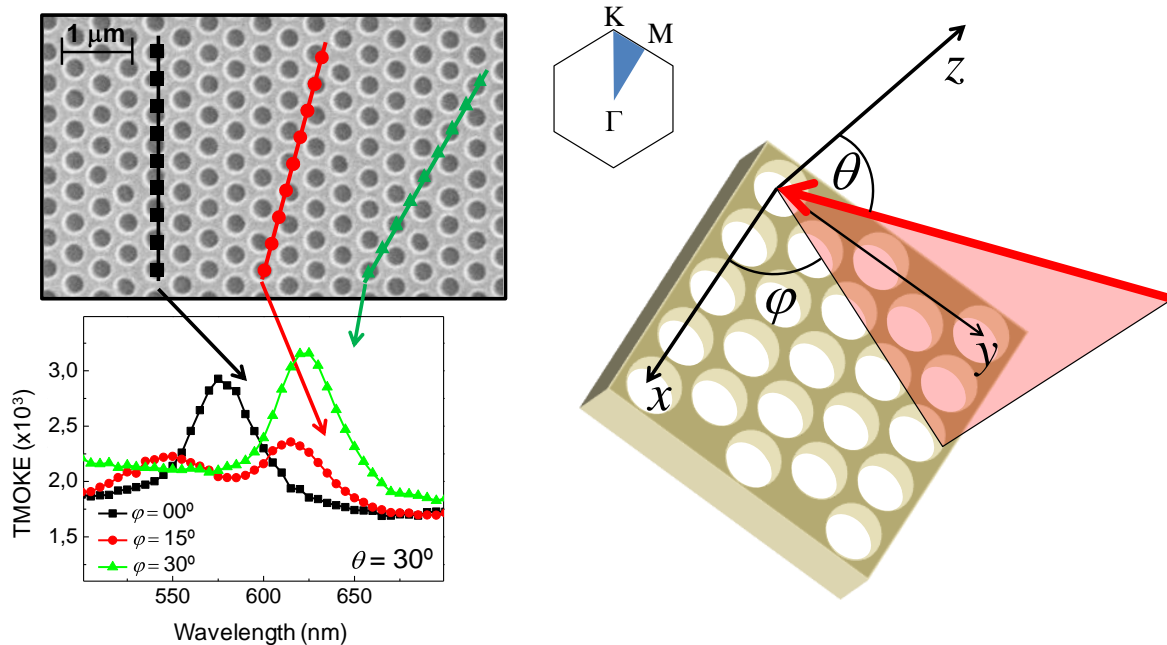


**Fig. 1:** Scanning Electron Micrograph of the Fe antidot array and a sketch showing the geometry and the first Brillouin zone of the in-plane lattice structure. Three characteristic TMOKE spectra obtained at different azimuth angles ( $\theta=30$  deg) showing the dependence of the TMOKE signal on the relative orientation of the impinging beam and the 2-D crystallographic high symmetry axis.

## Using Alternating Gradient Field Magnetometers for the characterization of the mechanical and magnetic behavior of magnetic nanoparticles in biological samples

V. Ferro<sup>1,2,3</sup>, J.J. Serrano<sup>1,2,3</sup>, T. Fernández<sup>1,2,3</sup>, M. Ramos<sup>1,2,3</sup>, C. Maestu<sup>1,2,3</sup>, F. del Pozo<sup>1,2,3</sup>  
<sup>1</sup> Biomedical Engineering and Telemedicine Centre (GBT), Centre for Biomedical Technology (CTB), Technical University of Madrid (UPM), Madrid, Spain  
<sup>2</sup> Biomedical Research Networking Center in Bioengineering, Biomaterials and Nanomedicine (CIBER-BBN), Spain  
<sup>3</sup> Community of Madrid Biomedical engineering programme (MADR.IB-CM), Madrid, Spain  
{vferro, milagros, cmaestu, fpozo}@gbt.tfo.upm.es, jjserran@etsit.upm.es, tfcabada@hotmail.com

The utility of magnetic nanoparticles (MNPs) has been proved with several in-vitro and in-vivo experiments. Their applications based on the interactions with static or time-varying magnetic fields, such as drug delivery, magnetic separation of labelled biological entities, magnetic resonance imaging contrast enhancement and, especially, the catabolism of tumours via hyperthermia, are currently some of the main and most promising focuses in biomedical investigation.

The characterization of the magnetic properties of the MNPs and their performance inside biological materials are improvable aspects, as well as the first steps for any experiment using them. At the moment there are no specific devices created for this purpose. As a consequence of this, the characterization of MNPs isn't good enough to determinate their behavior inside solid samples and biofluids. Therefore most of the results come from trial and error experiments.

Alternating gradient field magnetometers (AGFM) are fundamental instruments for characterizing magnetic materials. This type of magnetometer is extensively used in both laboratories and production environments for measuring the basic magnetic properties of materials as functions of magnetic field and, if desired, temperature. The AGFM is well-known because of its high sensitivity and low noise floor. Due to its features, the AGFM can be used for characterizing the magnetic and mechanical properties of MNPs.

The Princeton Measurements Corporation *MicroMag Model 2900 AGM System*<sup>®</sup>, installed in our laboratories as part of the Spanish Biomedical Research Networking Center in Bioengineering, Biomaterials and Nanomedicine MNPs Characterization Platform, offers the best combination of performance capabilities and can accommodate a large range of samples of very different properties, such as tissues or biofluids.

We have carried out a large number of experiments to prove that the AGFM is able to characterize MNPs inside biological samples. Figure 1 presents hysteresis loops resulting from experiments with 250 nm dextran-coated MNPs suspended in water infused inside human glioblastoma cells. It can be seen the only contribution come from the probe and the MNPs. Figure 2 shows normalized hysteresis loops, which are different between cultures with or without MNPs. Therefore, the AGFM is able to characterize the particles.

As can be seen in Figure number 3, the AGFM is able to discriminate the mechanical behavior of MNPs in liquid and solid sample. Using engineered MNPs (Magnetite MNPs dispersed in Triethylene glycol), constant measurements were taken while the sample evaporated. The influence of this evaporation was analyzed. It can be checked on Figure 3 that the hysteresis loop reaches a higher saturation when the sample dries, as well as the superparamagnetism is accentuated.

It has been also proved that the AGFM is able to detect low-concentrated (500 µg/ml) nanoparticles (Kisker's PMAV-250) inside 1321N1 human glioblastoma cell lines incubated

for three days. The samples were cultured on plastic cover slips, and the cationic peptide "protamine sulfate (PS)" was used (5  $\mu\text{g/ml}$ ) to increase the uptake of MNPs. The differences in the MNPs can be appreciated between Figure 4 (without PS) and Figure 5 (with PS). As can be seen in Figure 6, the AGFM can be used for characterizing the magnetic and mechanical properties of MNPs acquired by cells even without using PS. These experiments are the first step to discriminate the behavior of MNPs acquired by cells or situated on the extracellular matrix.

At the moment, we are focusing on the study of the differences between the magnetic and the mechanical properties of cell cultures with nanoparticles infused inside and outside of them. This way, we will know when MNPs have been acquired by cells. The final goal is to use AGFM combined with other techniques for the detection and the identification of engineered MNPs as contaminant in ex-vivo samples.

## References:

- [1] V. Ferro, J.J. Serrano, C. Maestú, C. Sánchez, M.C. Maicas, C. Aroca, M.M. Sanz, F. del Pozo, "El magnetómetro por gradiente alternante de campo: una nueva herramienta para la caracterización de nanopartículas magnéticas en biofluidos y tejidos biológicos", **Proceedings of the XXVI<sup>th</sup> Annual Congress of the Spanish Society of Biomedical Engineering (CASEIB 2008)**, Valladolid, October, 2008, pp.348-351, ISBN: 978-84-691-3640-9.
- [2] V. Ferro, J.J. Serrano, T. Fernández, M. Ramos, F. del Pozo, "Caracterización del comportamiento magnético y mecánico de nanopartículas en biofluidos y células con un AGFM", **Proceedings of the XXVII<sup>th</sup> Annual Congress of the Spanish Society of Biomedical Engineering (CASEIB 2009)**, Cádiz, November, 2009, pp.285-288, ISBN: 978-84-608-0990-6.

## Figures:

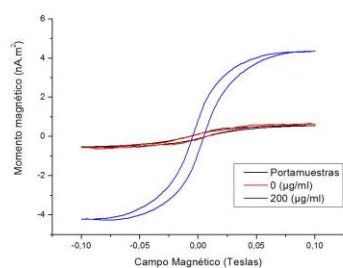


Figure 1

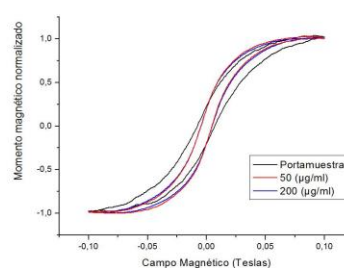


Figure 2

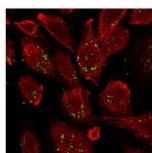


Figure 3

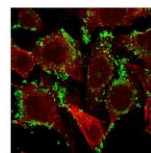


Figure 4

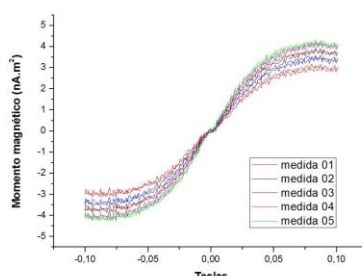


Figure 5

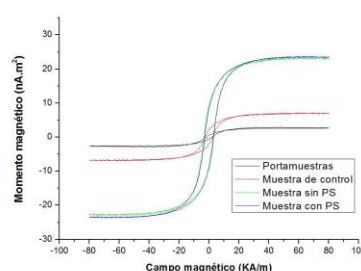


Figure 6

## **Interactions between Antitumoral Models of Ruthenium and DNA Purines in a Confined Environment (Nanostructured Silica Matrices)**

*Luís M. F. Lopes, Ana R. Garcia, Alexandra Fidalgo and Laura M. Ilharco*  
*CQFM - Centro de Química-Física Molecular and IN - Institute of Nanoscience and Nanotechnology, Instituto Superior Técnico, Universidade Técnica de Lisboa,*  
*Av. Rovisco Pais 1, 1049-001 Lisboa, Portugal*  
[luis.f.lopes@ist.utl.pt](mailto:luis.f.lopes@ist.utl.pt)

Although new cancer treatment strategies have been evolving towards specific pathways, notably those involved in cell signalling, the majority of cytotoxic metal complexes available and under research have as target the DNA, given its importance in replication process and cell viability. In order to achieve a clear understanding of the role of metal complexes on these processes, a wide range of studies centred on the interactions of the coordination complexes with DNA and its constituents and derivatives, as well as with other biological targets have been conducted. Some interaction mechanisms have been proposed based on theoretical approaches and experimental studies in homogeneous medium (aqueous or gaseous phase), but no so far in a confined environment. The binding of nucleic acid bases to the metal atoms of coordination complexes seems to be determinant on the antitumoral activity of those compounds.[1]

Among coordination compounds, the ruthenium complexes have been target of great attention as antitumoral agents, given their lower toxicity and higher specificity comparatively to platinum-based complexes. A few are presently standing clinical trials (phase II), namely NAMI-A (imidazolium [trans-tetrachloro(1H-imidazole)(S-dimethylsulfoxide)ruthenate(III)]) and KP1019 (indazolium [trans-tetrachlorobis(1H-indazole)ruthenate(III)]).

In the present work, some Ru(II) and Ru(III) complexes ( $\text{RuNO}(\text{NO}_3)_3$  and the ammine complexes  $\text{Ru}(\text{NH}_3)_6\text{Cl}_3$ ,  $\text{Ru}(\text{NH}_3)_6\text{Cl}_2$  and Ru-red) were coencapsulated with DNA purines (adenine (Ade) and guanine (Gua)) within nanostructured silica matrices prepared by a two-step sol-gel process. These Ru complexes were used as models and pro-drugs of antitumoral agents and their interactions with the DNA purines were investigated by infrared and UV-Visible spectroscopies.

This research shows that Ade interacts with the complexes, or with their decomposition products, only by hydrogen bonds (Figure 1). However, these interactions are strong enough to inhibit or delay the decomposition of the ammine complexes. Adenine showed also high affinity to the silica network, which increases with the amount of silanol groups on the matrix.

Guanine behaves differently with each complex: it interacts strongly with  $\text{RuNO}(\text{NO}_3)_3$ , since direct covalent bonding of the metal to the N7 or N9 of Gua was detected (Figure 2) [2]; on the other hand, the interactions with ammine complexes are much weaker given that only hydrogen bonds were confirmed. Guanine seems to have preferential interactions with the silanol or siloxy groups of the matrix, certainly by the carbonyl group, allowing the complexes to undergo further oxidation reactions.[3]

It was also proved that the nanostructure of the silica matrix plays an important role on the interactions established between the purines and the Ru complexes, namely the pore structure (shape and dimensions) and the amount of silanol groups, both largely affected by the nature of the dopants.

**References:**

- [1] M. J. Clarke, *Coord. Chem. Rev.*, **232** (2002) 69-93.  
[2] L. M. F. Lopes, A. R. Garcia, A. Fidalgo, L. M. Ilharco, *Langmuir*, **25** (2009), 10237-10242.  
[3] L. M. F. Lopes, A. R. Garcia, P. Brogueira, L. M. Ilharco, *J. Phys. Chem. B*, (accepted).

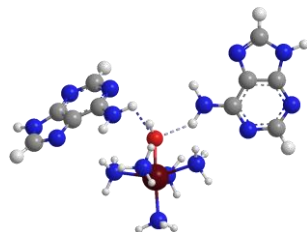
**Figures:**

Figure 1: Schematic representation of possible hydrogen bonds between Ade and the intermediate  $[\text{Ru}(\text{NH}_3)_5\text{OH}]^{2+}$

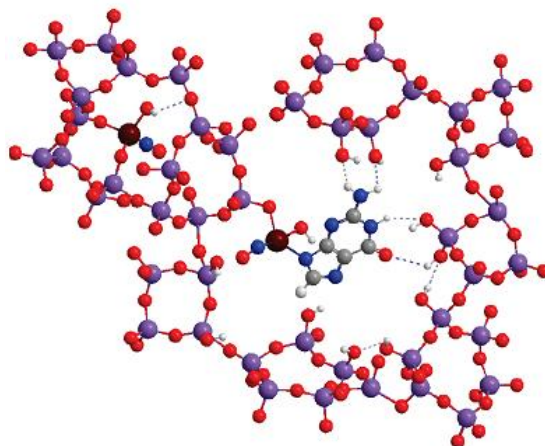


Figure 2: Proposed interactions between Gua and Ru(III) nitrosyl nitrate ( $\text{RuNO}(\text{NO}_3)_3$ ) within the silica matrix.

**Gold Nanoparticle-Based Immunoassay for detection of *Plasmodium falciparum* Hsp70**

B. Shenouda<sup>1,2</sup>, I. Gomes<sup>1,3</sup>, C. Sá e Cunha<sup>3</sup>, H. Azzazy<sup>2</sup>, M. Mota<sup>3</sup>, M. Prudêncio<sup>2</sup> and R. Franco<sup>1</sup>

<sup>1</sup> REQUIMTE, Departamento de Química, Faculdade de Ciências e Tecnologia, Universidade Nova de Lisboa, 2829-516 Caparica, Portugal

<sup>2</sup> Department of Chemistry, SSE # 1194, AUC Avenue, 74, New Cairo, 11835, Egypt

<sup>3</sup> Malaria Unit, Instituto de Medicina Molecular, Faculdade de Medicina da Universidade de Lisboa, 1649-028 Lisboa, Portugal

[r.franco@dq.fct.unl.pt](mailto:r.franco@dq.fct.unl.pt)

Biomedical nanotechnology presents revolutionary opportunities in the detection of pathogenic microorganisms. Despite its huge burden, with forty percent of the world's population at risk of infection, the diagnosis of malaria is often not straightforward and there is an urgent need to develop rapid, sensitive, and cost-effective tests for both high- and low-resource settings. We aim to design a gold nanoparticle (AuNP)-based rapid detection test (RDT) using specific antibodies to detect *Plasmodium falciparum* (malaria parasite) antigens in clinical specimens. The characteristics of the proposed malaria RDTs include reproducibility, acceptable high sensitivity and specificity, rapidity, ease of performance and interpretation, stability when stored, and capability of species differentiation, all at an affordable price [1].

Our approach is based on the utilization of mercaptoundecanoic acid (MUA)-capped AuNPs conjugated with 2E6 antibodies. These antibodies specifically recognize *Plasmodium falciparum* Heat Shock Protein 70 (PfHsp70). Heat Shock Proteins are immunodominant antigens recognized by the host immune system in various infectious diseases. In particular, PfHsp70 which possesses chaperone and anti-apoptotic activity has recently drawn attention as a novel therapeutic target [2]. The presence of parasitic Hsp70 in the pellet of saponin treated red blood cells of infected mice (and not uninfected mice or humans) was confirmed by Western blot (Figure 1). This result suggests that this antibody-antigen set could be used in the development of an RDT for malaria in clinical samples. PfHsp70 antigens will be purified from an overexpressing *E. coli* system using His-tag or immune-affinity chromatography, and utilized as proof-of-concept for the method.

The formation of the 2E6-AuNP bionano-conjugates was assessed using a previously established method based on  $\zeta$ -potential measurements ([3] and Figure 2), and conjugation stoichiometry was also verified by agarose gel electrophoresis. UV-visible spectrophotometry shows aggregation of the bionano-conjugates as a function of the solution pH, inducing a shift of the AuNP plasmon band corresponding to a red-to-blue color change of the solution. The pH at which this aggregation occurs can be related to the protonation state of superficial amino acid residues and may hence be used as an indirect evaluation of antibody-AuNP formation and surface alterations induced by antigen binding.

**References:**

- [1] D. Bell and R. W. Peeling, Nat Rev Microbiol, **4** (2006) S34
- [2] G. Misra and R. Ramachandran, Biophys Chem, **142** (2009) 55
- [3] I. Gomes, N.C. Santos, L.M.A. Oliveira, A. Quintas, P. Eaton, E. Pereira, R. Franco, J. Phys. Chem. C, **112** (2008) 16340

### Figures:

**Figure 1.** Western blot analysis, using 2E6 antibody, of saponin-treated pellets of red blood cells from mice infected with *Plasmodium berghei* (Inf); non infected mice (Non inf); or a healthy human donor (Hum)

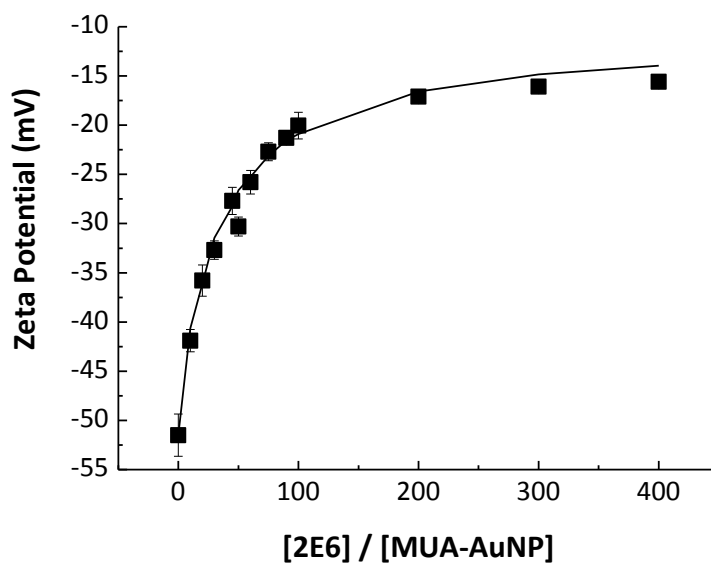
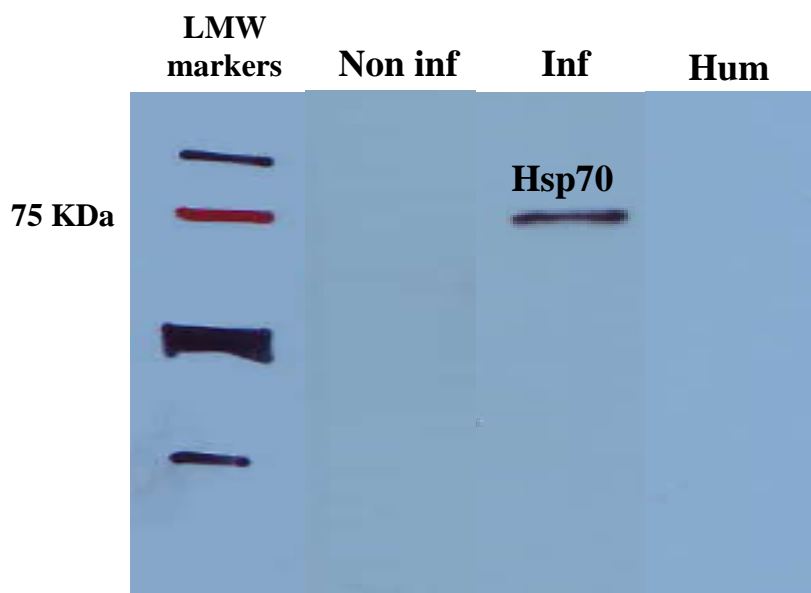


**Figure 2.** Zeta potential of each bionanoconjugate determined as a function of the [2E6] / [MUA-AuNP] ratio. Solid line represents fitting to a Langmuir adsorption isotherm.

**Acknowledgments:** FLAD (Luso-American Foundation), Portugal, is gratefully acknowledged for financial support to this work.

## **Fabrication by Dip-Pen Nanolithography of Polypyrrole Nanowires for DNA biosensors**

*T. Galán<sup>1,3</sup>, S. Oberhansl<sup>1,2</sup>, E. Martínez<sup>1,2</sup>, J. Samitier<sup>1,2,3</sup>.*

<sup>1</sup>*Nanobioengineering group, Institute for Bioengineering of Catalonia (IBEC), Josep Samitier 1-5, 08028, Barcelona, Spain.*

<sup>2</sup>*Networking Research Center on Bioengineering, Biomaterials and Nanomedicine (CIBER-BBN), Barcelona, Spain.*

<sup>3</sup>*Department of Electronics, University of Barcelona, c/ Martí i Franquès 1, 08028 Barcelona, Spain.*

[tgalan@ibec.pcb.ub.es](mailto:tgalan@ibec.pcb.ub.es)

Conducting polymers constitute an attractive alternative to metals and semiconductors as sensing elements in biosensor devices. They are low cost, easy processing materials at the micro and the nanoscale, with controllable mechanical and electrical properties and show high biocompatibility, a particularly important requirement for biomedical applications<sup>1</sup>. We propose the fabrication of conducting polypyrrole polymer nanowires, by the Dip-pen nanolithography method. This nanomaterial, would be used further on in the construction of a DNA sensor by depositing the polypyrrole nanowires between two metal contacts previously fabricated on top of a silicon oxide substrate. To address these challenges, Dip-pen<sup>2</sup> deposition combined with standard optical lithography will be used as main processing techniques.

Dip-pen nanolithography is a technique developed in 1999 by C. Mirkin et al.<sup>3</sup> where the ink is deposited onto a surface via cantilever. The use of the so called inkwells (microfluidic chips) enables the deposition of bio-molecules which are in a buffered solution. The cantilever is introduced in the wells, retracted abruptly and left drying to bring it into contact with the surface for the writing of the nanosize pattern (Fig.1).

Dip-pen experiments have been performed with a NSCRIPTOR system from Nanoink (Skokie, USA) at Room Temperature (20°C ±1°C) and relative humidity ranging from 30% to 40% on silicon oxide. An image of the written nanowires at 0,1, 0,5, 1,0 and 1,5 μm/s writing speeds, at 21°C and 40% of humidity is shown in Figure 2. The LFM (Lateral Friction Mode) has been obtained with the same tip and equipment used for writing. Several parameters influence the nanowire dimensions<sup>4,5</sup>, as the writing speed, the temperature and humidity, being these two last ones controlled by an environmental chamber (EChamber, Nanoink). Studies of the nanowire dimensions as a function of the writing speed and humidity at constant temperature were performed in order to determine the optimum deposition conditions. Figure 3 evidences the decay tendency of the size while increasing the speed, at Room Temperature and several humidities within the range of our study. Higher humidity increases the nanowire dimensions, so it should be also a parameter optimized when critical size tolerances are needed. Additionally, nanowire deposition between prepatterned metallic contacts have been achieved as seen in figure 4 by an AFM image showing a nanostructure located in a specific area.

Finally, we showed that it was possible to obtain polypyrrole nanowires with tailored dimensions (diameter) by controlling environmental conditions (temperature and humidity), and that we could deposit our structures in a certain location between electrodes for further processes.

### **References:**

- [1] Waneka AK, et.al. J. Phys Chem C, **111** (2007) 5218.
- [2] Tang Q, et.al. Sensor Actuat B-Chem, **13** (2008) 379.
- [3] C. Mirkin, et. al. Science, **283** (1999) 661
- [4] J. Lim, A Mirkin. Adv. Mater. **14**(2002) 20
- [5] Y. Im et al. Journal of Physics **38** (2006) 61-64

**Figures:**

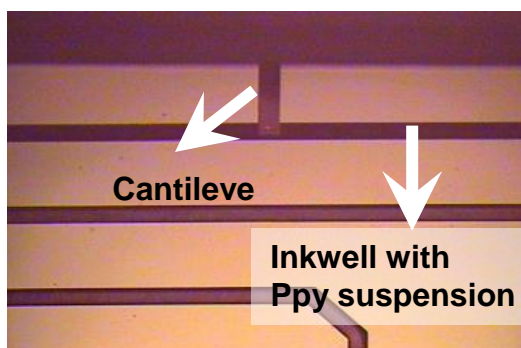


**Fig.1-** Process of loading the ink on the tip, by the help of the Inkwells

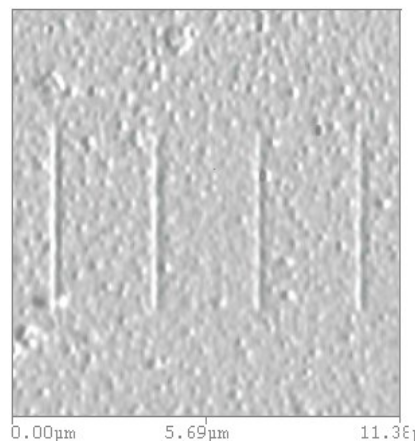


**Fig.2-** LFM image in contact mode of Nanowires at different writing speeds.

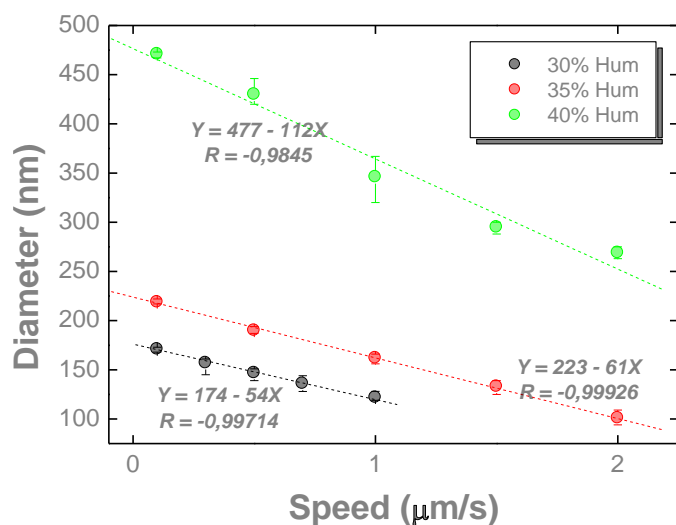


**Fig.3-** Dependence of the Nw diameter with the writing velocity, for different humidity values. Dashed lines correspond to the linear fits.

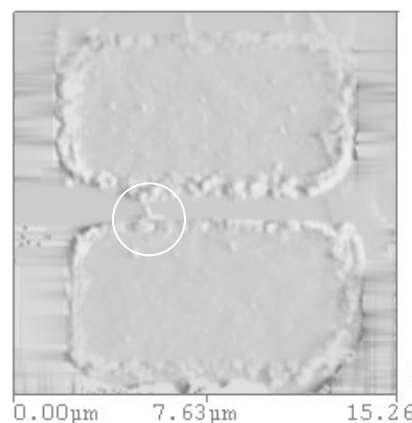


**Fig.4-** Topography AFM image of a Nanowire written in a gap between metallic contacts

## Maghemite Nanoparticles-Templated Assembly of Apoferritin Protein Functionalized with Carbohydrates for Targetting Cells

*Natividad Gálvez, Elsa Valero, Mariano Ortega, F. Javier López Jaramillo, Francisco Santoyo González, Juan de Dios López, Juan J. Delgado, José J. Calvino and José M. Domínguez Vera*

*Departamento de Química Inorgánica, Universidad de Granada, Spain, [ngalvez@ugr.es](mailto:ngalvez@ugr.es)*

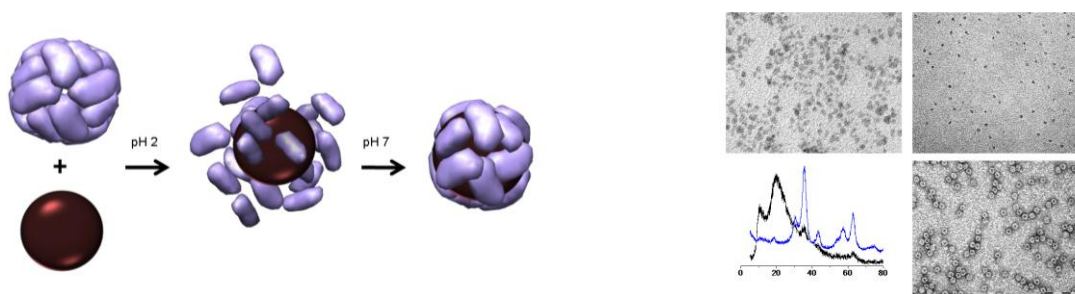
In the last few years there has been an enormous development in the synthesis and functionalization of inorganic nanoparticles for biomedical applications. Of particular interest is the case of magnetic nanoparticles where there is an outbreak of proposed nanostructures for imaging, magnetic hyperthermia or targeted drug delivery.

Non-invasive in vivo imaging (MRI, OI, PET CT...) has enormous potential for the early detection and treatment of disease. Imaging techniques using nonspecific-image contrast agents lack of the necessary specificity for obtaining quality imaging, particularly, in the early stages of disease. The identification of specific ligands to target tissues of interest opens the door for development of new probes that can specifically localize and image molecular events in the body in real time.

Magnetite and/or maghemite ( $\text{Fe}_3\text{O}_4/\gamma\text{-Fe}_2\text{O}_3$ ) nanoparticles have been used extensively as a model magnetic material in the biomedical research field. Considering that the magnetic properties and contrast enhancement capacity of nanoparticles are strongly dependent on various parameters, such as size, shape, surface properties and degree of aggregation, it is important to prepare nanoparticles with high saturation magnetization ( $M_s$ ) values, while maintaining single domain properties.

Moreover, numerous efforts have been devoted to achieve "active targeting" i. e., ligand-coated nanoparticles bearing an active functionality, such as a targeting molecule for a desired receptor, that enhance selectivity transport based on molecular recognition processes such as antigen-antibody or ligand-receptor interaction.

In this communication we describe a new synthetic method for obtaining carbohydrate-functionalized magnetic nanoparticles. Apoferritin, the cellular iron-storage protein, is a spherical shell composed of 24 polypeptide subunits surrounding a cavity of 8 nm. We used the dissociation at pH 2.0 of the apoferritin into its 24 subunits, followed by its reconstruction at pH 7 to encapsulate maghemite nanoparticles. It is worthy to pointing out that the native mineral formed inside the apoferritin is a ferrihydrite-magnetite core-shell structure of 5 nm of mean size.<sup>[1]</sup> We have lately shown that apoferritin shell can be successfully functionalized with different dyes or Quantum Dots, as a new type of dual-functional fluorescent-magnetic probes.<sup>[2]</sup> Herein, we have also succeeded in the functionalization of apoferritin with two types of monosaccharides. The immobilized carbohydrates retained their recognition abilities, as demonstrated by the strong affinity with their corresponding carbohydrate-binding lectins.



**References:**

- [1] N. Gálvez, B. Fernández, P. Sánchez, R. Cuesta, M. Ceolín, M. Clemente-León, S. Trasobares, M. López-Haro, J. J. Calvino, O. Stéphan, J. M. Domínguez-Vera, *J. Am. Chem. Soc.* **2008**, *130*, 8062–8068.
- [2] B. Fernández, N. Gálvez, R. Cuesta, A. B. Hungría, J. J. Calvino and José M. Domínguez-Vera. *Adv. Funct. Mater.* **2008**, *18*, 3931-35.

**Optimized fluorescent nanoparticles used for direct detection of GST fusion proteins.**

Beato JJ, Gomez E, Fernandez-Ponce C, Blanco E, Ramirez Del Solar M, Dominguez M, Garcia-Cozar F, Litran R.

The current development of life sciences is strongly linked to the availability of new experimental tools that enable the manipulation of biomolecules and the study of the biological process at the molecular level. We have optimized a synthetic process to obtain glutathione capped fluorescent CdS nanoparticles. Brightly fluorescents and biocompatible CdS quantum dots of different sizes can be obtained through our method based on four different heating steps. The optical behavior of the QDs has been evaluated studying both absorbance and fluorescence of the solutions containing the nanoparticles. For all samples the excitonic absorption onset clearly shows a blue shift in comparison to that of bulk CdS at 512nm, due to the quantum confinement effect. As the nanocrystal average size increases, the emission fluorescent band shows a red shift, from 440nm to 540nm. Both the study of the fluorescent efficiency as well as the fluorescent dynamic evolution provide information about the surface structure reconstruction of the quantum dot. We find a critical size at which, the quantum confinement effect as well as the surface/volume ratio give place to the highest fluorescent quantum yield and the largest fluorescent life time. We also show that optimized nanoparticles bound to Glutathione can directly bind Glutathion S-Transferase (GST) blotted onto PVDF membranes and thus are suitable for direct detection of GST fusion proteins.

## Modeling breakage properties of metallic nanowires with random orientations

S. Peláez<sup>1</sup>, C. Guerrero<sup>2,3</sup>, R. Paredes<sup>3,4</sup>, P. A. Serena<sup>1</sup>, P. García-Mochales<sup>5,\*</sup>

<sup>1</sup> Instituto de Ciencia de Materiales de Madrid,  
Consejo Superior de Investigaciones Científicas (CSIC), Madrid, Spain

<sup>2</sup> Departamento de Física, Facultad Experimental de Ciencias,  
La Universidad del Zulia (LUZ), Maracaibo, Venezuela

<sup>3</sup> Centro de Física, Instituto Venezolano de Investigaciones Científicas (IVIC), Venezuela

<sup>4</sup> Universidad Nacional Autónoma de México (UNAM), México, México

<sup>5</sup> Departamento de Física de la Materia Condensada, Facultad de Ciencias,  
Universidad Autónoma de Madrid (UAM), Madrid, Spain

\* [pedro.garciamochales@uam.es](mailto:pedro.garciamochales@uam.es)

During the last two decades, the study of the properties of nanowires has been one of the keystones of the development of nanotechnology since these nanoobjects exhibit electrical and mechanical properties of interest in fundamental knowledge as well as technological applications [1]. In particular, many experimental studies of electrical and mechanical properties of metallic nanowires have been addressed in order to describe the quantum features appearing due to electron transversal confinement. The standard approximation for the experimental study of such metallic nanowires includes the formation, elongation and breakage of ultranarrow nanocontacts, as for instance, those formed between an STM tip and a metallic surface. With the use of powerful computational resources and accurate description of the atomic interactions, many of the formation-breaking experiments can be reproduced “in silicon” [2], being possible even to analyse situations and structures that experimentally are difficult to address [3].

It has been stressed the importance of statistical studies of these phenomena [3, 4] because, given a particular initial geometrical configuration and temperature, each breakage event evolves differently, that is the standard approximation for the experimental study of metallic nanowires, where statistical data is accumulated during many indentation-retraction cycles.

However, the comparison between experimental results and the usual numerical simulations requires an additional element. Experimental data usually correspond to the statistical average of nanowire breaking events involving random stretching directions. In a standard experiment there is no reason that indicates that any particular orientation would be preferred during the nanowire formation and breakage. Therefore, to accomplish a complete statistical analysis equivalent to the experimental one, computational calculations must simulate breaking events on random stretching directions. This could be a potential problem since it is not easy to perform simulations with arbitrary (random) initial stretching directions. Fortunately, it is not necessary to compute “every” stretching orientation to get the statistical behaviour of the breaking nanowires.

In an experiment, the final stages and behaviour of a nanowire during its breakage are led by the type of crystalline structure closest to its elongation direction. So it should be in simulations. Therefore, it is needed only to analyse main crystalline orientations, those that show different structural type, and average their results according to their occurrences. I.e., to achieve orientation statistics in computational simulations, results from the main crystalline directions have to be merged with the appropriate weights. These weights will be proportional to the zone axis multiplicity [5]. Of course, each main direction must have an accurate

statistics to guarantee the correctness of the global results, but this is easily achieved performing many simulations with the same initial structure at a given temperature [3,4].

In this work we will present the method used to merge the statistical results corresponding to the three different stretching directions ([100], [110] and [111] for a *fcc* structure) in order to reproduce results from random orientations and compare with experimental findings. We will show the results on some properties of this weighted average for three metallic species (Ni, Al, Cu). As an example of these results, figure 1 shows for Ni nanowires the probability of obtain of a monomer, dimer or other structure as final configuration before the breakage.

## References:

- [1] Agraït, N.; Levy Yeyati, A.; Van Ruitenbeek, J.M. *Physics Report*, **2003**, 377, 81-279.
- [2] Barnet, R.N.; Landman, U.; *Nature* **1997**, 387, 788. Hasmy, A.; Medina, E.; Serena, P. A. *Phys. Rev. Lett.* **2001**, 86, 5574. Sen, P. et al.; *Phys. Rev. B* **2002**, 65, 235433; Hasmy, A. et al.; *Phys. Rev. B* **2005**, 72, 245405. Pauly, F. et al.; *Phys. Rev. B* **2006**, 74, 235106.
- [3] García-Mochales, P.; Paredes, R.; Peláez, S.; Serena, P.A.; *Nanotechnology* **2008**, 19, 225704. Peláez, S.; Guerrero, C.; Paredes, R.; Serena, P.A.; García-Mochales P. (2009). *Phys. Status Solidi C* **2009**, 6, 2133-2138.
- [4] García-Mochales, P. et al.; *Materials Science-Poland* **2005**, 23, 413. García-Mochales, P.; Peláez, S.; Serena, P. A.; Medina, E.; Hasmy, A. *Appl. Phys. A* **2005**, 81, 1545.
- [5] Rodrigues, V.; Fuhrer, T.; Ugarte, D. *Phys. Rev. Lett.* **2000**, 85, 4124.; González, J. C. et al.; *Phys. Rev. Lett.* **2004**, 92, 126102

## Figures:

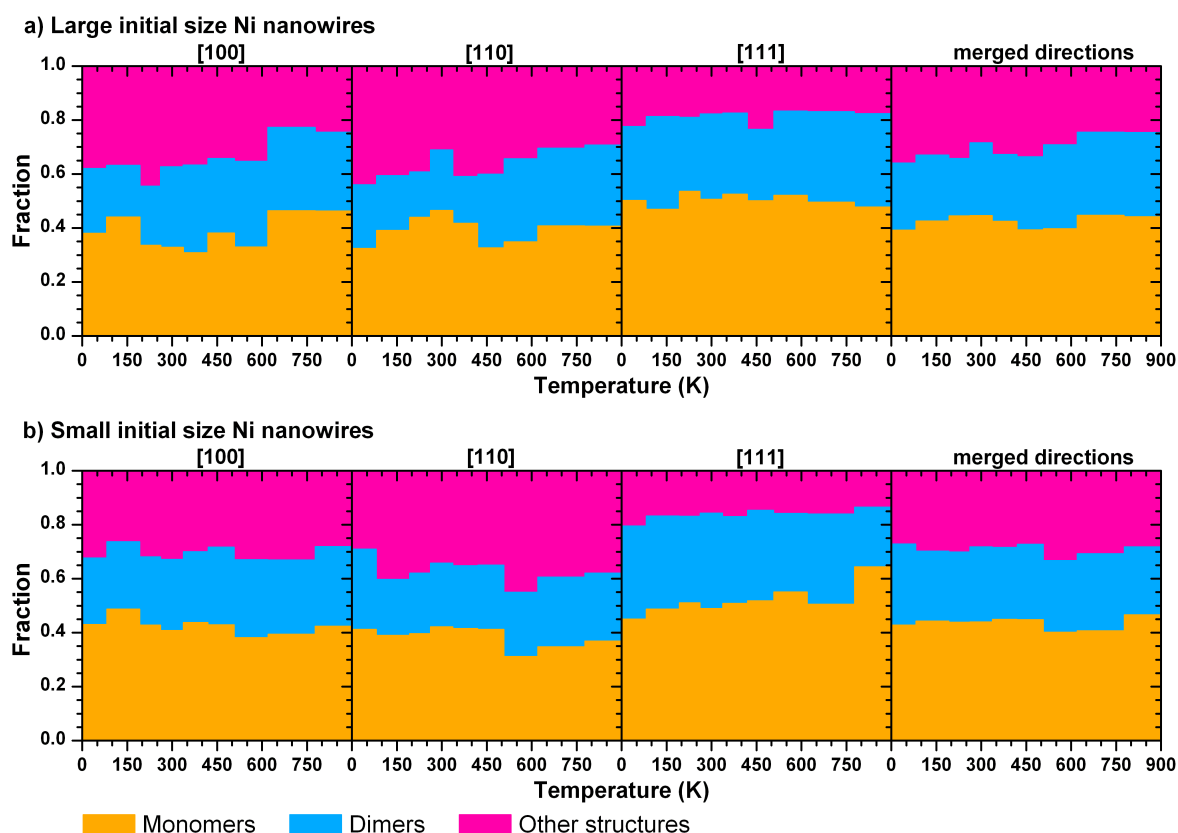


**Figure 1:** Fraction of monomers, dimers and more complex structures appearing during the Ni nanowire breaking process as functions of the temperature for Ni nanowires of large (~1000 atoms) (a) and small (~180 atoms) (b) initial size. Different columns correspond to nanowires stretched along [100], [110], [111] and random (merged) crystallographic directions.

## Magnetic fields interactions phenomena in guidance and focusing of magnetic micro and nanoparticles

R. A. García Mendoza<sup>1,2,3</sup>, J. J. Serrano Olmedo<sup>1,2,3</sup>, A. Mina Rosales<sup>1,2,3</sup>, F. del Pozo Guerrero<sup>1,2,3</sup>

<sup>1</sup> Bioengineering and Telemedicine Group (GBT), Biomedical Technology Center (CTB), Polytechnic University of Madrid (UPM), Avenida Complutense 30, "Ciudad Universitaria". 28040 – Madrid, Spain.

<sup>2</sup> Bioengineering, Biomaterials and Nanomedicine Network for Biomedical Research, Madrid, Spain.

<sup>3</sup> Biosciences Program MADR.IB-CM, Comunidad de Madrid  
[rgarcia@gbt.tfo.upm.es](mailto:rgarcia@gbt.tfo.upm.es), [jjherrero@etsit.upm.es](mailto:jjherrero@etsit.upm.es)

Fabrication of magnetic particles (MPs), either at micro or nano scale, it has been widely studied as well as some of their applications like cancer treatment, degenerative diseases diagnostic, contrast agents, etc.; but since Nanotechnology represents a new frontier between biology, chemistry and physics it is necessary do not leave out any phenomena like movement of MPs in viscous fluids under the action of static magnetic fields. All before could be important understand it to be able to control movement of the MPs [1], [2] and [3].

In this research, we present phenomena that involve movement of MPs. It must be note that movement can refer to guidance and focusing, and they are not the same. The first one represents the capacity to move MPs into a predefined path, the second one tries to agglomerate the biggest amount of MPs in a specific location. Both of them are under the influence of external magnetic field and immersed in a viscous medium. The identification of interaction phenomena can lead us to make an important differentiation of particles that could be used for biomedical applications.

Because the phenomena founded come from guidance and focussing of micro and nanoparticles experimentation, it is important to highlight that we had developed a methodology to obtain average velocity and their path into an essay tube filled of a medium whose viscosity is a little bit higher than water's, with which we make a comparative analysis [4]. Results have been successfully done, but this work is aimed at discussing two phenomena that appear in our methodology: 1) self-organization of MPs in presence of magnetostatic field, even if it is low (see Figure 1); and 2) agglomeration of MPs (see Figure 2). These phenomena are neither published nor explained until now.

Apparently, waiting for a better set of experiments to achieve better statistical results, it has been identified that self-organization experienced by MPs is memoryless; this is, even if MPs are introduced into the essay tube in random way, the phenomenon appears and has the same behavior. Therefore, it could be supposed repeatability. On the other hand, agglomeration phenomenon shows that MPs can keep their agglomeration position even without magnetostatic field influence. Both phenomena, well characterized, can lead to better control of MPs behavior for biomedical applications, which is our goal.

Future work is in the way to obtain better mathematical approximation of phenomena explained before, and to extend number of experiments to make sure implications of both of them and to offer a better statistical results as well as image background.

## References:

- [1] Correia A, **Nanociencia y Nanotecnología En España**. Fundación Phantoms, 2008, pp. 239.
- [2] Alexiou C, Diehl D, Henninger P, Iro H, Rockelein R, Schmidt W and Weber H, *IEEE Trans. Appl. Supercond.*, **A high field gradient magnet for magnetic drug targeting**, vol. 16, 2006, pp. 1527-1530 (ISSN: 1051-8223 ).
- [3] Gleich B, Hellwig N, Bridell H, Jurgons R, Seliger C, Alexiou C, Wolf B, Weyh T, *IEEE Transactions on Nanotechnology*, **Design and evaluation of magnetic fields for nanoparticle drug targeting in cancer**, vol. 6, 2007, pp. 164-170 (ISSN: 1536-125X).
- [4] R.A. García Mendoza, A. Macías Delgado, J.J. Serrano Olmedo, F. del Pozo Guerrero, *Libro de Resúmenes Congreso Anual de la Sociedad Española de Ingeniería Biomédica*, **Primeras Experiencias en Guiado y Focalización de Micro y Nanopartículas Magnéticas con fines Biomédicos**, 2009, p. 167 (versión completa en CD de Congreso).

## Figures:

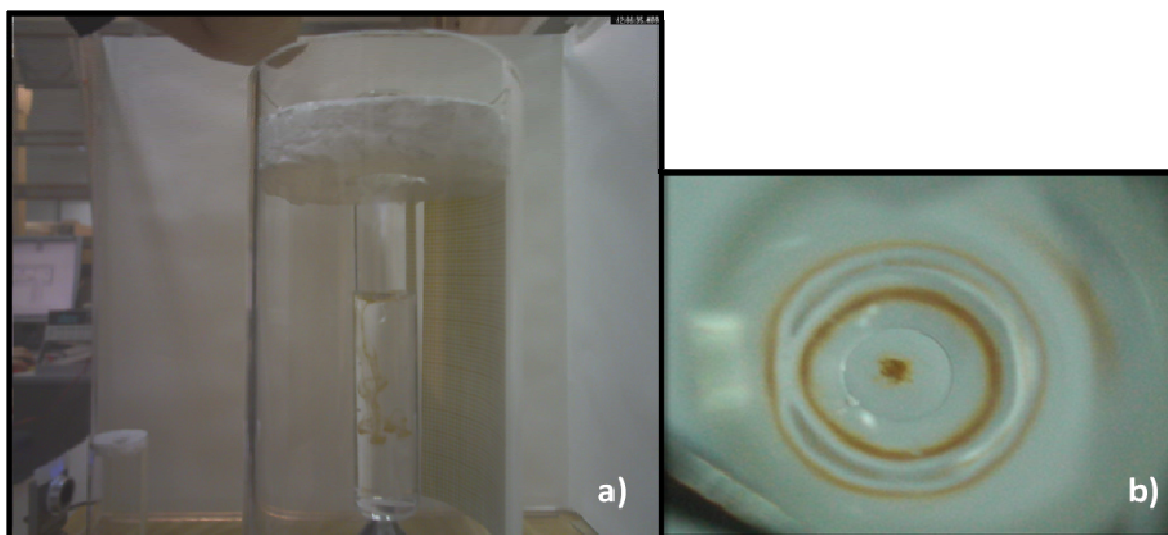


Figure 1. Phenomenon of self-organization under magnetostatic field using magnet plus cone and 1,31  $\mu\text{m}$  diameter MPs: in a) lateral view, and b) view from top of assay tube.

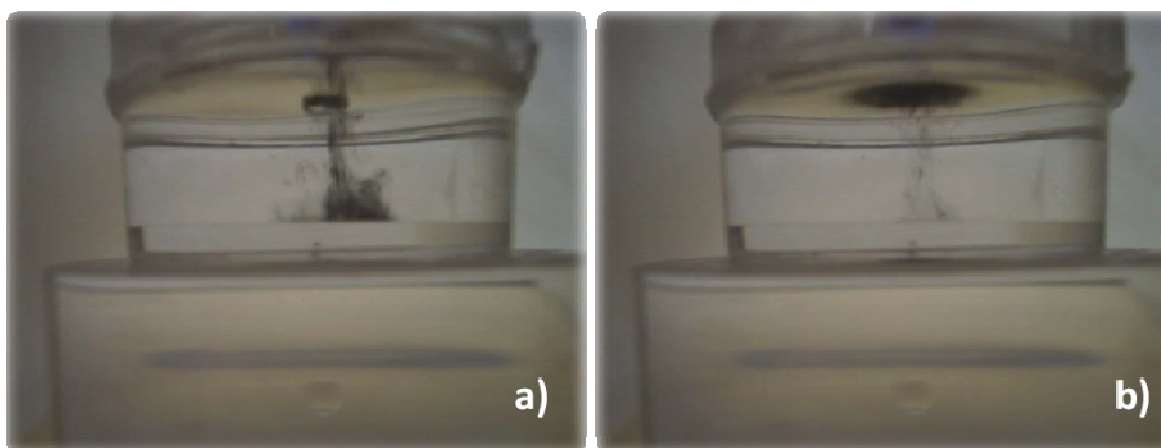


Figure 2. Phenomenon of agglomeration under magnetostatic field using magnet plus cone and 8  $\mu\text{m}$  diameter MPs: in a) response of MPs to magnetostatic field, and b) agglomeration of MPs.

**Manipulation of nanoparticles by arrays of electrodes: a theoretical analysis**

Antonio Ramos<sup>1</sup>, Antonio González<sup>2</sup>, Pablo García-Sánchez<sup>1</sup> and Antonio Castellanos<sup>1</sup>

<sup>1</sup>Dpto. Electrónica y Electromagnetismo, Reina Mercedes s/n, 41092

<sup>2</sup>Dpto. Física Aplicada III, Camino de los Descubrimientos s/n, 41012

Universidad de Sevilla, Sevilla, Spain

[pablogarcia@us.es](mailto:pablogarcia@us.es)

Electric fields are commonly used for the manipulation and control of nano/bioparticles [1]. Microelectrode structures represent an opportunity for direct actuation either on the liquid or suspended particles [2] and, when integrated in microchannels, electrodes make possible some standard processes in the “Lab-on-a-Chip” technology (i.e. pumping liquids [3], mixing analytes [4], sorting of cells [5],...)

In this work we analyze the motion of particles suspended in saline solutions on top of coplanar microelectrodes subjected to AC potentials. On one hand, the particles can undergo direct forces, as dielectrophoresis (DEP) or gravity. On the other hand, the particles can be dragged by the fluid flow. Upon application of an electric field, fluid flow in an electrolyte can be generated by either of the following mechanisms: electrothermal effect, AC electroosmosis and/or buoyancy. We also include in the analysis the random displacement of particles caused by Brownian motion.

As a model system, we consider an array of electrodes subjected to a travelling-wave potential (see Fig.1). We derive simple expressions for the magnitude of the forces on the particles and for obtaining estimates of the fluid velocity. From these expressions, we produce diagrams like those in Fig. 2, where we indicate which mechanism is dominating the motion of a particle (250 nm dia.) depending on the amplitude and frequency of an ac signal applied to an array of wavelength 100  $\mu\text{m}$ .

**References:**

- [1] H. Morgan and N.G. Green. *AC Electrokinetics: Colloids and Nanoparticles*. Research Studies Press Ltd. **2003**.
- [2] A. Ramos, H. Morgan, N.G. Green and A Castellanos. *J. Phys. D: Appl. Phys.* 31, 2338, **1998**.
- [3] A. Ramos. In *Microfluidics technologies for miniaturized analysis Systems*. Springer, **2007**.
- [4] N. Nguyen and Z. Wu. *J. Micromech. Microeng.* 15, R1-R16, **2005**.
- [5] S. Fiedler, S.G. Shirley, T. Schnelle, and G. Fuhr. *Analytical Chemistry*. 70, 1909, **1998**.

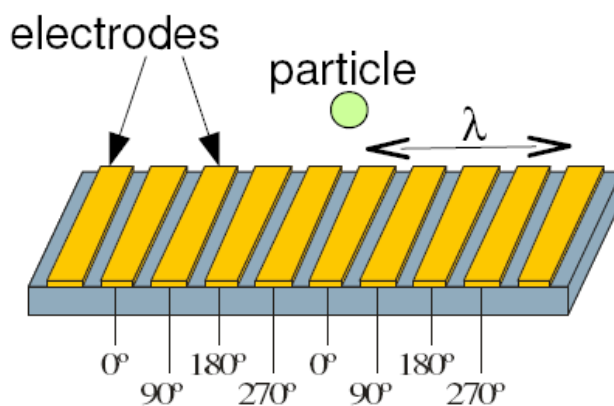


**Fig. 1.** Particle on top of an array of microelectrodes. AC signals of a given amplitude and frequency are applied to each electrode. The voltage on consecutive electrodes is phase shifted by  $90^\circ$ , generating a travelling-wave potential of wavelength  $\lambda$ .

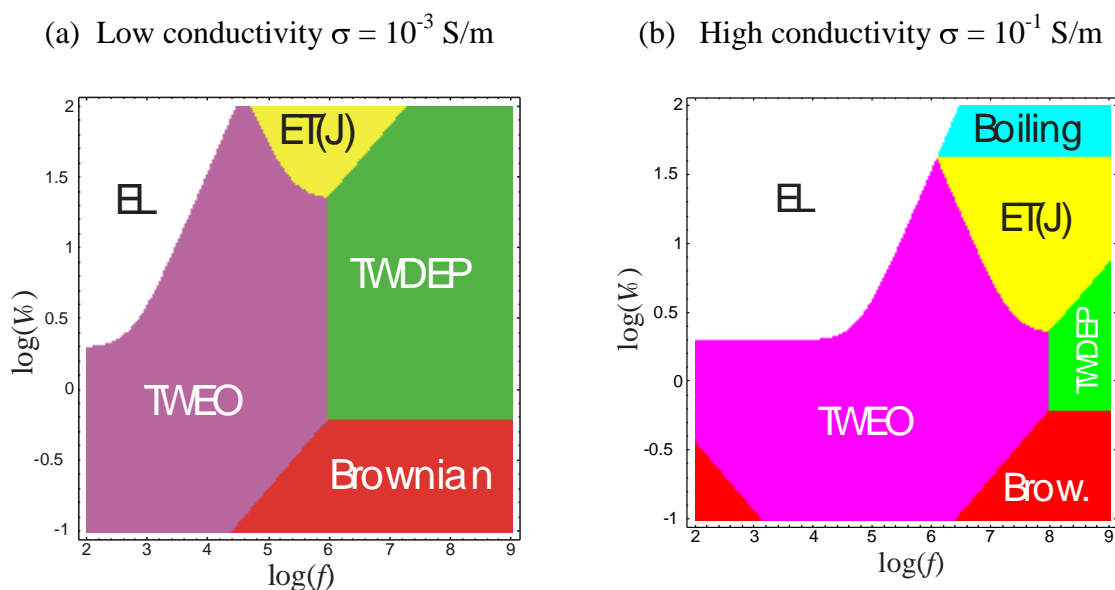


**Fig. 2.** The different regions indicate the mechanism dominating the motion of the particle (250nm dia.) as a function of the amplitude ( $V_0$ ) and frequency ( $f$ ) of the signal applied to a travelling wave array of  $\lambda=100\mu\text{m}$ . Two different conductivities are considered (a)  $10^{-3}$  S/m, and (b)  $10^{-1}$  S/m. The different mechanisms are: travelling-wave dielectrophoresis (TWDEP), travelling-wave electroosmosis (TWEO), electrothermal effect (ET) and Brownian motion. Water electrolysis (EL) can also be observed when the voltage drop at the electrodes is sufficiently high.

## **Enzyme immobilization based on sol-gel technology for pesticides determination**

*A. Navas Díaz, F. García Sánchez, A. Aguilar, I. Medina Lama, V. Bracho*

*Departamento de Química Analítica, Facultad de Ciencias, Universidad de Málaga,*

*29071 Málaga. Spain. e-mail: a\_navas@uma.es*

Environmental risks associated with pesticide use arise from both their toxicity and their tendency move with water. Because of increasing concerns over agricultural worker health and its potential environmental impacts, there is a growing interest to develop novel analytical methods capable of performing rapid detection of these compounds in the field.

The pesticides inhibition of biocatalytic properties of enzymes immobilized using sol-gel technology was studied using luminescence transduction strategies.

Based on the change in luminescent behaviour of enzymatic activity induced by the pesticides simple methods for investigation of the pesticides determination have been developed.

**Zero valent iron nanoparticles for in-situ soil remediation**

*Eunate Goiti, Marta Ocejo, María Moragues, Ekain Cagigal*  
*Labein-Tecnalia, Bizkaia Technology Park, Derio, Spain*  
[egoiti@labein.es](mailto:egoiti@labein.es)

The use of nanoscale zero valent iron particles (nZVI) for in-situ groundwater treatment and/or soil remediation is getting a lot of attention, due to the exceptional properties of these nanoparticles: nanoscale iron particles show higher surface area than microparticles, therefore nZVI show enhanced reactivity towards a wide range of contaminants, making it a promising technology in terms of sustainability and cost-effectiveness. However, high reactivity alone is not sufficient to make nZVI a good in situ remediation agent. Iron nanoparticles must also be readily dispersible in water such that they can migrate through water-saturated porous media to the contaminated area. Therefore, for the in situ remediation application colloidal stability of aqueous nZVI dispersion is a critical property.

In the present work, bare and biopolymer modified nZVI-based aqueous dispersions have been prepared by the standard borohydride method. By means of Transmission Electron Microscopy (TEM), Diffraction X-ray (DRX) and Z-potential measurements, the nanometer size, chemical structure and morphology has been evaluated. In addition, the stability of the dispersions with time has also been determined. The objective is to establish a comparison in terms of the above mentioned properties with iron microparticles and with some commercial iron nanoparticles. Furthermore, the reactivity of these four particles (micro, nano (bare and modified) and commercial) towards trichloroethylene (TCE) has been assessed.

**References:**

- [1] PG Tratnyek, RL Johnson, *Nanotoday*, **1** (2006) 44.
- [2] W Zhang, *J Nanoparticle Research*, **5** (2003) 323.
- [3] SM Ponder, JG Darab, TE Mallouk, *Environ Sci Technol*, **34** (2000) 2564.
- [4] F He, D Zhao, *Environ Sci Technol*, **39** (2005) 3314.

**Figure:**

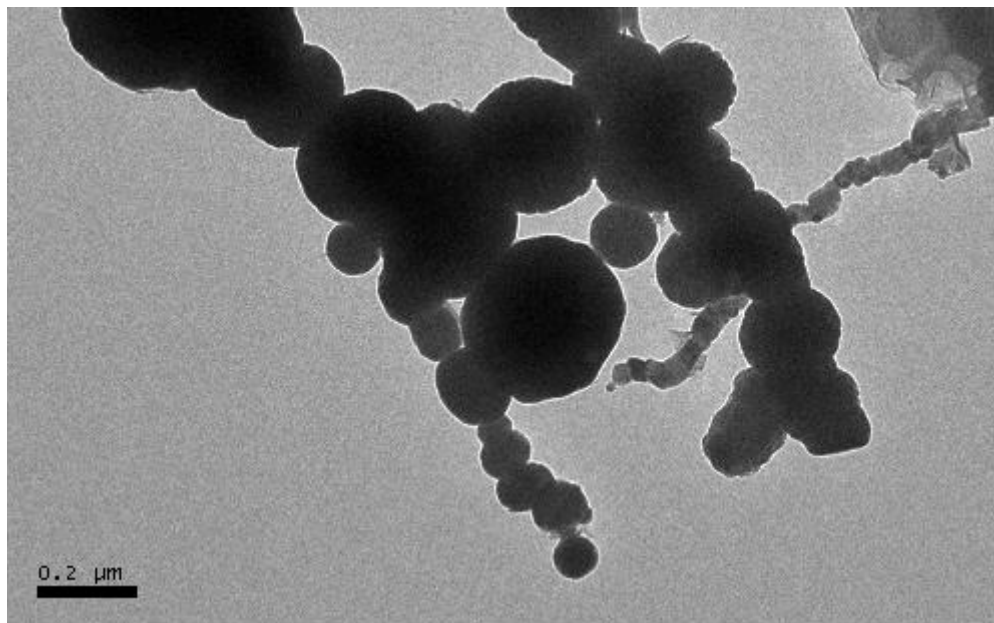


**Figure 1. TEM image of bare nZVI particles.**

## Tyrosinase-Gold Nanoparticles Conjugates on Nanostructured Gold Surfaces: Towards a Biosensor of Phenolic Compounds

*I. Gomes<sup>1</sup>, A. P. Serro<sup>2</sup>, A. P. Carapeto<sup>2</sup>, P. Paradiso<sup>3</sup>, J. Cortez<sup>1</sup>, S. Cardoso<sup>4</sup>, B. Saramago<sup>2</sup> and R. Franco<sup>1</sup>*

<sup>1</sup>*REQUIMTE, Departamento de Química, Faculdade de Ciências e Tecnologia, Universidade Nova de Lisboa, 2829-516 Caparica, Portugal*

<sup>2</sup>*Centro de Química Estrutural, Instituto Superior Técnico, Av. Rovisco Pais, 1049-001 Lisboa, Portugal*

<sup>3</sup>*Departamento de Engenharia de Materiais, Instituto Superior Técnico, Av. Rovisco Pais, 1049-001 Lisboa, Portugal*

<sup>4</sup>*Instituto de Engenharia de Sistemas e Computadores - Microsistemas e Nanotecnologias (INESC-MN) and Institute for Nanosciences and Nanotechnologies (IN, Associated Lab.), Rua Alves Redol 9, 1000-029 Lisboa, Portugal  
[inesgomes@dq.fct.unl.pt](mailto:inesgomes@dq.fct.unl.pt)*

The development of enzymatic biosensors based on the tyrosinase enzyme has attracted great interest for the detection of phenolic compounds (from, *e.g.*, pesticides, pollutants) in ground or wastewaters [1,2]. Our goal is to develop a biosensor based on conjugates of tyrosinase on gold nanoparticles (AuNPs), taking advantage of the high surface areas of AuNPs, its unique electrochemical properties and ideal protein conjugation chemistry afforded by suitable functionalization.

Self-Assembled Monolayers (SAM) of thiolates form nanostructured surfaces with a diversity of functionalities and chemical characteristics that can favor the immobilization of enzymes in gold surfaces [3]. The immobilization of enzymes and bioactive conjugates in this type of nanostructured gold surfaces is a highly suited strategy for the development of biosensors with high activity and specificity.

In the present work, the immobilization of tyrosinase-AuNP conjugates on SAMs of alkanethiols on nanostructured gold surfaces was studied by Quartz Crystal Microbalance (QCM) and Atomic Force Microscopy (AFM). AuNPs were functionalized with mercaptoundecanoic acid (MUA) and conjugated with tyrosinase. Tyrosinase (1.14.18.1) is a copper monooxygenase that catalyzes the *o*-hydroxylation of monophenols and the oxidation of *o*-diphenols to *o*-quinones. It contains a dicopper 2<sup>+</sup> center and its structure is found in three forms: *met*-tyrosinase, *oxi*-tyrosinase and *deoxy*-tyrosinase [4]. Conjugates were adsorbed on the surface of the piezoelectric quartz crystal coated with nanostructured gold, and the change in mass was measured as a shift in the oscillation frequency [5]. The alkanethiols used to build the different SAMs at the gold crystal surface have terminal groups with different chemical characteristics, namely cationic (11-amino-1-undecanethiol hydrochloride) or anionic (MUA).

The catalytic activity of the enzyme adsorbed on to the gold crystal was measured using a spectrophotometric assay to detect the formation of reaction products.

Preliminary QCM results show that the tyrosinase-gold nanoparticles conjugates have a high adsorption on the surface of the gold crystal (Figure 1) comparatively with the deposition of the gold nanoparticles on the cationic SAM.

The AFM images show a high immobilization of the conjugates on the cationic SAM on gold surface, when compared with the Au surface or cationic SAM on Au surface.

**References:**

- [1] Kim, G. *et al.*, *J. Environ. Monit.*, **10**, (2008), 632-637.
- [2] Abdullah, J. *et al.*, *Sensors and Actuators B*, **114**, (2006), 604-609.
- [3] Love, J.C. *et al.*, *Chem Rev.*, **105**, (2005), 1103-70.
- [4] Gormally, M. V. *et al.*, *Langmuir*, **25**, (2009), 10014-10019.
- [5] Gispert, M.P. *et al.*, *Surf. Interface Anal.*, **40**, (2008), 1529-1537.

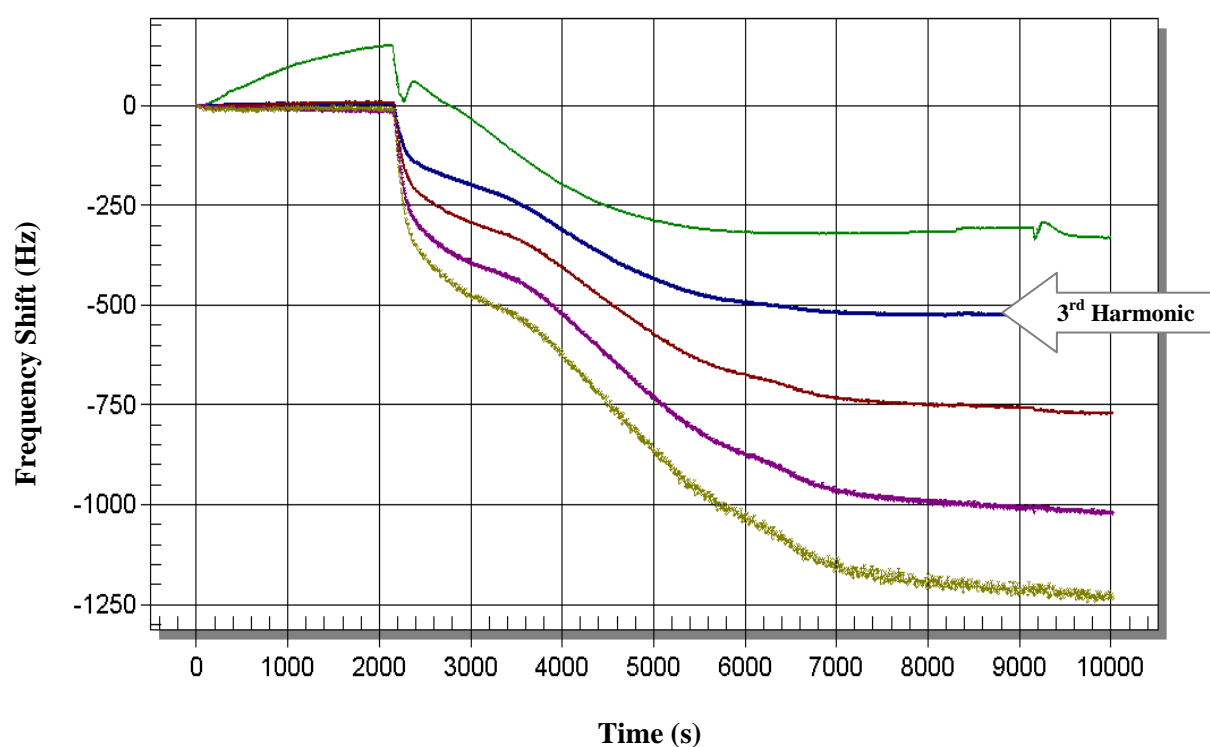


**Figure 1.** QCM profile for the deposition of the tyrosinase-AuNP conjugates on the cationic SAM on a gold crystal.

## Layer-by-Layer deposition of antimicrobial nanolayers on natural fibres

Ana P. Gomes<sup>1</sup>, João F. Mano<sup>2</sup>, João A. Queiroz<sup>3</sup>, Isabel C. Gouveia<sup>4</sup>

<sup>1</sup>Optical Centre, University of Beira Interior, 6201-001 Covilhã, Portugal

<sup>2</sup>IBB, 3B's Research Group, AvePark, Guimarães, Portugal

<sup>3</sup>Health Sciences Research Centre, University of Beira Interior, 6201-001 Covilhã, Portugal

<sup>4</sup>R&D Unit of Textile and Paper Materials, University of Beira Interior, 6201-001 Covilhã, Portugal

E-mail address: anapaula@ubi.pt

### Background:

The number of biofunctional textiles with an antimicrobial activity has increased considerably over the last few years [1,2,3]. Application is nowadays extended to biomedical products that will perhaps be the largest application of antimicrobial textiles [4,5]. Although synthetic antimicrobial agents used in textiles are very effective against a wide range of microorganisms, wearing these textiles can generate problems since health and environment risks can occur. In addition, the use of antimicrobial textiles in a continuous manner can lead to sensitization and bacterial resistance [1,4].

To minimize such risks, there is a great demand for antimicrobial textiles based on non-toxic and ecofriendly agents [6]. The relatively lower incidence of adverse reactions of natural products as compared to synthetic pharmaceuticals can be exploited as an attractive ecofriendly alternative for textile applications [6]. The Layer-by-Layer self assembly method (LbL) may provide new coatings or films that can be constructed by the alternate adsorption of oppositely charged polyelectrolytes at the surface of the material, easily obtained when the material is dipped in polyelectrolyte solutions, as first described by Decher and co-workers[7]. A deposition cycle creates a bi-layer and these cycles can be repeated as often as needed [8]. This opens the possibility of developing new functional textiles for biomedical applications.

Therefore, here we report the first results regarding the feasibility of LbL deposition of nanolayers of natural bioactive polyelectrolytes, to give antimicrobial properties to textiles.

### Materials and Methods:

The 2,2,6,6 – Tetramethyl-1-piperidinyloxy, free radical (TEMPO), Sodium Bromide, Sodium Hypochlorite 5%, Chitosan (CH) (low molecular weight), Acetic Acid, Alginate sodium salt (ALG), Sodium Chloride, Sodium Hydroxide and Hydrochloric acid were obtained from Sigma-Aldrich. All chemicals were of analytical grade and used as received. Chitosan (1 mg/mL), antimicrobial polyelectrolyte, and Alginate sodium salt (1 mg/mL) solutions were prepared by dissolving CH and ALG in 0.1 M CH<sub>3</sub>COOH and 0.5M NaCl solutions, respectively. The pH values were adjusted to 5 using 0,1M HCl and 1 N NaOH solutions.

To apply LbL technique, two samples of the substrate (cotton) were charged by immersing cotton samples in (TEMPO + NaBr + NaClO 5%, pH=10.5) solution under moderate stirring for 30 min and 120 min, respectively, followed by a rinse with deionized water, as described elsewhere [9,10]. Then, CH and ALG polyelectrolytes multilayer films were deposited over cotton by the LbL assembly where as CH was used as polycation and ALG as polyanion. For each layer deposition, the cotton substrate was immersed into the corresponding solution at room temperature and for 5 min, followed by rinsing with deionized water to remove the excess of polyelectrolyte. Since the cotton samples were charged negatively, the CH was deposited as the first layer. After the last deposition, the sample was dried in a desiccator at room temperature overnight

In order to monitor the LbL deposition of CH and ALG, three different methods were used: scan electron microscope (SEM) to evaluate surface changes of the fibers, color strength (K/S) using a reflectometer spectrophotometer, to evaluate the absorption of a cationic dye (Methylene blue), and Attenuated Total Reflectance FTIR, to evaluate chemical changes of the fibers.

The evaluation of the antibacterial activity of the functionalized samples was carried out according to the Japanese Industrial Standard JIS L 1902-2002, widely used for the antibacterial assessment of textile samples. The microorganisms selected include Gram-

positive and Gram-negative bacteria, *Staphylococcus aureus* and *Klebsiella pneumoniae*, respectively

### Results:

Figure 1 show the SEM microphotographs of the anionic cotton (controls), the (CH/ALG)<sub>5</sub> (5 cycles) samples and the samples that were washed after LbL deposition. The surface activation of cotton fibers by the TEMPO/NaBr/NaClO system under aqueous conditions, did not affect the original fibers since no damage can be observed (a). Moreover, the functionalized samples (CH/ALG)<sub>5</sub> show a large and heterogeneous deposition of polyelectrolytes (b). In contrast, the washed samples show a less but more uniform polyelectrolyte deposition (c).

Furthermore, the K/S values revealed a higher dye absorption on the treated fibers being in accordance with the higher deposition of CH/ALG layers, showing the success of the LbL assembly and fixation of those polyelectrolytes on the fibers.

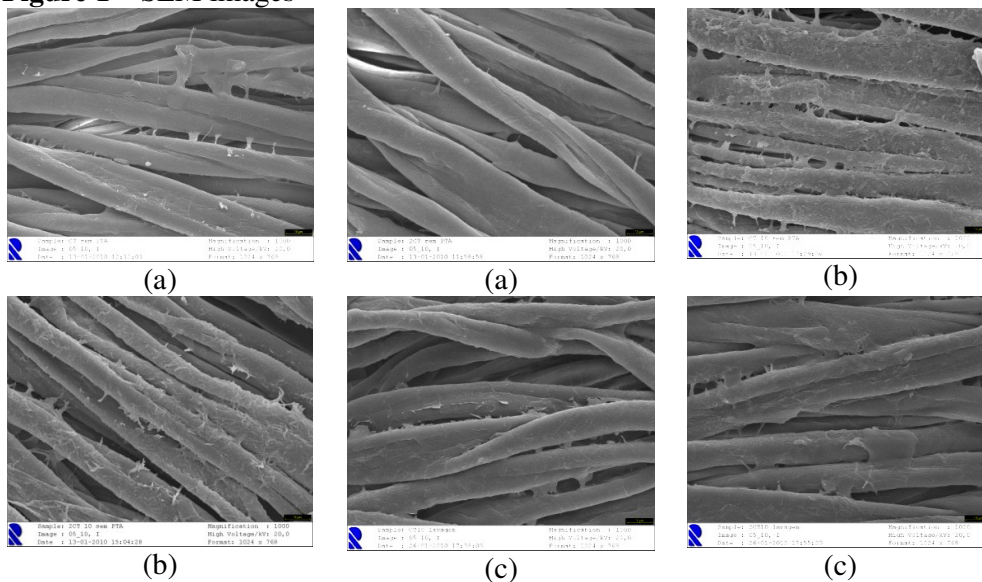
The results of the antibacterial assays against *S. aureus* and *K. pneumonia* revealed an antibacterial effect of LbL coated cotton textiles both for Gram-positive and Gram-negative bacteria. Further analysis, in particular, ATR FT-IR measurements will indicate the changes of surface chemistry.

Overall, the results showed a promising eco-friendly and simple technique to give textiles antimicrobial properties using natural antimicrobial agents. This method can open new avenues to the development of non-toxic and safe biomedical textiles.

### References:

- [1] Gao Y and Cranston R. Textile Research Journal **78-1**(2008) 68-72.
- [2] Papaspyrides CD, PavlidouS, Vouyiouka SN. J. Materials: Design and Applications. **223** (2009) 91-102
- [3] Singh R, Jain A, Panwar S, Gupta D and Khare SK. Dyes and Pigments **66** (2005) 99-102.
- [4] Kramer A, Guggenbichler P, Heldt P, Jünger M, Ladwing A, Thierbach H, Weber U and Daeshlein G. Biofunctional Textiles and the Skin. Curr Probl Dermatol. Basel, Karger, **33** (2006) 78-109
- [5] Zilberman M, Elsner J. Journal of Controlled Release **130** (2008) 202–215.
- [6] Joshia M, Wazed Ali S, Purwar R, Rajendran S. Indian Journal of Fibre & Textile Research **34** (2009) 295-304.
- [7] Decher, G.; Hong, J. D.; Schmitt, J. Thin Solid Films, **210-211** (1992) 831-835.
- [8] Ariga, K.; Hill, J.; Ji, Q. Phys. Chem. Chem. Phys., **9** (2007) 2319-2340.
- [9] Saito, T., Okita, Y., Nge, T., Sugiyama, J., Isogai, A. Carbohydrate Polymers **65** (2006) 435-440.
- [10] Dang, Z., Zhang, J., Ragauskas, A. Carbohydrate Polymers **70** (2007) 310-317

**Figure 1** – SEM images



## Strongly suppressed 1/f noise and enhanced magnetoresistance due to reduced interface mismatch in epitaxial Fe<V>/MgO /Fe magnetic tunnel junctions

*A. Gomez-Ibarlucea*<sup>1\*</sup>, *D. Herranz*<sup>1</sup>, *F. Bonell*<sup>2</sup>, *S. Andrieu*<sup>2</sup>, *C. Tiusan*<sup>2</sup>, and *F.G. Aliev*<sup>1</sup>

<sup>1</sup> Dpto. Física de la Materia Condensada, C-III, Universidad Autónoma de Madrid, 28049 Madrid, Spain

<sup>2</sup> Laboratoire of Physique des Matériaux, UMR CNRS 7556, Nancy Université, Vandoeuvreles-Nancy Cedex, France

(\*) [andres.gibarlucea@uam.es](mailto:andres.gibarlucea@uam.es)

It is well known that there is a small (about 4%) lattice mismatch between Fe and MgO that induces stress within MgO barrier, which is usually relaxed via dislocations and defects. These are responsible for the reduced TMR below its maximum value and also determine substantially the defect related 1/f noise. Recent attempts [1] to increase the tunnelling magnetoresistance (TMR), but only for relatively thick MgO barriers, have been focused on implementing some Fe alloy as ferromagnetic electrode to reduce the interface lattice mismatch.

In accordance with the previous report [1] alloying of Fe with V for the bottom electrode slightly improves the TMR value (Fig. 1a). We have also studied the evolution of the coercive field of soft and hard layers as function of the V doping (Fig 1b). Our findings suggest that changing the Vanadium doping of the electrodes we could tune TMR and modify the coercive field of the ferromagnetic layers.

The main result of our studies is experimental observation that the alloying of the Fe with V, through the reduced FeV/MgO interface mismatch in epitaxial magnetic tunnel junctions (MTJ's) with MgO barriers, notably suppress both nonmagnetic (parallel state) and magnetic (antiparallel state) normalised 1/f noise as well as enhances the TMR. Comparative study of the room temperature electron transport and low frequency noise in Fe<sub>1-x</sub>V<sub>x</sub>/MgO/Fe and Fe/MgO/Fe<sub>1-x</sub>V<sub>x</sub> MTJs with (0<x<0.25) reveals that relatively small Vanadium doping of the bottom electrode for x<0.16 reduces the normalized nonmagnetic 1/f noise (Hooge factor) in nearly 2 orders of the magnitude with moderate (about 10 %) increase of the TMR (Fig 2a). We attribute the enhanced TMR and suppressed 1/f noise to reduced misfit and dislocation densities. We also note that the doping provides minimum values of the nonmagnetic noise also corresponds to the maximum TMR values of about 200%.

For the further doping we found that the normalized nonmagnetic noise increases its value and the TMR decreases (Fig.2). Although the previous work [1] has demonstrated that increasing x should continue to decrease the lattice mismatch, we think that these results might be related to an increased structural disorder at FeV/MgO interface with increasing number of Fe or V atoms located in the metastable states. On the other side, we show that Vanadium substitution of the upper electrode results in a gradual suppression of the TMR and increasing of the nonmagnetic noise which is in accordance with structural analysis indicating growing influence of accumulated disorder with vanadium concentration for Fe/MgO/Fe<sub>1-x</sub>V<sub>x</sub> MTJs [1].

Finally, it is interesting to mention that, in the opposite to what could be expected from the previous reports observed the strong excess of the magnetic noise to be correlated with the bias dependence of TMR [2] pointing on the spin polarised electrons as a main source of the 1/f noise, in our experiment find an *increase of the TMR* value due to the Vanadium doping

accompanied by a strong decrease of the magnetic noise (Hooge in antiparallel state) (Fig. 2). This might indicate on the defects in the barrier as one of the sources of magnetic contribution to the  $1/f$  noise.

This work was supported by MICINN (MAT2009-10139), Consolider (CSD2007-00010), Integrated Action Project (France-Spain FR2009-0010) and CAM (P2009/MAT-1726).

## References:

- [1] F. Bonell et al. . IEEE TRANSACTIONS ON MAGNETICS, 45, **10** (2009), 3467.  
 [2] F.G. Aliev, R. Guerrero, D. Herranz, R. Villar, F. Greullet, C. Tiusan and M. Hehn , Appl. Physics Letters **91**, (2007), 232504.

## Figures:

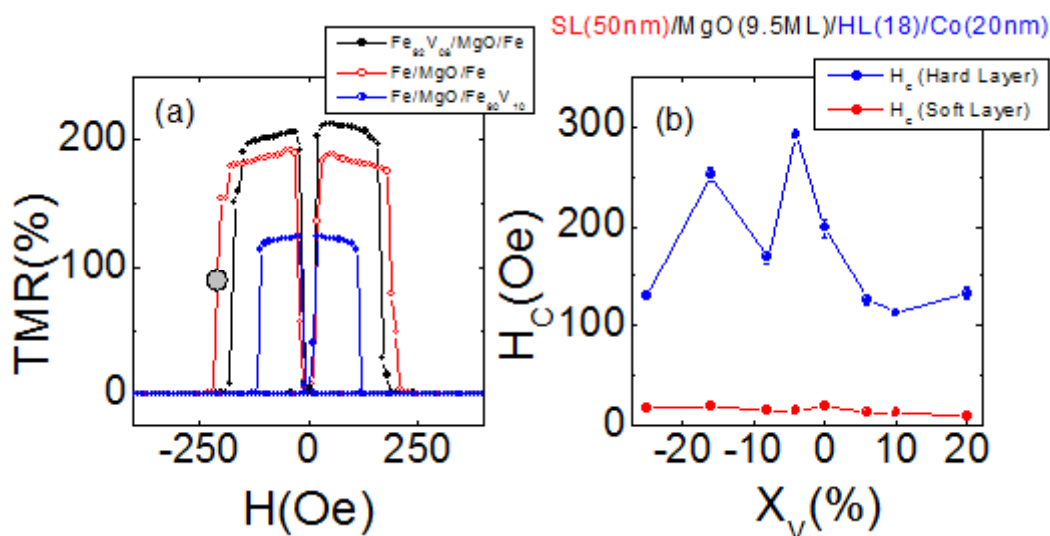


Figure 1 (a) Representative zero bias magnetoresistance for Fe<sub>0.92</sub>V<sub>0.08</sub>MgO/Fe (bottom electrode doped), Fe/MgO/Fe (non doped) and Fe/MgO/Fe<sub>0.9</sub>V<sub>0.1</sub> MTJs. (top electrode doped). (b) Averaged over samples coercive (switching as marked by gray dot) fields of the hard (upper) and soft (bottom) layers as a function of Vanadium concentration. Negative x values correspond to bottom, while positive to the upper electrode Vanadium concentration.

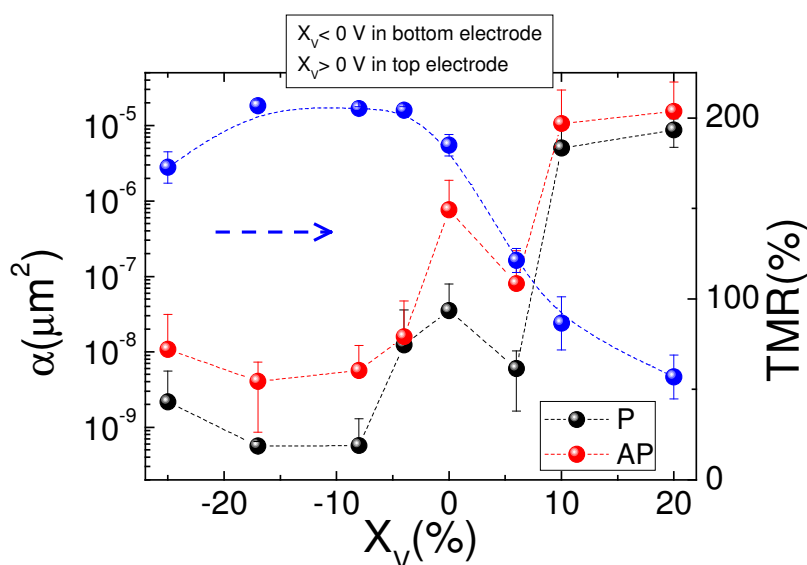


Figure 2: It is shown the variation of the averaged within each set of samples TMR and normalized  $1/f$  noise (Hooge parameter) with V substitution of bottom (negative x values) and upper (positive x values) electrodes.

## EFFECT OF IRS-4 KNOCK-DOWN IN PRO-APOPTOTIC TREATMENT BASED ON CARBOSILANE DENDRIMERS AS TRANSFECTION AGENTS IN HEPG2 CELLS.

S. García-Gallego<sup>a</sup>, B. Rasines<sup>a,c</sup>, V. Sánchez-Alonso<sup>b</sup>, R. Gómez<sup>a,c</sup>, L. G. Guijarro<sup>b</sup>, F. J. de la Mata<sup>a,c</sup>.

<sup>a</sup> Inorganic Chemistry Department, Universidad de Alcalá, E28871 Alcalá de Henares (Madrid), Spain. Email: javier.delamata@uah.es

<sup>b</sup> Biochemistry and Molecular Biology, Universidad de Alcalá.

<sup>c</sup> Networking Research Center on Bioengineering, Biomaterials and Nanomedicine (CIBER-BBN), Spain

### INTRODUCTION

Insulin receptor substrate-4 (IRS-4) is a scaffold protein that mediates the action of insulin and insulin-like growth factor-I (IGF-I) (a liver antiapoptotic factor) (1, 2). The knock-down of this protein in HepG2 cells leads to a sensitizing of the cells to several therapeutic drugs, by diminishing its protection to oxidative stress (3). The use of RNA interference as a technique for knocking-down proteins is principally limited by an effective delivery of siRNA into the target cells. Dendrimers are nanoparticles that are increasingly being used as oligonucleotide and drug delivery vehicles.

### RESULTS AND DISCUSSION

We present ammonium-terminated carbosilane dendrimers (CBS) (4,5) as a novel way to protect and transport siRNA in HepG2.

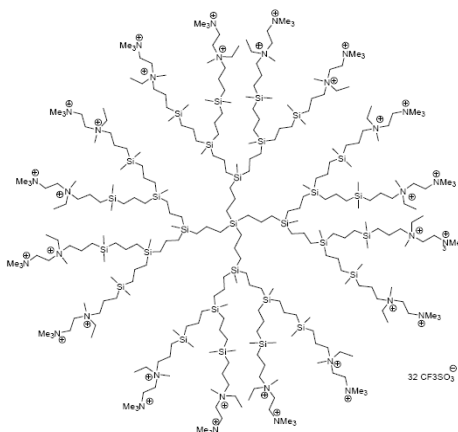


**Figure 1.** Carbosilane dendrimer on its third generation, 3G-CNN32,CF3SO3.

Initially, cytotoxicity assays of CBS in HepG2 revealed lower levels of toxicity, compared to usual commercial agents, such as Oligofectamine and Lipofectamine 2000. It was also demonstrated, by Western Blot, that CBS/siRNA dendriplexes transfected HepG2 and silenced IRS-4 expression. The second generation of the dendrimer with +/- charge ration of 2, was determined to have the highest transfection efficiency, while maintaining the lowest level of toxicity in these systems. Finally, it was demonstrated that transfected cells were up to 46% more sensitive to the pro-apoptotic treatment.

### References:

1. E. Cuevas et al. *J. Hepatol.*, 2007, 46, 1089-1098.
2. O. Escribano et al. *Hepatology*, 2003, 37, 1461-1469.
3. E. Cuevas et al. *J. Cell. Biochem.* 2009, 108, 1292-1301.
4. N. Weber et al. *J. Cont. Release*, 2008, 132, 55-64.
5. B. Rasines et al. *Dalton Transactions*, 2009, 40, 8704-8713.

**Magnetization process and magnetoresistance in tailored arrays of CoNi nanowires**

*L.G. Vivas<sup>a</sup>, M.Vázquez<sup>a</sup>, O. de Abril<sup>a</sup>, V.M. Prida<sup>b</sup>, V. Vega<sup>b</sup>*

*a) Instituto de Ciencia de Materiales, CSIC, 28049 Madrid, Spain*

*b) Departamento de Física, Universidad de Oviedo, 33007 Oviedo, Spain*

*[lauragv@icmm.csic.es](mailto:lauragv@icmm.csic.es)*

Dense arrays of magnetic nanowires prepared using suitable templates (i.e., electrochemical route) are receiving lately remarkable attention due to their unique physical and chemical properties which lead to a wide range of technological applications including various families of sensors, biomedical applications after suitable functionalization and high-density magnetic storage media<sup>1</sup>. Usually, due to the dominant shape anisotropy, magnetic nanowires are mainly magnetized along their axis. However, in particular cases, as for Co nanowires, magnetization can lie in a transverse orientation induced by their large magnetocrystalline anisotropy<sup>2</sup>.

Electrochemical conditions of preparation of arrays of nanowires inside anodic alumina templates play a decisive role to determine the magnetization easy axis. In this work, besides of the usual procedure of changing the nanowire physical dimensions, we chose to modify the CoNi-alloy composition introducing small amounts of Ni. In this way, we can control effectively the easy axis magnetization orientation and thus its magnetic properties.

Cylindrical pores in the anodic alumina template exhibit a self-organized hexagonal arrangement, which geometrical features are in the present case: 35 nm in diameter, 105 nm of interpore distance, and typically 1  $\mu\text{m}$  deep. CoNi nanowire arrays were electrodeposited into the anodic alumina templates, using suitable electrolytic baths<sup>3</sup>. Ni and Co nanowires were also deposited as reference samples. A thorough characterization of samples morphology and composition was performed using SEM (inset bottom) and XRD (inset up-right) techniques.

Hysteresis loops (M vs. H) measurements have been performed in a VSM magnetometer, and a detailed study of the M(H) curves dependence on the direction of the applied magnetic field (relative to the nanowires axis) is presented. In addition, magnetoresistance measurements (MR vs. H) were also performed as a function of the orientation of the applied field to determine its anisotropic behaviour (inset up-left). In this case, as top and bottom electrodes we used Au, thus enabling improved quality electrical contacts.

The results are discussed in terms of two distinct magnetization reversal mechanisms: coherent rotation and curling<sup>4</sup>, as can be derived from the angular dependence of the switching field. As the Ni content in CoNi alloy increases, from the angular dependence of the switching field we deduce a change in the reversal mechanism from curling to coherent rotation. This is further confirmed by the magnetoresistance (MR) measurements, where the bell-shape MR curve is ascribed to rotation mechanisms.

**References:**

[1] A. Fert, Rev. Mod. Phys., **80** (2008) 1517.

[2] Kleber R. Pirota and Manuel Vazquez, Advanced Engineering Materials, **12** (2005) 1113.

- [3] Kleber R. Pirota, Elvis L. Silva, Daniela Zanchet, David Navas, Manuel Vázquez, Manuel Hernández-Vélez and Marcelo Knobel, *Phys. Rev. B.*, **76** (2007) 233410.  
 [4] X. Tang, G. Wang, M. Shima, J. Mag. Magn. Mat., **309** (2007) 188.

**Figure:**

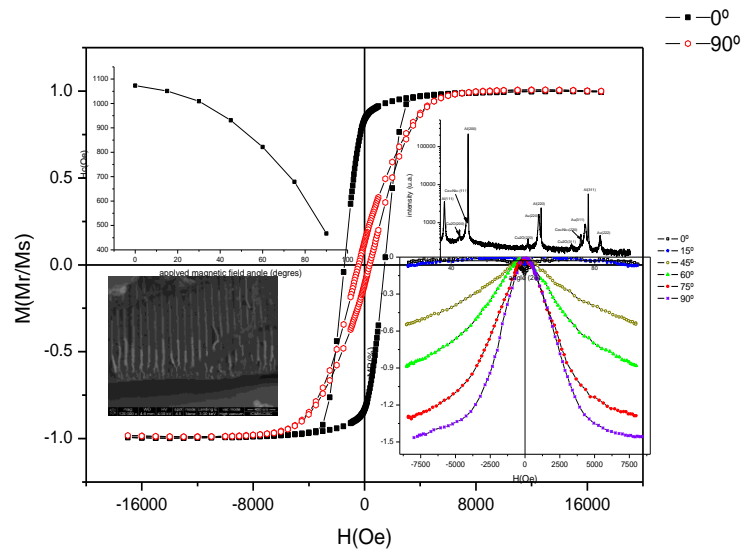


Fig 1: In-plane ( $0^\circ$ ) and out-of-plane ( $90^\circ$ ) hysteresis loops of CoNi nanowire arrays. Insets show coercivity variation with applied magnetic field angle (up-left), XRD pattern (up-right), SEM image (bottom-left) and MR curves (bottom-right).

## Synthesis of Substituted Tripod-Shaped Tri(*p*-phenylene)s

Jesús Hierrezuelo,<sup>1</sup> Elena Guillén,<sup>1</sup> J. Manuel López-Romero,<sup>\*1</sup> Rodrigo Rico,<sup>1</sup> M. Rosa López-Ramírez,<sup>2</sup> J.

Carlos Otero,<sup>2</sup>

<sup>1</sup> Dept. de Química Orgánica, Facultad de Ciencias, Universidad de Málaga, 29071 Málaga, Spain

<sup>2</sup> Dept. de Química Física, Facultad de Ciencias, Universidad de Málaga, 29071 Málaga, Spain

E-mail: [elenguillen@uma.es](mailto:elenguillen@uma.es)

For the development of organic thin films with applications in the construction of molecular scale devices it is needed *i*) the control of the orientation and spacing between functional groups in the film, *ii*) the availability of methods for the effective derivatization of the modified surface, and *iii*) for biological applications, the surface should resist the non-specific protein adsorption in order to avoid sensor contamination.<sup>1</sup>

We report here the synthesis of several tripod-shaped oligo(*p*-phenylene)s with each tripod leg composed of three or four phenylene units. Each leg is end-capped with an iodine atom, TMS or carboxyl group, and an ethoxy group is present at the functional arm. One of the tripods presents a methoxylated side substitution (Figure 1). The key step of the synthesis is the Pd-catalyzed Suzuki cross-coupling reaction<sup>2</sup> of the silicon derivative core molecule with the appropriate substituted *p*-biphenyl moiety. This synthesis represents a new and convergent strategy since iterative coupling of the substituted biphenyl building blocks with the first-generation tripods will allow the homologation of the tripod legs to reach giant tripod-shaped oligo(*p*-phenylene)s. Also, the iodine end-capped leg and the ethoxy group at the functional arm permit the design of the tripod for the nanostructuring of different surfaces and applications.<sup>3</sup> Geometry of some of the synthesized tripods was optimized by theoretical calculations (B3LYP/6-31G level of theory) combined with the analysis of their Raman bands.

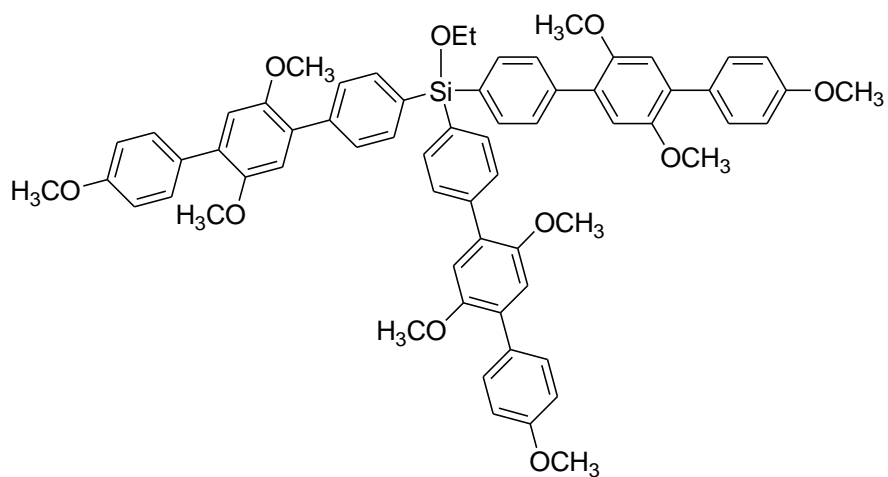
### References:

[1] (a) *Organic Thin Films for Waveguiding Nonlinear Optics*; Kajzar, F.; Swalen, J. D.; Eds.; Gordon & Breach: Amsterdam, **1996**. (b) Southern, E.; Mir, K.; Shchepinov, M. *Nat. Genet.* **1999**, *21*, 5-9. (c) Houseman, B. T.; Mrksich, M. *Angew. Chem., Int. Ed.* **1999**, *38*, 782-785.

[2] Miyaura, N.; Suzuki, A. *Chem. Rev.*, *95*, **1995**, 2457-2483

[3] (a) López-Romero, J. M.; Rico, R.; Martínez-Mallorquín, R.; Hierrezuelo, J.; Guillén, E.; Cai, C.; Otero, J. C.; López-Tocón, I. *Tetrahedron Lett.* **2007**, *48*, 6075-6079. (b) López-Tocón, I.; Peláez, D.; Soto, J.; Rico, R.; Cai, C.; López-Romero, J. M.; Otero, J. C. *J. Phys. Chem.* **2008**, *112*, 5363-5367. (c) Deng, X.; Mayeux, A.; Cai, C. *J. Org. Chem.* **2002**, *67*, 5279-5283. (d) Deng, X.; Cai, C. *Tetrahedron Lett.* **2003**, *44*, 815-817.

Figures 1



## Development of Nanoencapsulates for Nutritional Use

R. Rojo<sup>1</sup>, M<sup>a</sup> L. Mussons<sup>1</sup>, P. Gatón<sup>1</sup>, G. Antolín<sup>2</sup>, F. J. Gutiérrez<sup>1\*</sup>

<sup>1</sup>División Químico-Alimentaria, CARTIF Centro Tecnológico. Parque Tecnológico de Boecillo, parcela 205. 47151 Boecillo (Valladolid) España

<sup>2</sup>Dpto. de Ingeniería Química y Tecnología del Medio Ambiente. E.T.S.I. Industriales. Universidad de Valladolid. Paseo del Cauce s/n. 47011 Valladolid España  
[fragut@cartif.es](mailto:fragut@cartif.es)

Fundación CARTIF is a leading Applied Research Centre created in 1994 as a non-for-profit association focused on applied research in Boecillo, Valladolid, Spain. In October 2005, it was established as a Foundation. In 2009 CARTIF carried out 127 R&D and innovation projects and served 124 customers, enjoying a total income up to 13,74 m€. Nowadays, CARTIF is formed up by 200 people, mainly engineers, scientists and senior researchers and has an international dimension with 21 international projects out of the 2009 projects, with partners in almost all the EU-25 countries, the non-EU Mediterranean ones and Latin America.

**Fundación CARTIF** coordinates and participates in **DINAMO Project (Development of nanoencapsulates for Nutritional Use)** in cooperation with other four Spanish Technological Centres: Centro Nacional de Tecnología y Seguridad Alimentaria (CNTA), Navarra, Asociación de Investigación de la Industria Agroalimentaria (AINIA), Valencia, AZTI Tecnalia, País Vasco and the Instituto de Biotecnología, (INBIOTEC), León.

The main project objective is the implementation of techniques and procedures, which should allow applying nanotechnology in the food sector. It is expected the development of nanoencapsules containing active compounds to be used as additive.

Specially, protection to active compounds such as beta-carotene, docosahexaenoic acid and casein phosphopeptides is searched using covering materials as milky proteins ( $\beta$ -lactoglobulin, casein) or cyclodextrins, which allow to reach nanometric size without jeopardizing safety in human food.

The Project development steps are:

- Development of encapsulating technology. Evaluation of encapsulating bottom-up strategies mainly in order to obtain nanoencapsulates with possible nutritional use.
- Characterisation of the obtained encapsulates. During the Project development characterisation methods as Dynamic Light Scattering (DLS), Environmental Scanning Electron Microscopy (ESEM) and Size Exclusion Chromatography (SEC) were set to measure nanoparticles size and weight. Laser Doppler Velocitometry (LDV) technology was used to foresee suspended nanoparticles stability by means of the Zeta potential.
- Nanoencapsulates industrial feasibility was studied. An economical assessment of the selected techniques from the food process point of view will be carried out.
- Evaluation of nutritional safety and health aspects. Concerning nanoparticles safety in food uses, the (CE) 1333/2008 and (CE) 258/97 regulations of European normative state that every new food has to proof harmlessness before its commercialization. In the project, particularly, *in vivo* toxicity tests are being carried out with embryos of zebra fish to assess the toxicity of the nanoparticles.

This Project is granted by the Science and Innovation Office with the 2008-2011 National Programme of Applied Research, Applied Research - Technology Centre Subprogramme.



**Shaking molecules: detection of defects in SAMs of aliphatic amines with jumping mode AFM**

*José A. Heredia-Guerrero<sup>1</sup>, Miquel Salmerón<sup>2</sup>, Jesús J. Benítez<sup>1</sup>*

*<sup>1</sup>Instituto de Ciencia de Materiales de Sevilla. Centro Mixto CSIC-Universidad de Sevilla. Centro de Investigaciones Científicas Isla de la Cartuja. Avda. Americo Vespuccio 49, 41092 (Sevilla). Spain.*

*<sup>2</sup>Materials Sciences Division, Lawrence Berkeley National Laboratory, Berkeley, USA, and Materials Science and Engineering Department, University of California, Berkeley, USA*  
[alejandrohg@cartuja.csic.es](mailto:alejandrohg@cartuja.csic.es)

The alkylamine SAM formation on mica has been described as a two stage process [1]. The first one is relatively fast and comprises molecular adsorption on the substrate through an acid-base reaction, a process that is exclusively conditioned by the direct interaction between the amino end group and the adsorption sites on mica. The second stage is slow and consists in the diffusion and aggregation of scattered adsorbed molecules into self-assembled island takes place. This second stage is dominated by the attractive van der Waals interactions between alkyl chains and, consequently, is faster for longer chain alkylamines. In humid environments this accretion stage is followed by another very slow process characterized by molecular tilting within the islands. This was modeled by the penetration of water that from the environment, which protonates the amino groups and gives rise to an electrostatic repulsion.

In the present study, we have studied the effect of mechanical energy transfer from the tip of an Atomic Force Microscope (AFM) on the dynamics of self-assembly of a monolayer film of octadecylamine on mica, using jumping mode AFM [2]. The formation of the self-assembled film proceeds in two successive stages, the first being the fast adsorption from solution, which can be described by a Langmuir isotherm. This is followed by a second stage of slow aggregation and island growth. The dynamics of the second process can be altered by the addition of mechanical energy into the system through controlled tip-surface interactions. This leads to either the creation of pinholes as a consequence of vacancy concentration in defect-rich regions, as well as to the opposite phenomenon, the assembly of residual scattered molecules into more compact islands.

**References:**

- [1] Benítez J.J., Salmeron M., *J. Chem. Phys.*, **125** (2006) 044708.  
[2] de Pablo P.J., Colchero J., Gómez-Herrero J., Baró A.M., *Appl. Phys. Lett.*, 73 (1998) 3300

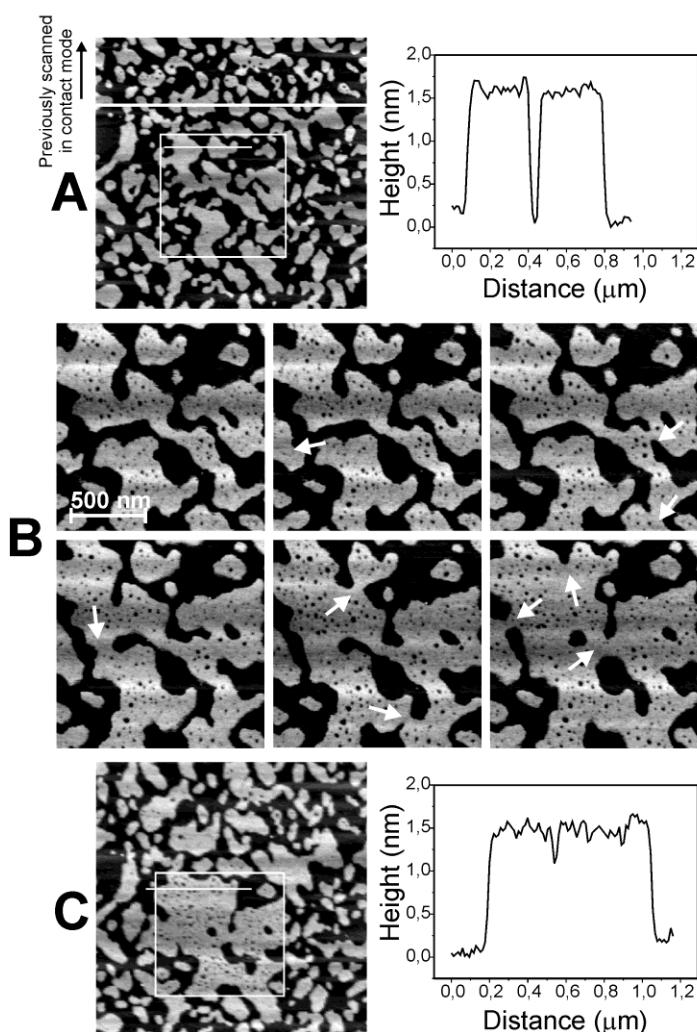


**Figure.** Topographic AFM image obtained in jumping mode over octadecylamine SAM islands on mica previously and partially scanned in contact mode by applying a positive 0.5nN force. The white horizontal line is the limit between the contact (upper part) and the contact preserved sides (lower part). Contact mode imaging causes island damage that is not observed when switching to jumping mode with identical set point. The image shows the initial stages of island aggregation. When the area marked by the white square is successively scanned in jumping mode (by increasing the set point to 2nN), pinholes and aggregation points (marked by arrows) are created (B). Images corresponds to 11, 15, 19, 21, 27 and 33 accumulated scans respectively (in each scans, every point is sampled four times). When the repetitive cycle ends, a larger range scan (jumping, set point 0.5nN) allows to distinguish the induced island aggregation at the repeatedly scanned area. Line profiles indicate no modification of island height along the experiment. The sample is prepared from an octadecylamine 15 mM solution and ripened for 48 hours.

## Oscillatory dependence of magnetoresistance with bias voltage in Fe/MgO/Fe/MgO/Fe epitaxial double magnetic tunnel junctions with dielectric breakdown

*D. Herranz<sup>1\*</sup>, F. Greullet<sup>2</sup>, C. Tiusan<sup>2</sup>, M. Hehn<sup>2</sup>, F.G. Aliev<sup>1</sup>*

<sup>1</sup> *Dpto. Física de la Materia Condensada, CIII, Universidad Autónoma de Madrid, 28049 Madrid, Spain*

<sup>2</sup> *Laboratoire of Physique des Materiaux, UMR CNRS 7556, Nancy Universite, Vandoeuvreles-Nancy Cedex, France*

(\* Presenting author: [david.herranz@uam.es](mailto:david.herranz@uam.es))

Double magnetic tunnel junctions present novel promising for applications devices in which electron transport through central nanometer size magnetic electrode could be influenced by charge quantization, quantum well effects, spin accumulation and spin torque.

Here we present detailed investigation at the room temperature electron transport in epitaxial Fe(100)/MgO/Fe/MgO/Fe double magnetic tunnel junctions (DMTJ's) with dielectric breakdown in the barrier. Figure 1 shows magnetization of the MTJs, it's TEM (Transmission Electron Microscopy) analysis and tunneling magnetoresistance (TMR) at room temperature. The reduced TMR is due the Nitrogen doping of the barrier which reduces effective barrier height of MgO and therefore minimizes the possible damage from the breakdown over the flatness of the central Fe electrode. As a consequence, the breakdown voltage of the barrier was always essentially below 1V. The tunnel magneto resistance (TMR) at zero bias in our "fresh" samples is close to 30% (Fig.1), however after application of about ~500mV the TMR decreases down to 4%. The change in the TMR and the magnetic transitions for the three electrodes, as shown in Fig.2, indicate indirectly that the dielectric breakdown in the barrier decreases the effective MgO thickness. We believe that the breakdown of the doped MgO barrier could result in the local displacement of the atoms where a local amorphization in the barrier appears near "hot-spot" concentrating the current. For the DMTJ's with "pinhole" we observed periodic changes in resistance as a function of bias voltage which are in satisfactory agreement with recent first principal calculations by Wang *et al.* [1], that considering formation of quantum well states in the middle Fe free layer (see arrows in Fig. 3). The bias dependence of the tunneling magnetoresistance varies strongly with the direction of external magnetic field indicating possible local spin torque effects in the breakdown region

In conclusions, the oscillatory dependent TMR in the DMTJ's with dielectric breakdown indicate the local resonant tunneling through the quantum well states in the middle free layer, possibly affected by spin torque effects. A simple model which suggests local amorphization of the MgO barrier and intact central free Fe layer close to the breakdown region qualitatively explains the main experimental observations.

This work was supported by MICINN (MAT2009-10139), Consolider (CSD2007-00010), Integrated Action Project (France-Spain FR2009-0010) and CAM (P2009/MAT-1726).

### References:

- [1] Y. Wang, Z.-Y. Lu, X. Zhang, X. Han, Phys. Rev. Lett. **97**, 087210 (2006)
- [2] T. Nozaki, N. Tezuka, K. Inomata, Phys.Rev.Lett. **96**, 027208 (2006)
- [3] I. Theodonis, A. Kalitsov, N. Kioussis, Phys.Rev.**B76**, 224406 (2007)

Figures:

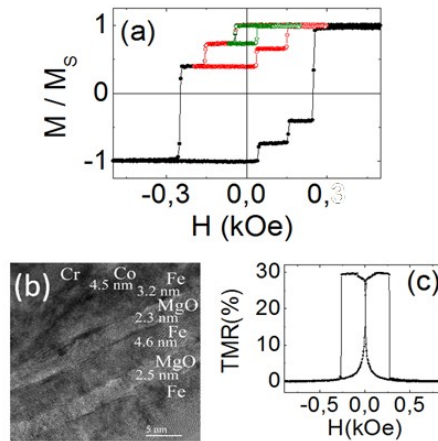


FIG.1 (a) Magnetization vs. field for unpatterned DMTJ. The black line corresponds to the top electrode, the green to the middle and the red to the bottom electrode. (b) Cross-sectional TEM image of the DMTJ. (c) Typical zero bias TMR measured before the breakdown.

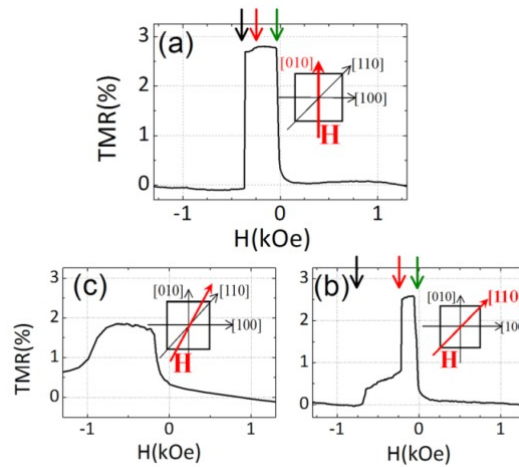


FIG.2 Zero bias TMR after breakdown: (a-c) show correspondingly TMR measured with magnetic field applied along the (easy axis (EA), hard axis (HA) and intermediate state (IA), respectively. The arrows show the coercive field of the different layers (green for the middle, red for the bottom and black for the top electrodes).

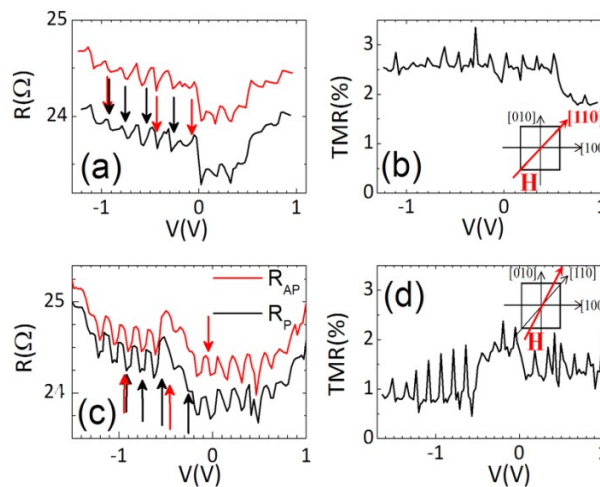


FIG.3 (a), (c) Resistance vs. bias measured for parallel (black line) and antiparallel (red line) states with magnetic field applied along the HA and IA respectively. The arrows show the theoretical predictions by Wang *et al.* [1] for the resonant tunneling in the parallel state with QWS above (red arrows) and below (black arrows) Fermi level. Parts (b,d) show TMR vs. bias for magnetic field applied along the HA and IA directions.

## Modification of a Regenerated Cellulose Membrane with Lipid Nanoparticles and Layers. Nanoparticle Preparation, Morphological and Physicochemical Characterization of Nanoparticles and Modified Membranes.

*J. Hierrezuelo<sup>1</sup>, J. Benavente<sup>2</sup>, M. I. Vazquez<sup>2</sup>, R. Rico<sup>1</sup>, E. Guillén-Ruiz<sup>1</sup>, J. M. López-Romero<sup>1</sup>, M. R. López-Ramirez<sup>3</sup>.*

*<sup>1</sup>Departamento de Química Orgánica, <sup>2</sup>Departamento de Física Aplicada I, <sup>3</sup>Departamento de Química Física. Facultad de Ciencias. Universidad de Málaga. E-29071 Málaga. Spain. [jhierrezuelo@uma.es](mailto:jhierrezuelo@uma.es)*

The modification of solid substrates and membranes using biomaterials is an attractive field of research for developing new devices such as biosensors, structured multilayers or controlled-release delivery systems [1-3].

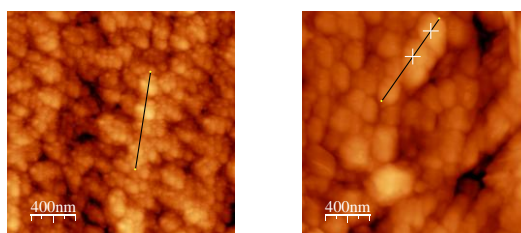
On the other hand, encapsulation technologies are utilized in the medical, pharmaceutical and cosmetic industries for the development of controlled-release delivery systems.

Ultrasound and high-pressure homogenized lipid (lecithin-triesterine) nanoparticles were prepared and embedded into a regenerated cellulose commercial membrane (RC-MD); this support was also modified by deposition of a lecithin-triesterine layer. The lipid nanoparticles, RC-support and modified membranes were topographically and chemically characterized by atomic Force Microscopy (AFM) and Raman spectroscopy. Electrical parameters (conductivity and capacitance) of both the original and modified membranes in the dry state were determined by the impedance spectroscopy (IS) technique using a parallel resistance-capacitance equivalent circuit as a model. The results allow the lipid particle inclusion to be distinguished from the lipid layer deposition. Moreover, the paper shows the possibility of lipid nanoparticle inclusion into a solid support whilst maintaining particle integrity.

### References:

- [1] C. M. Niemeyer, C. A. Mirking. Nanobiotechnology, Wiley-VCH, Weinheim, (2004).
- [2] D. S. Goodsell. Bionanotechnology, Wiley-Liss, New Jersey, (2004).
- [3] V. Kochev, M. Karabaliev. Wetting films of lipids in the development of sensitive interfaces. An electrochemical approach. *Adv. Colloid Interface Sci.* **107** (2004) 9-26.

### Figures:



## Engineering of gemcitabine-loaded poly(D,L-lactide-co-glycolide) nanoparticles by flow focusing for cancer treatment

Holgado M.A.<sup>1</sup>, Martín-Banderas L.<sup>1</sup>, Arias J.L.<sup>2</sup>, Alvarez-Fuentes J.<sup>1</sup>, Fernández-Arévalo M.<sup>1</sup>

<sup>1</sup>Department of Pharmacy and Pharmaceutical Technology, Faculty of Pharmacy, University of Seville, Spain.

<sup>2</sup>Department of Pharmacy and Pharmaceutical Technology, Faculty of Pharmacy, University of Granada, Spain.

holgado@us.es

### Introduction

Gemcitabine is a nucleoside analogue that despite its efficient antitumor activity, suffers from several drawbacks including a very short plasma half-life, thus generating the need to use high doses, simultaneously leading to severe dose-limiting side effects [1]. Drug delivery systems are intended to protect drugs from biological metabolization and elimination, and to induce the highest therapeutic effect with minimal toxicity [2, 3]. Recently [4, 5], we have developed a flow focusing (FF) method to encapsulate biomolecules into biodegradable poly(D,L-lactide-co-glycolide) (PLGA) particles. This technique allows the easy formulation of polymeric colloids with interesting drug carrying properties: more narrow size distribution particles, great drug entrapment efficiency and drug loading values and very slow (biphasic) drug release. In order to obtain gemcitabine-loaded PLGA nanoparticles with a narrow size distribution and the best drug loading properties, we investigated the best formulation conditions: the influence of the liquid flow rates of the FF device and the drug concentration.

### Materials and Methods

*Synthesis of the gemcitabine-loaded PLGA nanoparticles:* a water-in-oil emulsion was prepared by mixing appropriate volumes of a gemcitabine aqueous solution with 1 mL of a 1 % (w/v) PLGA and 0.5 % (w/v) Ethocel solution in ethyl acetate. This emulsion was used as focused fluid in a simple flow focusing nozzle [Avant 2 (D = 100  $\mu$ m), Ingeniatrics Tecnologías S.L., Spain] fixed at different flow rates (table 1). Distilled water was used as focusing fluid. PLGA nanoparticles were formed into a 0.3 % (w/v) PVA solution. The ethyl acetate content was reduced to a very minimum by using a rotary evaporator. Then, they were freeze-dried and stored at  $\approx 4$  °C until use.

*Characterization methods:* the mean particle size and particle size distributions of gemcitabine-loaded PLGA nanoparticles were measured at  $\approx 25$  °C by laser scattering (Partica LA-950V2, Horiba). Gemcitabine loading was determined by reverse phase-high performance liquid chromatography (RP-HPLC) (Hitachi LaChrom® (D-7000) Series HPLC system). Gemcitabine content was expressed in terms of gemcitabine entrapment efficiency (EE, %) [2]. The production performance (%) was also determined [6]. In order to establish the variations in particle size, a statistical analysis was performed by the use of the Student's *t*-test. Values with  $p < 0.05$  and  $p < 0.01$  were considered as significantly different.

### Results and Discussion

Under the best FF conditions, this method allowed the formation of well-stabilized spherical nanoparticles with an average diameter of  $\approx 600$  nm and a narrow size distribution (table 1). Particle morphology was not influenced by the FF conditions. On the opposite, the flow rates of the focused and focusing fluids clearly determined the particle diameter: respectively, the slower and the faster flow rates determined the formation of much smaller particles. In general, a good linear relationship between theoretical and experimental size values was found and, thus, it could be theoretically calculated the experimental conditions needed to achieve any given size.

In addition, FF allows obtaining suitable gemcitabine entrapment efficiencies ( $\approx 30$  %). Gemcitabine entrapment was not significantly influenced by the drug concentration in solution. However, an increase in the volume of the aqueous drug phase determined a very significant reduction in the entrapment efficiency (table 2). Compared to non-loaded PLGA, particle geometry did not vary significantly when gemcitabine is encapsulated (figure 1), as was previously observed with other biomolecules [4, 5].

We hypothesize that the approximation of the hydrophilic drug molecules from the aqueous phase to the hydrophobic polymeric matrix is not thermodynamically favoured. Hence, only the favourable

electrostatic interaction between this positively charged chemotherapy agent and the negatively charged polymer could be responsible for the gemcitabine loading into the PLGA nanoparticles.

## Conclusions

The optimal formulation conditions to obtain gemcitabine-loaded PLGA nanoparticles by FF suitable for parenteral administration have been determined. Further experiments are under development to enhance drug loading. The *in vitro* drug release and the antitumor activity are also under investigation.

## Acknowledgements

Financial support from Junta de Andalucía, Spain, under Project P06-CTS-01688 is acknowledged.

## References

- [1] Reddy LH, Couvreur P. *Curr Pharm Design* **14** (2008) 1124.
- [2] Arias JL, Reddy LH, Couvreur P. *J Drug Target* **17** (2009) 586.
- [3] Couvreur P, Vauthier C. *Pharm Res* **23** (2006) 1417.
- [4] Holgado MA, Arias JL, Cózar MJ, Álvarez-Fuentes J, Gañán-Calvo AM, Fernández-Arévalo M. *Int J Pharm* **358** (2008) 27.
- [5] Holgado MA, Cózar-Bernal MJ, Salas S, Arias JL, Álvarez-Fuentes J, Fernández-Arévalo M. *Int J Pharm* **380** (2009) 147.
- [6] Arias JL, Martínez-Soler GI, López-Viota M, Ruiz MA. *Lett Drug Des Discov* **7** (2010) 70.

## Figures and Tables

**Figure 1.** Scanning electron microscopy (SEM) picture of the gemcitabine-loaded PLGA nanoparticles.

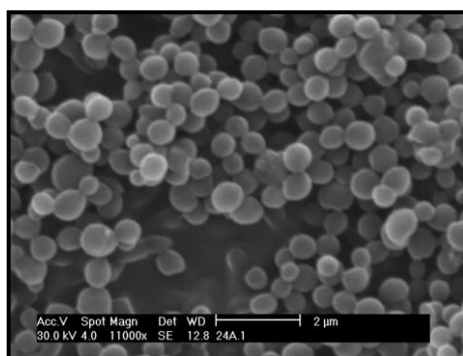


**Table 1.** Formulations of PLGA particles obtained by flow focusing (FF) under different preparation conditions.

Formulation	Flow rate of the focused fluid (mL/h)	Flow rate of the focusing fluid (mL/min)	Theoretical size (μm)	Experimental size (μm)
1	0.3	1.1	1.8	7
2	0.3	1.2	1.8	4.2
3	0.3	2	1.4	1.1
4	0.3	1.2	1.8	4.3
5	0.1	1.2	1.0	1.0
<b>6</b>	<b>0.1</b>	<b>2</b>	<b>0.7</b>	<b>0.6</b>
7	0.05	2	0.5	0.5

**Table 2.** Size and gemcitabine entrapment efficiency (EE) of gemcitabine-loaded PLGA nanoparticles (flow rate of the focused fluid: 0.1 mL/h; flow rate of the focusing fluid: 2 mL/min).

Formulation	Volume of the aqueous phase (μL)	Gemcitabine concentration (mM)	Production performance (%)	Size (μm)	Gemcitabine EE (%)
6.1	50	50	38.83	0.68	34.44
6.2	50	100	46.50	0.81	23.58
6.3	100	50	69.50	Very high polydispersion	11.43

**Magnetization reversal and the intermediate state stability in thin Co-films***O. Idigoras, P. Vavassori, J. M. Porro and A. Berger**CIC nanoGUNE Consolider, Tolosa Hiribidea 76,**E-20018 Donostia-San Sebastian, Spain*[o.idigoras@nanogune.eu](mailto:o.idigoras@nanogune.eu)

The process of magnetization reversal is a fundamental aspect of magnetism and of crucial relevance in many industrial applications, which explains why it is a very active area of research. In this work we have conducted a Kerr effect microscopy study for the purpose of analysing the microscopic effects that occur during magnetization reversal at different applied field directions in order to understand the underlying physics.

Co-films with uniaxial in-plane anisotropy have been grown by means of UHV sputter deposition. This specific magneto-crystalline anisotropy of the samples has been achieved by means of epitaxial growth onto single crystal Si(110) wafer substrates and the use of a suitable template layer sequence [1].

The magnetization reversal and the intermediate domain stability have been analysed by means of an EVICO@ Kerr effect microscope for various angles of the externally applied field. Images taken in the positive saturation state, during reversal and at the negative saturation state are shown in Figure 1 for different applied field angles. Specifically, we have studied the reversal for the applied field oriented along the easy axis, 30° away from the easy axis and 60° away from the easy axis. Initially the sample is always saturated positively and the magnetization is uniform in all three cases. However, as we remove the positive field and start applying the field in the opposite direction, i.e. applying a negative field, we can observe different reversal behaviors for different applied field orientations just before and during the magnetization switch. In the first case (Figure 1 (a2)) (external field applied along the easy axis) the magnetization is still uniform without any domain state before the switch, however for the other two cases (Figure 1 (b2, c2)) intermediate multi-domain states are visible due to partial switching of the local magnetization structure.

To represent the entire magnetization reversal sequence in a compact and quantitative way, we developed a new representation method. In this method, all data that are contained in an entire image sequence (movie) are condensed into a single picture. If we quantify the numbers of pixels per gray scale in a Kerr microscope image, a histogram of the magnetization distribution can be obtained. A color coded scheme is then utilized to display different probabilities of each histogram point in order to obtain a single line representation for each applied field value (each Kerr microscope image). Combining all such lines for different applied field strengths produces a local magnetization probability vs. field picture of the magnetization reversal as shown in Figure 2. This new magnetization reversal representation contains substantially more information than a single magnetic hysteresis loop. With this representation method we can examine and quantify different effects that can take place during magnetization reversal such as, domain creation, uniform rotation of the magnetization and sample size avalanches.

Using this new method we have analyzed the magnetization reversal along different external applied fields directions: along the easy axis, 30° and 60° away from the easy axis (Figure 2). We have observed that the stability range of intermediate non-uniform magnetization states, that are absent for the easy axis reversal, is increasing as we go further away from the easy axis. When the external field is applied along the easy axis, the magnetization reversal is fully correlated without any intermediate stable domain creation, consistent with describing the reversal as a macro-spin process. (Figure 2 (a)). However, if we go away from the easy axis the magnetization reversal is no longer a sample size avalanche and intermediate stable

states start appearing. For the external field applied  $30^\circ$  away from the easy axis, we already have (meta-)stable multi-domain states (Figure 2 (b)). Moreover, the field range in which such domain states occur, increases as one increases the angle away from the easy axis. For a field  $30^\circ$  away from the easy axis, the field range of these intermediate domains is between  $-2.2$  mT and  $-2.7$  mT, while for fields  $60^\circ$  away from the easy axis (Figure 2 (c)) the field range increased to  $-1.74$  mT to  $-2.77$  mT.

In addition to these non-uniform reversal states, we can also observe a uniform magnetization rotation for these last two cases as we increase the strength of the applied field opposite to the magnetization direction. Here, the magnetization distribution peak does not remain at the full positive saturation value, but starts bending towards the negative saturation state prior to the domain state reversal.

We acknowledge funding from the Department of Industry, Trade, and Tourism of the Basque Government and the Provincial Council of Gipuzkoa under the ETORTEK Program, Project No. IE06-172, as well as from the Spanish Ministry of Science and Education under the Consolider-Ingenio 2010 Program, Project No. CSD2006-53. P.V. also acknowledges support through the Marie Curie International Reintegration Grant within the 7th European Community Framework Programme, (Grant Agreement No. PIEF-GA-2008-220166) and finally the Basque Government for the Formación de Investigadores fellowship No. BFI09.284.

## References:

[1] Yang W., Lambeth D.N. and Laughling D.E. Journal of Applied Physics. **Vol 85, 8** (1999)

## Figures:

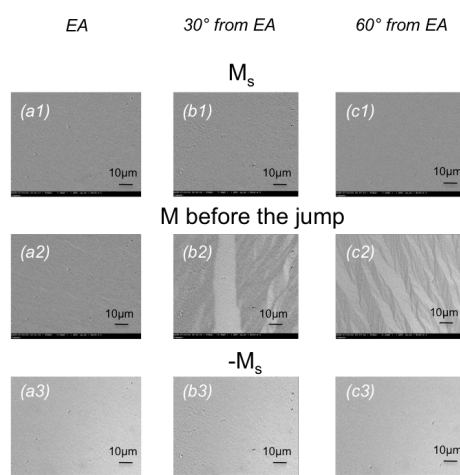


**Figure 1** Kerr microscope images (physical dimensions  $55 \mu\text{m} \times 42 \mu\text{m}$ ) of magnetization states in a uniaxial Co sample: at positive saturation, near or during reversal (external applied field a2:  $-3.09$  mT b2:  $-2.59$  mT c2:  $-2.29$  mT) and for negative saturated states. The external field is applied along a) the easy axis b)  $30^\circ$  away from the easy axis and c)  $60^\circ$  away from the easy axis.

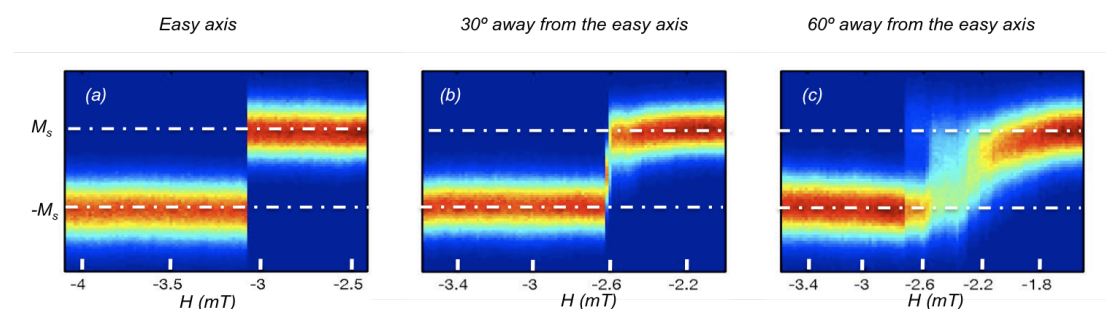


**Figure 2** Magnetization reversal in a uniaxial Co sample using a histogram representation method: External field applied along a) the easy axis b)  $30^\circ$  away from the easy axis and c)  $60^\circ$  away from the easy axis.

## Optical scattering forces generated by high numerical aperture microscope objectives

Ignacio Iglesias<sup>1</sup> and Juan José Sáenz<sup>2</sup>

<sup>1</sup>*Depto. de Física, Universidad de Murcia, Campus de Espinardo (CIOyN Bldg.), 30100 Murcia, Spain*

<sup>2</sup>*Depto. de Física de la Materia Condensada, Universidad Autónoma de Madrid, 28049 Madrid, Spain*

**E-mail:** iic@um.es

**KEY WORDS:** optical forces, optical trapping, high numerical aperture microscope objectives.

A detailed description of the dynamics of particles trapped or moved by light is needed for an increasing number of applications. The characteristics and control of light-induced trajectories of particles in fluids[1] or the precise stiffness determination when small trapped particles confined by light are used as probes in force microscopy[2] are just two examples.

It has been shown that the forces involved can be classified as conserving or not mechanical energy. In the past, only the conservative term, arising from the gradient of the optical intensity distribution, was considered[3]. Recently, the relevance of the force generated by the radiation pressure has also been highlighted[4, 5]. Although this term has been traditionally assumed to be the only non-conservative contributor to the total force field, with small Rayleigh particles, another term may be crucial: the force generated by the curl of the spin angular momentum of the light field[6].

While the contribution to the total force of the spin angular momentum has been studied for optical fields in optical lattices[6-8], we demonstrate here how this term also plays a significant role in the total non-conservative force emerging in the focal volume of high numerical aperture objectives.

1. Sun, B., et al., *Brownian vortexes*. Physical Review E (Statistical, Nonlinear, and Soft Matter Physics), 2009. **80**(1): p. 010401-4.
2. Ghislain, L.P. and W.W. Webb, *Scanning-force microscope based on an optical trap*. Opt. Lett., 1993. **18**(19): p. 1678.
3. Ashkin, A., et al., *Observation of a single-beam gradient force optical trap for dielectric particles*. Opt. Lett., 1986. **11**(5): p. 288.
4. Sun, B., Y. Roichman, and D.G. Grier, *Theory of holographic optical trapping*. Opt. Express, 2008. **16**(20): p. 15765-15776.
5. Roichman, Y., et al., *Influence of Nonconservative Optical Forces on the Dynamics of Optically Trapped Colloidal Spheres: The Fountain of Probability*. Phys. Rev. Lett, 2008. **101**: p. 128301.
6. Albaladejo, S., et al., *Scattering forces from the curl of the spin angular momentum of a light field*. 2009.
7. Zapata, S., et al., *Deterministic ratchet from stationary light fields*. arXiv, 2009.
8. Albaladejo, S., et al., *Giant enhanced diffusion of gold nanoparticles in whirlights fields*. Nano Lett., 2009.

Supported in part by Fundación Seneca (Region de Murcia, Spain), grant 4524/GERM/06

## Adsorption of palladium ions by magnetite nanoparticles

D. Jimenez de Aberasturi, I. Ruiz de Larramendi, R. Pinedo, I. Gil de Muro,

J.I. Ruiz de Larramendi and T. Rojo

Departamento de Química Inorgánica, Facultad de Ciencia y Tecnología,

Universidad del País Vasco UPV/EHU, Apdo.644, 48080 Bilbao, Spain

*djimenezdeab001@ikasle.ehu.es*

Platinum group metals (PGMs) which are widely used in car catalytic converters have been in high demand, in spite of a low natural abundance in the earth crust. Due to scarcity and high value of these metals, there is an increased interest towards their recovery from wastes such as spent catalyst. Palladium together with platinum is the metal more used as catalyst. This metal is generally fixed in the washcoat surface of the catalytic converter and allows the oxidation of carbon monoxide (CO) and hydrocarbons (HC) in order to decrease the contamination caused by car exhaust fumes [1].

Several works have been dedicated to the recovery of metals by different methods including solvent extraction, ion exchange, membrane separation and so on, but most of these methods suffer from some drawbacks such as high capital and operational costs. Therefore, efforts are made to develop low-cost materials for the recovery of metals and the use of nanoparticles is a really good alternative.

Nanomaterials have been shown to possess distinctive mechanical, magnetic, optical, electronic, catalytic and chemical properties that contribute to promising applications in electronics, energy, biomedicine, environmental remediation and recently recovery of metals [2 - 4]. Their small size gives them a high surface area-to-volume ratio and facilitates the interaction with several kinds of chemical species. As magnetic separation has been shown to be a useful solid-solid phase separation technique, magnetic nanoparticles like magnetite nanoparticles are excellent candidates for adsorption of different metals [5].

In the present work we conduct a research on the adsorption of palladium from hydrochloric acid solution onto magnetite ( $\text{Fe}_3\text{O}_4$ ) nanoparticles. The magnetite nanoparticles have been synthesized by several methods, such as co-precipitation, freeze drying, polyol and modified polyol [6-7]. The analysis of X-ray powder diffraction indicated that all the samples were a single phase of magnetite. The transmission microscopy analysis shows that depending on the synthesis method different average particle sizes are obtained (see table 1).

For the adsorption experiments, 1mg of the different  $\text{Fe}_3\text{O}_4$  nanoparticles were re-dispersed with 1 ml of TMAOH (tetramethylammonium hydroxide) and added into a 10 ml dissolution of 8.58 ppm of Pd. The pH of the solution was adjusted at 2.5 and the contact time was 2 hours under sonication.

The aqueous phase was separated from solid phase by magnetic settlement applying external magnetic field. The liquid phase was analyzed by ICP-MS in order to determine the concentration of the palladium cations that have not been adsorbed into magnetite nanoparticles. This way was possible to calculate the percentage of palladium recovered from the initial dissolution.

The results show that with the polyol method only a 70% of the palladium present in the initial dissolution is adsorbed onto the magnetite ( $\text{Fe}_3\text{O}_4$ ) nanoparticles. This low percentage can be explained due to the organic coating of the magnetite nanoparticles. The freeze drying method allows a 79 % of palladium adsorption, while the co-precipitation allows an 85 %. The best results are obtained with the modified polyol method, where the smallest nanoparticles are observed and a 90% of palladium can be adsorbed. The adsorption values are summarized in table 1.

Table 1.- Nanoparticle average sizes and Pd adsorption percentage

Synthesis Method	Nanoparticle Average Size (nm.)	% Pd adsorption
Co-Precipitation	7	85
Freeze drying	8.5	79
Polyol	9	70
Modified polyol	2.6 and 10	90

These results point out that all of these methods are adequate for the synthesis of magnetite nanoparticles, which can be used for the adsorption of palladium. However, the modified polyol shows the best performance for the separation of palladium from diluted hydrochloric acid solutions.

#### References:

- [1] M.Moldovan; Sebastien Rauch, *Surf. Interface Anal.* 2003; 35: 354–359 (2003).
- [2] J. Salado, M. Insausti, I. Gil de Muro, L. Lezama, T. Rojo *J. Non-Crystal. Solids* 354 5207-5209(2008).
- [3] Wei-xian Zhang, *Journal of Nanoparticle Research* 5: 323–332, (2003).
- [4] Xiao-qin Li, Daniel, *Critical review in Solid State and Material Science* 31:111-122 (2006)
- [5] A. Uheida, M. Iglesias, *J. Colloid and interface Science* 301, 402–408 (2006)
- [6] Y.F Shen, J. Tang, Z.H Nie, *Separation and Purification tech.* 68 312-319 (2009)
- [7] S.Sun, H.Zeng, D.B. Robinson, *J.Am.Chem Soc* 126, 273 (2004)

**Basal cytotoxicity of single wall carbon nanotubes on a human endothelial cell line (HUVEC)**

*Jos A<sup>1</sup>, Gutiérrez-Praena D<sup>1</sup>, Pichardo S<sup>1</sup>, Sánchez-Grandados E<sup>2</sup>, Grilo A<sup>2</sup>, Cameán AM<sup>1</sup>*

*<sup>1</sup>Area of Toxicology, Faculty of Pharmacy, University of Seville, Profesor García González nº2, 42012, Seville, Spain*

*[angelesjos@us.es](mailto:angelesjos@us.es)*

*<sup>2</sup> University Hospital Virgen de Valme. Avda. Bellavista s/n, 41014 Seville, Spain.*

Carbon nanotubes (CNTs) are among the nanoparticles with higher potential for biomedical uses. They consist on carbon atoms arranged in a series of condensed benzene rings rolled-up into a tubular structure. CNTs can be classified in two general categories: single-walled nanotubes (SWNT) which have diameters from 0.4 to 2.0 nm and lengths in the range of 20-1000 nm, and multi-walled nanotubes (MWNT) that are bigger objects with diameters in the range of 1.4-100 nm and lengths from 1 to several  $\mu\text{m}$ .

CNTs have interesting physicochemical properties which make CNTs a unique material with the potential for diverse applications, including biomedical [1]. Therefore, it is necessary to know the toxic effects that they can induce, even more when the human exposure will increase in the near future.

CNTs toxicity has been previously studied mainly in pulmonary and dermal cells due to the importance of these exposure ways. But nanoparticles can translocate from the uptake sites to the blood circulation or the lymphatic system, resulting in distribution throughout the body [2]. Thus, the vascular endothelium is going to be in contact with them and can suffer from their toxic effects.

In this sense, in the present study the vascular endothelium cell line (HUVEC) was used to explore the basal cytotoxicity involved in SWCNT pathogenicity. Cells were exposed to concentrations between 0 and 800  $\mu\text{g}/\text{mL}$  SWCNT for 24h and 48h. The basal cytotoxicity biomarkers studied were protein content (PT), neutral red uptake (NR), a tetrazolium salt metabolization (MTS) and Trypan Blue Exclusion Test (TBET).

NR assay, MTS assay, and PT results all showed a decrease in a time and concentration-dependent manner. TBET also showed a decreased in the viability of the cells. The most sensitive biomarker was the MTS reduction with a mean effective concentration (EC50) of 81.25  $\mu\text{g}/\text{ml}$  after 48h exposure, indicating impairment of mitochondrial dehydrogenases activity. The results obtained indicate that SWCNT can induce cytotoxicity in HUVEC cells.

Acknowledgments: authors thank Consejería de Salud de la Junta de Andalucía (Project PI-00192/2007) the financial support of this study.

## References:

- [1] A. Bianco, K. Kostarelos, C.D. Partidos, M. Prato, *Chemical Communications* **7** (2005) 571–577.  
 [2] E. Casals, S. Vázquez-Campos, N.G. Bastús, V. Puentes. *Trends in Analytical Chemistry* **27** (2008) 672-683.

## Figures:

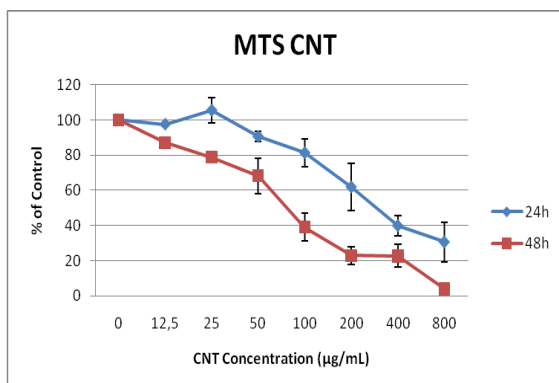


Figure 1. MTS reduction in Huvec cells exposed to SWCNT for 24 and 48h.

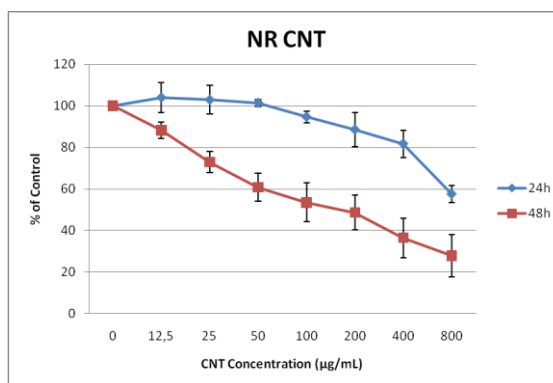


Figure 2. NR uptake in Huvec cells exposed to SWCNT for 24 and 48h.

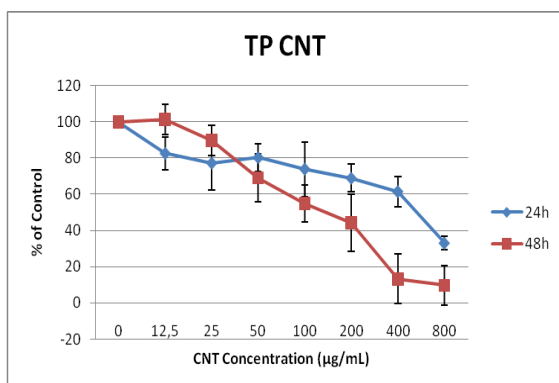


Figure 3. Total Protein content in Huvec cells exposed to SWCNT for 24 and 48h.

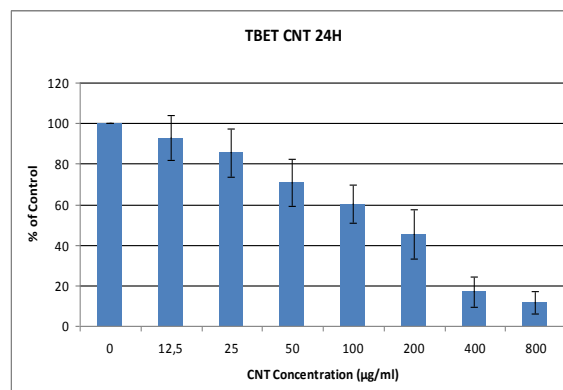


Figure 4. TBET in Huvec cells exposed to SWCNT for 24h.

**Nanobiotechnologies and nanomedicine:  
Organizational and market challenges in a technology convergence scenario**

*Esteve Juanola-Feliu<sup>1</sup>, Josep Samitier<sup>1,2,3</sup>, Jaume Valls-Pasola<sup>4</sup>*

<sup>1</sup>*CEMIC-Department of Electronics, University of Barcelona, Martí i Franquès 1, Planta 2, 08028 Barcelona, Spain, [ejuanola@el.ub.es](mailto:ejuanola@el.ub.es)*

<sup>2</sup>*IBEC-Institute for Bioengineering of Catalonia, Baldri Reixac 10-12, 08028 Barcelona, Spain*

<sup>3</sup>*CIBER-BBN-Biomedical Research Networking Center in Bioengineering, Biomaterials and Nanomedicine, María de Luna 11, Edificio CEEI, 50018 Zaragoza, Spain*

<sup>4</sup>*Department of Economics and Business Organization, University of Barcelona, Av. Diagonal 690-696, 08034 Barcelona, Spain*

In a European context of knowledge-based and information driven society, Spain is evolving to a new economic model for sustainable growth. Among all the research priorities and market opportunities, findings suggest that the commercialization of the nanobiotechnologies developed in Spain is a big issue for technology transfer and innovation managers. A subsequent analysis suggests that Spanish universities and science and technology parks are key players in the area of nanobiotechnology transfer and innovation, and thus they have a fundamental role in fostering the innovation and creativity that are emerging from the social and industrial nano-revolution, with special attention being paid to the nanomedicine sector.

The atomically precise manufacturing (APM) is expected to provide a wide array of practical and profitable technologies and products as research and development in nanotechnology proceeds. Indeed, nanotechnology is widely predicted to drive the next “industrial revolution” [1], one referred to as “the materials age” and which is the result of a sequence of preliminary revolutions in electronics, ICT and biotechnology [2].

Scientific papers and patents in the nanotechnology sector have grown exponentially over the last two decades. Products based on nanotechnology are already in use and analysts expect markets to grow by hundreds of billions of euros during the present decade. After a long R+D incubation period, several industrial segments are already emerging as early adopters of nanotech-enabled products and findings suggest that the Bio&Health market is among the most challenging ones during the next years.

In this context, nanobiotechnology is a rapidly advancing area of scientific and technological opportunity that provides advances into the food industry, energy, environment and medicine. This new discipline is placed at the interface of physical and biological sciences and has the potential of revolutionizing medicine when the tools, ideas and materials of nanoscience and biology are combined (Figure 1).

In the nanomedicine case, there is a wide range of technologies that can be applied to medical devices, materials, procedures, and treatment modalities. A closer look at nanomedicine introduces emerging nanomedical techniques such as nanosurgery, tissue engineering, nanoparticle-enabled diagnostics, and targeted drug delivery. According to an expert group of the European Medicines Evaluation Agency (EMA), the majority of current commercial applications of nanotechnology to medicine are devoted to drug delivery. On the other hand, novel applications of nanotechnology include tissue replacement, transport across biological barriers, remote control of nanoprobe, integrated implantable sensory nanoelectronic systems and multifunctional chemical structures for targeting of disease.

Nanotechnology implies a new approach to research strategies and it is needed to enhance co-location and coordination, as well to improve integration between public and private partners, encouraging multidisciplinary training programmes and working teams and helping to identify new solutions and products [3]. Bozeman [4] points out that the arrival of a radically new technology generates new knowledge dynamics, new roles of the institutions and new technological and industrial opportunities. Clustering in nanotechnology has interesting dynamics and the success and failure of a cluster to be stimulated is in part related to the degree of success in agglomeration of technology platforms [5]. As a result, academics and policy makers are investigating the performance of inventors working in the emerging field of nano science and technology, as well as the effectiveness of different institutional regimes [6]. Actually, the scientific and technical challenges of working at this scale are huge, and

future progress depends not only on the sharing of knowledge about tools and techniques but also on the exchange of expertise regarding the atomic and molecular interactions along this new scientific frontier. Furthermore, nanomanipulation equipment is relatively scarce, and cooperation is thus crucial at this time. This can be achieved by sharing equipment and knowledge in networks and virtual teams, as well as by the setting up of cooperative, multidisciplinary and public-private ventures such as Minatec (Grenoble) in France or MESA+ (Twente) in The Netherlands. In Barcelona, for instance, there is a process of clustering and alliances focused on the nanomedicine niche as a strategy to “catch up” the windows of opportunity currently offered by biotechnology and nanotechnology.

In summary, a survey about nanobiotechnology commercialization is given laying emphasis on nanomedicine and its Spanish context, in which research and medical applications are heavily funded by governments and private sector. The performance of the Spanish universities and science and technology parks is considered in terms of efficiency and competitiveness enhancing ecosystems for private-public partnerships in the field of nanobiotechnologies and improving their market position in the global knowledge-based economy.

## References:

- [1] European Commission (2002). «Press Release: European Union Research Drives Nanotechnology Revolution», Directorate-General Research, <http://ec.europa.eu/research/press/2002/pr1206en.html>
- [2] Uwe B. Sleytr (2006). NANOBIO TECHNOLOGY, An Interdisciplinary Challenge. Center for NanoBiotechnology University of Natural Resources and Applied Life Sciences Vienna. <http://www.scribd.com/doc/2409974/NanoBioTechnology-an-interdisciplinary-challenge-2006>
- [3] Morrison M. (2005). «Seventh Nanoforum Report: European Support for Nanotechnology Small and Medium-sized Enterprises», Institute of Nanotechnology, [www.nanoforum.org](http://www.nanoforum.org)
- [4] Bozeman B., Laredo P., Mangematin V. (2007). «Understanding the emergence and deployment of “nano” S&T», *Research Policy*, Vol. 36, p. 807-812.
- [5] Douglas K.R.R., Rip A., Mangematin V. (2007), «Technological agglomeration and the emergence of clusters and networks in nanotechnology», *Research Policy*, Vol. 36, p. 871-879.
- [6] Bonaccorsi A., Thoma G. (2007). «Institutional complementarity and inventive performance in nano science and technology», *Research Policy*, Vol. 36, p. 813-831

## Figures:

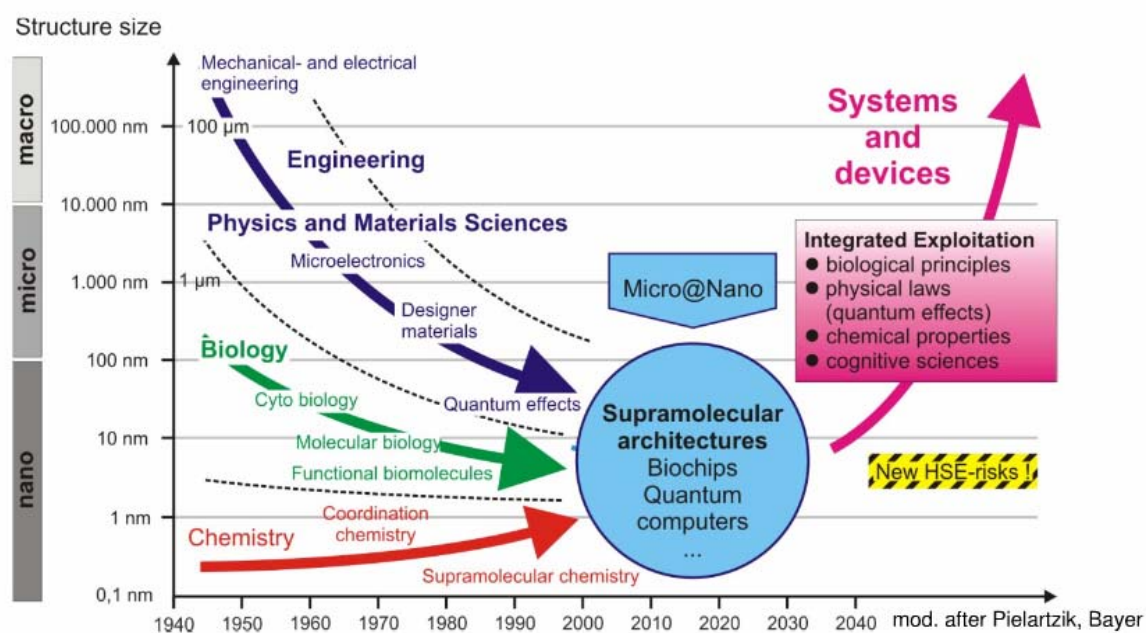


Figure 1. Convergence of technologies and revolutionary performance of the nanotechnology [2].

## **Spectroscopic Studies on Biocompatibility of Multiwalled Carbon Nanotubes with Cell Culture Media**

Dr Gautam Kaul

Biochemistry Division, National Dairy Research Institute, (I.C.A.R.) (Government of India) Karnal-132001, Haryana India.

\*Dr. Gautam Kaul, Incharge S.B Lab.-I, Biochemistry Division, National Dairy Research Institute, (Government of India) Karnal-132001 (Haryana) India Tel.:+91-184-2259133  
Fax: + 91-184-2250042, e-mail address: [gkndri@gmail.com](mailto:gkndri@gmail.com)

The biocompatibility of any material is compulsory before it can be used further for biological applications. All possible bio-applications of carbon nanotubes will require their compatibility with biological milieu. The present study has been conducted to elucidate the interaction of purified multiwalled carbon nanotubes (MWCNT) with cell culture media and its components by UV/Vis absorbance and fluorescence spectroscopy. The Minimal essential media a commonly used cell culture media was used along with/without fetal calf serum in this study, containing many components like phenol red (pH indicator), proteins, vitamins, hormones etc. The absorbance spectroscopy shows change in the spectrum of media on addition of nanotubes indicating the interaction between MWCNTs and cell culture media. Florescence studies were conducted to further elucidate the interaction of individual components of cell culture media with nanotubes. Fluorescence spectroscopy revealed reduction in emission features associated with the components of the media upon addition of MWCNTs. Interaction established between MWCNT and cell culture media have been correlated with biocompatibility and established.

**Key words:** MWCNTs; Cell culture medium; Spectroscopy; Biocompatibility

## A Butterfly-like model for non-covalent functionalization of MWCNTs as a biocompatible nanoglycoarrays.

Noureddine Khiar,<sup>a</sup> Mohyeddin Assali,<sup>a</sup> Raquel Navas,<sup>a</sup> Juan Francisco Moya,<sup>a</sup>  
Inmaculada Fernández,<sup>b</sup> Lama Arafat,<sup>b</sup> Rachid Baati.<sup>c</sup>

<sup>a</sup>*Instituto de Investigaciones Químicas, C.S.I.C-Universidad de Sevilla, c/. Américo Vespucio, 49, Isla de la Cartuja, 41092, Sevilla, Spain.* <sup>b</sup>*Departamento de Química Orgánica y Farmacéutica, Facultad de Farmacia, Universidad de Sevilla, 41012, Sevilla, Spain.* <sup>c</sup>*Université de Strasbourg Faculté de Pharmacie CNRS/UMR 7199, Laboratoire des Systèmes Chimiques Fonctionnels BP 60024, 74 route du Rhin, 67400 Illkirch France. e-mail: [Kхийar@iiq.csic.es](mailto:Kхийar@iiq.csic.es).*

Carbon nanotubes (CNTs) have received an unrivalled interest as consequence of their unique structural, mechanical, electrical, and optical properties.<sup>1</sup> To date, CNTs are being actively investigated in a wide range of scientific areas,<sup>2</sup> These applications have been hampered by the insolubility of CNTs in most organic solvent, and in water. To overcome the drawbacks of insolubility, the surface functionalization of the CNT sidewalls has emerged as a powerful strategy to exfoliate CNTs resulting in the preparation of stable aqueous/organic suspensions. So far many strategies have been developed to exfoliate CNTs into solution including covalent and no-covalent functionalization.<sup>3,4,5</sup> Herein we disclose the use of sugar based tetrabenzo[a,c,g,i]fluorene (Tbf) amphiphiles with large flat aromatic group, as a new molecular scaffold for the non-covalent functionalization of CNTs, comparing with sugar based pyrene amphiphiles giving rise to robust water soluble nanoglycoarrays with a biomimetic presentation of carbohydrates on their surface (scheme 1).



## **Cationic Surfactants Based on Renewable Raw Materials: New Emulsifiers for Elaboration of Nanoparticles of Dispersed Oil**

*Plamen Kirilov, Hakima Azira, Loïc Lemiègre, Thierry Benvegnu, Fabrice Goursaud, Daniel Plusquellec*

*Ecole Nationale Supérieure de Chimie de Rennes, CNRS UMR 6226, Campus Beaulieu  
Avenue Général Leclerc CS 50837, F-35708 Rennes, France*

[plamen.kirilov@ensc-rennes.fr](mailto:plamen.kirilov@ensc-rennes.fr)

The development of surfactants based on natural renewable resources is a concept that is gaining recognition in cosmetic and detergent industries. This new class of biodegradable and biocompatible surfactants is a response to the increasing consumer demand for products that are both greener and more efficient. In order to achieve these objectives, it is necessary to use renewable low-cost materials that are available in large quantities and to design molecular structures that show improved performance, favourable ecotoxicological properties and reduced environmental impact.<sup>1</sup>

Several families of surfactants were prepared using environmentally friendly processes (without solvent or pollutants) and envisaging industrial scaling up. Their production permits to valorise various products and by-products of the sugar and oleochemical industries or derived from marine resources. Sugars<sup>2</sup> or betaine<sup>3</sup> were used as polar heads, and natural Tropical or European oils as raw materials for the lipophilic part of the surfactants. Cationic surfactants from glycine betaine (esters and amides carrying stearic and oleic alkyl chains) or non-ionic surfactants from different sugars were obtained by green solvent-free processes: the reaction takes place in the reagent in excess which is then recycled. For example, esterification reactions of glycine betaine were carried out with recyclable saturated or unsaturated fatty alcohols of various lengths (lauric, stearic or oleic alcohols) at 130°C, in the presence of biodegradable methane sulfonic acid and under reduced pressure to provide glycine betaine ester-type surfactants (Figure 1).

The physicochemical properties of the synthesized surfactants were evaluated: they exhibit attractive surface-tension, and remarkable foaming, surfactant and emulsifying capability. For example concerning emulsifying properties, we followed the O/W emulsion ageing by photodensitometry vs. pH medium in order to compare the capacity of glycine betaine stearic and oleic esters and amides to stabilize oil droplets (Figure 2). These investigations showed the importance of the surfactant type on the stability of obtained emulsions and could define the kind of surfactant applications. A highly biodegradable emulsifying formulation called Emulgreen<sup>®</sup> is currently under industrial development.

To conclude, a wide range of original surfactants derived from renewable resources were developed with potential applications, notably, in detergency and cosmetic industry. The production of these entirely natural molecules may substitute the petrochemical products classically used.

### **References:**

- [1] T. Benvegnu, D. Plusquellec, L. Lemiègre, in *Monomers, Polymers and Composites from Renewable Resources 2008*, M. N. Belgacem, A. Gandini, Eds. Elsevier Limited: Amsterdam.
- [2] M. Roussel, T. Benvegnu, V. Lognoné, H. Le Deit, I. Soutrel, I. Laurent, D. Plusquellec, *Eur. J. Org. Chem.*, **20** (2005) 3085 – WO2003104248.
- [3] F. Goursaud, M. Berchel, J. Guilbot, N. Legros, L. Lemiègre, J. Marcilloux, D. Plusquellec, T. Benvegnu, *Green Chem.*, **10** (2008) 310 - WO2005121291.

## Figures:

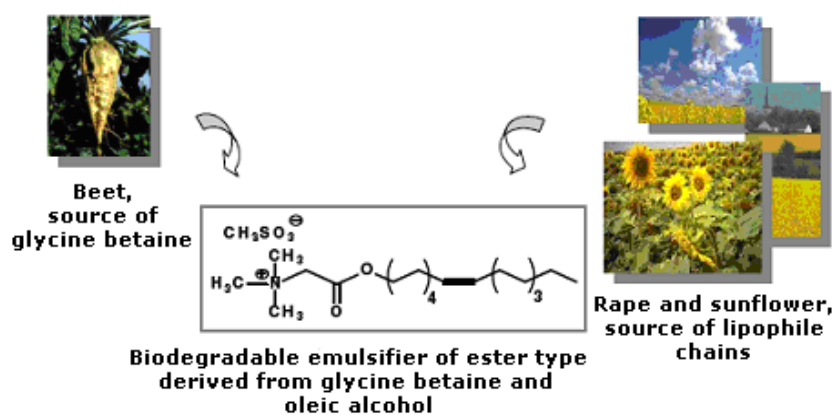


**Figure 1.** Ester type of biodegradable emulsifier obtained from renewable raw materials.

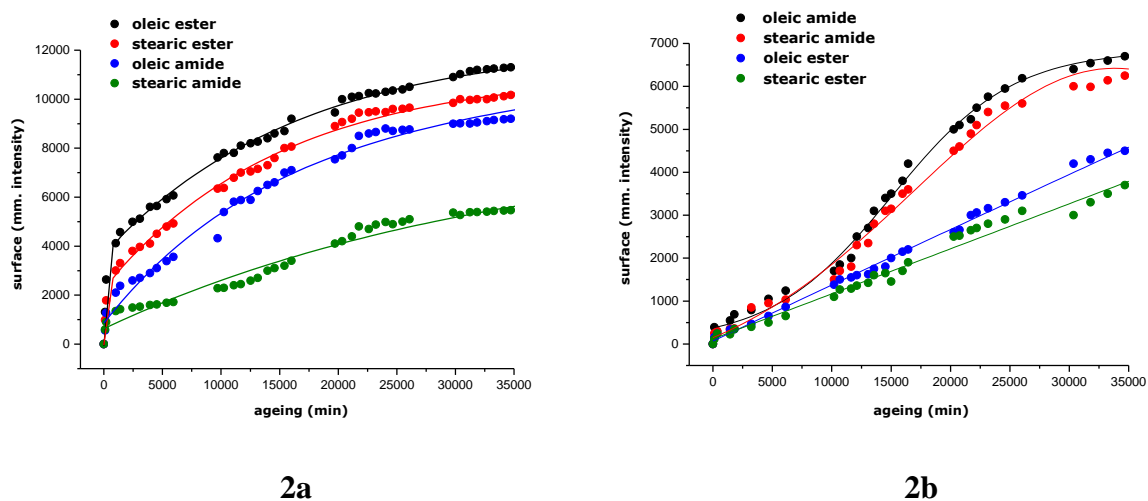


**Figure 2.** Surface variation of the serum peak area (formed during the creaming process) vs. time for emulsions stabilized by glycine betaine esters and amides at neutral pH (2a) and at acid (2b) pH.

## Nanotechnology approaches for improved based-drug delivery systems of the immunomodulatory neuropeptide vasoactive intestinal peptide

*Rebecca Klippstein<sup>1</sup>, Paula M. Castillo<sup>1</sup>, Rafael Fernandez-Montesinos<sup>1</sup>, Ana P. Zaderenko<sup>2</sup> and David Pozo<sup>1</sup>*

<sup>1</sup>*CABIMER-Andalusian Center for Molecular Biology and Regenerative Medicine (CSIC-University of Seville, UPO, Junta de Andalucía), Seville, Spain*

<sup>2</sup>*Department of Physical, Chemical and Natural Systems, UPO-University Pablo de Olavide, Seville, Spain*

[david.pozo@cabimer.es](mailto:david.pozo@cabimer.es)

In spite of sustained interest in therapeutic applications of vasoactive intestinal peptide (VIP), and the fact that its administration could be largely improved by attachment to functionalized metal nanoparticles, no methods have been described so far to obtain them. The primary aim of the current study was to provide a method for silver nanoparticle conjugation to VIP that would be also useful for tailor-made applications based on nanoparticle multifunctional capabilities (Fernandez-Montesinos et al. 2009). The biological features of VIP are of particular interest to develop multifunctional nanoparticles for innovative therapeutic approaches for human diseases with inflammatory or autoimmune components (Pozo 2008; Delgado et al. 2004). VIP is a 28-aminoacid peptide (His-Ser-Asp-Ala-Leu-Phe-Thr-Asp-Thr-Tyr-Thr-Arg-Leu-Arg-Lys-Gln-Met-Ala-Met-Lys-Lys-Tyr-Leu-Asn-Ser-Val-Leu-Asn) that was initially isolated from the gastrointestinal tract due to its capacity as a vasodilator (Said and Mutt 1970). VIP was subsequently identified in the central and peripheral nervous systems, and recognized as a widely distributed neuropeptide. VIP exerts its biological functions through interaction with VPAC specific receptors belonging to the class II G protein-coupled receptors. Among its physiological roles, VIP and VPAC receptors have shown their relevance as endogenous factors that regulate inflammatory immune responses and immune tolerance, emerging as a very promising therapeutic factor (Pozo 2003; Pozo and Delgado 2004; Pozo et al. 2007). The mechanisms involved include the deviation towards Th2-driven inflammatory pathways, the specific recruitment and development of Th2 cells, and the peripheral expansion of regulatory T cells (Pozo et al. 2009; Chorny et al. 2005; Gonzalez-Rey et al. 2007). Also, VIP and VPAC receptors are overexpressed in 100% of human prostate cancers (Reubi and Maecke 2008; Reubi 2003). In spite the fact that the structure-function relationships of VPAC receptors are well known, the structure-function relations for VIP are however poorly understood. In this sense, VIP has been shown to have diffuse pharmacophoric domains, with important amino acids all along the peptide for binding to VPAC1 and VPAC2 receptors (Ceraudo et al. 2008). Photoaffinity labelling, molecular dynamic simulation and ligand docking studies have determined that the C-terminal part of VIP from Phe<sup>6</sup> to Asn<sup>28</sup> interacts with the N-terminal ectodomain of human VPAC1 receptor. Recently, it has been shown that the N-terminus of VIP also interacts with the human VPAC1 receptor N-terminal domain. VIP was conjugated to tiopronin-capped silver nanoparticles of a narrow size distribution, by means of proper linkers, to obtain VIP functionalized silver nanoparticles with two different VIP orientations Ag@tiopronin@PEG@succinic@[His]VIP and Ag@tiopronin@PEG@VIP[His]. VIP intermediate nanoparticles were characterised by TEM, FTIR, Raman, <sup>1</sup>H-NMR and TOCSY. VIP functionalized silver nanoparticles cytotoxicity was determined by LDH release from mixed glial cultures prepared from cerebral cortices of 1-3 days-old C57/B1 mice. Cells were used for LPS stimulation at day 18-22 of culture. Mixed cultures were checked by immunocytochemistry for high enrichment of GFAP and CD68 positive reactive cells, identifying astrocytes and microglia, respectively. Supernatants from mixed glial cells cultures were harvested 24 hours after treatment, and IL-6, TNF- $\alpha$ , and IL-10 production was

determined by ELISA. Two different types of VIP functionalized silver nanoparticles were obtained; both expose the C-terminal part of the neuropeptide, but in the first type VIP is attached to silver nanoparticle through its free amine terminus Ag@tiopronin@PEG@succinic@[His]VIP while in the second type, VIP N-terminus remains free Ag@tiopronin@PEG@VIP[His]. VIP functionalized silver nanoparticles did not compromise cellular viability and inhibited microglia-induced stimulation under inflammatory conditions. Treatment of primary mixed glial cultures with Ag@tiopronin@PEG@Succinic@[His]VIP or Ag@tiopronin@PEG@VIP[His] nanoparticles with a final concentration of functionalized VIP of  $10^{-8}$ M resulted in an inhibition of LPS-induced production of IL-6 and TNF- $\alpha$  and an increase of IL-10. We have exploited the potential of nanoparticle functionalization as an alternative approach to improve the therapeutic prospect of the endogenous cytokine-like peptide VIP. Our results showed the proof-of-concept for its use, as the chemical synthesis procedure developed to obtain VIP functionalized silver nanoparticles rendered functional products, in terms of biological activity, without any observed cytotoxic effects. The present work provides functional data that demonstrates that VIP can be conjugated to tiopronin-capped silver nanoparticles in two alternative orientations, involving or not the VIP N-terminus, without loss of biological activity. This information is especially valuable for other studies aiming at including VIP in formulations where the possibility of chemical synthesis constraints exists depending on the nanosurface to be functionalized. Our study provides for the first time a proof-of-principle to enhance the therapeutic potential of VIP with the valuable properties of metal nanoparticles for imaging, targeting, and drug delivery. Our study provides for the first time a proof-of-principle to encourage the development of VIP-based nanoparticles that exploit the valuable properties of silver nanoparticles for imaging, targeting, and drug delivery.

## References:

- Ceraudo, E., Y. V. Tan, P. Nicole, A. Couvineau, and M. Laburthe. 2008. The N-Terminal Parts of VIP and Antagonist PG97-269 Physically Interact with Different Regions of the Human VPAC1 Receptor. *J Mol Neurosci* 36 (1-3):245-248. .
- Chorny, A., E. Gonzalez-Rey, A. Fernandez-Martin, D. Pozo, D. Ganea, and M. Delgado. 2005. Vasoactive intestinal peptide induces regulatory dendritic cells with therapeutic effects on autoimmune disorders. *Proc Natl Acad Sci U S A* 102 (38):13562-13567.
- Delgado, M., D. Pozo, and D. Ganea. 2004. The significance of vasoactive intestinal peptide in immunomodulation. *Pharmacol Rev* 56 (2):249-290.
- Fernandez-Montesinos, R., P. M. Castillo, R. Klippstein, E. Gonzalez-Rey, J. A. Mejias, A. P. Zaderenko, and D. Pozo. 2009. Chemical synthesis and characterization of silver-protected vasoactive intestinal peptide nanoparticles. *Nanomed* 4 (8):919-930.
- Gonzalez-Rey, E., A. Chorny, and M. Delgado. 2007. Regulation of immune tolerance by anti-inflammatory neuropeptides. *Nat Rev Immunol* 7 (1):52-63.
- Pozo, D. 2003. VIP- and PACAP-mediated immunomodulation as prospective therapeutic tools. *Trends Mol Med* 9 (5):211-217.
- Pozo, D. 2008. Immune-based disorders: the challenges for translational immunology. *J Cell Mol Med* 12 (4):1085-1086.
- Pozo, D., P. Anderson, and E. Gonzalez-Rey. 2009. Induction of Alloantigen-Specific Human T Regulatory Cells by Vasoactive Intestinal Peptide. *J Immunology* 183:4346-4359.
- Pozo, D., and M. Delgado. 2004. The many faces of VIP in neuroimmunology: a cytokine rather a neuropeptide? *FASEB J*. 18 (12):1325-1334.
- Pozo, D., E. Gonzalez-Rey, A. Chorny, P. Anderson, N. Varela, and M. Delgado. 2007. Tuning immune tolerance with vasoactive intestinal peptide: a new therapeutic approach for immune disorders. *Peptides* 28 (9):1833-1846.
- Reubi, J. C. 2003. Peptide receptors as molecular targets for cancer diagnosis and therapy. *Endocr Rev* 24 (4):389-427.
- Reubi, J. C., and H. R. Maecke. 2008. Peptide-based probes for cancer imaging. *J Nucl Med* 49 (11):1735-1738.
- Said, S., and V. Mutt. 1970. Polypeptide with broad biological activity: isolation from small intestine. *Science* 169:1217-1218.

## Decrease of the adhesion force with vapor pressure

Mariana Köber<sup>1</sup>, Enrique Sahagún<sup>2</sup>, Pedro García-Mochales<sup>2</sup>, Fernando Briones<sup>1</sup>, Mónica Luna<sup>1</sup>, Juan José Sáenz<sup>2</sup>

<sup>1</sup>Instituto de Microelectrónica de Madrid (IMM-CSIC), Isaac Newton 8, 28760 Tres Cantos, Spain

<sup>2</sup>Departamento de Física de la Materia Condensada, Universidad Autónoma de Madrid, 28049 Madrid, Spain  
[mariana.koeber@imm.cnm.csic.es](mailto:mariana.koeber@imm.cnm.csic.es)

Experimental evidence of a monotonous decrease of the capillary forces between hydrophilic surfaces with increasing relative humidity from 0 to 100% is presented. In concordance with the results of a theoretical simulation, we identified the objects' shape as the origin of different adhesion force vs. RH behaviours when treating with nanoscale objects. If the water neck is formed between a flat surface and a nanometric object presenting a truncated cone shape the adhesion force decreases with increasing vapour pressure. The variety of meniscus force behaviours found for different shapes emphasizes the importance of geometry in capillary phenomena at the nanometric scale.

Moisture alters the cohesion among particles in powders and the adhesion of particles to surfaces. The principal reason for this effect is the formation of a liquid neck or meniscus at the contact region between particles or between the particles and the surface. The attractive force caused by such a liquid meniscus is called "capillary force" and it generally predominates (for hydrophilic surfaces) over other surface forces under ambient conditions [1]. A profound understanding of capillary forces is essential in the studies of the behaviour of powders and soils [2], friction, hydrophobic interactions, and has implications in industries as pharmaceutical (colloid stability, suntan creams), food engineering (the cleaning of food) [3], and new materials (coatings, lubricants).

Atomic Force Microscopy (AFM) allows for the investigation of adhesion forces between bodies of micro or nanometer sizes and plays, therefore, a major role in the studies of capillarity. In this study, AFM experiments were performed using sharp as well as dull Si tips and flat mica surfaces. Adhesion force vs. environmental water pressure curves were obtained by measuring force vs. distance curves (from which adhesion forces were extracted) [4] while increasing the relative humidity slowly from 0 to 100%. In order to preserve small tip apex dimensions very low normal loads have been applied. When using sharp Si tips the adhesion force decreases monotonously with increasing water vapour pressure (Fig. 1, left), while it shows a maximum behaviour when using larger (> 15nm) tips (not shown here). While the maximum behaviour has been reported reiterately [1, 5-11], we found no reference to a strict decrease of the adhesion force with increasing humidity in literature.

A simple model explaining the experimental findings has been developed, based on a previously described model [12], using continuum theory and the formation of minimum energy water necks. The model suggests that, when bringing a hydrophilic nanoscale object in proximity to a hydrophilic surface the object's shape is a decisive factor for determining the adhesion behaviour with humidity. While conical shapes present increasing  $F_{adh}$  vs.  $H$  curves, sharp and nearly flat caps yield decreasing curves (Fig. 1, right). Curved tips, in turn, show the well known force curves displaying a maximum.

Experimental and theoretical results are consistent if we assume that the "small" tips, preserved up to what the SEM can elucidate, exhibit a nanometer sized flat surface free of asperities. The Nanosensors Si tip is likely to exhibit a flat surface after entering into first contact with the stiff mica sample since Nanosensors Si cantilevers are aligned parallel to the <110> direction [13] (thus the <110> direction is perpendicular to the cone axis) along which cracks are easily propagated resulting in a nearly perfectly flat fracture surface [14].

The results imply that the undesirable sticking effect between surfaces occurring at increasing relative humidity could be avoided by controlling the shape of the surface asperities at the nanometric scale. Furthermore, for a correct interpretation of AFM adhesion maps the tip size and shape have to be taken into account – hydrophilic samples do not necessarily yield a

capillary force increase with increasing moisture.

## References:

- [1] H.-J. Butt, and M. Kappl, *Adv. Colloid Interface Sci.* **146**, 48 (2009).
- [2] L. Bocquet, E. Charlaix, S. Ciliberto & J. Crassous, *Nature* **396**, 735-737 (1998).
- [3] W. Liu, P.J. Fryer, Z. Zhang, Q. Zhao and Y. Liu, *Innovative Food Science and Emerging Technologies* **7**, 263–269 (2006).
- [4] Weisenhorn, A. L.; Hansma, P. K.; Albrecht, T. R.; Quate, C. F. *Appl. Phys. Lett.* **54**, 2651 (1989).
- [5] O H Pakarinen, A S Foster, M Paajanen, T Kalinainen, J Katainen, I Makkonen, J Lahtinen and R M Nieminen, *Modelling Simul. Mater. Sci. Eng.* **13**, 1175–1186 (2005).
- [6] D. B. Asay and S. H. Kim, *J. Chem. Phys.* **124**, 174712 (2006).
- [7] A. Fukunishi and Y. Mori, *Advanced Powder Technol.* **17**, 567–580 (2006).
- [8] M. Farshchi-Tabrizi, M. Kappl and H. -J. Butt. *Journal of Adhesion Science and Technology* **22**, 181–203 (2008).
- [9] X. D. Xiao, and L. M. Qian, *Langmuir* **16**, 8153 (2000).
- [10] O. Stukalov, C. A. Murray, A. Jacina, and J. R. Dutcher, *Rev. Sci. Instrum.* **77**, 033704 (2006).
- [11] . M. He, A. S. Blum, D. E. Aston, C. Buenviaje, R. M. Overney and R. Luginbühl, *J. Chem. Phys.* **114**, 1355-60 (2001).
- [12] E. Sahagún, P. García-Mochales, Sacha G.M. and J.J. Sáenz, *Phys. Rev. Lett.* **98**, 176106 (2007)
- [13] <http://www.nanosensors.com/faq.html>
- [14] A. George, G. Michot, *Mater. Sci. Eng. A* **164**, 118 (1993); R. Pérez and P. Gumbsch, *Phys. Rev. Lett.* **84**, 5347 (2000)

## Figures:

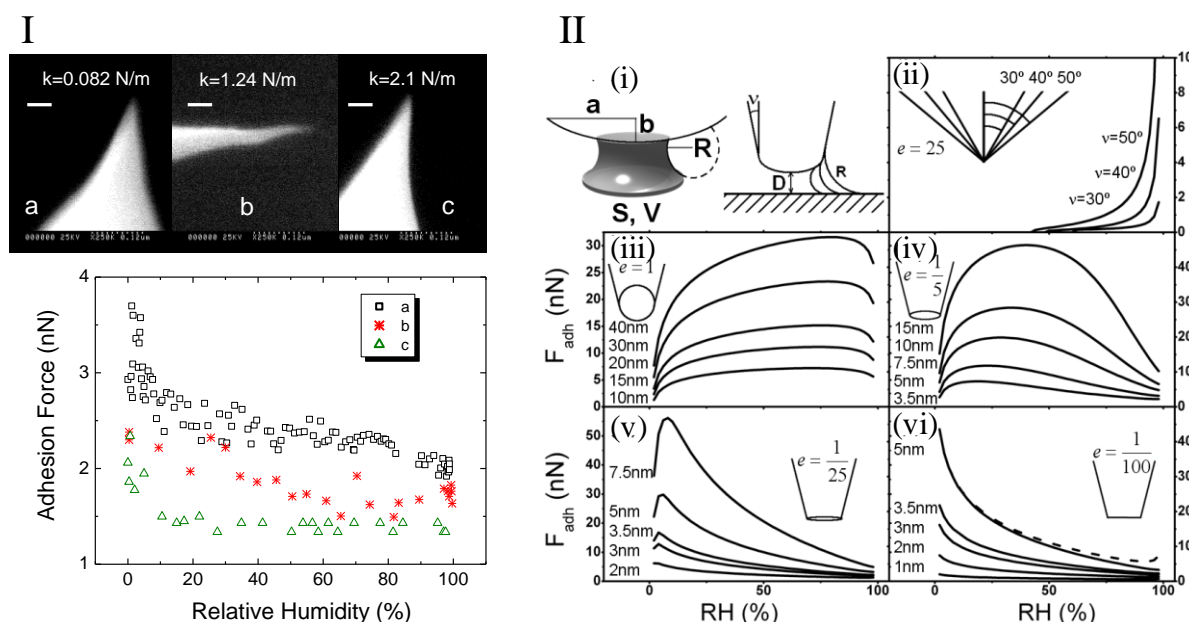


Fig. 1 Experimental (I) and model (II) curves of the adhesion force vs. relative humidity.

Top left (I): SEM images showing three tips after they had been used to measure the adhesion force with flat mica surfaces (the scale bar represents 60 nm). Bottom left (I): adhesion force as a function of the relative humidity for the three sharp Si tips. Nominal tip radii are 7 nm for (a) and (c) and 2 nm for (b). II. (i) Scheme of the modelled tip geometry and water meniscus (ii-vi)  $F_{adh}$  vs humidity curves calculated with the ellipsoid model ( $D = 0.2$  nm) for different values of the tip apex form factor  $e = b/a$  ( $e = 25, 1, 0.2, 0.04$  and  $0.01$ , respectively) and the ellipsoid transverse semi axis  $a$ . In (b) we show the results for a quasi conical tip ( $b/a = 25, a = 5$  nm) for different aperture angles. In (iii-vi) solid lines are results for tips with  $v = 10^\circ$  and different  $a$  (curve labels correspond to  $a$  values used). In (vi) the dashed line corresponds to a quasi-truncated tip with  $a = 5$  nm and  $v = 30^\circ$ .

## Photoresponsive Amphiphiles Based on Azobenzene Glycerol Conjugates for Drug Delivery

Christian Kördel, Achim Wiedekind, Prof. Rainer Haag  
Freie Universität Berlin, Institut für Chemie und Biochemie  
Takustr. 3, 14195 Berlin, Germany  
[chriskoe@chemie.fu-berlin.de](mailto:chriskoe@chemie.fu-berlin.de)

The photoisomerisation of azobenzenes has shown great practicality<sup>[1]</sup>. The thermodynamically favoured *trans* isomer can be switched to the *cis* isomer within minutes by light (~360 nm). Back switching to the *trans* isomer can be achieved either by heat or by light (~450 nm). This photoswitching is used for controlling the expression of genes or the function of proteins<sup>[2]</sup> as well as in liquid crystals.<sup>[3]</sup> Making use of the large change in geometry, we are interested in changing the properties of an amphiphile consisting of a dendritic polyglycerol head and a hydrocarbon tail. The micelles are able to incorporate guests, like drugs or dyes, into the hydrophobic core.

In this work, photoresponsive amphiphiles, whose hydrophobic and hydrophilic part is separated by an azobenzene, are examined.

The azobenzene switch bears an aliphatic chain on one side and on the other side a polyglycerol (PG) dendron (Figure 1). The length of the chain is varied from C11 to C16 as well as the size of the generation of the PG dendron (generation 2 and 3). After photoisomerization from *trans* to *cis* the critical micelle concentration (cmc) is increased. First results for G2azoC11 show a doubled cmc after switching (Figure 2). In the all-*trans* state the cmc is 4E-5 mol/l, whereas after the light-induced switching the cmc is 8E-5 mol/l. The steric demand of one molecule at the air-water interface also increased from 0.25 nm<sup>2</sup> to 0.33 nm<sup>2</sup>. We observe a ten-fold increase in cmc upon switching by increasing the PG generation to G3. For the unswitched all-*trans* state the cmc is 7.7 E-6 mol/l, whereas after isomerization the cmc increased to 6E-5 mol/l. The steric demand for one molecule at the air-water interface now changes from 0.7 nm<sup>2</sup> to 1 nm<sup>2</sup>. The lower cmc for the G3 compared to the G2 compound is expected due to the growth of the hydrophilic part.

## References:

- [1] A. Teitel, *Naturwissenschaften*, **44**, (1957) 370.  
[2] A. Yamazawa, X. Liang, H. Asanuma, M. Komiyama, *Angew. Chem. Int. Ed.* **39**, (2000) 2356.  
[3] A. Natansohn, P. Rochon, *Chem. Rev.*, **102**, (2002) 4139–4175.

## Figures

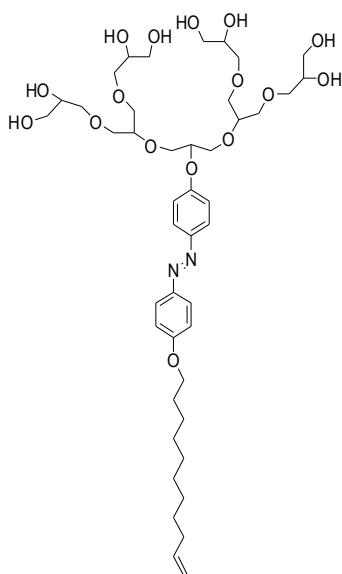


**Figure 1:** G2azoC11

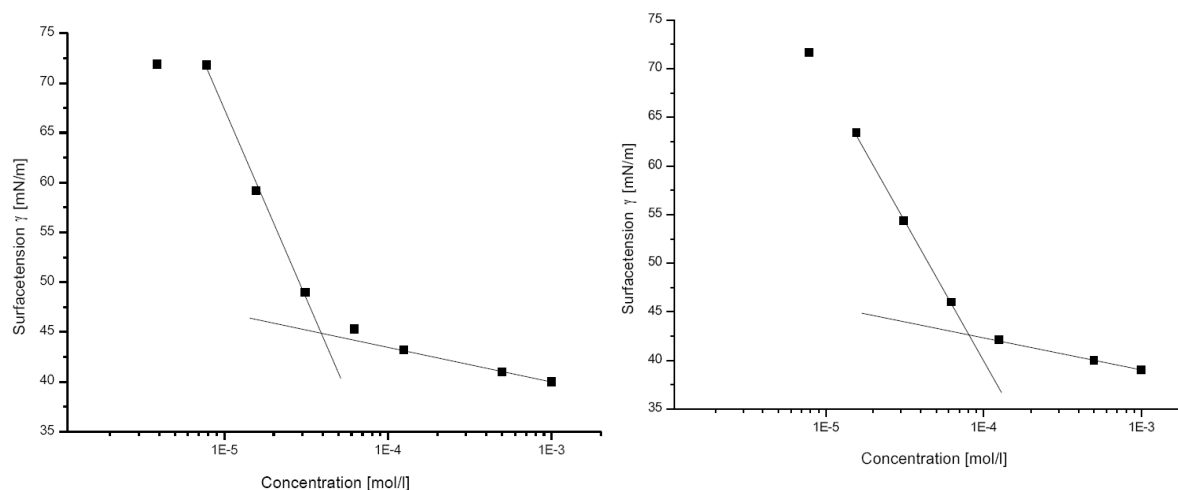


**Figure 2:** *left:* cmc measurement for *trans* G2azoC11, cmc =  $3.9 \times 10^{-5}$  mol/l; *right:* cmc measurement after irradiation with 350 nm for 12 h, cmc =  $8.0 \times 10^{-5}$  mol/l.

## Tuning exchange bias in Ni/FeF<sub>2</sub> heterostructures using antidot arrays

*M. Kovylnina*<sup>1,\*</sup>, *M. Erekhinsky*<sup>2</sup>, *R. Morales*<sup>3</sup>, *J.E. Villegas*<sup>4</sup>, *Ivan K. Schuller*<sup>2</sup>, *A. Labarta*<sup>1</sup> and *X. Batlle*<sup>1</sup>

<sup>1</sup> *Dept. Física Fonamental and Institut de Nanociència i Nanotecnologia (IN2UB),  
Universitat de Barcelona, 08028 Barcelona, Catalonia, Spain*

<sup>2</sup> *University of California-San Diego, La Jolla 92093, California, USA*

<sup>3</sup> *Universidad de Oviedo-CINN, Oviedo 33007, Spain*

<sup>4</sup> *Universite Paris Sud, 91405 Orsay, France*

*miroslavna@ffn.ub.es*

The microscopic origin of exchange bias (EB) represents one of the challenges in solid state physics, despite the extensive experimental and theoretical investigations [1]. We used focused ion beam lithography to fabricate a series of ordered arrays of Ni/FeF<sub>2</sub> antidots to get a deeper insight of EB in nanostructures (Figure 1). Ni/FeF<sub>2</sub> heterostructures were deposited by electron beam evaporation onto (110) MgF<sub>2</sub> single-crystal substrates of 70 nm of antiferromagnetic (AF) FeF<sub>2</sub>, 50 nm of ferromagnetic (FM) Ni and 4 nm of Al. The antidots were fabricated in a square array, with antidot size of 200 nm and periodicity ranging from 100 to 900 nm (antidot density, AD, from 5% to 24 %). Magnetoresistance measurements were used to determine the EB field in the temperature range 4.2–300 K, in both the parallel and transversal configurations, after field cooling (Figure 2). For small/large cooling fields, the magnetoresistance curves display a shift towards negative/positive fields. At intermediate cooling fields (CF), two MR peaks are observed (one shifted to negative and the other to positive fields), whose relative height and area depend on CF. However, the absolute value of the EB field is almost independent of CF. This suggests that the AF domain size is comparable to or larger than the FM domain size, so each FM domain couples mostly to one AF domain with a particular direction of the EB [2]. The transition from positive to negative EB can be systematically tuned with AD. The onset of positive EB appears at a CF one order of magnitude lower for AD=24 % than the unpatterned samples. These results are a consequence of the energy balance and suggest that the nanostructure plays a key role in the formation of pinned, uncompensated spin regions in the FeF<sub>2</sub> layer. The non-interfacial magnetic moments created at the antidot faces favor the onset of positive EB at lower CF [3].

The financial support of the Spanish MICINN (MAT2009-08667 and CSD2006-00012), Catalan DURSI (2009SGR856) and the U.S. Air Force are recognized.

### References:

- [1] O. Iglesias, A. Labarta, and X. Batlle, *J. Nanoscience and Nanotechnology*, **8**(2008) 2761.
- [2] O. Petravic, Z.P. Li, Igor V. Roshchin, M. Viret, R. Morales, X. Batlle, and I. K. Schuller, *Appl. Phys. Lett.*, **87** (2005) 222509; I.V. Roshchin, O. Petravic, R. Morales, Z.P. Li, X. Batlle and I.K. Schuller, *Euro. Phys. Lett.*, **71** (2005), 297.
- [3] M. Kovylnina, M. Erekhinsky, R. Morales, J. Villegas, I.K. Schuller, A. Labarta and X. Batlle, *Appl. Phys. Lett.* **95** (2009) 152507.

Figures:

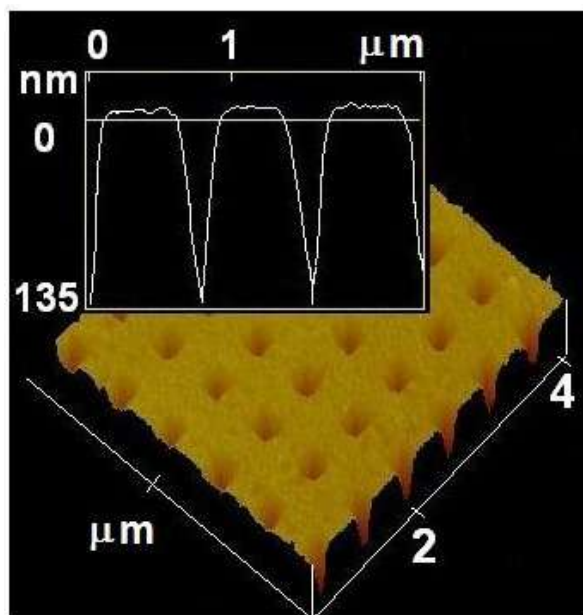


**Figure 1.** Atomic force microscopy image for  $AD = 0.12$ ; The inset shows that the antidot is carved through the whole depth of the heterostructure.

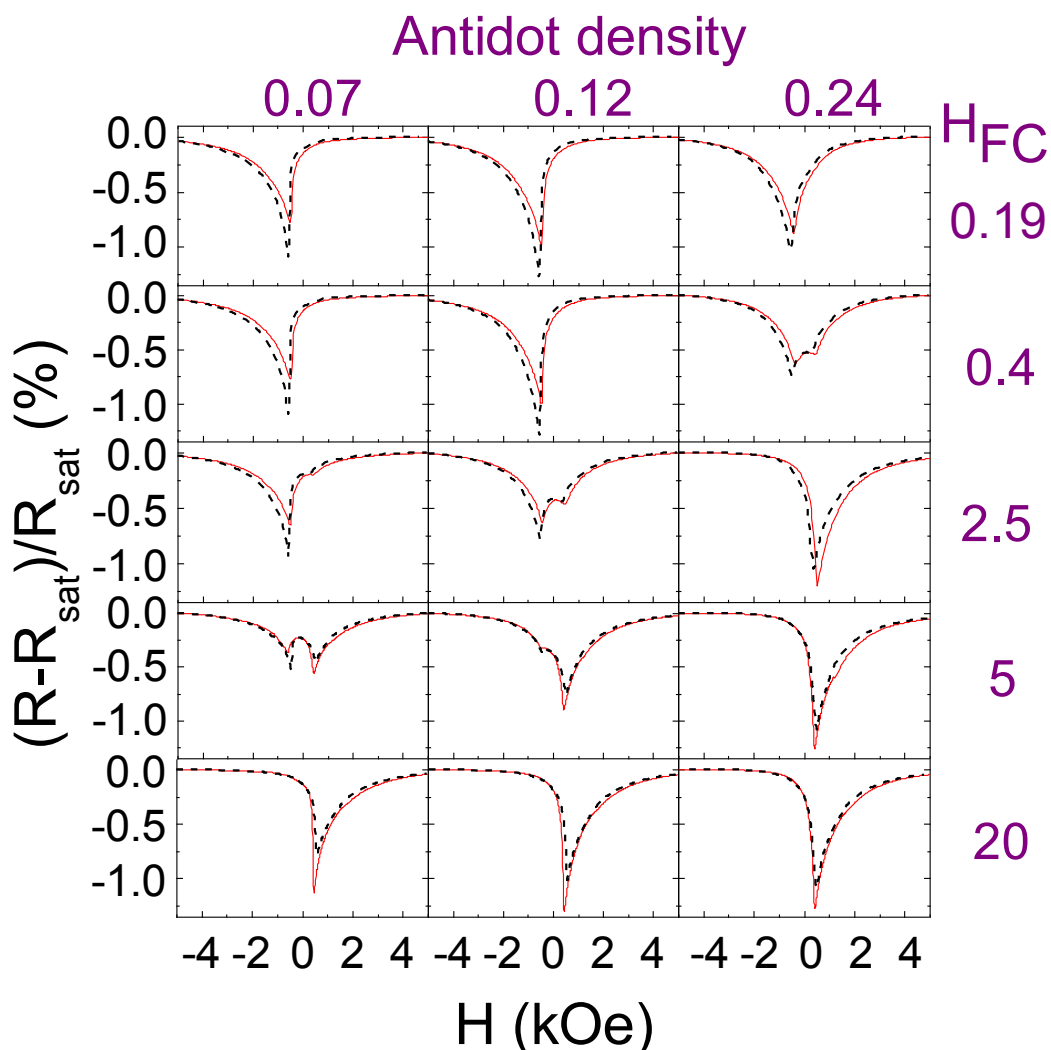


**Figure 2.**  $(R(H) - R_{\text{sat}})/R_{\text{sat}}$  measured at 4.2 K as a function of  $H$  applied parallel to the current, after cooling under  $H_{\text{FC}} = 0.19, 0.4, 2.5, 5$  and  $20$  kOe, for  $AD = 0.07, 0.12$  and  $0.24$ . The solid (red)/dash (black) line corresponds to the decreasing/increasing field branches.

## **Enhanced emission in self assembled photonic crystals by hybrid photonic-plasmonic modes**

M. López-García, J.F. Galisteo-López, A. Blanco, C. López

*Instituto de Ciencias de Materiales de Madrid (CSIC), c/ Sor Juana Inés de la Cruz 3, 28049, Cantoblanco, (Madrid) Spain*

[mlopez@icmm.csic.es](mailto:mlopez@icmm.csic.es)

A. García-Martín

*Instituto de Microelectrónica de Madrid (CSIC), c/ Isaac Newton 8, 28760, Tres Cantos, (Madrid) Spain*

Coupling between plasmonic and photonic systems has become one of the most efficient ways to obtain small scale waveguiding and emitting devices [<sup>i</sup>]. In this work, a novel structure for obtaining enhanced emission in a hybrid plasmonic-photonic structure is presented. The samples under study consist of large area close-packed ordered monolayers of dye doped polystyrene spheres grown on a thin (60nm) gold film. This system allows surface resonant plasmonic modes to couple efficiently to photonic ones leading to the formation of localized surface plasmon polariton (SPP) modes, propagating waveguide modes and hybrid ones [<sup>ii</sup>].

The dispersion relation of these modes is retrieved by means of angle and polarization resolved reflectance measurements for different crystallographic orientations. Comparison with calculated reflectance spectra as well as the spatial distribution of the electric field in the system allows us to identify different mode types. Field enhancement inside the spheres is seen to be much larger than that obtained for similar samples grown on dielectric substrates evidencing the role of the metallic layer in preventing leakage losses into the substrate [<sup>iii</sup>].

Finally we have studied the effect of such field enhancement on the emission of the dye by studying angle and polarization resolved photoluminescence (PL). We have observed that enhanced emission is obtained for those modes where the field is mainly concentrated in the region containing the emitter (i.e. polymeric spheres). A comparison with a reference system non structured thin dye doped polymer films deposited on gold, further points to the efficiency of our samples to obtain enhanced emission. The spectral tunability of the mode dispersion with sphere size makes this system a versatile one for many applications involving efficient emitting devices.

## References:

- <sup>i</sup> R.F. Oulton, V.J. Sorger, T. Zentgraf, R-M. Ma, C. Gladden, L. Dai, G. Bartal and X. Zhang, *Nature*, **461**, 629 (2009).
- <sup>ii</sup> R.M. Cole, Y. Sugawara, J.J. Baumber, S. Mahajan, M. Abdelsalam and P.N. Barlett, *Phys. Rev. Lett*, **97**, 137401 (2006).
- <sup>iii</sup> Y. Kurokawa, H. Miyazaki, Y. Jimbo, *Phys. Rev. B*, **69**, 155117 (2004).

## Figures :

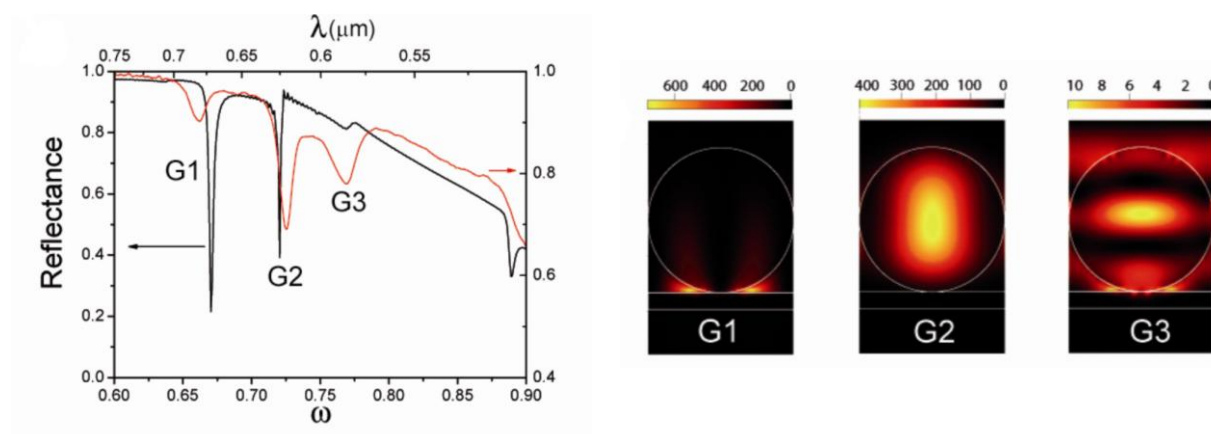


Figure 1: Left : Calculated (black curve) and measured (red curve) normal incidence reflection spectra of a ML of 520nm PS spheres grown on a gold substrate. Right: Total field intensity distribution of selected modes (as indicated in spectra).

## Technetium derivatives of Dawson Heteropolyanions: Redox properties and $\alpha_1/\alpha_2$ Relative Stability

XavierLópez, Susanna Romo, Israël-Martyr Mbomekallé, Donna McGregor, Lynn Francesconi, Josep M. Poble

*Departament de Química Física i Inorgànica, Universitat Rovira i Virgili, Marcel·li Domingo s/n, 43007 Tarragona, Spain*

*Javier.lopez@urv.cat*

This work analyzes the differences in the redox behavior between the well-known  $\alpha_1$  and  $\alpha_2$  positional isomers of the technetium-monosubstituted Dawson anion,  $[P_2W_{17}TcO_{62}]^{n-}$  [1]. The results, based on cyclic voltammetry (CV) measurements and density functional (DFT) calculations, show these two isomers' relative stability upon the number of electrons that the Tc ion carries. The  $\alpha_1$  form gains relative stability as the systems gets reduced from  $d^0$  for Tc(VII) to  $d^3$  for Tc(IV). The most stable oxidation state observed for technetium is Tc(V). In this case, the  $\alpha_1$  isomer is computed  $4.0 \text{ kcal mol}^{-1}$  more stable than  $\alpha_2$ , whereas in fully oxidized form, Tc(VII),  $\alpha_2$  is more stable by  $-3.6 \text{ kcal mol}^{-1}$ . This gain in stability for  $\alpha_1$  correlates with Tc orbital energies obtained with DFT calculations [2]. The first unoccupied molecular orbital of the  $\alpha_1$  isomer lays lower than its  $\alpha_2$  homologue, traducing into a more exothermic reduction process for  $\alpha_1$ . The same stabilization of  $\alpha_1$  vs. the number of d electrons added has been observed in other  $P_2W_{17}MO_{62}$  systems ( $M = V, Mo, Re$ ). CVs also show, and DFT calculations explain, why isomer  $\alpha_1$  can not be oxidized to Tc(VII) in aqueous media, whereas it is possible for the  $\alpha_2$  isomer. Such a general behavior can be applied to systems containing other M ions. The pH influence on the reduction potentials has also been investigated. As in other polyoxometalate systems, increasing the pH shifts the reduction

potentials towards more negative values. In addition, one-electron waves that appear close (or as a single two-electron one) to each other at low pH values split as pH is increased, although isomer  $\alpha_1$  and  $\alpha_2$  also show differences in this issue. At high pH, both isomers feature a pH-independent first reduction wave.

### References:

- [1] Howell, R. C.; Nilges, M. J.; Mbomekallé, I. M.; Lukens, Jr., W. W.; McGregor, D.; Belford R. L.; Francesconi, L. C. *Inorg. Chem.*, submitted to publication.  
 [2] López, X.; Bo, C.; Poblet, J. M. *J. Am. Chem. Soc.* **124** (2002) 12574.

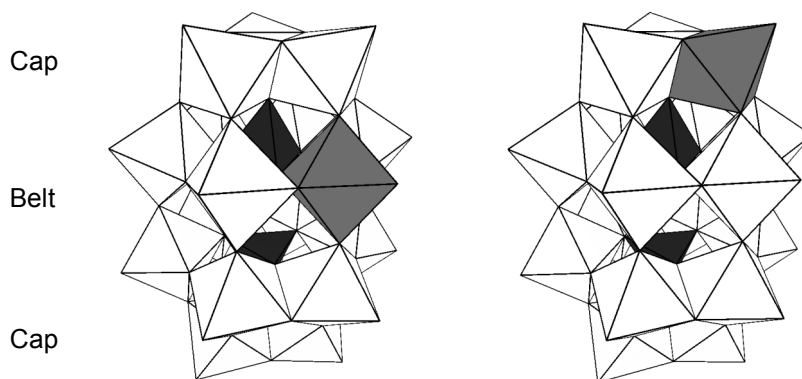


**Figure 1.**  $\alpha_1$  (left) and  $\alpha_2$  forms of the  $P_2MW_{17}O_{62}$  Dawson anion. White and gray octahedra are  $WO_6$  and  $MO_6$  units, respectively. Black tetrahedra are  $PO_4$  moieties.

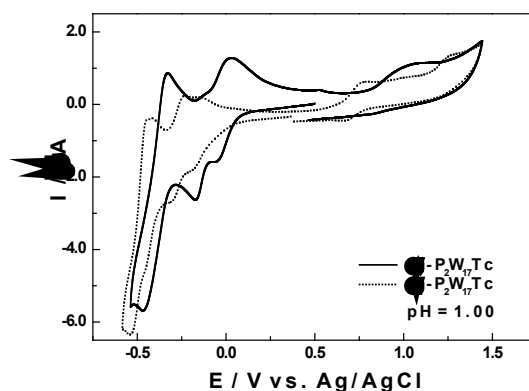


**Figure 2.** Cyclic voltammograms of **1** (solid line) and **2** (dotted line) in 0.2M  $Na_2SO_4 + H_2SO_4$  pH 1. Working electrode: glassy carbon; reference electrode: Ag/AgCl; Scan rate:  $10 \text{ mV}\cdot\text{s}^{-1}$ ; polyoxometalate concentration: 0.2 mM.

## Nanotechnology-based new systems in drug delivery

*Martín-Banderas, L.; Holgado M.A.; Muñoz-Rubio, I; Cózar, M.J.; Álvarez-Fuentes, J.; Durán, M.; Arias, J.L.<sup>1</sup>; Fernández-Arévalo, M*

*Dept. Pharmacy and Pharmaceutical Technology, Univ. Sevilla, Spain*

*<sup>1</sup>Dept. Pharmacy and Pharmaceutical Technology, Univ. Granada, Spain*

[luciamartin@us.es](mailto:luciamartin@us.es)

### Introduction

At present 95% of all new potential therapeutics have poor pharmacokinetics and biopharmaceutical properties. Nanotechnology plays an important role in therapies by lowering doses required for efficiency as well as increasing the therapeutic indices and safety profiles of newer therapeutics. Here, there are reported three experimental examples of delivery nano-systems based on a biodegradable polymer, poly(D,L-lactide-co-glycolide) (PLGA) or natural phospholipids obtained by two different technologies which are briefly described below.

### Materials and Methods

#### Technologies

Two mechanical technologies were employed to produce nanoparticles containing different active molecules.

*Flow Focusing (FF).* This is a simple atomization technique based on the combination of a specific geometry and hydrodynamic forces. FF provides a remarkable accuracy in size, narrow size dispersion, and feasibility [1-4]. The phenomenon is characterized by the presence of a steady micro-jet which is “sucked” through a small orifice, and eventually breaks up into droplets of well-defined size and structure (Figure 1a).

*High pressure homogenization (HPH).* A fluid mechanical process that involves the subdivision of particles or droplets into micron sizes. The process occurs in a special homogenizing valve creating conditions of high turbulence and shear, combined with compression, acceleration, pressure drop, and impact which cause the disintegration of particles and dispersion throughout the product (Figure 1b).

#### Production of nanosystems. Experimental examples:

1. PLGA-Gemcitabine nanoparticles for oral administration. Gemcitabine is a water soluble anticancer drug with very short plasma half-life. To obtain the nanoparticles, FF technology was used. In this case, a primary o/w emulsion was carried out by dispersing a gemcitabine aqueous solution into a PLGA solution in ethyl acetate. This o/w emulsion was sprayed inside a hot chamber. The resulting solid polymeric particles were collected at the bottom of the chamber.
2. PLGA-  $\Delta^9$ -THC ( $\Delta^9$ -tetrahydrocannabinol) or CB13 nanoparticles for oral administration. THC and its derivatives are small oily molecules, recently accepted for neurology pain treatment. Nanoparticulated systems containing THC can avoid the drug accumulation on adipose tissue, among other advantages. In this case, drug and polymer were co-dissolved in ethyl acetate and used as focused fluid in a simple FF nozzle. Particles were produced inside a polyvinyl alcohol (PVA) bath under continuous agitation, and then particles were centrifuged and washed three times.
3. Lipid Nanoparticles (LN) for topical administration. These kinds of particles, among other advantages, allow achieved high levels of hydration by increasing the occlusion grade [5]. We prepared vitamin E loaded nanoparticles based on a mixture of fatty alcohols and a surfactant (Mygliol 813; Compritol ATO; Monostearin, Span 60, 0.25%) using HPH equipment (1 cycle, 1000 bar, 75 °C) (Panda 2K, Niro Soavi).

**Characterization methods:** *Particulate size.* Particles diameters were measured by photon correlation scanning (PCS) using a Partica LA-950V2 analyzer (Horiba). *Zeta potential ( $\zeta$ )* measurements were carried out in using a Malvern Zetasizer (UK) (PBS 7.4, 25°C). *Drug content* was determined by HPLC on a Hitachi LaChrom<sup>®</sup> (D-7000) Series HPLC system. *Scanning electron microscopy (SEM)* was used to evaluate nanoparticles aspect and morphology.

### Results and Discussion

Several methods to obtain drug loaded-nanoparticles using two different technologies (FF, HPH) have been developed. Drugs having radical different physicochemical and biopharmaceutical properties have been assayed. By FF (PLGA nanoparticles), particles around 1  $\mu\text{m}$  in diameter and narrow size distribution have been obtained (CV  $\leq$  10%). Zeta potential for PLGA nanoparticles were lightly

negative ( $\zeta \sim -20$  mV) which points out a favourable nanoparticles up take on Peyer's patch. Lipid nanoparticles (230 - 280 nm in diameter, Figure 2b,c) were obtained in two different internal structures: solid (SLN, perfect matrix) and nanostructured lipid carrier (NLC, imperfect matrix) according to the assayed formulations.

### Conclusions

The present study shows that Flow Focusing and HPH are suitable technologies to produce solid polymeric and lipid nanoparticles with uniform shape, mean size and size distribution.

We have established the possibility to obtain PLGA nanoparticles containing water and no-water soluble drugs with suitable properties for oral administration. Lipid nanoparticles for topical administration have been also produced with real small sizes allowing high levels of occlusion and hydration. FF technology is characterized by a high control on particle diameter and can also predict final particle diameter [1]. HPH can produce particles at very high rate (10L/h) in a continuous manner keeping constant high temperatures required for lipid formulations production.

### Acknowledgements

I. Muñoz-Rubio and M. Durán are grateful for the financial support from Consejo Andaluz de Colegios Oficiales de Farmacéuticos and University of Sevilla, Spain (Grant of Plan Propio of Investigación). Financial support from Junta de Andalucía, Spain, Projects P09-CTS-5029, is also gratefully acknowledged.

### References:

- [1] Gañán Calvo, A.M. Phys Rev Lett **80** (1998) 285-288
- [2] Martín-Banderas L. et al. Small., **1** (2005) 688-692
- [3] Martín-Banderas L. et al. Adv. Mat., **18** (2006) 559-64
- [4] Martín-Banderas L. et al. Int J Pharm **324** (2006) 19-26
- [5] Lippacher, A; Muller, RH; Mader, K. Int J Pharm **214** (2001) 9-12
- [6] Ingeniatics Tecnologías S.L. (Seville, Spain)

### Figures:

**Figure 1.** Technologies employed to produce drug-loaded nanoparticles: (a) Simple FF nozzle [6]; (b) scheme of the main pieces of HPH equipment

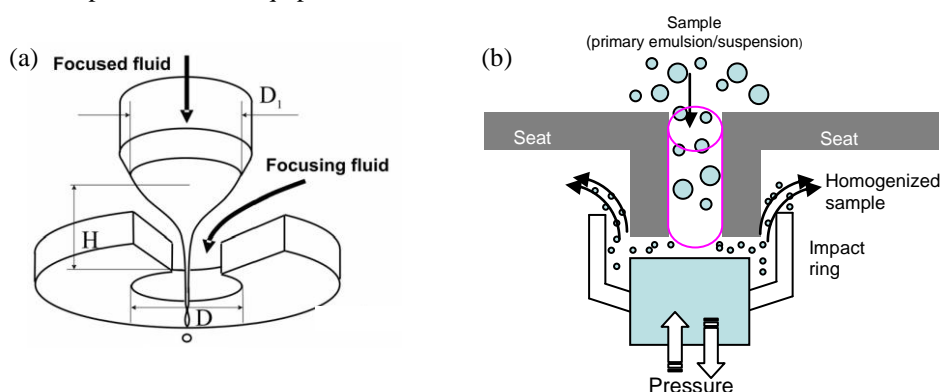
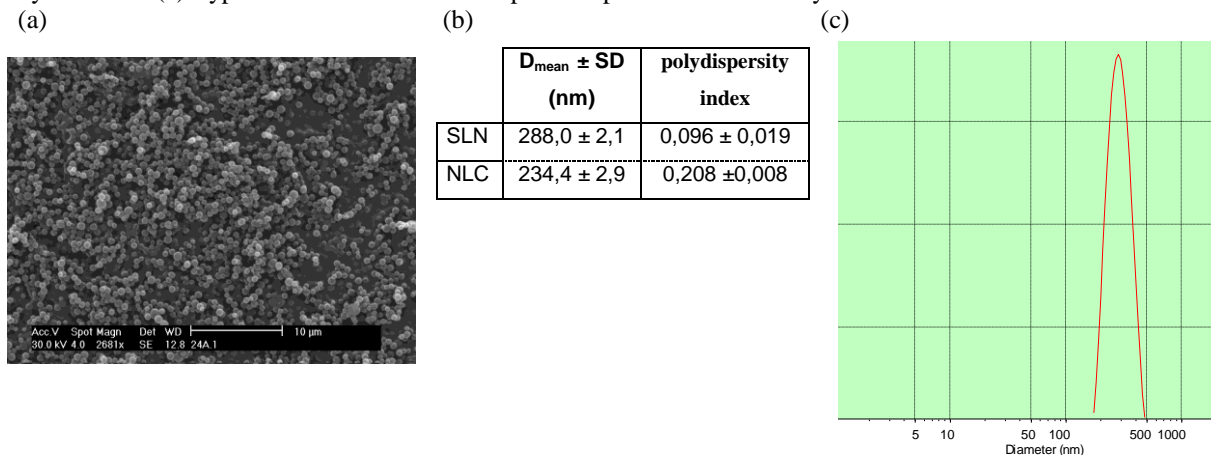


**Figure 2.** (a) SEM image of PLGA-Gemcitabine nanoparticles; (b) Mean diameter for SLN and NLC produced by HPH and (c) Typical size distribution for lipid nanoparticles obtained by HPH



## Metal oxides nanofibers obtained by electrospinning

*F. Martín<sup>a</sup>, H. Soussi<sup>a</sup>, E. Navarrete<sup>b</sup>, E.A. Dalchiele<sup>c</sup>, D. Leinen, L. Martínez<sup>c</sup>, J.R. Ramos-Barrado<sup>b</sup>*

*(a) Departamento de Ingeniería Química (b) Departamento de Física Aplicada I. Universidad de Málaga. Spain (c) Instituto de Física, Facultad de Ingeniería, Universidad de la República, Montevideo, Uruguay*

*(\*) [marjim@uma.es](mailto:marjim@uma.es)*

Nanoscale materials, such as nanowires, nanorods, nanowhiskers, and nanofibers have recently attracted attention due their exceptional properties and novel applications [1]. It has been demonstrated that metal oxide can readily be synthesized in these morphologies by electrospinning of sol-gel or polymeric solutions. Electrospinning technique is a relatively simple and versatile method for fabricating fibers with diameters ranging from tens of nanometers to micrometers. Typically in this technique, a polymer solution or melt is ejected from a small opening or a nozzle under the influence of a strong electrostatic field of negative or positive polarity. Electrostatic charges built upon the surface of the pendant drop induce the formation of a jet, which is subsequently stretched by a combination of superficial charge repulsion, superficial tension and viscosity, and finally, as the jet accelerated towards the collector, the solvent evaporated, leaving ultrathin fibers on the collector. If a metal oxide precursor is mixed or dissolved into the polymer, and the polymer is removed afterwards, for example by calcinations, it is possible to obtain metal oxide thin fibers.

The main objectives of this work were to investigate the effects of polymer and metal oxide precursor concentrations, electrostatic polarity, field strength, and calcination conditions on the morphological appearance and crystal structure of the resulting fibers. Also was an objective to apply the obtained fibers to functional devices, in our case they were used as anode materials for lithium batteries. But these ceramic fibers have other potential applications as membranes or catalysts. As example, rutile fibers were obtained by electrospinning of a mixture of titanium isopropoxide and a high molecular weight polyvinylpyrrolidone (PVP) at 20 kV with negative polarity. The PVP was removed by calcination in air at 600°C during two hours. If the fibbers are calcined at 400°C, then anatase structure could be obtained. If a salt of lithium is added to the initial polymeric solution, then  $\text{Li}_4\text{Ti}_5\text{O}_{12}$  with a spinel structure can be obtained [2,3] when the fibbers are calcined in air at 800 °C.  $\text{Li}_4\text{Ti}_5\text{O}_{12}$  has been studied as a candidate for negative active electrodes [4] for rechargeable lithium-ion batteries. The spinel  $\text{Li}_4\text{Ti}_5\text{O}_{12}$  is extremely tolerant to cycling because the volume of the cubic unit cell changes less than 1%

Figure 1, shows a SEM image of nanofibers as-spun. The figure 2 shows a distribution of rutile fiber diameters which range is between few to hundreds nanometers.

Acknowledgements: The financial support of this research was provided by the MEC (Acción Complementaria EXPLORA ENE2007-29042E/ALT).

### References:

[1] C. Feng, K. C. Khulbe, T. Matsuura, Journal of Applied Polymer Science, 115, (2010), 756.

- [2] Hai-Wei Lu, Wei Zeng, Yue-Sheng Li, Zheng-Wen Fu, *Journal of Power Sources* 164 (2007) 874.
- [3] Junrong Li, Zilong Tang, Zhongtai Zhang, *Electrochemistry Communications* 7 (2005) 894.
- [4] Hao Ge, Ning Li, Deyu Li, Changsong Dai, Dianlong Wang, *Electrochemistry Communications* 10 (2008) 1031.

**Figures:**

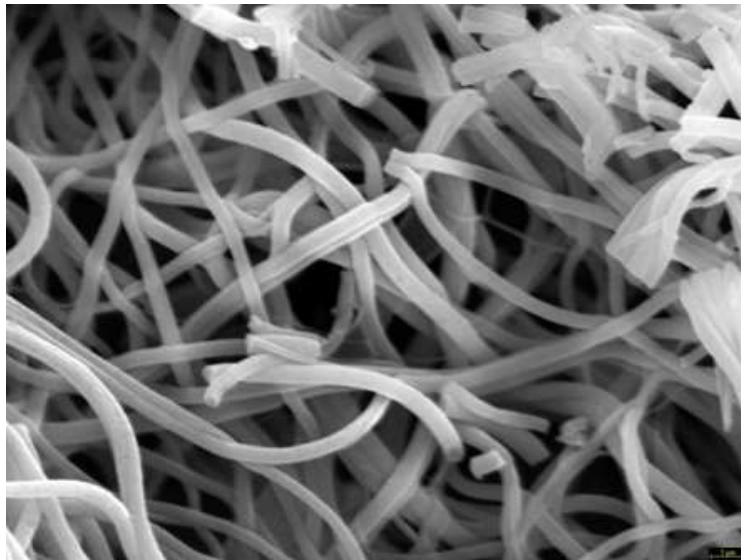


**Figure 1: PVP nanofibers as spun**

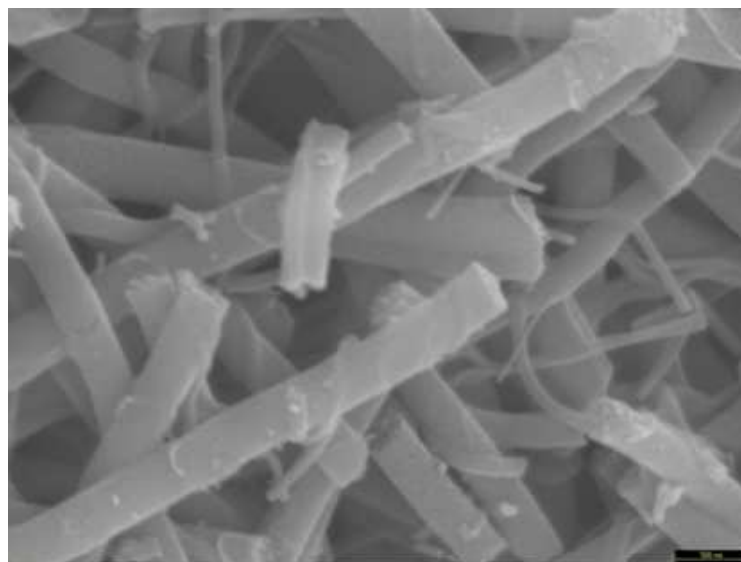


**Figure 2: Rutile fibers with different diameters**

## Information processing needs and challenges in the context of Nanomedicine

**Fernando Martín-Sánchez, Guillermo López-Campos, Victoria López-Alonso**

*Medical NanoBioInformatics Department, Institute of Health Carlos III, Majadahonda, Madrid, Spain*  
[fms@isciii.es](mailto:fms@isciii.es)

Nanomedicine, defined “as the application of nanotechnology in view of making a medical diagnosis or treating or preventing diseases”[1], opens new research avenues which increasingly demand sound methods and tools for data and knowledge management. For this reason, a new sub-discipline of Biomedical Informatics named “Nanoinformatics” [2] has been proposed as a way to facilitate the access of researchers, clinicians and other health professionals to the relevant information that is needed for the advancement of nanomedicine.

The main contributions of nanoinformatics that can support the effective processing of information in this field are summarized in Figure 1. They include: -nanomaterial characterization databases, -standardization and controlled vocabularies and taxonomies for nanomedicine, -data and image analysis techniques and -modelling and simulation (and even prediction) of biological behaviour of nanomaterial. Here follows a succinct description of each of them:

- Nanomaterial characterization databases. Nanoinformatics is contributing to the development of data repositories in the context of nanomedicine [3]. Nanolibraries and databases with information about physical-chemical, biological and toxicological properties of nanoparticles are already available. However, important challenges remain in integrating and providing a unified interface for these resources. This represents a key aspect in order to study the biocompatibility of nanomaterials. There is a clear need of new tools to define and store the minimum information associated with the characterization of nanoparticles. Again, nanomedicine poses new challenging issues for informatics in terms of integrating nanomaterial data with biological and clinical information that is already available in biomedical databases.
- Standardization and controlled vocabularies and taxonomies for nanomedicine. The large amount of experimental and bibliographic data that is being produced on a daily basis requires the setting up of information-based models and tools that allow for the sharing of all these data. Taxonomies, ontologies and controlled vocabularies are central issues in this regard [4]. To facilitate data interoperability in all areas of nanomedicine, from atomic and molecular level to the clinical level, there is a need to develop nano-ontologies to achieve a conceptual (semantic) consensus of terminology, for the development of nanotechnology applications in Health.
- Data and image analysis techniques. Once those data were available, it would be possible to use advanced informatics techniques (such as data and text mining) in order to extract new knowledge based on previous results [5]. Advances in nanomedicine are expected to produce less invasive and more precise imaging modalities, however due to the size and properties of nanoparticles, image processing methods will require considerable computational power in order to efficiently manage the huge amount of data about nanoparticles that will be generated along the process and new image analysis techniques will be needed in order to correlate theoretical discoveries with experimental results.

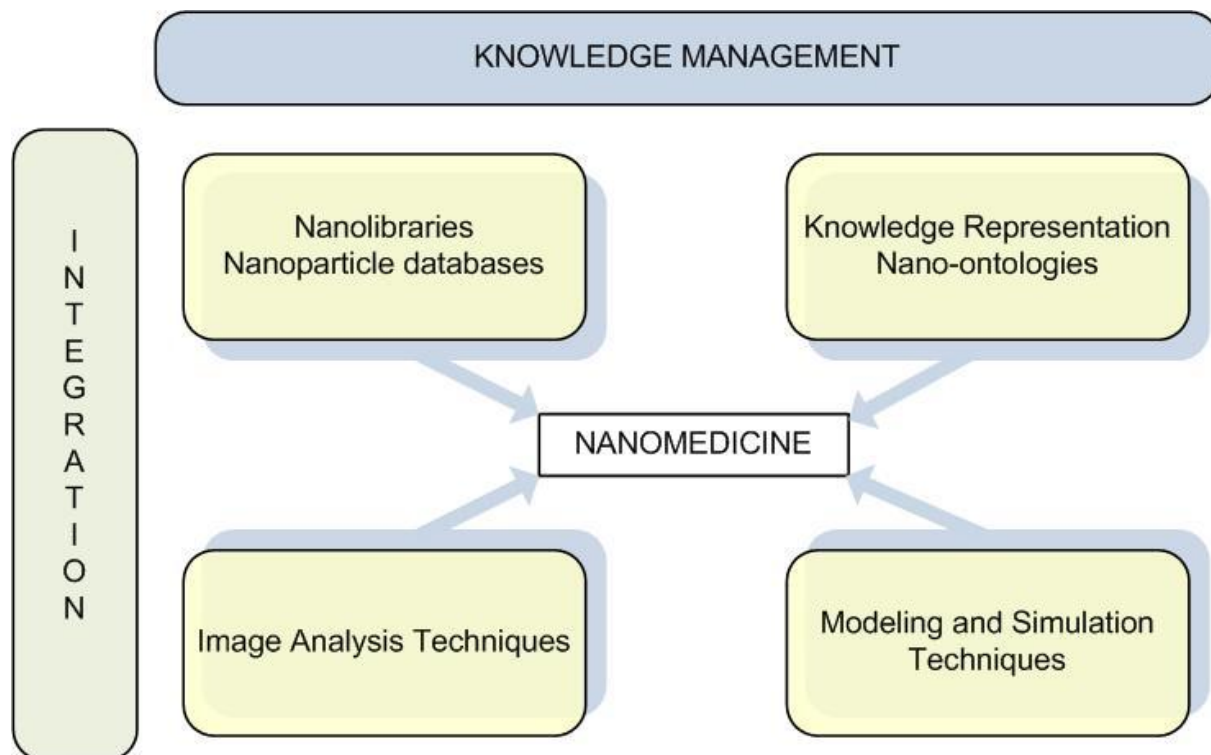
- Modelling and simulation (and even prediction) of biological behaviour of nanomaterials. The analysis of positive and negative effects of nanoparticles based on “in vitro” or “in vivo” studies is expected to be complemented with “in silico” modeling and simulation techniques that will be used to predict nanoscale biomedical systems behaviour.

In summary, the term nanoinformatics encompasses the application of computer technologies, information science and molecular simulations, arising as a key methodology in the short-term development of nanomedicine.

### References:

- [1] European Medicines Agency. (2006) EMEA/CHMP/79769/2006  
 [2] Martín-Sánchez, V. López-Alonso, I. Hermosilla-Gimeno and G. Lopez-Campos. Lecture Notes in Computer Science (2008). Vol. 5178, pp 50-57.  
 [3] López-Alonso V; Hermosilla-Gimeno I; Lopez-Campos G; *et al.* AMIA Annual Symposium Procs (2008) pp 1046.  
 [4] Gordon N, Sagman U (2003). Canadian Institute of Health Research & Canadian NanoBusiness Alliance  
 [5] Chiesa S, García-Remesal M, de la Calle G, de la Iglesia D, *et al.* Procs of the KES 2008 symposium (2008) pp 50-57.

**Figure 1.** The four main areas of research in Nanoinformatics are supported by integration of biomedical resources and knowledge management processes.



## First studies with a new wide frequency range device for the induction of hyperthermia in magnetic fluids, for magnetic fluids experimentation in biomedical applications

A.Mina Rosales<sup>1,2,3</sup>, J.J. Serrano Olmedo,<sup>1,2,3</sup> C. Maestú Unturbe<sup>1,2,3</sup>, R. García Mendoza<sup>1,2,3</sup>, F. del Pozo Guerrero<sup>1,2,3</sup>.

<sup>1</sup> Bioengineering and Telemedicine Group (GBT), Biomedical Technology Center (CTB), Polytechnic University of Madrid (UPM), Avenida Complutense 30, "Ciudad Universitaria". 28040 – Madrid, Spain.

<sup>2</sup> Bioengineering, Biomaterials and Nanomedicine Network for Biomedical Research, Madrid, Spain.

<sup>3</sup> Biosciences Program MADR.IB-CM Comunidad de Madrid  
[amina@gbt.tfo.upm.es](mailto:amina@gbt.tfo.upm.es), [ajserran@etsit.upm.es](mailto:ajserran@etsit.upm.es)

Hyperthermia (Greek word for "overheating") is defined as the phenomenon that occurs when a body is exposed to an energy generating source that can produce a temperature change inside, 42-45<sup>0</sup>C range [1-2] along a given time. The excitation should be retained for a minimum period of 30 minutes, to produce cell death by thermal destruction in the treatment area. Generation of magnetic hyperthermia is performed through changes of the magnetic induction in magnetic nanoparticles (MNPs) that are embedded in viscous medium. The MNPs have the capacity to absorb energy from an alternating magnetic field to generate heat. The main applications of this technique are identified in cancer therapy and delivery of drugs into specific sites.

In this work we present a new device for hyperthermia induction in magnetic fluids. The device was completely designed and built by our research-group and presents advantages as compared to commercial devices. One of them, and the most important one, is the ability to achieve a wide range of working frequencies from 9 KHz to 2MHz, whilst the commercial equipment generally can handle only one frequency or very short frequency range. Another advantage is the possibility to use different signals like sinusoidal, square, pulse sequences configurations, etc.; our purpose is to study the phenomena of the heat generation by changing the excitation signal. This could be the way to optimize the magnetic hyperthermia induction parameters.

The hyperthermia device basically consists of a signal generator, an amplifier, a copper coil, a cooling system, an optical temperature sensor, control software, multimeter and the probe (Figure 1). The amplifier has a wideband frequency range (9KHz-2MHz) and a linear output up to 1000W. The selected signal passes through the amplifier and feeds the copper coil, where is produced the magnetic field. The cooling system serves to keep controlled and fixed the environmental temperature, so isolating the sample from the thermal external influence. In order to know the temperature inside the sample it is used an optical temperature sensor with a range of 0 to 120<sup>0</sup>C and 0.02<sup>0</sup>C resolution. We have control software to avoid undesired changes in the magnetic field due to spurious fluctuations in the delivered power. The probe is an adiabatic chamber made of borosilicate. As well as we had made this device, we are making a theoretical approximation on the thermal system response to be able to obtain the specific absorption rate (SAR) and the other interesting parameters.

To show the functionality of our device, we present results about the behavior of some MNPs [3]. The methodology consists in the application of a magnetic field 2.8 kA/m intensity and 1.8MHz frequency for 45 minutes. We continue to record the temperature for 15 minutes without excitation to observe the heat dissipation. The description of the samples used for the study is in Table 1. The time-dependent temperature curves are shown in figure 2. The highest

observed temperature change correspond to the smallest diameter (15 nm) MNPs, as expected.

Sample	Coating	Diameter MNPs (nm)	Amount of sample ( $\mu$ liters)	Concentration
Magnetita	Dextran	20	200	10mg/ml
Magnetita	Dextran	50	200	10mg/ml
Endorem	Varios	15	200	-

Table1. Description of the samples used for the study.

## References:

- [1] Pankhurst QA, Conolly J, Jones S K, Dobson J. Applications of magnetic nanoparticles in biomedicine. *Journal of physics. D, applied physics* 36(13), (2003), pp. R167.
- [2] Lee SW, Bae S, Takemura Y, Yamashita E, Kunisaki J, Zurn S, Kim CS, Magnetic Properties, Self-Temperature Rising Characteristics, and Biocompatibility of  $\text{NiFe}_2\text{O}_4$  Nanoparticles for Hyperthermia Applications, *Magnetics, IEEE Transactions on*, vol. 42, (2006) pp. 2833-2835.
- [3] Mina Rosales A., Ma. A. Peramo Serrano, J.J. Serrano Olmedo, F. del Pozo Guerrero, Generación de hipertermia mediante campos magnéticos alternos, aplicada en muestras con nanopartículas magnéticas: fenómenos físicos y primeros resultados, Congreso Anual de la Sociedad Española de Ingeniería Biomédica, (2010), pp 166.

## Figures:

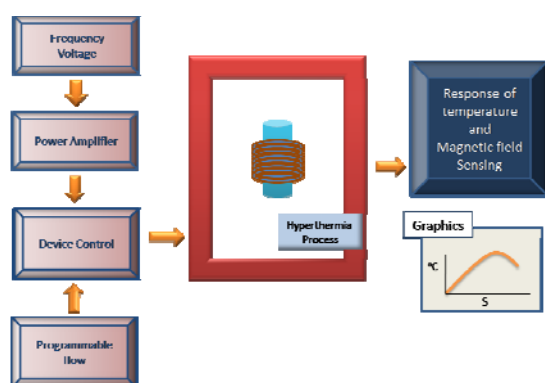


Figure1. Scheme of hyperthermia device

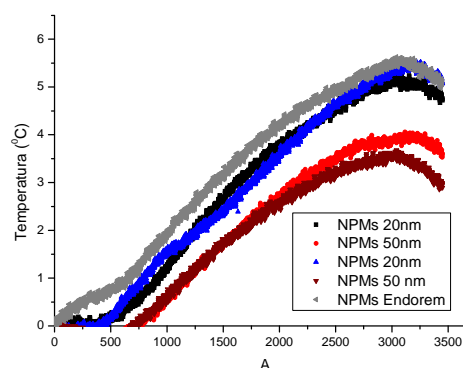


Figure2. Time-dependent temperature curves of the samples in 1.8 MHz and 2.6 kA/m.

## Electron excitations of carbon nanostructures by the CNDOL Hamiltonian

A.L. Montero<sup>a,b)</sup>, M.E. Fuentes<sup>c)</sup>, E. Menéndez<sup>d)</sup>, W. Orellana<sup>e)</sup>, C. Bunge<sup>f)</sup>, L.A. Montero<sup>a)</sup> and J.M. García de la Vega<sup>b)</sup>

a) *Laboratorio de Química Computacional y Teórica, Facultad de Química, Universidad de la Habana, 10400 Havana, Cuba*

b) *Departamento de Química Física Aplicada, Facultad de Ciencias, Universidad Autónoma de Madrid, 28049 Madrid, Spain*

c) *Laboratorio de Química Computacional, Universidad Autónoma de Chihuahua, 31000 Chihuahua, Mexico*

d) *Departamento de Física, Facultad de Ciencias, Universidad de Chile, Las Palmeras 3425, 780-0024 Ñuñoa, Santiago, Chile*

e) *Departamento de Ciencias Físicas, Universidad Andrés Bello, Av. República 220, 837-0134 Santiago, Chile*

f) *Instituto de Física, Universidad Nacional Autónoma de México, México*  
[ana.montero@uam.es](mailto:ana.montero@uam.es)

Real scenarios at nanoscopic levels involve irreducible large molecular systems that are characterized by complex environments and non-periodic arrangements of different bodies. Consideration of electron densities and exchange by means of appropriate Hamiltonians of the complete system is required to obtain more reliable computational models, including bonding. Electronic state properties of such systems, like fullerenes [1] and nanotubes [2], represent a very active field of research nowadays where, for example, the interaction with the light is important.

CNDOL (Complete Neglect of Differential Overlap considering the L azimuthal quantum number), is an *a priori* and approximate quantum mechanical Hamiltonian [3] that consists in a simplified Hartree-Fock (HF) procedure comprising all valence electrons. It is provided as a good starting point to build molecular wave functions, which are further variationally improved by applying large-scale singly-excited configuration interaction (CIS) as a straightforward procedure for modeling electron excitation processes of big polyatomic systems[4].

In the present work we want to show the performance of the CNDOL formalism to model the electronic properties of different carbon nanostructures. The predicted electron transition energies and related properties of the isolated fullerene ( $C_{60}$ ), van der Waals cluster models of them  $(C_{60})_n$  and zig-zag like  $(n,0)$  single walled carbon nanotubes (SWCNT), are analyzed and compared with available experimental data. The optical spectrum of the isolated fullerene and their cluster models show similarities. However, the appearance of allowed electron transitions at lower energies in van der Waals complexes in concordance with the experimental spectra, could be considered as an evidence of intermolecular interaction phenomena during excitations. The CNDOL calculations of  $(5,0)$ ,  $(9,0)$  and  $(13,0)$  SWCNT's, performed over a set of increasingly long, although finite lengths, show that it is

important to consider finite models of SWCNT's with length larger than 3 nm in order to simulate realistic properties corresponding to experimental systems. The absorption spectrum obtained for (5,0) SWCNT is in nice agreement with the experimental data [5]. Both, the (5,0) and (13,0) SWCNTs do not show a decrease in the lowest energy excited states when the length increases, in contrast to the (9,0) SWCNT, which show more favoured conditions for photo-excitations when became longer.

### References:

- [1] A. A. Voityuk and M. Duran, *Journal of Physical Chemistry C*, **112** (2008) 1672.
- [2] A. López-Bezanilla, F. Triozon, S. Latil, X. Blase, and S. Roche, *Nano Letters*, **9** (2009) 940.
- [3] L. A. Montero, L. Alfonso, J. R. Alvarez, and E. Perez, *International Journal of Quantum Chemistry*, **37** (1990) 465.
- [4] L. A. Montero-Cabrera, U. Röhrig, J. A. Padron-García, R. Crespo-Otero, A. L. Montero-Alejo, J. M. García de la Vega, M. Chergui, and U. Röthlisberger, *The Journal of Chemical Physics*, **127** (2007) 145102.
- [5] Z. M. Li, Z. K. Tang, H. J. Liu, N. Wang, C. T. Chan, R. Saito, S. Okada, G. D. Li, J. S. Chen, N. Nagasawa and S. Tsuda, *Physical Review Letters*, **12** (2001) 127401.

## Design and Construction of an Ultra High Vacuum Integral Low Energy Electron Mössbauer Spectrometer for Surface Analysis

*M. Monti, J.R. Gancedo, M. Gracia, J. de la Figuera and J.F. Marco*  
*Instituto de Química Física "Rocasolano", CSIC, Serrano 119, 28006 Madrid, Spain*  
*mmonti@iqfr.csic.es*

Mössbauer spectroscopy is regarded generally a bulk technique. However, it is known from many years [1] that it can be converted into a surface sensitive technique by means of the detection of the conversion electrons emitted subsequently to the nuclear de-excitation that follows the nuclear resonant absorption. Both the theoretical and experimental aspects of this variant of the technique (known as CEMS, Conversion Mössbauer Electron Spectroscopy) are well established and it has been successfully applied to the study of many different problems. One of the limitations of CEMS from the point of view of the surface analyst is that its surface sensitivity is lower than that of other standard analytical techniques such as XPS or AES. While the depth probe in these latter techniques is around 3-5 nm, the depth probe in CEMS is around 300 nm. This is related to the much higher energy of the conversion electrons (7.3 keV in the case of  $^{57}\text{Fe}$ ), which, obviously, can travel much longer distances in the solid.

After the emission of the conversion electrons a complex reorganisation of the different atomic shells takes place bringing about the emission of Auger electrons of different energies, fluorescent X-rays and shake-off electrons. Monte Carlo calculations show that, in iron, every single Mössbauer event is accompanied by 6.5 ionizations. From those, 1.5 correspond to resonant electrons of high energy (K and L conversion electrons and KLL, KLM y KMM Auger electrons) and 5.0 to LMM, MMM and MMN Auger electrons with energies lower than 100 eV and shake-off electrons with energies lower than 15 eV. It has been suggested [2] that the surface sensitivity of Mössbauer spectroscopy could be enhanced by detecting these low energy electrons since it is thought that they represent more than 50% of the total emitted electrons and their range in the solid is within a few nanometers. This variant of Mössbauer spectroscopy is known as ILEEMS (Integral Low Energy Electron Mössbauer Spectroscopy).

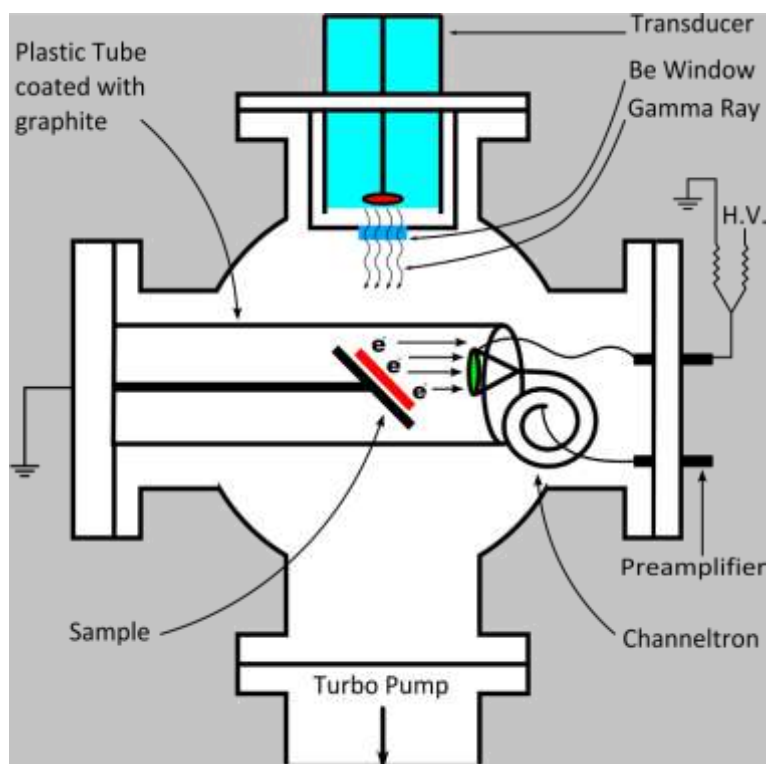
From the experimental point of view, ILEEMS is a technique which needs to be operated at least under high vacuum conditions using a channeltron as electron detector. Since most of the channeltrons have a low efficiency for the detection of low energy (<1 keV) electrons, a positive bias has to be applied to the cone entrance of the channeltron in order to accelerate the less energetic electrons increasing in that way the efficiency in their detection.

We report here on the design and construction of an ultra high vacuum ILEEM spectrometer aimed at the chemical, structural and magnetic characterization of iron-containing surfaces and nanostructures. The design allows the operation of the spectrometer as a stand alone device for the characterisation of samples produced ex-situ or as an accessory instrument coupled to an UHV chamber for the study of samples produced in UHV conditions.

We have carried out experiments to optimize the operational conditions of the spectrometer and we are currently involved in the study of carefully prepared samples with a well-defined layer structure to quantify the surface sensitivity of the technique. The results are compared with those obtained from XPS.

**References:**

- [1] J.R. Gancedo, M. Gracia y J.F. Marco, *Hyperfine Interact.* **66** (1991) 83.  
[2] E. De Grave, R.E. Vandenberghe y C. Dauwe, *Hyperfine Interactions* **161** (2005) 147.

**Figure:**

*Fig.1 Schematic drawing of ILEEMS system.*

## Investigation of Ionic Water Flow Over a Carbon Nanotube: Stick-Slip Mechanism

*F. Moradi, R. Kalantarinejad, N. M. Asghari, and M. Bahrani*

*Aerospace Research Institute, Ministry of Science, Research and Technology, Tehran, Iran  
[moradi@mail.ari.ac.ir](mailto:moradi@mail.ari.ac.ir)*

### Introduction

At early 2001, Kral and Shapiro reported the possibility of generating an electric current by making a liquid flow over some metallic carbon nanotubes [1]. This theory was proved by the experimental production of a CNT-based flow sensor which indicated the generation of an induced voltage in nanotube bundles because of a ionic liquid flow with a number of different velocities [2]. Although Ghosh and his coworkers believe in the main role of pulsating asymmetrical ratchets to explain the transduction mechanism of this sensor [2], there are other suggested models involving phonon wind drag, columbic fields [1], electrokinetic mechanism [3] and a stick-slip flow [4].

The logarithmic dependence of induced voltage on the liquid velocity and also respectively, direct and reversed relation between voltage and liquid's polarity and viscosity are some remarkable properties of the produced sensor, to which is asserted that the stick-slip model has the most conformity. Such a mechanism is based on the alternative adsorption and desorption of ions dissolved in solid-like water layer pinning to nanotube surface.

### Molecular Dynamics Simulations

In this work we use molecular dynamics simulations to demonstrate the manner of a ionic flowing water around a carbon nanotube and therefore to investigate the possibility of the stick-slip model. Therefore a metallic (5,5) carbon nanotube immersed in a sodium chloride solution, is computationally simulated by NAMD software [5]. We also use langevin dynamics to appoint a constant temperature in an NVT ensemble.

In spite of some nanoseconds of simulation, we observe that not only sodium ions, contrary to Persson's anticipation [4], don't adsorb on CNT surface, but also such a pristine nanotube is so much hydrophobic that water molecules don't approach its surface closer than  $3.2 \text{ \AA}$ , "Fig 1". This space resembles the CNT-liquid interface thickness, while introducing a nanotube into water [1,2]. However, there are some differences with what has been reported for  $\text{Na}^+$  ( $5.5 \text{ \AA}$ ) and  $\text{Cl}^-$  ( $5.3 \text{ \AA}$ ) equilibrium distances from CNT surface according to Ghosh et. al *ab initio* studies [6].

We also perform the radial distribution calculations for  $\text{Na}^+$  and  $\text{Cl}^-$ , to evaluate the arrangement over carbon nanotube's surface.

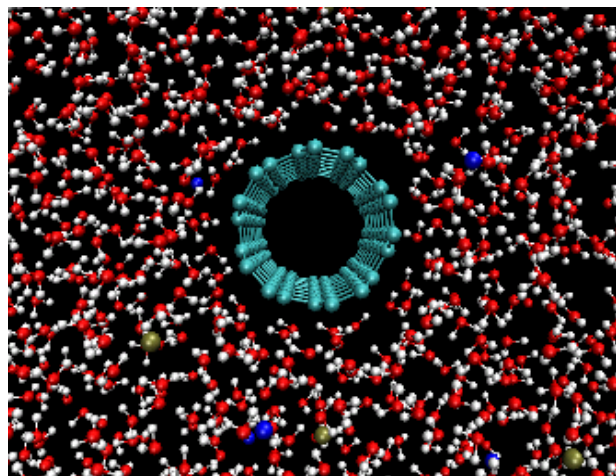
### Ab initio Studies

The minimum approaching distance of positive sodium ions to carbon nanotube surface is applied to investigate the interaction of one  $\text{Na}^+$  on nanotube density of states, according to density functional theory (DFT). For this purpose we use Siesta code [7] and the pseudopotential approximation. The obtained results indicate some noteworthy changes in the electronic density of states of the nanotube.

Finally it seems that flowing water can force a few of positive ions to approach nanotube surface up to a  $3.2 \text{ \AA}$  distance, that is a bit similar to what Persson et. al suggest as an arrangement of positive ions on water-CNT interface layer, but there is an obvious contradiction to the theory of ions' periodically adsorption and desorption on nanotube external surface as the transduction mechanism of charge transfer in nanotube due to flowing of water over it.

**References:**

- [1] P. Král and M. Shapiro, “Nanotube electron drag in flowing liquids”, *Physical Review Letters*, **vol. 86**, (2001) pp.131-134.
- [2] S. Ghosh, A. K. Sood, and N. Kumar, “Carbon nanotube flow sensors”, *Science*, **vol. 299**, (2003) pp.1042-1044.
- [3] A. E. Cohen, “Carbon nanotubes provide a charge”, *Science*, **vol. 300**, (2003) pp.1235-1236.
- [4] B. N. J. Persson, U. Tartaglino, E. Tosatti, and H. Ueba, “Electronic friction and liquid-flow-induced voltage in nanotubes”, *Phys. Rev. B*, **vol. 69**, no. 23, (2004) pp.235410-235415.
- [5] J. C. Phillips, R. Braun, W. Wang, J. Gumbart, E. Tajkhorshid, E. Villa, C. Chipot, R.D. Skeel, L. Kale, K. Schulten, “Scalable molecular dynamics with NAMD”, *J. Comp. Chem*, **vol. 26**, (2005) pp. 1781–1802.
- [6] S. Ghosh, V. Gadagkar, and A.K. Sood, “Strains induced in carbon nanotubes due to the presence of ions: *ab initio* restricted Hartree-Fock calculations”, *Chem. Phys. Lett.*, **vol. 406**, (2005) pp.10-14.
- [7] J. M. Soler, E. Artacho, J. D. Gale, A. García, J. Junquera, P. Ordejón, and D. S. Portal, “The SIESTA method for *ab initio* order-*N* materials simulation”, *Journal of Physics: Condensed Matter*, **vol. 14**, no. 11, (2002) pp. 2745-2781.

**Figures:**

**Figure 1.** Snapshot of the simulated carbon nanotube immersed in a solution of  $\text{Na}^+$  (blue) and  $\text{Cl}^-$  (green), showing the hydrophobic surface of carbon nanotube.

## **Health Impact of Engineered Metal and Metal Oxide Nanoparticles: Response, Bioimaging and Distribution at Cellular and Body Level**

E.Rojas<sup>1</sup>, I.Llarena<sup>1</sup>, A. Gonzalez<sup>2</sup>, I. Estrela<sup>3</sup>, E.Donath<sup>3</sup>, Ch.Gao<sup>4</sup>, S.T.Larsen<sup>5</sup>,  
K.Savonailen<sup>6</sup>, S.E.Moya<sup>1</sup>

<sup>1</sup>CIC biomaGUNE, San Sebastián, Spain

<sup>2</sup>University of Vigo, Vigo, Spain

<sup>3</sup>University of Leipzig, Leipzig, Germany

<sup>4</sup>Zhejiang University, Hangzhou, China

<sup>5</sup>National Research Centre for the Working Environment, Copenhagen, Denmark

<sup>6</sup>Finish Institute of Occupational Health, Helsinki, Finland

Email: smoya@cicbiomagune.es

Metal oxide and metal NPs are widely used in various industrial processes and common products. Some examples of these are TiO<sub>2</sub> and ZnO as catalysts and UV protectors, CuO in anti-fouling paints, Al<sub>2</sub>O<sub>3</sub> as a surface protector, CeO<sub>2</sub> in polishing, and various rare earth oxides in electronics, among many other applications.

Metal and metal oxide NPs may be toxic for two reasons: i) They may possess increased catalytic activity due to nanoscale structure or chemical modification of their surface. These catalytic properties may interfere with numerous intracellular biochemical processes. ii) The decomposition of NPs and subsequent ion leakage may result in a continuous formation of free radicals and metal ions, which may heavily interfere with the intracellular free metal ion homeostasis, which requires that metal ions are kept at extremely low levels in the cytoplasm.

Previous research and hypothesis suggest that the particle size, shape, chemical composition and the chemistry of the capping agent determine the catalytic properties and surface activity of NPs as well as the materials where the NPs are incorporated. These properties are important for the applications of the NPs and must be studied in the context of their effects on human health.

Our approach to the problem is multidisciplinary and involves:

- 1) Characterization of commercially available NPs, and the fabrication and characterization of NPs with specific properties and with either fluorescence or radioactive labelling.
- 2) Technical development and analysis of the uptake, distribution and release of NPs *in vivo* and in cells.
- 3) Understanding the interaction of NPs with cellular and extra-cellular components
- 4) Determination of physiological effects of NPs *in vitro*.
- 5) Risk of exposure and toxicological effects of metal and metal oxide NPs.

## Design and production of cannabinoids-loaded PLGA nanoparticles for treatment of neuropathic pain

*Muñoz-Rubio, I., Martín-Banderas L., Álvarez-Fuentes J., Cózar-Bernal M.J., Holgado, M.A., Fernández-Arévalo, M.*

*Department of Pharmacy and Pharmaceutical Technology, Faculty of Pharmacy, University of Seville, Spain.  
inmmunrub@alum.us.es*

### Introduction

The pain reduces the quality of life for millions of patients around the world and drug treatments currently available, normally opioids and anti-inflammatory drugs, are not effective in many clinical situations. Cannabinoids have anti-nociceptive mechanisms different from those used by the drugs currently employed, providing a new line for the treatment of pain that is unresponsive to drug treatments presently available [1]. Oral administration is one of the routes most commonly used for drug administration. However, it is not feasible when the actives present unfavourable conditions: not adequate physicochemical properties for intestinal absorption, stability or solubility problems and clear decrease in bioavailability by first-pass hepatic effects, as the cannabinoids [2]. In this work, the preparation of cannabinoid-loaded poly(D,L-lactide-co-glycolide) (PLGA) particles using two methods, the flow focusing (FF) [3] technology and the traditional emulsion solvent evaporation method (SEV), is described. The main goal is to compare the effect of both methodologies on the geometry, particle size, surface characteristics and physicochemical properties of the formulations [4, 5].

### Materials and Methods

*Materials:*  $\Delta^9$ -Tetrahydrocannabinol ( $\Delta^9$ -THC) and 1-Naphthalenyl[4-(pentyloxy)-1-naphthalenyl]methanone (CB 13) (Tocris, Great Britain), Resomer® RG 502 (PLGA) (Boehringer Ingelheim, Germany), sorbitan monoestearate (Span 60®) (Sigma-Aldrich, Spain), ethyl acetate (Panreac, Spain) and polyvinyl alcohol (Mowiol® 3-96) (Fluka, Germany) were used as materials.

*Formulation of the cannabinoids-loaded PLGA particles:* Nanoparticles, with a theoretical cannabinoid loading of 2 % (w/v), were prepared using two different methods:

- (a) Emulsion-solvent evaporation method (SEV). An o/w emulsion was prepared to obtain solid PLGA nanoparticles. As oil phase a co-solution of cannabinoid (0.1 mL, 2 % w/v) and PLGA (1 mL, 10 %w/v) in ethyl acetate (EA) was prepared. This solution was added dropwise to a 0.3 % (w/v) PVA solution under sonication. The recently prepared emulsion was diluted by adding 20 mL of a 2 % (w/v) PVA solution, stirred at r.t. for 4h. After this, particles were collected by centrifugation (10000 rpm, 4°C, 10 min) and washed three times with distilled water. Finally, particles were freeze dried and stored at 4°C [6].
- (b) Flow focusing method (FF). In this case, to produced the o/w emulsion a simple FF nozzle [*mod.* Avant 2 (D = 50  $\mu$ m), Ingeniatics Tecnologías S.L., Spain] was used. As oil phase (focused fluid) ( $Q_o = 0.2$  mL/h), PLGA-drug solution was prepared as previously described. As aqueous phase (focusing fluid) ( $Q_w = 2$  mL/min) distilled water was used. The emulsion production was carried out inside a 0.3 % (w/v) PVA bath under continuous agitation for 4h. After this, particles were treated in the same way as previously described [7].

*Characterization methods:* the mean particle size and particle size distributions were measured at room temperature by laser scattering (Partica LA-950 V2, Horiba). Geometry and surface morphology were determined by scanning electron microscopy (SEM) (Philips XL-30, Philips Electron Optics). In order to characterize surfaces of particles the zeta potential (ZP) of them were measured in a NaCl 0.9% (w/v) solution at r.t. (Malvern Mastersizer 2000). Cannabinoids content was determined by HPLC (Hitachi LaChrom® (D-7000) Series) and expressed in terms of loading (% w/w).

### Results and discussion

Related to particle size, SEV method ( $0.35 \pm 0.24$   $\mu$ m and  $0.55 \pm 0.46$   $\mu$ m for CB 13 and  $\Delta^9$ -THC respectively) allowed obtaining smaller particles than the FF technology ( $0.84 \pm 0.12$   $\mu$ m and  $0.93 \pm 0.12$   $\mu$ m for CB 13 and THC respectively). Nevertheless, a narrower particle size distribution was obtained by FF (figure 1a). This is especially interesting considering the biopharmaceutical influences that can be derived.

Morphology and aspect studies by SEM, showed that particles were spherical, smooth and non-aggregated (figures 1b and 1c) in both cases. As it can be seen, the technique of microencapsulation did not seem to influence the final particles morphology and aspect.

Concerning to the electrical surface properties, the ZP values obtained showed that the electrophoretic properties are not similar for non-loaded and cannabinoids-loaded particles. Moreover, ZP values for CB13-loaded nanoparticles were less negative than for  $\Delta^9$ -THC particles, not depending on preparation method (Table 1). This

point out those CB13 particles was less hydrophobic than  $\Delta^9$ -THC particles; maybe by reason of the presence of CB13 on particles surfaces. CB13 molecular structure is less hydrophobic than  $\Delta^9$ -THC one. Probably, during the drying process, the CB13 molecules tend to go towards the external aqueous phase being trapped on the surface of the particle.

Results obtained for drug content are summarized in Table 2. In both cases, SEV and FF methods provided nanoparticles with high drug contents. In case of CB13, nanoparticles drug content was higher (around 50% w/w) than for  $\Delta^9$ -THC not depending on the production technique employed but rather the molecule structure.

## Conclusions

We have analyzed two formulation procedures, the classic SEV and the novel FF technique, for the preparation of spherical PLGA particles loaded with cannabinoids. Compared to SEV, it was found that FF allowed obtaining particles with a clear more narrow size distribution. Importantly, the nanoparticles obtained by FF showed more suitable physicochemical properties to through membranes resulting in a new alternative in neuropathic pain treatment by oral administration.

## Acknowledgements

I. M-R. is specially grateful for the financial support from Consejo Andaluz de Colegios Oficiales de Farmacéuticos, Spain. Financial support from Junta de Andalucía, Spain, Project P09-CTS-5029, is also gratefully acknowledged.

## References

- [1] Pertwee RG, Prog. Neurobiol., **63** (2001) 569.
- [2] Attal N, Brasseur L, Guirimand D, Clermond-Gnamien S, Atlami S, Bouhassira D, Eur. J. Pain, **8** (2003) 173
- [3] Gañán-Calvo, A. M. *Phys Rev Lett*, **80** (1998), 285-288.
- [4] Munjal M, ElSohly MA, Repka MA, AAPS Pharm. Sci. Tech., **7(3)** (2006) 71
- [5] Thumma S, ElSohly MA, Zhang SQ, Gul W, Repka MA, Eur. J. Pharm. Biopharm., **70(2)** (2008) 605
- [6] Holgado MA, Arias JL, Cózar MJ, Álvarez-Fuentes J, Gañán-Calvo AM, Fernández-Arévalo M. Int. J. Pharm. **358** (2008) 27.
- [7] Gañán-Calvo, A. M., Martín-Banderas, L., González-Prieto, R et al.. Int J Pharm **324** (2006), 19-26
- [8] Holgado MA, Cózar-Bernal MJ, Salas S, Arias JL, Álvarez-Fuentes J, Fernández-Arévalo M. Int. J. Pharm. **380** (2009) 147.

**Figure 1.** (a) Typical particle size distribution obtained for cannabinoid-loaded PLGA particles prepared by methods assayed. (b) Scanning electron microphotographs of  $\Delta^9$ -THC-loaded PLGA particles obtained by SEV and by FF (c).

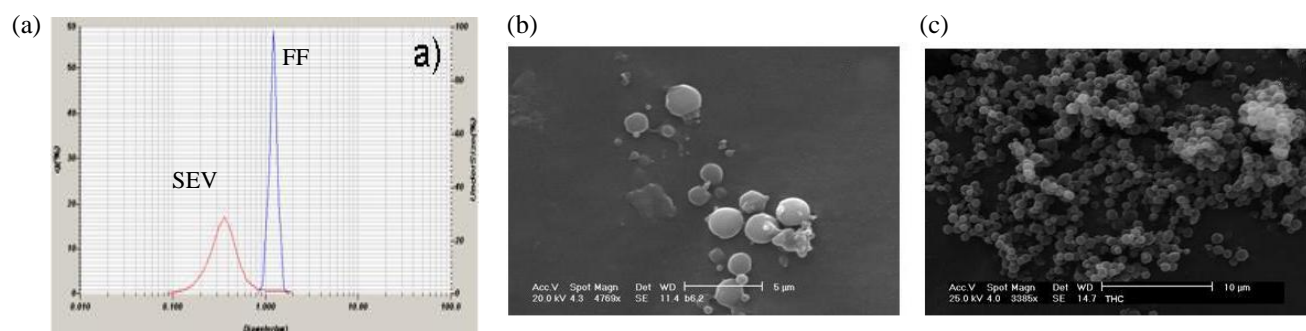


**Table 1.** Zeta potential values (mV  $\pm$  SD) in NaCl 0.9% w/v for loaded and non-loaded particles

FORMULATION	NON-LOADED	CB13	$\Delta^9$ -THC
SEV	-13,34 $\pm$ 0,75	-7,24 $\pm$ 0,76	-11,30 $\pm$ 0,63
FF	-14,21 $\pm$ 0,8	-8,69 $\pm$ 0,43	-12,02 $\pm$ 0,67

**Table 2.** Cannabinoids loading values (% w/w  $\pm$  SD)

FORMULATION	CB 13	$\Delta^9$ -THC
SEV	45,28 $\pm$ 21,65	39,68 $\pm$ 6,34
FF	47,60 $\pm$ 14,10	31,89 $\pm$ 9,92

## **Enzyme immobilization based on sol-gel technology for pesticides determination**

*A. Navas Díaz, F. García Sánchez, A. Aguilar, I. Medina Lama, V. Bracho*

*Departamento de Química Analítica, Facultad de Ciencias, Universidad de Málaga,*

*29071 Málaga. Spain. e-mail: a\_navas@uma.es*

Environmental risks associated with pesticide use arise from both their toxicity and their tendency move with water. Because of increasing concerns over agricultural worker health and its potential environmental impacts, there is a growing interest to develop novel analytical methods capable of performing rapid detection of these compounds in the field.

The pesticides inhibition of biocatalytic properties of enzymes immobilized using sol-gel technology was studied using luminescence transduction strategies.

Based on the change in luminescent behaviour of enzymatic activity induced by the pesticides simple methods for investigation of the pesticides determination have been developed.

## Uniform YF<sub>3</sub>:Yb,Er up-conversion nanophosphors of various morphologies synthesised in polyol media through an ionic liquid.

*Nuria O. Nuñez,<sup>a</sup> Marta Quintanilla,<sup>b</sup> Eugenio Cantelar,<sup>b</sup> Fernando Cussó,<sup>b</sup> and Manuel Ocaña<sup>a</sup>.*

<sup>a</sup>*Instituto de Ciencia de Materiales de Sevilla, CSIC-US, Americo Vespucio 49, 41092, Isla de la Cartuja, Sevilla, Spain.*

<sup>b</sup>*Depto. Física de Materiales, C-IV, Universidad Autónoma de Madrid, Spain*

[nurianu@icmse.csic.es](mailto:nurianu@icmse.csic.es)

### Abstract

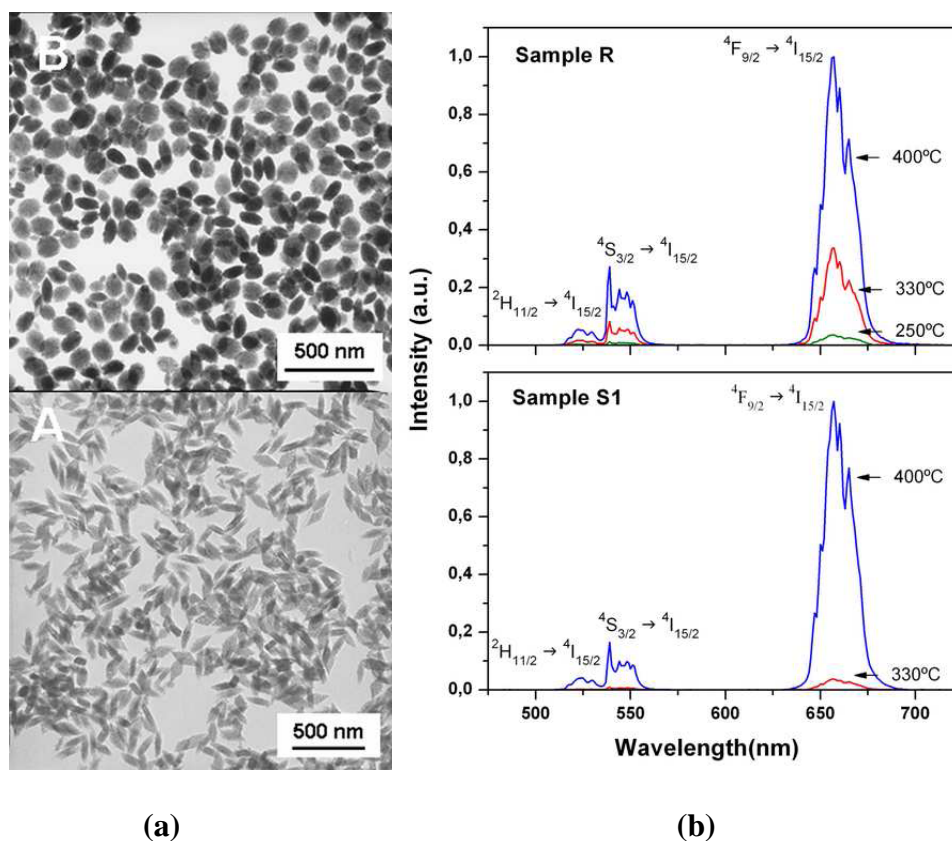
We describe a facile procedure for the synthesis at low temperature (120°C) of waterdispersible uniform YF<sub>3</sub>:Yb,Er up-conversion nanophosphors of various morphologies (rhombic and spheroidal) by homogeneous precipitation in polyol solutions containing different lanthanide salts and an ionic liquid (1-Butyl, 2-methylimidazolium tetrafluoroborate) as fluoride source. It is shown that the shape of the obtained nanoparticles is mainly determined by the nature of both, the polyol and the lanthanide precursors, which also affects to their colloidal stability in water suspensions. These morphological differences are explained on the basis of a different mechanism of particle formation. The efficiency of the up-conversion processes in the synthesised rhombic and spheroidal nanoparticles is also comparatively analysed and the observed differences are justified on the basis of the different impurities incorporated to the nanophosphors during their synthesis process.

**Key words:** Nanoparticles · Luminescence · Rare earth · Yttrium fluoride · Upconversion.

### References:

- [1] Nuñez NO, Ocaña M, *Nanotechnology*, **18** (2007) 455606.
- [2] Nuñez NO, Míguez H, Quintanilla M, Cantelar E, Cussó F, Ocaña M, *Eur J Inorg Chem*, (2008) 4517.
- [3] Ocaña M, Rodriguez-Clemente R, Serna CJ, *Adv Mater*, **7** (1995) 212.
- [4] Cao C, Qin W, Zhang J, Zhang J, Wang Y, Jin Y, Wei G, Wang G, Wang L, *J Nanosci Nanotechnol*, **8** (2008) 1384.
- [5] Li Z and Zhang Y, *Nanotechnology*, **19** (2008) 345606.
- [6] Weng F, Chen D, Wang Y, Yu Y, Huang P, Lin H, *Ceram Int*, **35** (2009) 2619.
- [7] Zhang T, Guo H, Qiao YM, *J Lumin*, **129** (2009) 861.
- [8] Wang GF, Qin WP, Zhang JS, Zhang JS, Wang Y, Cao CY, Wang LL, Wei GD, Zhu PF and Kim R, *Opt Mater*, **31** (2008) 296.
- [9] Wang GF, Qin WP, Wei GD, Wang LL, Zhu PF, Kim RJ, Zhang DS, Ding FH, Zheng KZ, *J Fluor Chem*, **130** (2009) 158.
- [10] Wei Y, Lu F, Zhang X, Chen D, *Materials Letters*, **61** (2007) 1337.

## Figures:



(a) TEM images of  $\text{YF}_3:\text{Yb,Er}$  nanoparticles [samples R (A) and S1 (B)] obtained at  $120^\circ\text{C}$  in different solvents from different Y precursors and variable solvent/IL ratio, (b) Comparison of the intensities of the  $\text{Er}^{3+}$  up-conversion emissions for samples R and S1 annealed at different temperatures. The different bands have been labelled according with the corresponding optical transition, arising from different emitting  $\text{Er}^{3+}$  levels and ending in the  $\text{Er}^{3+}$  ground state ( $4I_{15/2}$ ).



Dispersion of rhombic  $\text{Er,Yb;YF}_3$  nanophosphors (sample R) in water showing UC luminescence sample when excited at  $980\text{ nm}$ : (left) total UC, (center) UC viewed through a red filter, (right) UC viewed through a green filter. The photograph has been taken using a LUMIX DMC-digital camera (1 second exposure at ISO 400).

## Optomechanical multiplexed detection with large arrays of cantilevers

*Charis Orfanidou<sup>1,2</sup>, Priscila M. Kosaka<sup>1</sup>, Johann Mertens<sup>1</sup>, Oscar Ahumada<sup>2</sup>, Nicolas Francisco Martínez<sup>2</sup>, Antonio Salvador Matar<sup>2</sup>, Carlos García<sup>2</sup>, Jorge Ramírez<sup>2</sup>, Hien-Duy Tong<sup>3</sup>, Montserrat Calleja<sup>1</sup>*

<sup>1</sup>*Bionanomechanics Lab-Instituto de Microelectrónica de Madrid- CSIC, Isaac Newton 8 (PTM), Tres Cantos 28760, Madrid, Spain*

<sup>2</sup>*Mecwins S.L., Santiago Grisolia, Tres Cantos 28760, Madrid, Spain*

<sup>4</sup>*Nanosens, Berkelkade 11, NL 7201 JE Zutphen, The Netherlands*

[charis.orfanidou@imm.cnm.csic.es](mailto:charis.orfanidou@imm.cnm.csic.es)

There is an increasing interest in micromechanical sensors that feature a compact size combined with very high sensitivity and short response times. Cantilever-based sensing is emerging as a capable sensing platform with the advantage of being relatively cheap to mass-produce. Micro-fabrication technologies have allowed for the design of micro-cantilevers optimized for various types of sensing applications, as well as for the manufacturing of large arrays of cantilevers, making it possible to use various sensors in parallel. These cantilever-based sensors are proving to be quite competitive with current sensing technologies due to their high sensitivity and fast response time, given their small size (micrometers to nanometers).

In most cantilever-based sensing applications, one surface of the cantilever beam is rendered sensitive to a specific target molecule of interest, while the opposing surface is chemically passivated. When these target molecules interact with the sensitized surface of the cantilever, a surface stress can be induced. The difference in surface stress induced on the sensitive relative to the passive surface of the cantilever results in a measurable mechanical deflection. Cantilever deflections are monitored as a direct measure of adsorption-induced surface stress. In the MecWins platform, the displacement of the read-out laser beam provides a fast acquisition and the capability to detect the full 3D profile of cantilever arrays of any size, shape and number of elements. Any cantilever design and cantilever number can be addressed by Mecwins technology.

We present here for the first time measurements performed in a completely automatic way of arrays of 4x4 groups of 8 cantilevers that make possible the detection of a total of 128 different molecules. As a key application for DNA detection, the biosensing principle applied by Mecwins is based on the role of hydration forces in controlled bilayers[1]. In the experiment involving DNA, a solution containing end-thiolated single stranded DNA (ssDNA) molecules is introduced into a cell containing the above mentioned chip, which has one surface coated with gold. The ssDNA molecules adsorb on the gold surface of the cantilever through the strong gold-thiol bond forming a self-assembled monolayer (SAM). Figure 1 shows the profile of 11 chips with a total of 88 cantilevers. Figure 2 presents the response of the 88 cantilevers to a hydration cycle. The key capabilities of this novel instrumentation are: a highly multiplexed detection together with an accurate control of the gas environment.

### References:

[1] Mertens, J., Rogero, C., Calleja, M., Ramos, D., Martín-Gago, J.A., Briones, C. & Tamayo, J., *Nature Nanotechnology* **3** (2008) 301.

Figures:

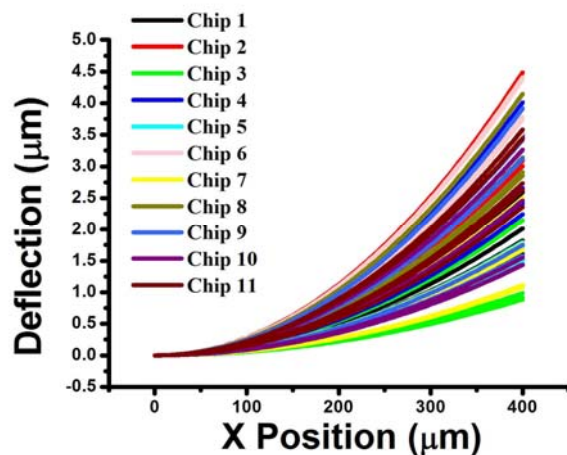


**Figure 1.** Simultaneous measurement performed by the Mecwins platform in 11 different chips comprising 8 cantilevers each chip. Information from the full profile of 88 cantilevers is obtained.

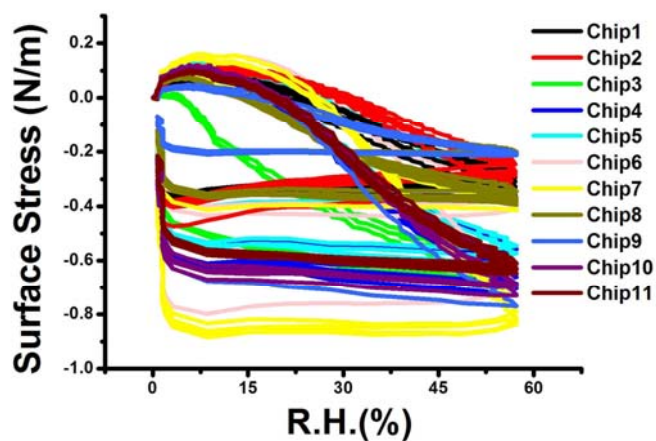


**Figure 2.** The described instrument is capable of multiplexed measurements in controlled gas environment (a mixture of dry and water saturated nitrogen in this experiment). Here the response of ssDNA sensitised cantilevers is shown. Measurements are performed simultaneously in 88 cantilevers from 11 chips. The results show a very good reproducibility of the DNA layers, with similar responses to changes in relative humidity. The cantilevers also show comparable mechanical responses to the hydration changes.

**Functionalisation of textile fibres with metal nanoparticles**

*Inês V. Osório<sup>a</sup>, Ricardo Ramos<sup>b</sup>, Leonor Soares<sup>c</sup>, Eulália Pereira<sup>c</sup>, Rui Igreja<sup>b</sup>, Ricardo Franco<sup>a</sup>, João Cortez<sup>a</sup>*

*<sup>a</sup>REQUIMTE, Departamento de Química, Faculdade de Ciência e Tecnologia da Universidade Nova de Lisboa, Campus de Caparica, 2829-516 Caparica, Portugal*

*<sup>b</sup>CENIMAT, I3N, Faculdade de Ciências e Tecnologia, Universidade Nova de Lisboa, 2829-516 Caparica, Portugal*

*<sup>c</sup>REQUIMTE, Departamento de Química, Faculdade de Ciências da Universidade do Porto, R. Campo Alegre, 687, 4169-007 Porto, Portugal*

[ines.osorio@dq.fct.unl.pt](mailto:ines.osorio@dq.fct.unl.pt)

There is need in the textile market for technologies that warrant efficient shielding for high and persistent levels of electromagnetic (EM) radiation, mitigating its effects on humans. In particular, applications for Individual Protective Equipment (IPE) are sought by the industry and military, for protection of individuals that are exposed for long and frequent periods to non-ionising EM radiation (from electronic equipment). EM radiation is critical to many aspects of modern life (e.g. telecommunications), and there is increasing public concern on its effects, given some studies indicate increased rates of maladies such as cancer and leukemia[1]. In particular, EM fields generated at near-field by mobile phones or far-field by e.g. radiofrequency towers causes most concern[2,3]. There is, thus, a concomitant interest and demand for EM shielding (EMS) technologies for IPE.

We propose the concept of deposition or immobilisation of a nanometric layer of metal nanoparticles (NPs) on the surface of textile fibres, resulting in high levels of conductivity that lead to EM field dissipation by the textiles through a Faraday Cage effect[4].

Our approach, in departure from previous methodologies, will be: (i) the direct growth of metal nanoparticles (NPs) on the textile fibre surfaces, and (ii) the targeted use of specific ligands to ensure the immobilisation of metal nanoparticle (NPs). This rational design will permit low temperature immobilisation of metal NPs onto different fibre compositions in a targeted manner by controlling the NP amount immobilised onto the fibres, thus providing a tuneable EMS for a wide range of EM frequencies; allow the production of EMS clothing with high standards of comfort and resistance to washing and wear, at a low cost.

Here we report our first results on the first approach (direct growth of NPs on the fibres). The growth of silver nanoparticles (AgNPs) on cotton fibres surfaces has been reported by Lee et al. [5] in an ethanol solution. Since this approach is not feasible at an industrial scale, we developed a modified method in aqueous solution. The method simply consists of placing a sample of wool or cotton fabric in water and adding buthylamine and silver nitrate, at 45°C in constant agitation. The samples were analysed by ICP to determine the concentration of silver in the treated fibres grown as AgNPs. The results (Table 1) showed an increase in the amount of silver per weight of sample (mg/mg) for both wool and cotton when the reaction was carried out in aqueous solution when compared to an absolute ethanol solution. This suggests that the growth of AgNPs directly on the fibres is more efficient in aqueous solution than in absolute ethanol.

In accordance to the second approach (synthesise first NPs in solution and then bind them to the fibres), we have synthesised AgNPs following the borohydrate method[6]. This method also uses water as solvent and the AgNPs obtained have a average size of 8-10 nm(Fig. 1). A stability study of these particles showed they aggregated at NaCl concentrations greater than 40 mM and at pH lower than 4.

The fibres treated followed both approach are presently being analysed by SEM to observe how the AgNPs are formed and bound to both textiles. Moreover, conductivity and shielding measurements will be performed on the treated fabrics to verify that the fibres treated in aqueous solution block the EM radiation and were bestowed with a high conductivity levels

This work is part of the project QREN-ADI-5518-METALFUN, funded by the ERDF via QREN (Quadro de Referência Estratégico Nacional), a Portuguese funding body, in collaboration with Devan-Micropolis, Moreira da Maia, Portugal. The authors also wish to acknowledge the collaboration of Eng. Raquel Vieira (Micropolis) in this work.

### References:

1. Funk R., Monsees T., Ozkucur N. *Progr. Histochem. Cytochem.* 43 (2009) 177–264
2. <http://www.who.int/mediacentre/factsheets/fs322/en/index.html>, WHO study, June 2007.
3. Kundi M., Mild K., Hardell L., Mattsson M. 2004. *J. Toxicol. Environmental Health, Part B*, 7:351–384.
4. Gindrup W., Vinson, R. 1998, United States Patent 5786785.
5. 11. Lee H., Park H., Lee Y., Kim K. and Park S. *Chem. Commun.* 28 (2007) 2959–2961.
6. Hynning D. and Zukoski, C. (1998) *Langmuir*, 14, 7034-7046.

Figure 1. TEM photograph of AgNPs synthesized.

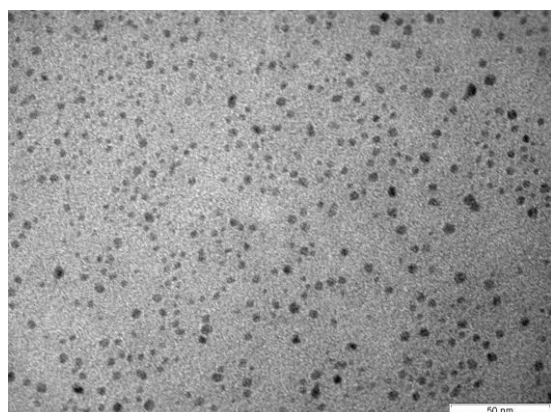


Table 1. Results of ICP in mg of Ag per mg of sample.

Solvent\Sample	Wool	Cotton
Water	7,19	12,33
Absolute ethanol	1,75	3,85

## Design and development of the CEM metrological long range scanning probe microscope

*Milagros Ozaita, Laura Carcedo, Emilio Prieto.*

*Spanish Centre of Metrology (CEM), Alfar 2, Tres Cantos (Madrid), Spain*  
[mmozaita@cem.mityc.es](mailto:mmozaita@cem.mityc.es); [lcarcedo@cem.mityc.es](mailto:lcarcedo@cem.mityc.es); [eprieto@cem.mityc.es](mailto:eprieto@cem.mityc.es)

The continuing miniaturization process in science and technology demands high resolution measurements with very low uncertainties (even below the nanometer level). Scanning Probe Microscopes (SPMs) have proved to be a unique and very efficient tool to investigate and characterize different surface properties at scales ranging from hundreds of microns down to tenths of a nanometer. The use of SPMs has become a very popular technique in science, technology research, and even in industry, but in order to ensure comparability of the obtained data traceability to the SI unit metre must be established.

This technique is applied to all sorts of disciplines such as precision engineering, semiconductor fabrication, material science, crystallography, life sciences and many others. There are two main reasons for this success. First, SPMs provide very good lateral and vertical resolution in comparison with other traditional techniques and local or average information of the surface can be inferred. Second, a variety of samples can be analyzed without any particular preparation or damage. The main drawbacks of the method are the small scan range (of the order of tens of micrometers in the lateral directions and of a few micrometers in the vertical direction), long scanning times and problems related to the properties of the standard piezo-tube scanners such as hysteresis, creep and drift.

SPMs, as well as any other instruments for which quantitative analysis is important, should be metrologically traceable, i.e. a measurement result should be related to a reference through a documented unbroken chain of calibrations, each contributing to the measurement uncertainty. For this application, the “reference” is the definition of the metre through its practical realization. In Spain, The Spanish Centre of Metrology (CEM) is the Institution in charge of realizing and maintaining such National Standard.

In conventional SPMs (C metrological category of the metrological classification <sup>[1]</sup>) positioning is established by the voltage applied to piezos and the calibration relies on the usual physical transfer standards. Category B SPMs make use of a variety of different sensors such as strain gauges, encoders and capacitive or inductive sensors. Calibration is achieved by attaching interferometers or with physical transfer standards. Our goal is to go beyond this and build a Class A SPM with integrated laser interferometers in all the three axes. Traceability to the SI unit meter will rely on the wavelength of the lasers. It is important to emphasize that the interferometric system will perform a continuous monitoring and active control during measurements.

Our metrological SPM (class A) will contribute to reinforce the Spanish traceability chain (fig.1) by performing the calibration of physical transfer standards (step height, pitch, critical dimension standards) that will be used to calibrate categories B and C SPMs. One of our objectives is to extend the calibration capabilities of the SPM to large scanning areas and step heights. This will allow us to certify standards compatible with other instruments such as profilers or interference microscopes. According to the above motivations we are going to build a system that will combine a high precision and long range three dimensional nanopositioning and nanomeasuring machine (NMM) <sup>[2]</sup> -with a resolution of 0.1 nm over the range 25 mm x 25 mm x 5 mm- and a versatile scanning probe microscope as the sensor for surface analysis.

The NMM machine has been developed by the Institute of Process Measurement and Sensor Technology of the Technical University of Ilmenau and is manufactured by SIOS<sup>[3]</sup>. This machine includes three miniature HeNe laser interferometers used for position measurement and control at the nanometer scale, and allows Abbe offsets of less than 0.1 mm. They are installed in a thermally stable metrology frame, and the traceable measurements of objects can be done relative to it. The samples under study will be placed on the base plate of a corner mirror structure (three mirrors built as a solid corner mirror). The mirrors reflect the beams of the interferometers. In addition, the angular position of the corner mirror will be controlled by two angular sensors and the corner mirror itself will be moved by a 3D stage. The stage will operate in a closed loop controlled by the interferometric system.

The SPM machine will be adapted from the original Cervantes AFM<sup>[4]</sup> from Nanotec Electronica to allow compatibility with the NMM design. In order to improve the dynamic behaviour of the measuring system, an ultrafast piezo coupled to the cantilever holder will be added and allowed to move in the z axis. The SPM will be capable of operating in basic and advanced SPM modes including: contact mode, non-contact mode, diverse dynamic modes, measurement of electrostatic force, magnetic force and nanolithography (controlled nanomanipulation of the surface).

### References:

- [1] T. Dziomba, L. Koenders, G. Wilkening, Proceedings of SPIE, **5965** (2005) 59650C.1-59650C.12
- [2] E. Manske, R. Mastylo, T. Hausotte, N. Hofmann, G. Jäger, "Advances in Traceable Nanometrology with the Nanopositioning and Nanomeasuring Machine" in "Nanoscale Calibration Standards and Methods: Dimensional and Related Measurements in the Micro- and Nanometer Range" edited by G. Wilkening, L. Koenders, Wiley-VCH Verlag GmbH & Co. KGaA, Weinheim, p 47-59, (2005).
- [3] SIOS Meßtechnik GmbH,  
[http://www.sios.de/ENGLISCH/PRODUKTE/NMM\\_ENGL.PDF](http://www.sios.de/ENGLISCH/PRODUKTE/NMM_ENGL.PDF), as of 02/2010
- [4] Nanotec Electronica, <http://www.nanotec.es/products/cervantes.php>, as of 02/2010

### Figures:

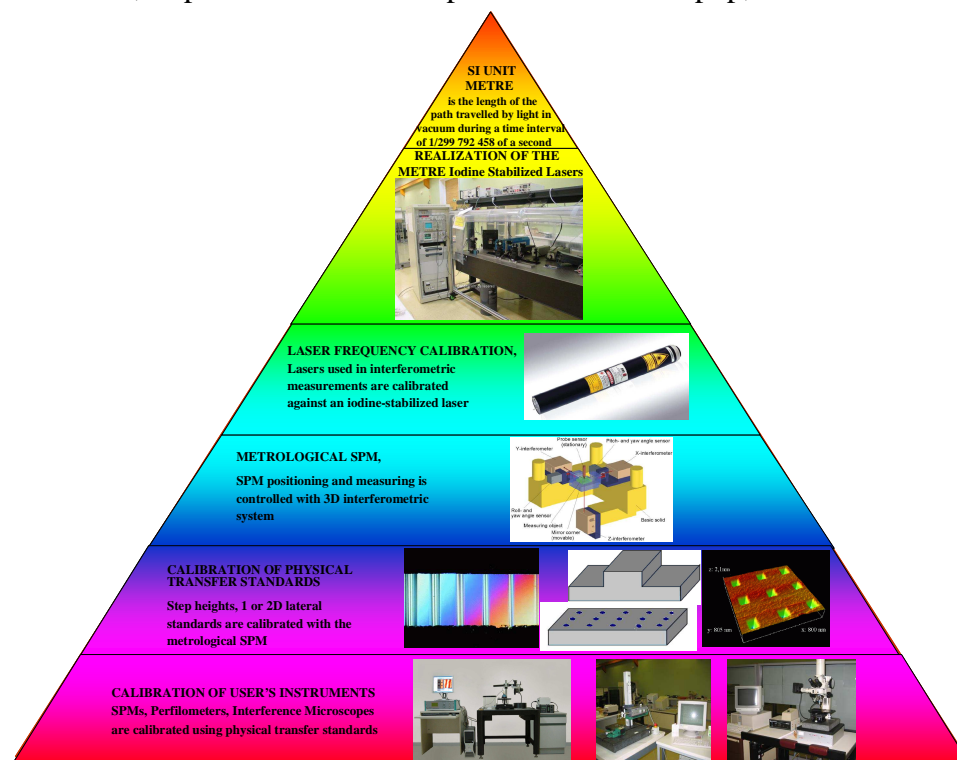


Figure 1. Traceability chain for scanning probe microscopes

## Simultaneous ir (1064 nm) pulsed laser deposition and annealing of zno films with an splitted 1064 nm beam

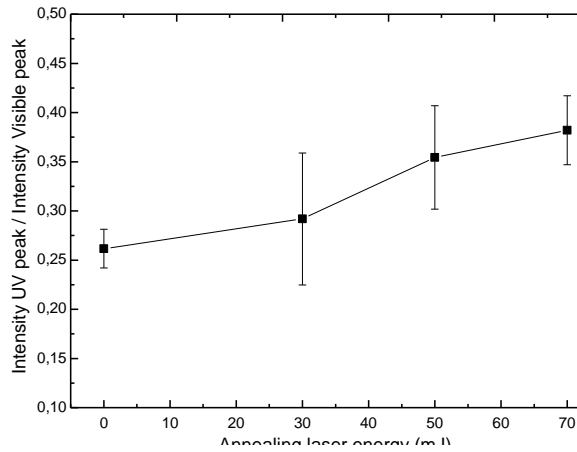
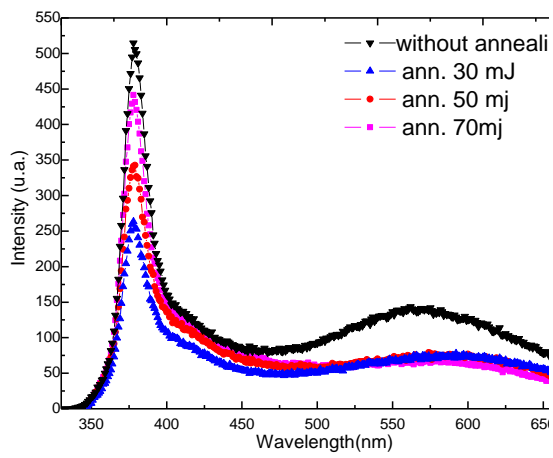
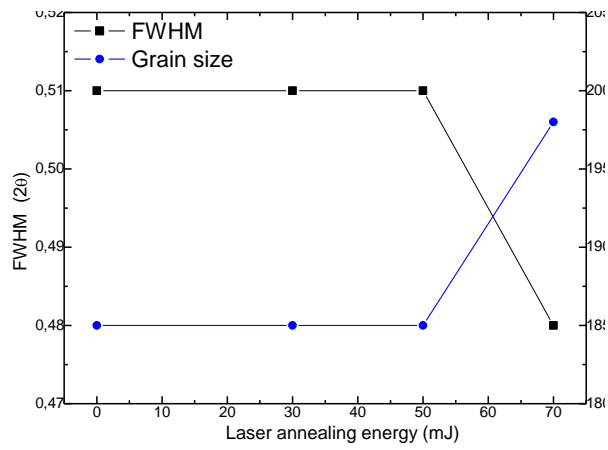
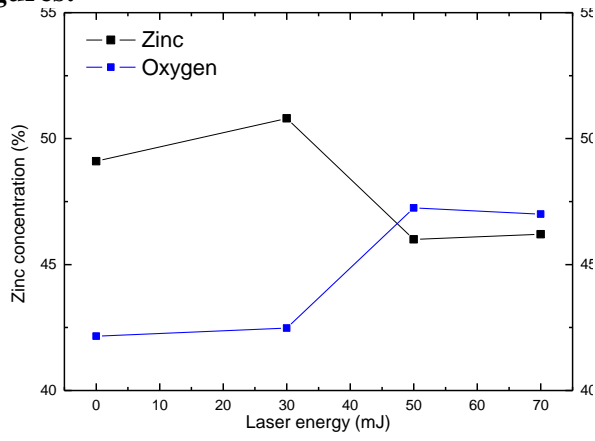
*Padilla Rueda Diana, Vadillo José Miguel, Laserna J. Javier*  
*Laser Laboratory, University of Malaga, Málaga, Spain*  
[laserna@uma.es](mailto:laserna@uma.es)

Zinc Oxide (ZnO) thin films had been elaborated at room temperature using an innovative PLD system with a simultaneous IR pulsed laser annealing of the substrate during the deposition. The deposition was performed using sintered ZnO targets under a 2 mbar oxygen pressure. The IR laser (Nd:YAG, 1064 nm), was splitted in two different beams used for the ablation process with a constant fluence ( $7 \text{ J/cm}^2$ ) and to heat the substrate surface. The chemical composition and morphological, structural and optical properties of thin films has been studied as a function of laser annealing fluence. With the increasing in the annealing laser fluence, the oxygen concentration in the films, the cristalinity of thin films in the preferentially direction (002) and the grain size increases, while there the film thickness and the optical transmittance decreases. The optical gap shifts to low values (3.28 eV) regardless the laser annealing fluence. The PL spectra shows two main bands centered around 370 and 570 nm. Our studies have demonstrate that the intensity of the UV band increases with the laser annealing, while the intensity of the visible band decreases. This evidence is in agreement with the change in the films stoichiometry, so that our instrumental approach allows the obtention of films with tailored characteristics over substrates that it can not be directly heated.

### References:

- [1] Te-Wei Chiu, Kazuhiko Tonooka and Naoto Kikuchi. *Thin Solid Films* **516** (2008) 5941–5947
- [2] F.O. Adurodija, H. Izumi, T. Ishihara, H. Yoshioka, M. Motoyama, K. Murai. *Vacuum* **67**,(2002), 209–216.
- [3] M. Rusop, K. Uma, T. Soga, T. Jimbo. *Materials Science and Engineering B* **127** (2006) 150–153.
- [4] S. Venkatachalam, Y. Kanno and S. Velumani. doi:10.1016/j.vacuum.2009.10.025.
- [5] M.P.Bole,D.S.Patil, *Journal of Physics and Chemistry of Solids*, **70**, (2009), 466–471.
- [6] F. K. Shan, G. X. Liu, W. J. Lee, G. H. Lee, I. S. Kim, and B. C. Shin. *Applied Physics Letters* **86** (2005),221910.
- [7] I. Ozerov , M. Arab, V. I. Safarov, W. Marine, S. Giorgio, M. Sentis and L. Nanai. *Applied Surface Science* **226** (2004) 242–248
- [8] Hongxia Li, Hong Liu, Jiyang Wang, Shushan Yao, Xiufeng Cheng, R.I. Boughton. *Materials Letters* **58** (2004) 3630– 3633

Figures:



## Colloidal nano- and microparticles towards sensing applications in biology

*Wolfgang Parak*

Philipps Universität Marburg, Fachbereich Physik, Renthof 7, 35037 Marburg. Germany  
[wolfgang.parak@physik.uni-marburg.de](mailto:wolfgang.parak@physik.uni-marburg.de)

Nanomedicine nowadays is a popular key word in the media, though everyone seems to associate it with different visions, hopes, and even fears. From the point of view of a materials scientist it will be pointed out what new materials will be possible, how they will be designed, and which properties they could offer for diagnosis and treatment. It will be critically discussed that though sophisticated materials with advanced novel properties will be available in the future, they do not automatically match the requirements and demands of clinicians. The discussion is centred around one example, multifunctional polyelectrolyte capsules which might act as a "nano-submarine" for in vivo sensing and delivery, which is used to highlight promising interfaces between both disciplines.

### References:

- [1] C. Röcker, M. Pözl, F. Zhang, W. J. Parak, G. U. Nienhaus, "A quantitative fluorescence study of protein monolayer formation on colloidal nanoparticles", *Nature Nanotechnology* 4, 577-580 (2009).
- [2] P. Rivera Gil, S. de Koker, B. G. de Geest, W. J. Parak, "Intracellular processing of proteins mediated by biodegradable polyelectrolyte capsules", *Nanoletters* 9, 4398-4402 (2009).
- [3] J. Peteiro-Cartelle, M. Rodríguez-Pedreira, F. Zhang, P. Rivera Gil, L. L. del Mercato, W. J. Parak, "How colloidal nano- and microparticles could contribute to medicine - a personal perspective both from the eyes of physicians and materials scientists", *Nanomedicine* 4, 967-979 (2009).

## Synthesis and Characterization of Porous Materials Prepared by Templating in Oil-in-Alcohol Highly Concentrated Emulsions

L. A. Pérez-Carrillo\*, C. Solans, J. Esquena.

*Institute for Advanced Chemistry of Catalonia, IQAC-CSIC, c/Jordi Girona, 18-26, Barcelona, Spain.*

\*e-mail: lourdesapc31@hotmail.com

Highly concentrated emulsions are an interesting class of emulsions characterized by an internal phase volume fraction exceeding 0.74, the critical value of the most compact arrangement of uniform, undistorted spherical droplets [1-3]. Consequently, their structure consists of deformed (polyhedral) and/or polydisperse droplets separated by a thin film of continuous phase, a structure resembling gas-liquid foams [1-3].

In the present work, the main objective was to obtain porous materials with very high pore volume, by templating in highly concentrated emulsions. The porous materials were prepared by polymerizing in the external phase of highly concentrated emulsions, which consisted of hydrocarbon droplets dispersed in a furane derived alcohol (Oil-in-Alcohol highly concentrated emulsions). The emulsions were prepared by stepwise addition, with mechanical stirring, of the hydrocarbon (80 wt%) to the furane derived alcohol phase (20 wt%), which already contained a suitable emulsifier [4,5]. The droplet size of highly concentrated emulsions was studied by optical microscopy and by laser diffraction on emulsions diluted after preparation. The image obtained by optical microscopy of the highly concentrated emulsion of furane derived alcohol, with a particle size between 17 and 18  $\mu\text{m}$  of diameter, is show in Fig. 1.

The polymerization reaction was carried out by the addition of small amounts of hydrochloric acid. The porous polymer monoliths were purified by soxhlet extraction for 48 hours. In order to confirm that polymerization had occurred the chemical composition of the materials was studied with an IR Spectroscopy (FTIR). Large monoliths could be obtained, and its internal structure was observed by SEM. Figure 2 shows the image of an example of the macroporous network of a polymer monolith, with pore sizes around 15  $\mu\text{m}$ . It can be observed that the structure of the porous polymer material is similar to that of the highly concentrated emulsion, which acted as template.

### References

- [1] K. J. Lissant, *Journal of Colloid and Interface Science*, 22 (5), (1966), 462-368.
- [2] H. M. Princen. *Journal of Colloid and Interface Science*, 71 (1), (1979), 55-66.
- [3] C. Solans, J. Esquena, N. Azemar, C. Rodríguez and H. Kunieda. In: D.N. Petsev (Ed.), *Emulsions: Structure, Stability And Interactions*. Amsterdam: Elsevier, 2004, 367-394.
- [4] J. Esquena, GSR Ravi Sankar, and C. Solans, *Langmuir*, 19 (2003), 2983-2988.
- [5] J. Esquena and C. Solans, book of *Emulsions and Emulsion Stability*, Chapter 6 *Highly Concentrated Emulsions as Templates for Solid Foams*, 245-260.

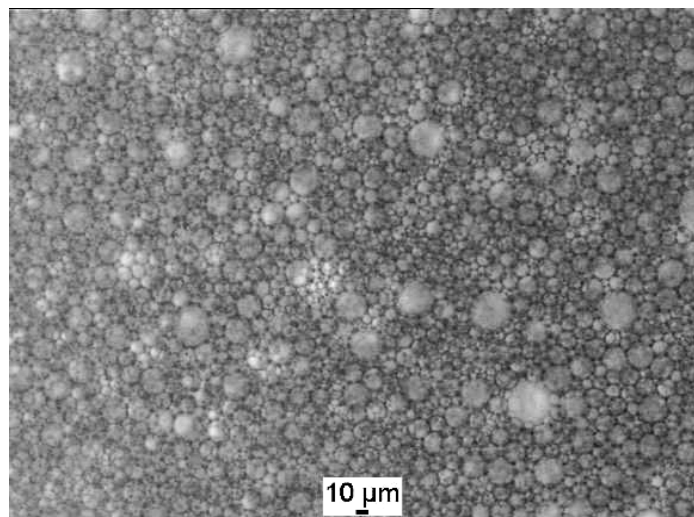
**Figures**

Fig. 1. Highly Concentrated Emulsion consisting in hydrocarbon droplets dispersed in furane derived alcohol.

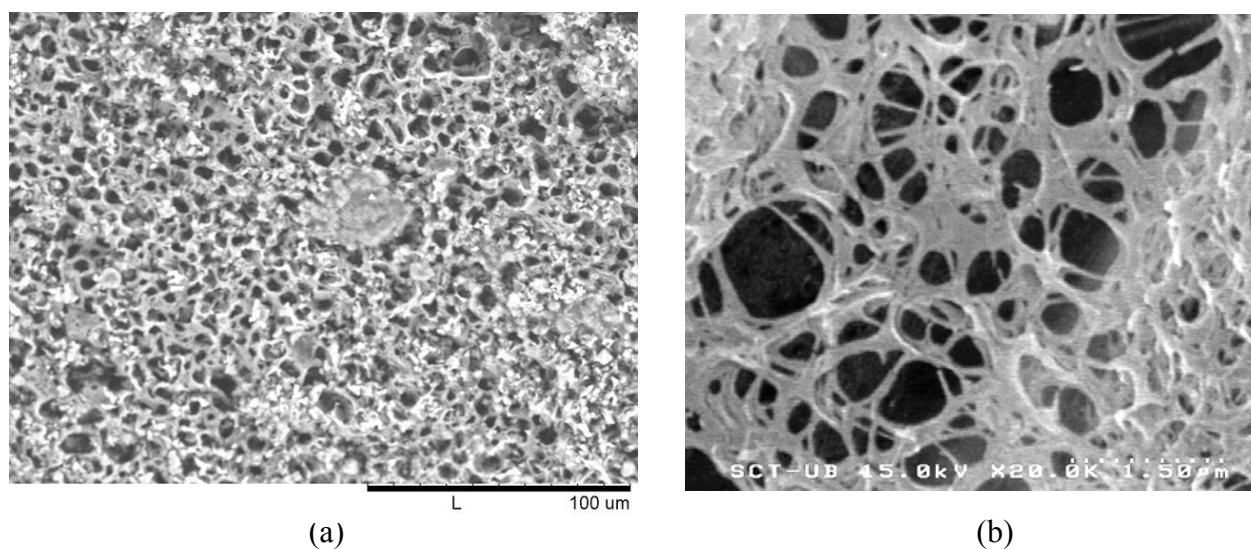


Fig. 2. Polymer macroporous materials, as observed at low magnification (a) and high magnification (b).

**Acknowledgements**

The authors acknowledge to CONACYT, México for the postdoctoral scholarship give to Lourdes Adriana Pérez Carrillo, to CSIC for the financial support PIFC00\_08\_00022 through the Proyecto Intramural de Frontera. The authors also acknowledge Yolanda Castro, Alicia Durán, from The Institute for Ceramic and Glass, Madrid, Spain, and Juan Manuel Diez Tascón from the National Institute for Carbon, Oviedo, Spain, for useful discussions.

## Simulation and impedance analysis of carbon nanotube thin films

*Jordi Pérez-Puigdemont, Nuria Ferrer-Anglada*

*Departament de Física Aplicada (UPC), Campus Nord - Edifici B4/B5 C/ Jordi Girona Salgado, 1-3 , Barcelona, Spain*

[jordi.perez@fa.upc.edu](mailto:jordi.perez@fa.upc.edu)

We numerically simulated carbon nanotube thin films as in a nano nano-version of the frenchFrench game called mikadoMikado, in which the assuming carbon nanotubes as were straightthe sticks. With In these simulations we studied the topological and geometric properties of the nanotubes network's topological and geometric properties, such as percolation threshold, path length and distance between nodes. Also, we We also described the electron's behaviour of electrons inside in the network under an AC field, giving insights about and this enabled us to determine the mean number of nodes they crossed by it, as well as the distance they travelled through in the network. We measured the impedance  $Z(f)$ , from DC to hundreds of MHz, of several thin films with different varying nanotube densities and sample sizes. Through We used the simulation's and measurement's results we to explained the features of the  $Z(f)$ 's features behaviour, such as like the real part's of the onset frequency. And by changing the length of the sample's length we found that the onset frequency depends on the density of the nanotube density, as is reported in some several articles [1, 2], but also on the sample length of the sample. This double dependence is explained by means of the complexity of the conducting path.

### References:

- [1] H. Xu, S. Zhang, S. M. Anlage, L. Hu and G.Grüner. Phys. Rev. B. **77**, **7** (2008). 075418
- [2] B. E. Kilbride, J. N. Coleman, J. Fraysse, P. Fournet, M. Cadek, A. Drury, S. Hutzler, S. Roth, and W. J. Blau, J. Appl. Phys. **92** (2002)4024

## Surface anisotropy, orbital moment and biomedical applications in magnetic nanoparticles

N. Pérez<sup>(a)</sup>, P. Guardia<sup>(a)</sup>, A.G. Roca<sup>(b)</sup>, M.P. Morales<sup>(b)</sup>, C.J. Serna<sup>(b)</sup>, F. Bartolomé<sup>(c)</sup>, L.M. García<sup>(c)</sup>, J. Bartolomé<sup>(c)</sup>, A. Labarta<sup>(a)</sup>, X. Batlle<sup>(a)</sup>

<sup>a</sup> Dept. Física Fonamental and Insitut de Nanociència i Nanotecnología IN2UB, U. Barcelona, Martí i Franqués 1, 08028 Barcelona, Spain

<sup>b</sup> ICMN-CSIC, Sor Juana Inés de la Cruz 3, Cantoblanco 28049, Madrid, Spain

<sup>c</sup> Dept. Física de la Materia Condensada, U. Zaragoza and ICMA-CSIC, Pedro Cerbuna 12, 50009 Zaragoza, Spain

[nicolas@ffn.ub.es](mailto:nicolas@ffn.ub.es)

Magnetic nanoparticles (NP) systems have long been subject to study finite-size and surface effects [1]. Besides, their potential application for biomedical purposes relies on high quality magnetic materials. The thermal decomposition of an organic iron precursor in an organic medium [2] allows the preparation of highly crystalline iron oxide NP with excellent magnetic parameters [3]. Particles in the 5-50 nm range were synthesized in the presence of a variety of coatings with controlled shapes. All the materials show a narrow size distribution with high crystal quality. Saturation magnetization was size independent in the 5-20 nm range and almost reached the expected value for bulk magnetite at low temperatures, higher in those NP with the surfactant covalently bonded to the surface. In 5 nm particles the surface contribution to magnetic anisotropy could be established via an analytical method that relies on the  $T \ln(t/t_0)$  scaling and demonstrates that surface anisotropy causes the broadening of their energy barrier distribution [4,5]. X-ray absorption spectra (XAS) suggested charge transfer from the NP to the covalent bonded surfactant. X-ray magnetic circular dichroism (XMCD) confirmed the dependence of the magnetic moment on the surface bond and suggested that the orbital momentum is more effectively quenched in covalently bonded NPs. Besides, the low-temperature  $\langle S_z \rangle = 3.63 \mu_B/f.u.$  obtained in the latter, is very close to those reported for bulk samples (3.90-3.95  $\mu_B/f.u.$ ). High resolution TEM suggests that the foregoing is related to the crystal quality of the NP [6].

### Acknowledgements

MEC (NAN2004- 08805-CO4-02, NAN2004-08805-CO4-01, CONSOLIDER CSD2006-12, MAT2005-02454 and MAT2006-03999), Generalitat de Catalunya (2005SGR00969)

### References:

- [1] X. Batlle and A. Labarta, J. Phys D: Appl. Phys 35, R15 (2002)
- [2] J. Park et al., Nat. Mat.3, 891 (2004)
- [3] P. Guardia et al., J. Magn. Magn. Mat. 316, e756 (2007)
- [4] N. Pérez et al., Nanotechnology 19, 475704 (2008)
- [5] O. Iglesias et al., J. Magn. Magn. Mat. 140-144, 399 (1995)
- [6] N. Pérez et al., Appl. Phys. Lett. 94, 093108 (2008)

## Cu/SiO<sub>2</sub> films for 3D filling in microelectronic applications by an organometallic chemical liquid deposition (OMCLD) route

Kilian Piettre<sup>a,b</sup>, Virginie Latour<sup>a</sup>, Olivier Margeat<sup>c</sup>, Clément Barrière<sup>a</sup>, Marina Proust<sup>b</sup>,  
Benoît Riou<sup>b</sup>, Bruno Chaudret<sup>a</sup>, Pierre Fau<sup>a\*</sup>

<sup>a</sup> Laboratoire de Chimie de Coordination, 205, route de Narbonne, 31077 Toulouse,

<sup>b</sup> STMicroelectronics, 16, rue Pierre et Marie Curie, 37071 Tours

<sup>c</sup> Université de la Méditerranée, Faculté des Sciences, 163 av Luminy, 13288 Marseille

[Kilian.Piettre@lcc-toulouse.fr](mailto:Kilian.Piettre@lcc-toulouse.fr)

Organometallic chemistry has recently been emphasized [1] in microelectronics processes and new cost effective copper deposition films have been proposed [2, 3]. In this talk, we present a fully liquid method to specifically produce thin conductive copper films on silicon substrates at specific temperature and under specific H<sub>2</sub> pressure. Metallization of the surface will be achieved by simultaneous decomposition under reducing H<sub>2</sub> gas of a copper precursor ((N-N'-diisopropylactemidinato) copper (I)) in the presence of a silica source (tetraethoxysilane TEOS). This unique organometallic approach allows the formation of adherent copper/SiO<sub>2</sub> clusters around 100 nm thick, on silicon surfaces presenting a large aspect ratio. The continuous precursor availability in the liquid phase during deposition will allow good coverage of both walls and bottom structures and evenly deposit (figure 1)+.

The copper precursor decomposition is followed by nuclear magnetic resonance (NMR) monitoring and TEOS hydrolysis and condensation reactions are controlled by the precursor chemistry. The reaction pathways involved in the formation of these composite films are detailed and the process parameters are discussed. The resulting films are characterized by scanning electron microscopy (SEM), focused ion beam (FIB), back-scattered electrons (BSE) and X-rays diffraction (XRD). The resulting Cu/SiO<sub>2</sub> films present the double interest of forming an adherent copper layer directly on silica surfaces thanks to SiO<sub>2</sub> anchoring, and behave as an effective catalyst layer for a further deposition of thick copper by electroless technique. This approach can easily be extended to other classes of organometallic precursors and brings a new example of the growing role of organometallic chemistry solutions in the field of the actual microelectronic challenges.

[1] G. A. Somorjai, F. Tao and J. Y. Park, *Top. Catal.*, **2008**, 47, 1

[2] C. Barrière, P. Fau et al. *J. Mater. Chem.*, **2008**, 18, 3084–3086

[3] O. Margeat, C. Barrière, P. Fau, B. Chaudret, **2009**, FR2929449\_WO200912514

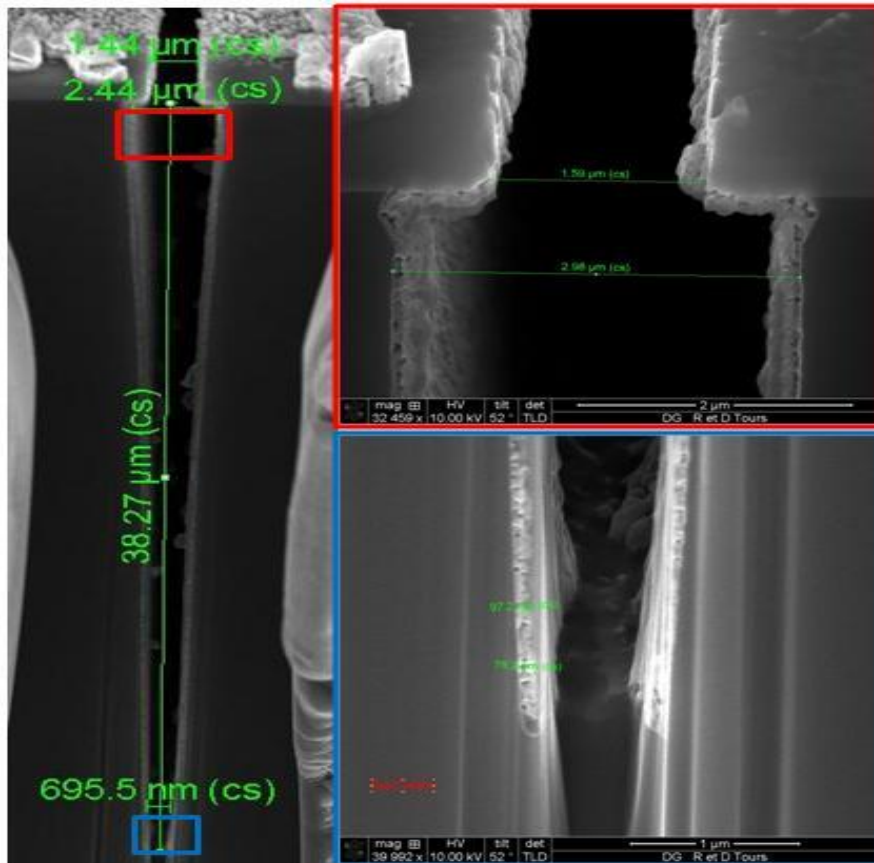


Figure 1: FIB pictures of Cu/SiO<sub>2</sub> deposit : panoramic view and dimension of the trench (left), top of the trench (top right) and bottom of the trench (bottom right)

## Studies of encapsulation of new antitumoral fluorescent compounds in nanoliposomes for drug delivery purposes

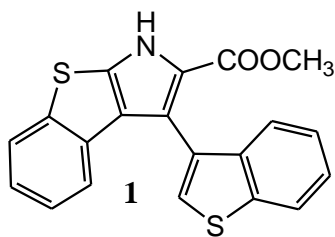
Maria-João R. P. Queiroz,<sup>1</sup> Ana S. Abreu,<sup>1,2</sup> Elisabete M.S. Castanheira,<sup>2</sup> Paula M.T. Ferreira<sup>1</sup>

<sup>1</sup>Centro de Química (CQ-UM) and <sup>2</sup>Centro de Física (CFUM), Universidade do Minho, Campus de Gualtar, 4710-057 Braga, Portugal

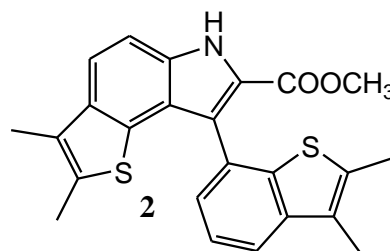
[mjrpg@quimica.uminho.pt](mailto:mjrpg@quimica.uminho.pt)

Nanosized liposomes are among nanotechnological delivery methods for chemotherapeutic drugs in the treatment of cancer. This nanotechnology can potentially overcome many common pharmacologic problems, such as those involving solubility, *in vivo* stability, pharmacokinetics, tumor uptake and toxicity [1,2]. Liposomes are closed spherical vesicles consisting of a lipid bilayer that encapsulates an aqueous phase in which hydrophilic drugs can be stored, while water insoluble compounds can be incorporated in the hydrophobic region of the lipid bilayer [3].

In this work, new synthetic fluorescent antitumoral compounds **1** and **2** [4] were encapsulated in nanosized liposomes of DPPC (dipalmitoyl phosphatidylcholine), egg lecithin (phosphatidylcholine from egg yolk) and DODAB (dioctadecyldimethylammonium bromide). The phospholipids DPPC and egg lecithin (Egg-PC) are neutral components of biological membranes, while cationic liposomes based on the synthetic lipid DODAB have been used as vehicles for DNA transfection and drug delivery [5].



Methyl 3-(benzo[*b*]thien-3-yl)benzothieno[2,3-*b*]pyrrole-2-carboxylate



Methyl 8-(2,3-dimethylbenzo[*b*]thien-7-yl)-2,3-dimethyl-6*H*-thieno[2,3-*e*]indole-7-carboxylate

Monodisperse and nanosized liposomes were prepared by injection of an ethanolic solution of the lipid in an aqueous media under vigorous stirring, above the lipid melting transition temperature ( $T_m \sim 41$  °C for DPPC and 45 °C for DODAB). The hydrodynamic diameters of  $87 \pm 11$  nm for DPPC,  $51 \pm 2$  nm for Egg-PC and  $268 \pm 37$  nm for DODAB were obtained by dynamic light scattering.

The effect of compounds **1** and **2** on the *in vitro* growth of three human tumor cell lines, breast adenocarcinoma (MCF-7), non-small cell lung cancer (NCI-H460) and CNS cancer (SF-268), was evaluated after a continuous exposure of 48h. Values of compound concentrations able to inhibit 50% of cell growth ( $GI_{50}$ ) are shown on Table 1. The benzothieno[2,3-*b*]pyrrole **1** showed the best results, exhibiting lower  $GI_{50}$  values than compound **2** in the three tumor cell lines, being significantly more potent against the MCF-7 and NCI-H460 tumor cell lines.

**Table 1 .** Effect of compounds **1** and **2** on the growth of three human tumor cell lines

Compounds	GI <sub>50</sub> (μM)		
	MCF-7	NCI-H460	SF-268
<b>1</b>	7.9 ± 0.1	7.9 ± 1.8	14.1 ± 3.0
<b>2</b>	20.1 ± 16.7	16.7 ± 8.6	16.5 ± 9.4

Results represent means ± SEM of 3-4 independent experiments performed in duplicate.

Doxorubicin was used as positive control, GI<sub>50</sub>: MCF-7 = 42.8 ± 8.2 nM;

NCI-H460 = 94.0 ± 8.7 nM and SF-268 = 94.0 ± 7.0 nM.

The intrinsic fluorescence of compounds **1** and **2**, due to its high sensitivity and dependence on the solvent, was used to obtain information about compounds location in the nanoliposomes prepared. Fluorescence emission and anisotropy measurements were performed below (gel phase) and above (liquid crystalline phase) the lipid transition temperature (figure). The results indicated that compound **1** preferential location is at the lipid bilayer, near the polar head groups, while compound **2** prefers generally a more fluid environment. These encapsulation experiments are relevant for further studies involving drug delivery applications in cancer treatment.

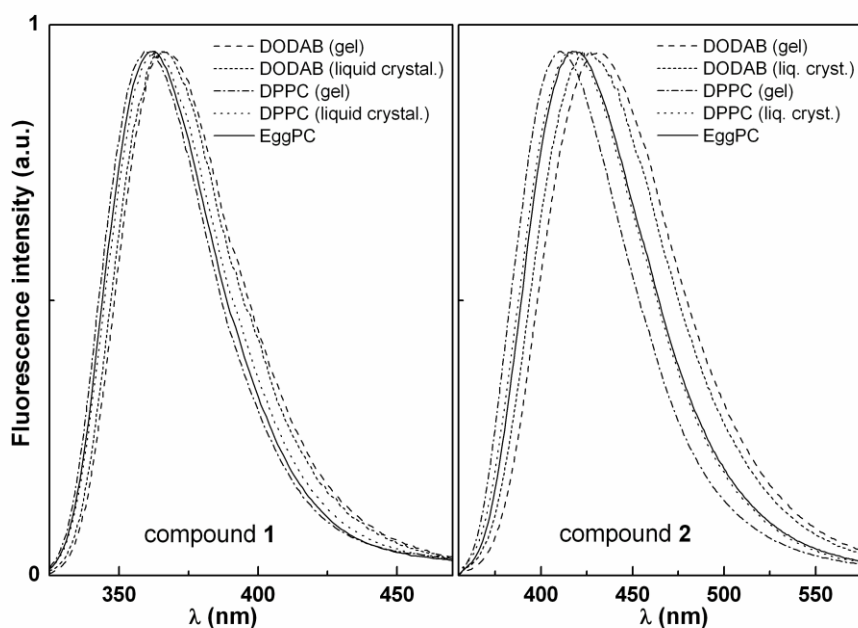


**Figure:** Normalized fluorescence emission spectra of compounds **1** and **2** incorporated in nanoliposomes of DPPC, Egg-PC and DODAB.

**Acknowledgments:** This work was funded by Foundation for Science and Technology (FCT-Portugal) through CFUM, CQ-UM, Project PTDC/QUI/81238/2006 and Post-doc. grant of A.S. Abreu (SFRH/BPD/24548/2005).

#### References:

- [1] T. L. Andresen, S. S. Jensen, K. Jorgensen, *Prog. Lipid Res.* **44** (2005) 68-97.
- [2] N. A. Ochekepe, P. O. Olorunfemi, N. C. Ngwuluka, *Tropical J. Pharm. Res.* **8** (2009) 265-274; 275-287.
- [3] Y. Malam, M. Loizidou, A.M. Seifalian, *Trends Pharmacol. Sci.* **30** (2009) 592-599.
- [4] A. S. Abreu, N. O. Silva, P. M.T. Ferreira, M.-J. R.P. Queiroz, M. Venanzi *Eur. J. Org. Chem.* (2003), 4792-4796.
- [5] M. C. Pedroso de Lima, S. Simões, P. Pires, H. Faneca, N. Düzgünes, *Adv. Drug Deliv. Rev.* **47** (2001) 277-294.

## Using biomolecules with micro and nanosystems: electrically aligned microtubules as a foundation for further integration

*Ruben Ramalho<sup>a,b,\*</sup>, Helena Soares<sup>a,c</sup>, Susana Cardoso<sup>b,e</sup>, Luís V. Melo<sup>b,d</sup>*

*<sup>a</sup>Instituto Gulbenkian de Ciência, R. da Quinta Grande 6, Oeiras, Portugal*

*<sup>b</sup>Instituto Superior Técnico, Av. Rovisco Pais, Lisboa, Portugal*

*<sup>c</sup>Escola Superior de Tecnologia de Saúde de Lisboa, Lisboa, Portugal*

*<sup>d</sup>IN, Lisboa, Portugal*

*<sup>e</sup>INESC-MN, R. Alves Redol 9, Lisboa, Portugal*

*[\\*rubendrr@igc.gulbenkian.pt](mailto:rubendrr@igc.gulbenkian.pt)*

Proteins in living cells are excellent examples of highly efficient nanodevices, whose functions are not limited to catalysing and participating in chemical reactions, but also include structuring the cell – often by self assembling into specialized structures such as those that make up the eukaryotic cytoskeleton – and generating forces used for intracellular transport, cellular remodelling or cellular motion (or, in fact, motion of the entire organism). A good example are microtubules, self-assembling anisotropic cytoskeletal polymers, which form a network that interacts with many of the cell's proteins and structures, including motor proteins – responsible for intracellular transport – and other cytoskeletal structures. This makes them a possible foundation for integrating and controlling other biomolecules.

When attempting to use these molecules with existing micro- and nano-electronic technology, there is a challenge in organising and controlling them. With this challenge in mind, we have previously shown [1] that microtubules can be aligned in bulk by a high electric field (~ 400 KV/m).

To study the possible use of microtubules in bionanotechnology, we have reproduced the previous bulk alignment experiment on a custom-made chip containing thousands of separate alignment experiments over distances in the order of 5 to 20  $\mu\text{m}$ , which allowed us to use fields up to 1 MV/m. Using Atomic Force Microscopy, we observed the successful alignment of microtubules by the applied field, and present the results here.

To continue exploring the possibilities of this method, we have produced a simplified glass chip to be used with an optical microscope in order to further characterize microtubule alignment and interaction with associated proteins. The preliminary results from this chip will also be presented.

### References:

[1] Ramalho, R., Soares, H. & Melo, L., *Mat. Sci. Eng. C*, **27**(2007), 1207-1210

## PREPARATION AND CHARACTERIZATION OF SINGLE-CRYSTALLINE SILICON NANOWIRE ARRAYS

Enrique A. Dalchiele<sup>1</sup>, Francisco Martín<sup>2</sup>, Dietmar Leinen<sup>2</sup>, Ricardo E. Marotti<sup>1</sup> and José R. Ramos-Barrado<sup>2</sup>

<sup>1</sup>*Instituto de Física, Facultad de Ingeniería, Herrera y Reissig 565, C.C. 30, 11000 Montevideo, Uruguay.*

<sup>2</sup>*Laboratorio de Materiales y Superficie (Unidad Asociada al CSIC). Departamentos de Física Aplicada & Ingeniería Química, Universidad de Málaga, Campus de Teatinos s/n, E29071 Málaga, Spain.*

[barrado@uma.es](mailto:barrado@uma.es); [dalchiel@fing.edu.uy](mailto:dalchiel@fing.edu.uy)

In the last years, one-dimensional (1D) nanostructured materials, such as semiconductor nanowires have attracted much attention because of their special physical properties and their potential applications in various fields [1]. It has been demonstrated that compared to the two dimensional thin film semiconductors, 1D materials exhibit superior optoelectronic, mechanical and thermal properties. On the other hand, silicon (Si), is as a consequence of its excellent performance, the most important semiconducting material since the Si-based devices have dominated microelectronic technology for many decades. In the last years, silicon nanowires (SiNWs), have attracted much attention because of their unique properties and their compatibility with the Si-based microelectronics. Then, SiNWs are attractive for applications in field-emission devices, chemical sensors, spintronics and photonics [2].

In the present work SiNW arrays have been synthesized by self-assembly electroless metal deposition (EMD) nanoelectrochemistry. The synthesized SiNW arrays have been submitted to SEM, TEM and HRTEM studies.

The SEM images of a typical SiNW array synthesized by the SAEMD-nanoelectrochemistry approach on n-type Si(100) substrate (30 min etching) are shown in Fig. 1. SEM observations reveal that large quantities of silicon nanowires arrays could be produced on the silicon wafer chip. The density of SiNW arrays (Fig. 1a) is about  $10^9/\text{cm}^2$ , which shows little changes with different etching times. Figure 1b shows the cross-section details of the SiNW array in which all SiNWs are distinguishable and most of them are vertical to the wafer surface, exhibiting a length about 30  $\mu\text{m}$  and diameters in the range of 100-160 nm.

Furthermore, the morphology and structure of SiNWs have been characterized in detail using TEM and HRTEM analysis. The SiNW were single crystalline, as shown by the FFT pattern (inset of Fig. 2) and HRTEM image of the Si lattice of a SiNW in Fig. 2. A further detailed analysis of HRTEM indicates that the axial crystallographic orientation of the SiNWs is the [100] direction, which is identical with the orientation of the initially used silicon wafer.

### References:

- [1] B. K. Teo and X. H. Sun, Chem. Rev., **107** (2007) 1454.
- [2] Z. Huang, H. Fang and J. Zhu, Adv. Mater., **19** (2007) 744.

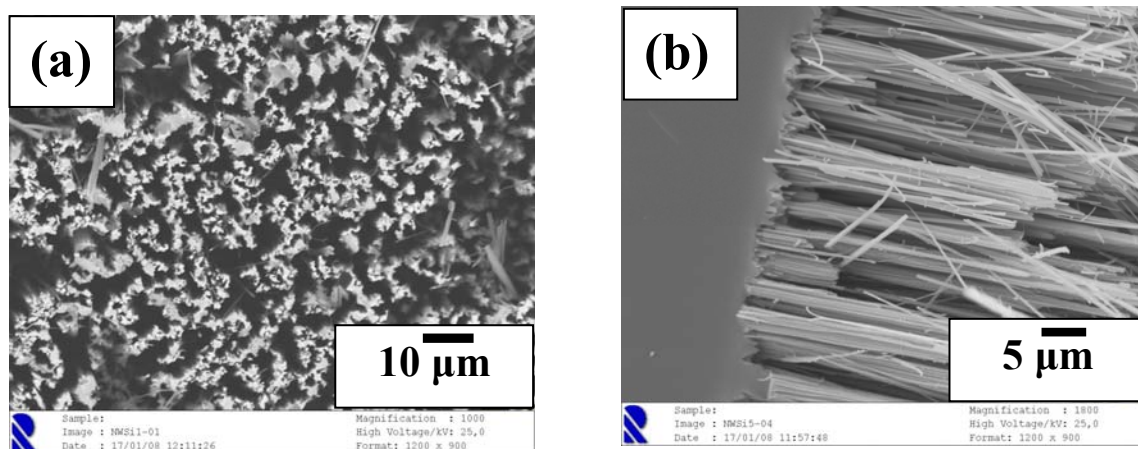


**Figure 1:** SEM images of SiNW arrays: (a) top view and (b) cross-sectional view.

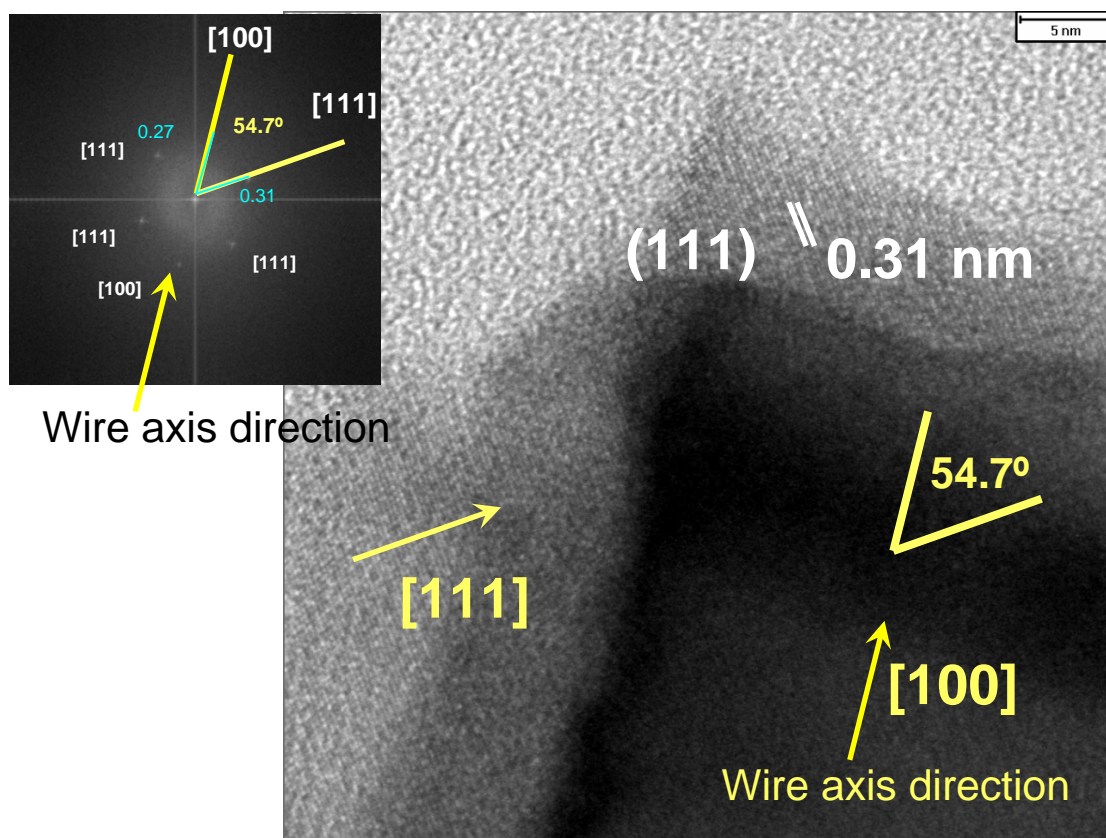


**Figure 2:** Typical HRTEM of an individual Si nanowire. Inset: FFT of the HRTEM image.

**Luminescent nanocomposites for photonic sensing**

<sup>1</sup>F.J. Aparicio, <sup>1</sup>I. Blaszcyk-Lezak, <sup>1</sup>A. Borrás, <sup>2</sup>M. Holgado, <sup>1</sup>J.R. Sanchez-Valencia,  
<sup>3</sup>A. Griol, <sup>4</sup>H. Sohlström, <sup>4</sup>M. Antelius, <sup>1</sup>A.R. González-Elípe, <sup>1</sup>A. Barranco

<sup>1</sup>Instituto de Ciencia de Materiales de Sevilla CSIC-Universidad de Sevilla, c/Américo  
Vespucio 49 41092 Sevilla Spain

<sup>2</sup>Centro Láser, Universidad Politécnica de Madrid, Spain

<sup>3</sup>Nanophotonics Technology Center, UPLV, Valencia, Spain.

<sup>4</sup>Royal Institute of Technology, KTH, Stockholm, Sweden

[angelbar@icmse.csic.es](mailto:angelbar@icmse.csic.es)

This communications reports about a novel synthetic methodology that permits a tailored deposition of dye containing nanometric thin films over photonic structures for the fabrication of luminescent sensing photonic chips. This new procedure is based on the room temperature partial polymerization of the dye molecules in a remote Ar glow discharge. As a result of this one step solventless process a polymeric nanocomposite thin film is produced containing some dye molecules that keep intact their optical activity and sensor response. In addition this synthetic strategy permits the use of additional precursors in order to control the dye molecules aggregation and therefore modified the fluorescent and absorption response of the nanocomposite. The thin films are flat homogenous mechanically stable, insoluble and well adhered to the substrate. These materials can be processed in order to produce micrometric patterns for photonic applications. The mechanical, structural, optical and luminescent properties of the films deposited by this new procedure make such materials ideal candidates for their integration in photonic structures for environmental sensing applications. For example this synthetic methodology has been recently used for the deposition of optical NO<sub>2</sub> sensing nanocomposites [1] and for the controlled introduction of solid organic luminescent planar defects within self assembly 3D photonic crystals [2]. The fabrication strategy developed is fully compatible with the current micro- and optoelectronic technology permitting the use of temperature sensitive substrates and is scalable at the wafer level. Examples of the integration of the luminescent nanocomposite as active layers in photonic structures will be shown.

**References:**

[1] I. Blaszcyk-Lezak, F.J. Aparicio, et al., J. Phys. Chem. C, **1** (2009) 431.

[2] F.J. Aparicio, G. Lozano, et al., Chem. Mater., **2** (2010) 379.

## Synthesis and evaluation of magnetic poly(styrene/divinylbenzene/acrylic acid) microspheres for applications in bio-molecular recognition.

*C. Rodríguez, E. Castro, J.R. Marín, P. Bilbao and J.M. Cuevas  
GAIKER Technology Center. Parque Tecnológico, Edificio 202,  
48170, Zamudio (Spain)  
[rodriguezcg@gaiker.es](mailto:rodriguezcg@gaiker.es)*

### Abstract

In the present work, the polymerization of styrene-divinylbenzene-acrylic acid monomers by precipitation polymerization<sup>1</sup> with the inclusion of magnetite nanoparticles has been used for the magnetic microspheres formation and use in biomedical application. These magnetic microspheres contain –COOH functional groups, provided by the acrylic acid monomer, suitable for the antibodies coupling and biorecognition of the carcinoembryonic antigen CEA<sup>2-4</sup>. In general, biological interactions with engineered nanoparticles are strongly dependent on variables such as size, morphology, surface charge and reactivity, defects in the nanoparticle surface, elemental composition (core composition) and surface functionalization which directly impact biocompatibility<sup>5</sup>.

The research is based on the synthesis and characterization of different magnetic microspheres, studying the influence of the acrylic acid concentration in the final size copolymer and consequently, in the efficiency of the antibody coupling between the primary amino groups (-NH<sub>2</sub>) and the carboxyl functional groups (-COOH) of the polymeric surface.

Three magnetic microspheres have been synthesized with different ratios of monomers styrene:divinylbenzene:acrylic acid named M1, M2 and M3, from low to high concentration of acrylic acid and a fixed weight of magnetite nanoparticles (≈10 nm) for all of them. The particle size, analyzed by scanning electronic microscopy (SEM) (Figure 1), and transmission electronic microscopy (TEM), decreases as it increases the acrylic acid concentration (from 0,5 to 0,17 μm approximately) and the saturation magnetization values, measured in an electromagnet, also changed with the size of particle, Figure 2.

The presence of the –COOH groups in the polymeric surface and the –NH and C=O groups after the covalent bounding of the antibodies has been shown by Fourier transform infrared spectroscopy (FTIR).

Molecular techniques, as ELISA assay<sup>6</sup>, have allowed quantification of the antibodies coupling and have showed high efficiencies of covalent bound of the added antibody in the case of the magnetic beads that contain the highest concentration of acrylic acid monomer (M2 and M3).

## References:

- [1]. M. D. Shultz, J. R. Marin, S. H. Naik, J. Wilkins, J. M. Laza, J. L. Vilas, M. Rodriguez, N. Perez, and E. E. Carpenter, *Journal of Applied Physics*, **105** (1009) 07B318.
- [2]. C.N. Ramchand, P. Pande, P. Kopcansky, *Ind. J. Pure Appl. Phys.*, **39** (2001) 683.
- [3]. A. Elaissari, M. Rodriguez, F. Meunier, C. Herve, *J. Magn. Magn. Mater.*, **225** (2001) 127.
- [4]. S. Hallier-Soulier, E. Guillot, *J. Appl. Microbiol.*, **89** (2000) 5.
- [5]. *Nanoparticles and Nanodevices in Biological Applications: The INFN Lectures-V.1*, (2009), Bellucci S. (Ed).
- [6]. Sirley V. Pereira, Germán A. Messina, Julio Rab., *Journal of Chromatography B*, **878** (2010) 253–25.

Figure 1.

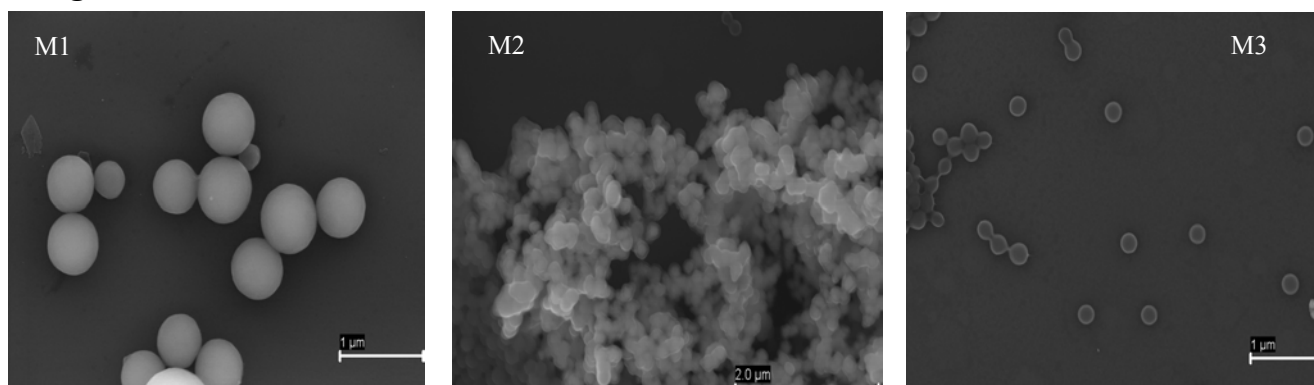
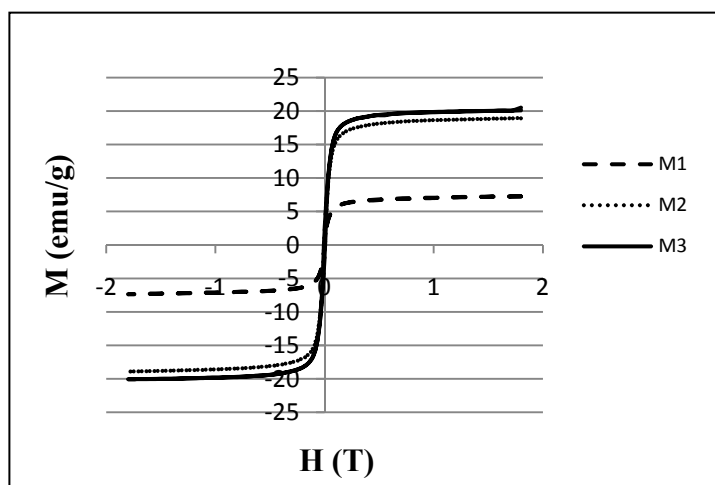


Figure 2.



## Thermal decomposition of cerium propionate in oxidant atmosphere to obtain ceria nanocrystalline films at low temperature

*P. Roura\**, *J. Farjas\**, *J. Camps\**, *S. Ricart<sup>&</sup>*, *N. Mestres<sup>&</sup>*, *T. Puig<sup>&</sup>* and *X. Obradors<sup>&</sup>*

*\*University of Girona, Campus Montilivi, Edif. PII, E17071 Girona, Catalonia, Spain*

*<sup>&</sup>Institut de Ciència de Materials de Barcelona (CSIC), Campus de la UAB, 08193*

*Bellaterra, Catalonia, Spain*

*[pere.roura@udg.es](mailto:pere.roura@udg.es)*

Ceria-based oxides deserve great attention because of their broad range applications covering fields as diverse as catalysis [1], electrolyte materials for fuel cells [2], oxygen sensors [3] and buffer layers for coated superconductor architectures [4]. This last application requires the epitaxial crystallization of a multilayered structure of several oxides on metallic Ni-W tapes. Nanometric buffer layers of (Y)ZrO<sub>2</sub> and CeO<sub>2</sub> are usually grown between the upper YBa<sub>2</sub>Cu<sub>3</sub>O<sub>7</sub> superconductor layer and the substrate to promote epitaxy while avoiding interdiffusion [4].

Chemical solution deposition offers a low cost route for obtaining such multilayers with good chemical purity and thickness control [5, 6]. The precursors are decomposed by thermal treatment in inert atmosphere to avoid substrate oxidation [7]. However, this practice is detrimental for the CeO<sub>2</sub> quality because elimination of carbonaceous residues is achieved at the expense of partial reduction of Ce<sup>4+</sup> to Ce<sup>3+</sup> [8].

In this communication, we will present our recent results on the thermal decomposition of cerium(III) propionate in atmospheres with varying oxygen partial pressure. It is shown that the decomposition temperature is as low as 300°C in air and that crystallization and oxidation of Ce<sup>3+</sup> to Ce<sup>4+</sup> occurs before complete decomposition has been achieved so that nanocrystalline CeO<sub>2</sub> layers can be obtained at a temperature range where oxidation of the metallic substrate is negligible.

A range of thermoanalytical techniques has been applied to characterize the decomposition processes. In particular, mass spectroscopy of the volatile species has proven essential in elucidating the microscopic processes leading from propionate to ceria nanoparticles. The degree of crystallization of the intermediate and final products has been analyzed by x-ray diffraction (XRD) and transmission electron microscopy (TEM), whereas the cerium oxidation state has been quantified by x-ray photoelectron spectroscopy (XPS) and by magnetic susceptibility measurements (SQUID).

This work has been funded by the Spanish Plan Nacional de Materiales through projects MAT2009-08385 and MAT2008-01022.

### References:

- [1] A. Trovarelli, Catal. Rev. Sci. Eng., **38** (1996) 439.
- [2] E. P. Murray, T. Tsai and S.A. Barnett, Nature, **400** (1999) 649.
- [3] N. Izu, W. Shin, N Murayama, Sens. Actuators B, **93** (2003) 449.
- [4] A. Goyal, M. Parans Paranthaman and U. Schoop, MRS Bull. **29** (2004) 552.
- [5] R. Schwartz, T. Scheneller and R. Waser, C.R.Chimie, **7** (2004) 433.
- [6] M. W. Rupich, D. T Verebelyi, W. Zhang, T. Kodenkandath and X. Li, MRS Bull. **29** (2004) 572.
- [7] M. Coll, J. Gazquez, F. Sandiumenge, T. Puig, X. Obradors, J. P Espinos and R. Hühne, Nanotechnology, **19** (2008) 395601.
- [8] S. Masson, P Holliman, M. Kalaji and P. Kluson, J. Mat. Chem. **19** (2009) 3517.

## Figures:

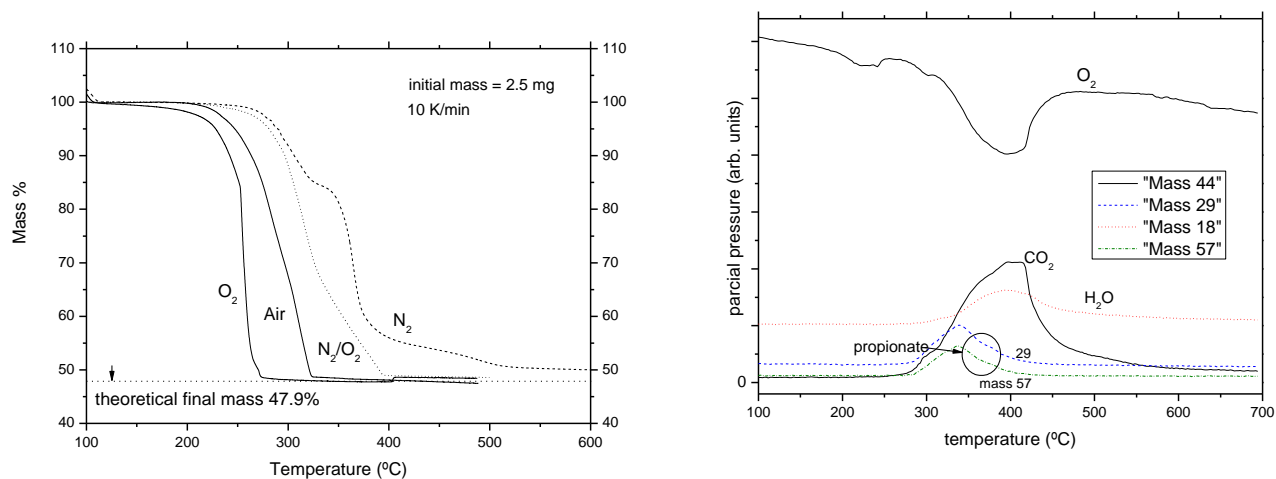


Figure 1.- a) Thermogravimetric curves showing the mass loss when cerium propionate is heated at constant rate in atmospheres with varying oxygen partial pressure; b) the mass spectroscopy curves of the main volatile species detected in air.

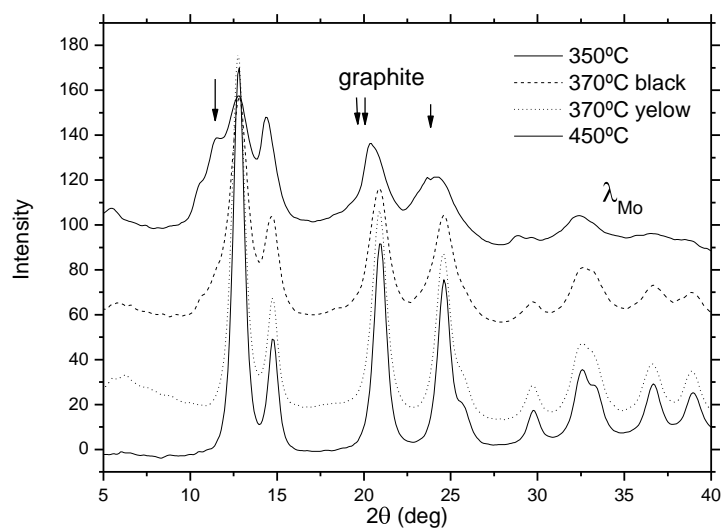


Figure 2.- X-ray diffraction curves obtained at different steps of the decomposition process. The peaks corresponding to CeO<sub>2</sub> are already present before decomposition has finished.

## Label-Free Optical Fiber Sensing Platform based on Lossy Mode Resonances Supported by Transparent Conducting Oxides

*Carlos Ruiz, M. Hernaez, I. Del Villar, I. R. Matias, F. J. Arregui*  
Public University of Navarra, Campus Arrosadia, Pamplona, SPAIN  
[carlos.ruiz@unavarra.es](mailto:carlos.ruiz@unavarra.es)

Thin-film coated optical waveguides can support different types of resonances [1]. Among them, surface plasmon resonances (SPR) have focused the attention of the scientific community motivating hundreds of publications and sensing applications as a label free sensing platform [2]. Besides, optical fiber SPR configuration can overcome some of the limitations of the traditional Kretschmann-based SPR configurations such as the utilization of a prism and a monochromatic light source and permits remote sensing and multiplexing between multiple SPR-based devices [3]. A second type of resonance is known as lossy mode resonances (LMR) [4]. Even though LMR-based optical fiber sensors are independent of light polarization and can overcome some of the traditional limitations of SPR-based optical fiber sensors they have not been as widespread as SPR-based optical fiber sensors. Additionally, LMR-based devices permit to tune the sensitivity of the resonance in the spectral range by simply adjusting the absorbing thin-film fabrication parameters or by selecting the appropriate material. LMR-based devices also permit the utilization of an additional coating adhered to the metal layer in order to detect diverse substances or chemical compounds [5]. Indium tin oxide (ITO) coated optical fibers have been already studied in literature as LMR-based refractometers with a resonance wavelength in the infrared region [4-5].

Here, it is described the fabrication of LMR-based refractometers by means of the deposition of a thin aluminium doped zinc oxide (AZO) film onto the optical fiber core. The AZO film is deposited onto the optical fiber core as described elsewhere [6]. The deposition process basically consisted of a prior fiber cleaning process in order to remove the optical fiber cladding followed by a sol-gel dip-coating deposition process. The AZO film of thickness ~115 nm fabricated onto the optical fiber is shown in the SEM image of *Fig. 1*.

AZO coated optical fibers were connected in a typical transmission setup as it is represented schematically in *Fig. 2*. A halogen lamp (ANDO Inc.) was used as the excitation source at one end of the fiber and a spectrometer (HR4000, Oceanoptics Inc.) was used in order to collect the light at the opposite end of the fiber. Absorbance spectra (see *Fig. 3*) were obtained when the AZO sensitive region (see detail in *Fig. 1*) was immersed in different glycerin/water concentration solutions from 0% to 75% corresponding to 1.33, 1.35, 1.37, 1.39, 1.41 and 1.43 refractive index units (RIU) respectively, estimated at 20 °C and 590nm. Here, the wavelength at maximum absorbance (resonance wavelength) is shifted to larger wavelengths as the external medium refractive index is increased. The resonance wavelength shift is represented in *Fig. 4*, showing a variation of approximately 1100 nm/RIU.

To sum up, AZO coated optical fibers have been fabricated and characterized as LMR-based refractometers in the visible spectral region in a simple and straight-forward way. Finally, LMR-based devices presented here, could be the first step towards a vast field of applications in chemistry, or biology by the only addition of the specific outer coating in the same manner as SPR-based sensors already did.

### References:

- [1] Yang & Sambles, *J. Mod. Opt.*, **44**, 1155-1163, 1997.
- [2] J. Homola, *Anal. Bioanal. Chem.*, **377**, 528-539, 2003.
- [3] B. Lee, S. Roh, J. Park, *Sens. Actuators B*, **15**, 209-221, 2009.
- [4] I. Del Villar, C. R. Zamarreño, M. Hernaez, F. J. Arregui, I. R. Matias, *J. Lightwave Tech.*, **28(1)**, 111-117, 2010.
- [5] C. R. Zamarreño, M. Hernaez, I. Del Villar, I. R. Matias, F. J. Arregui, *Sens. Actuators B*, (in press)
- [6] Keh-moh Lin y Paijay Tsai., *Mat. Sci. & Engineering B*, **139**, (2007) 81-87.

Figures:

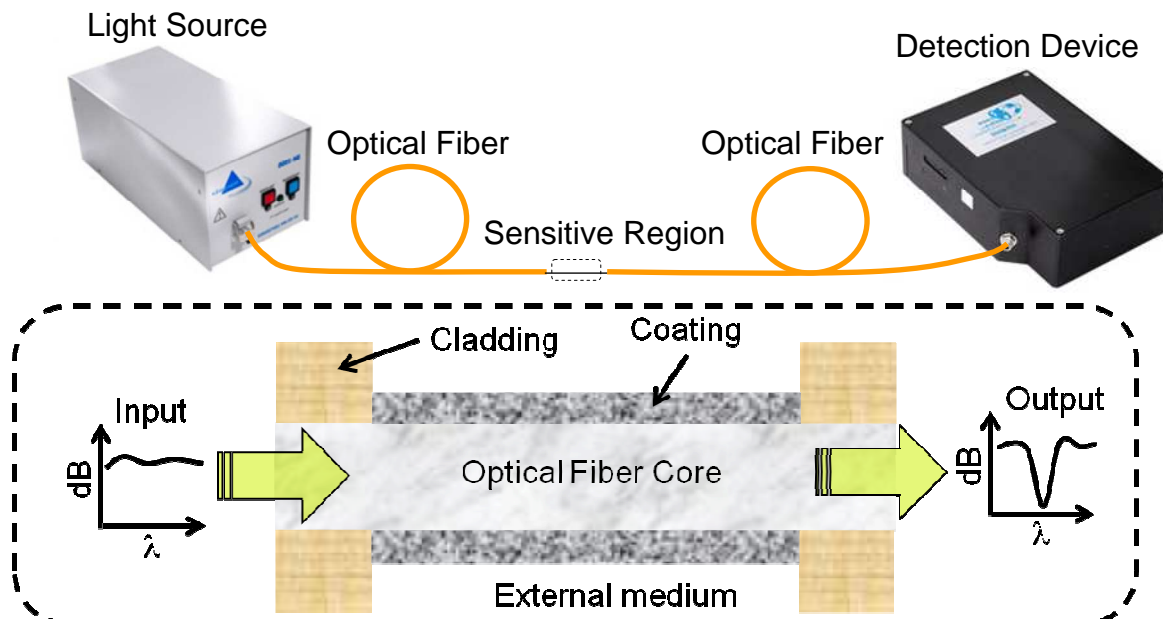


Fig2: Optical fiber transmission setup and detail of the sensitive region.

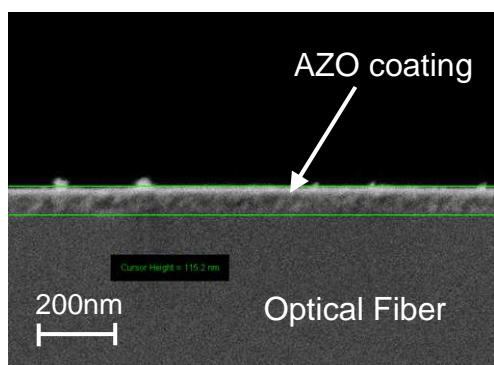


Fig1: SEM image of an AZO coated optical fiber.

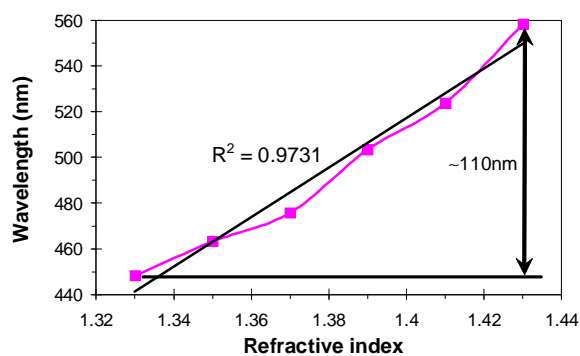


Fig4: Resonance wavelength shift as a function of the external refractive index.

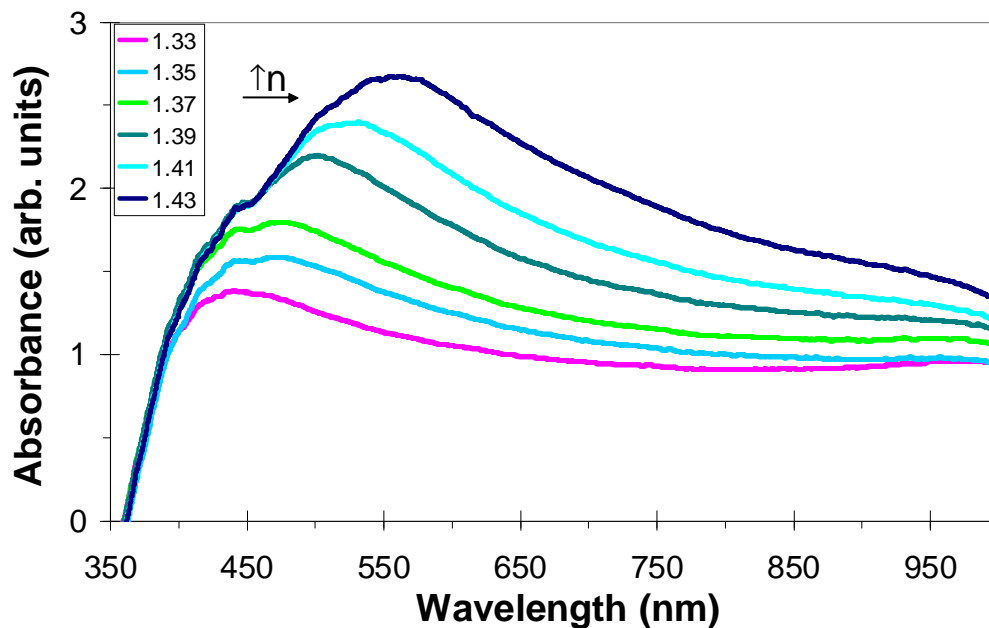


Fig. 3: Absorbance spectra obtained when the sensitive region was immersed in different glycerin/water concentration solutions of refractive indices 1.33, 1.35, 1.37, 1.39, 1.41, 1.43.

## Dendrimeric-Nanocarriers for easy *in vitro* detection of allergic reactions induced by $\beta$ -lactams

Ruiz-Sánchez, A.J.<sup>1</sup>, Vida, Y.<sup>1</sup>, Montañez, M.I.<sup>2</sup>, Kehr, S.<sup>3</sup>, Suau, R.<sup>1</sup>, Blanca, M.<sup>2</sup>,  
Mayorga, C.<sup>2</sup>, Torres, M. J.<sup>2</sup>, De Cola, L.<sup>3</sup>, Perez-Inestrosa, E.<sup>1</sup>

<sup>1</sup> Department of Organic Chemistry. Faculty of Sciences. University of Málaga,  
Campus Teatinos s/n, 29071, Málaga, Spain

<sup>2</sup> Fundación IMABIS, Hospital Carlos Haya, Málaga, Spain.

<sup>3</sup> Physikalisches Institut, University of Münster, Mendelstrasse, D-48149 Münster, Germany  
[ajruizs@uma.es](mailto:ajruizs@uma.es)

Immediate allergic reactions to  $\beta$ -lactams are mainly diagnosed by a compatible clinical history and the presence of skin test positive and/or *in vitro* test to different  $\beta$ -lactams determinants. In some cases, when skin tests are negative, a controlled administration of the drugs may be necessary although neither is free of risk, especially in persons with anaphylactic reactions. The determination of specific immunoglobulin E antibodies, IgE (antibody associated with an allergic response) in serum is a very valuable method to confirm the diagnosis, although it is not as sensitive as skin testing. An improvement in the *in vitro* techniques is therefore needed to enhance diagnosis in allergic patients. Diagnostic testing in the immunological setting is primarily concerned with the recognition and confirmation of the presence of IgE antibodies.<sup>1</sup> The analytical challenges of an *in vitro* test are therefore related with sensitivity (i.e. lowest detectable concentration) and specificity (i.e. accuracy for the analyte or group of analytes required). The analytical sensitivity and specificity have an important influence on the clinical sensitivity and specificity of the method. The binding of an immunoreactive component such as an analyte-specific antigen to a specific antibody immobilized on a solid-phase support is the essential, common feature of solid-phase immunoassay techniques. Such techniques are used to measure circulating levels of a number of markers used as guidance in the management of patients with specific clinical symptoms. For example, the RadioAllergoSorbent Test (RAST) shown in Figure 1 is a blood test used to determine what a person is allergic to, based on the amount of IgE reacting specifically with suspected or known allergens.<sup>2</sup>

Conjugation of BL to a macromolecular carrier has been used as a tool for the *in vivo* and *in vitro* tests for diagnosing IgE mediated reactions. Classical conjugation of HSA (Human Serum Albumin) with penicillins generates the benzylpenicilloyl determinant (BPO), the major antigenic structures.<sup>3</sup>

PLL (Poly-L-Lysine) is a versatile homopolymer that has been extensively used as a precursor of drug-polymer conjugates.<sup>4</sup> However this approach, due to differences in the degree of polymerization and subsequent functionalisation frequently lacks of reproducibility.

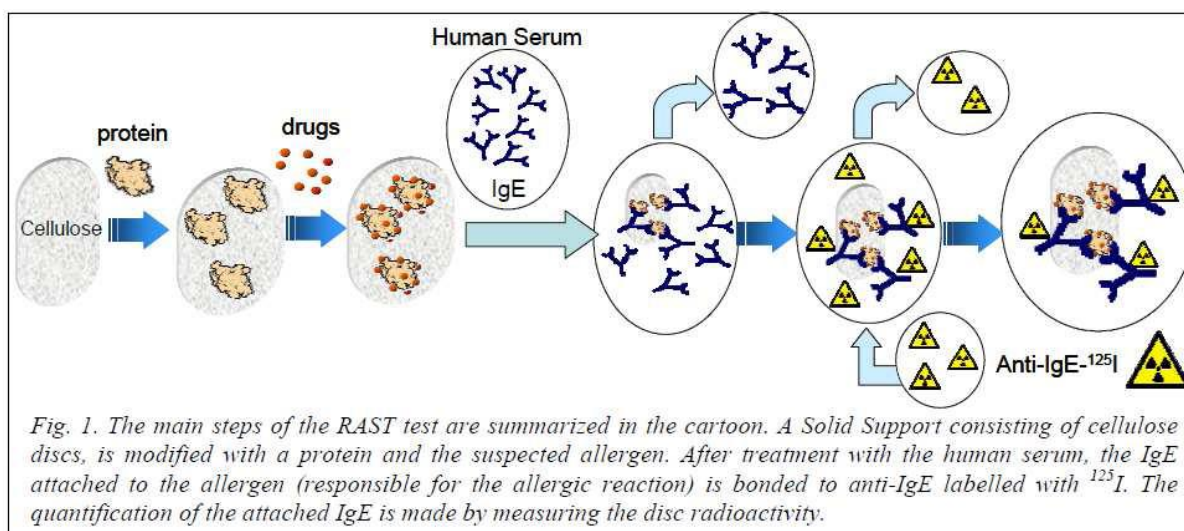
Dendrimers can be considered the most versatile, compositionally and structurally controlled synthetic nanoscale building blocks available today.<sup>5</sup> Artificial antigens have been synthesized and they have shown that these hapten dendrimer conjugates are recognized by IgE directed to BL, emulating the *in vivo* drug conjugates to proteins.<sup>6,7</sup>

The shift from cellulose (fibrous and rough surface, with holes that can host the dendrimer) to nano/microstructure transparent surface as zeolites seems to be an important improvement in our system.

Zeolite L is a microporous crystalline material featuring a one dimensional channel system. The length of these cylindrically shaped crystals can be tuned from 30 nm to about 10 microns. Zeolite L can be prepared with different aspect ratios (i.e. length / diameter),

forming either thin discs or long cylinders. [1] A. Zabala Ruiz, D. Brühwiler, L.-Q. Dieu, G. Calzaferri, in *Materials Syntheses, A practical Guide*, Eds. Schubert U., Hüsing N., Laine R., Springer, Wien, (ISBN 978-3-211-75124-4), 2008, 1.

The surface of zeolites L has been functionalized with hapten dendrimer conjugates. The novel organic-inorganic hybrid materials have been characterized by IR, XPS, zeta potential and ninhydrin test proving the successful covalent anchoring of the dendritic macromolecules to zeolites L. RAST analysis using them is going to be done as soon as possible.



## References:

- [1] Torres MJ, Blanca M, de Weck A, Fernandez J, Demoly P, Romano A, Abereer W and ENDA and the EAACI interest group on drug hypersensitivity. *Allergy* **2003**; 58, 961.
- [2] Blanca, M., Mayorga, C., Sanchez, F., Vega, J. M., Fernandez, J., Juarez, C., Suau, R., Perez-Inestrosa, E. *Allergy* **1991**, 46, 632.
- [3] *The Antigens* Vol 5 New York. Academic Press. **1977**, 73-245
- [4] G. Thoma, J. T. Patton, J. L. Magnani, B. Ernst, R. Oehrlein, R. O. Duthaler, *J. Am. Chem. Soc.* 1999, **121**, 5919
- [5] *Dendrimers and Dendrons: Concepts, Synthesis, Application*. Wiley-VCH: Weinheim, Germany, **2001**
- [6] F. Sánchez-Sancho, E. Pérez-Inestrosa, R. Suau, C. Mayorga, M. J. Torres, M. Blanca. *Bioconjugate Chem.* **2002**, 13, 647.
- [7] M. I. Montañez, E. Perez-Inestrosa, R. Suau, C. Mayorga, M. J. Torres, M. Blanca. *Biomacromolecules.* **2008**, 9, 1461.
- [8] A. Zabala Ruiz, D. Brühwiler, L.-Q. Dieu, G. Calzaferri. *Materials Syntheses, A practical Guide*, Eds. Schubert U., Hüsing N., Laine R., Springer, Wien, (ISBN 978-3-211-75124-4), **2008**, 1.

## Liquid Crystalline-ZnO Nanoparticle Hybrids

S. Saliba,<sup>a,b</sup> M. L. Kahn,<sup>a\*</sup> J.-D. Marty,<sup>b\*</sup> Y. Coppel,<sup>a</sup> C. Mingotaud,<sup>b</sup> B. Chaudret<sup>a</sup>

<sup>a</sup> University of Toulouse ; Laboratoire LCC; CNRS UPR 8241, 205 route de Narbonne, 31077 Toulouse, France.

<sup>b</sup> University of Toulouse; Laboratoire IMRCP; UMR CNRS 5623, 31062; Toulouse, France.

[saliba@chimie.ups-tlse.fr](mailto:saliba@chimie.ups-tlse.fr)

ZnO is a well known wide-gap semiconductor with a band-gap value of 3.37 eV displaying luminescent properties in the near UV and visible regions of the spectrum.<sup>1</sup> Such nanoparticles (NPs) are highly interesting in the manufacture of electronic and photonic devices.<sup>2,3</sup> Combining ZnO NPs and liquid crystals (LCs) may lead to new hybrids with unique properties and controlled organization.<sup>4,5</sup> To elaborate such materials two strategies can be envisaged; a) combining preformed ZnO NPs with a compatible LC and b) the *in-situ* growth of NPs inside the liquid crystalline host. We have developed both strategies using the thermotropic liquid crystal 4'-(6-aminohexyloxy) biphenyl-4-carbonitrile (6OCBNH<sub>2</sub>) as host and obtained new organic/inorganic organized materials. The general synthesis of ZnO NPs is being carried out *via* a straight forward organometallic method previously reported by our group.<sup>6</sup>

First strategy involved the mixing of a solution of OA-protected ZnO nanoparticles with a solution of 6OCBNH<sub>2</sub>. The ligand exchange was confirmed by <sup>1</sup>H-NMR and DOSY experiments. Dispersion of these NPs in 6OCBNH<sub>2</sub> did not disrupt the mesomorphic behaviour of the latter as proven by DSC and POM. The combination of ZnO NPs and 6OCBNH<sub>2</sub> in solution does not quench the optical properties of any of the components and we therefore obtain a hybrid material that exhibits interesting emission properties in the UV region of the spectrum.

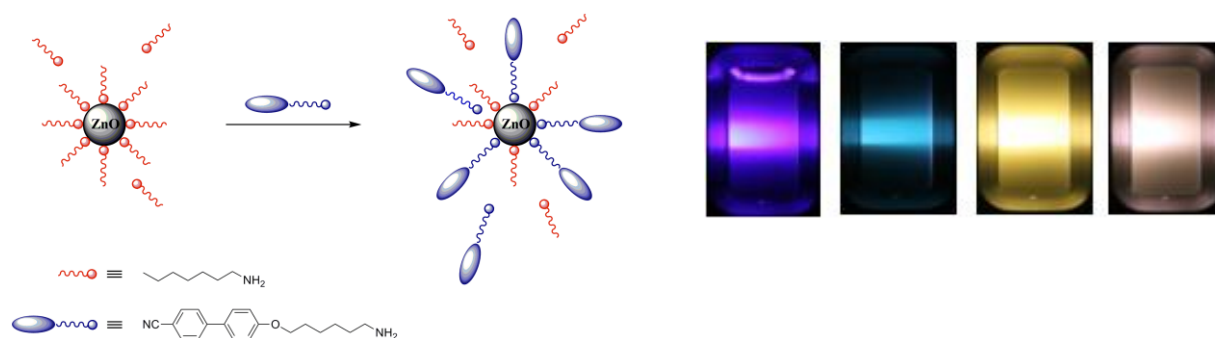
The second strategy was the direct synthesis of ZnO NPs in 6OCBNH<sub>2</sub>. This has resulted in the formation of well dispersed spherical nanoparticles of an average diameter of 5 nm. The formation of ZnO inside the LC host had no unfavourable effects on the luminescent properties of ZnO. Emissions corresponding to a variety of regions in the visible spectrum, depending on excitation wavelength, were observed. The *in-situ* growth of ZnO NPs in LC mixtures (6OCBNH<sub>2</sub>/5CB) is currently being investigated.

To our knowledge we have developed novel liquid crystal hybrid materials containing ZnO NPs. Besides their interesting optical properties, we have the possibility to control the organization of particles using the alignment properties of the LC.

## References:

- [1] Huang, M. H.; Mao, S.; Feick, H.; Yan, H. Q.; Wu, Y. Y.; Kind, H.; Weber, E.; Russo, R.; Yang, P. D. *Science*, **292** (2001), 1897-1899.
- [2] Rodriguez, J. A.; Jirsak, T.; Dvorak, J.; Sambasivan, S.; Fischer, D. *J. Phys. Chem. B.*, **104** (2000), 319-328.
- [3] Noack, V.; Weller, H.; Eychmuller, A. *J. Phys. Chem. B.*, **106** (2002), 8514-8523.
- [4] Kinkead B., Hegmann T., *J. Mater. Chem.*, **20** (2010), 448-458.
- [5] Cseh L., Mehl G. H., *J. Mater. Chem.*, **17** (2007), 311-315.
- [6] Monge, M.; Kahn, M. L.; Maisonnat, A.; Chaudret, B. *Angew. Chem.-Int. Edit.* **2003**, *42*, 5321-5324.

## Figures:



**Quantum dots in aqueous medium. Size, quantum efficiency and stability.**

S. Sánchez Paradinas, J. F. Boyero Benito, M. J. Almendral Parra, A. Alonso Mateos, J. J. Criado Talavera, Emilio Rodríguez Fernández.

*Department of Analytical Chemistry, Nutrition and Food Science. University of Salamanca.*

*Plaza de la Merced s/n., 37008 Salamanca, Spain. +34 923 29 44 83*

*e-mail: [ssparadinas@usal.es](mailto:ssparadinas@usal.es); [jfbb@usal.es](mailto:jfbb@usal.es), [almendral@usal.es](mailto:almendral@usal.es)*

Semiconductor nanocrystal quantum dots (QDs) have been explored as fluorescent biological labels due to their photostable, size-tunable, narrow bandwidth photoluminescence and chemically functionalizable surfaces.<sup>1</sup> The unique optical properties of QDs make them appealing as fluorophores in a variety of biological investigations, in which traditional fluorescent labels based on organic molecules fall short of providing long-term stability and simultaneous detection of multiple signals.<sup>2</sup> Currently, there are lots of essays trying to improve the methods of synthesis of QDs and it can be considered a powerful area that involves several fields of science.<sup>3</sup>

Organic solvent approach for these QDs synthesis is complex and harmful to the environment and the "as-prepared" QDs cannot be directly used in biological applications due to their hydrophobic character.

Our studies report an easy strategy to synthesize highly luminescent, water soluble and biocompatible CdS NCs by the reaction of Cd<sup>2+</sup> and S<sup>2-</sup> in the presence of mercaptoacetic acid (MAA) as capping agent (stabilizant), under normal pressure and atmospheric temperature (Fig. 1 y 2). We also systematically investigate the influence of various experimental variables, including the pH (Fig. 3 y 4) value, Cd-to-S ratio (Fig. 5) as well as Cd-to-MAA ratio, on the optical properties and the growth rate of CdS NCs. Through the temporal evolution of the UV-VIS absorption and PL emission spectra (Fig. 6) we have studied mean particle size and size distribution of CdS NCs (foto). This highly luminescent water-soluble QD can be expected to be very promising biological label.

There is quite a wide range of available methods of CdSe nanoparticles preparation but these techniques have many inherent limitations, such as the utilization of high toxic precursors, in particular organometallic cadmium and selenium compounds, high temperatures, high-energy irradiation, and others.

Our studies have been focused on the development of a synthesis of water-soluble CdSe quantum dots. Due to the difficulties of the reaction in organic medium, our method for the preparation of CdSe QDs consists in using CdCl<sub>2</sub> and Na<sub>2</sub>SeSO<sub>3</sub> as precursors (pH=4-5, Fig. 9) and mercaptoacetic acid (Fig. 10) as a stabilizing agent in aqueous medium (Fig. 6 y 8).

The Na<sub>2</sub>SeSO<sub>3</sub> has a very slow kinetic hydrolysis at 4°C. In these conditions the nanocrystals have a high quantum efficiency (IF~1000u with slits of 3 nm). The stability of the QDs is longer than 100 days (Fig. 11).

<sup>1</sup> J. O. Winter, N. Gomez, S. Gatzert. *Colloids and Surfaces A: Physicochem. Eng. Aspects* 254 (2005) 147-157.

<sup>2</sup> Igor L. Medintz, H. Tetsuo Uyeda, Ellen R. Goldman, Hedi Mattoussi. *Nature Materials* 4, 435 - 446 (2005)

<sup>3</sup> A. M. Smith, S. Nie. *The Analyst* 129 (2004) 672

## CdS QDs

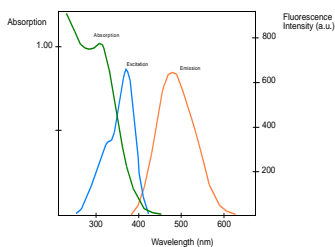


Fig. 1- Absorption, excitation and emission spectrum of CdS QDs



Fig. 3- Colour of the CdS QDs with different pH

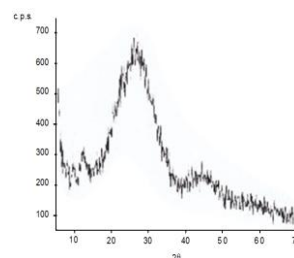


Fig. 2- X-Ray diffractogram of

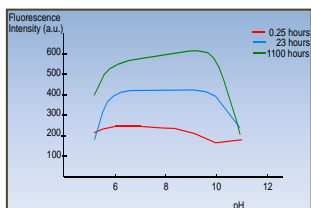


Fig. 3- Dependence of the PL emission intensity on the pH, at different times. Choice of the optimal pH for the synthesis

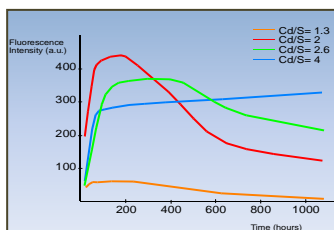


Fig. 4- The optimum conditions of quantum yield and stability are achieved for Cd-to-S ratios higher

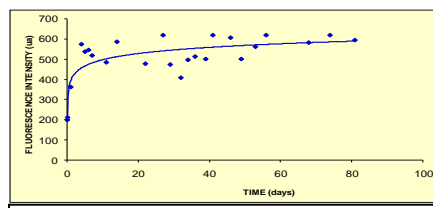


Fig. 5- Temporal evolution of CdS QDs

## CdSe QDs

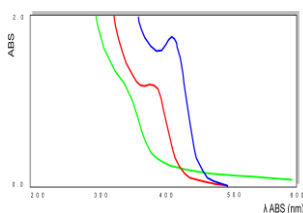


Fig. 6- Temporal evolution of CdSe QDs absorption spectrum

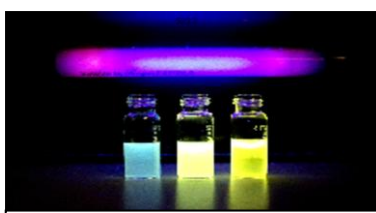


Fig. 7- Different colours of CdSe quantum dots with different amounts of Cd and Se

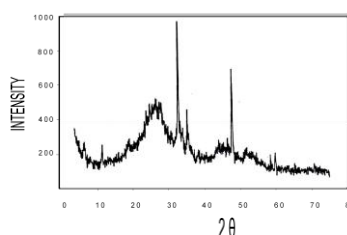


Fig. 8- X-Ray diffractogram of

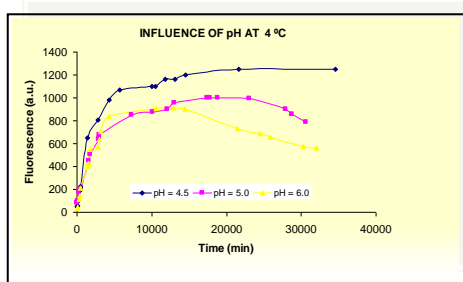


Fig. 9

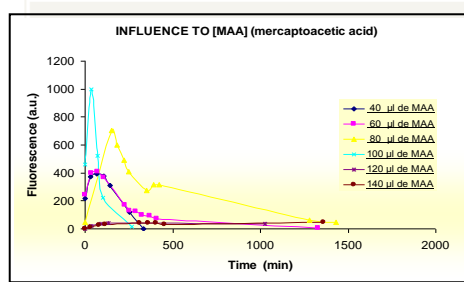


Fig. 10

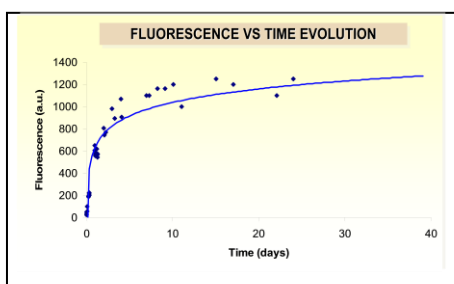


Fig. 11

## Non innocent oxoanions encapsulated in Ferritin for SPECT imaging

*Purificación Sánchez<sup>a</sup>, José M. Domínguez-Vera<sup>a</sup>, Natividad Gálvez<sup>a</sup>, Susana Trasobares<sup>b</sup>, Miguel López-Haro<sup>b</sup>, Jose J. Calvino<sup>b</sup>, Alberto Roger<sup>c</sup>, Henrik Braband<sup>c</sup>.*

<sup>a</sup>*Departamento de Química Inorgánica. Universidad de Granada, 18071 Granada, Spain,*

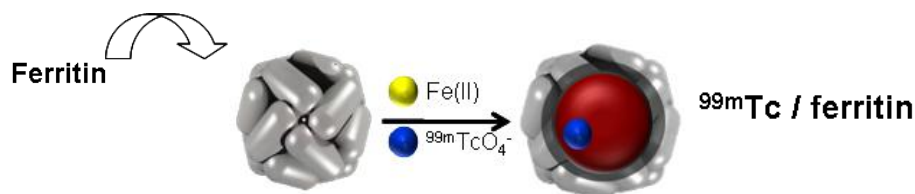
<sup>b</sup>*Departamento Ciencia de Materiales e Ingeniería Metalúrgica y Química Inorgánica, Universidad de Cádiz, Campus Río San Pedro, 11510 Cádiz, Spain,*

<sup>c</sup>*Fachbereich Chemie-Biochemie, Universität Zürich, Winterthurerstrasse 190, 8057 Zürich, Switzerland*

[mpsansan@ugr.es](mailto:mpsansan@ugr.es)

In the last years the preparation of nanostructured materials has attracted great interest. Considerable research efforts have been focused on the preparation of bifunctional metallic nanoparticles, it means particles having several different properties: magnetic, optical, electrical, radioactive or catalytical. This kind of particles has biomedical potential interest by itself and can be also used as precursors for the fabrication of technological devices, through controlled deposition following a bottom up approach.<sup>1</sup>

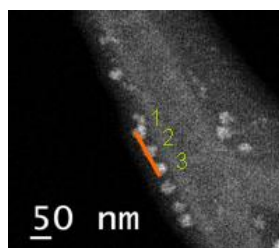
Experimental results concerning the synthesis of apoferritin-encapsulated particles containing the native ferrihydrite iron(III) mineral and different iron/oxo-anions, such as iron vanadate, iron phosphate, iron molybdate, iron arsenate or pertechnetate, and **HAADF-TEM, EELS**, characterization is presented. In the case, of the pertechnetate, the radionuclide encoded apoferritin nanoparticles can have a new potential to be used for diagnosis and radiotherapy treatment of tumor cells, and for radioimmunotherapy and radioimmunodetection of different cancers.



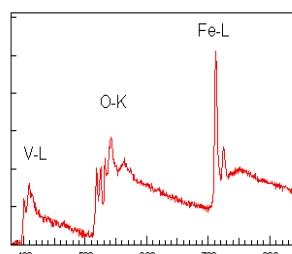
The <sup>99m</sup>Tc apoferritin encapsulation can be a useful tool to increase the therapeutic efficacy of a drug by increasing its circulation time, by decreasing its adverse side-effects and with appropriate functionalization by delivering it to regions of the body not normally accessible to the free drug. Ft/Tc nanoparticles supply a new modality for diagnosis (SPECT *Single Photon Emission Computed Tomography*). The coelution of Tc and protein was an indication that <sup>99m</sup>Tc was attached to apoferritin.

EELS, data of the vanadate/ferritin system show homogeneous particles with signals O (~532 eV), Fe (~708 eV) and V (~512 eV), and a relation Fe/V = 2.30.

This represents a new approach for the incorporation of anion radiotracers for therapy and diagnosis.



HAADF for three consecutive particles



EEL spectra in the energy loss region

**References:** [1] Jinhao Gao, Hongwei Gu and Bing Xu *Acc. Chem. Res.*, **2009**, *42* (8), pp 1097–1107

## Tunable in plane optical anisotropy of Ag nanostructures growth on columnar SiO<sub>2</sub> template thin films

Juan R. Sánchez-Valencia<sup>1\*</sup>, Johann Toudert<sup>1</sup>, Ana Borrás<sup>1</sup>, Carmen López-Santos<sup>1</sup>, Angel Barranco<sup>1</sup>, I. Ortega Feliu<sup>2</sup> and Agustín R. González-Elipé<sup>1</sup>

<sup>1</sup> Instituto de Ciencia de Materiales de Sevilla (CSIC-Univ. Sevilla), c/Américo Vespucio 49, 41092, Sevilla, Spain.

<sup>2</sup> Centro Nacional de Aceleradores, Universidad de Sevilla, Avenida Thomas A. Edison 7, 41092 Sevilla, Spain

\*corresponding author e-mail: jrsanchez@icmse.csic.es

### Abstract

Metal nanoparticles (MNPs) have been the focus of many studies during the last decades because of their applications in optical devices, as sensors and in SERS.[1] The control of the MNPs shape, size and organization supported in solid substrates is synthetic priority objective since these parameters control the spectral response of the material and its performance in a wide variety of applications.[2]. In fact, an active research has been carried out to grow 2D assemblies of elongated MNPs with a high aspect ratio and a parallel orientation (nanostripes) or parallel chains of MNPs with a strong optical anisotropy in the plane of the substrate (in-plane anisotropy) for the fabrication of dichroic filters, polarized light nanosources or materials showing high second-order non-linearities.[3-4] Among the different methods used to fabricate MNPs in a controlled way, the physical vapor deposition of metals onto substrates presenting a 1D periodic roughness has been reported to promote the growth of silver nanostripes or chains of silver nanoparticles oriented in the plane of the substrate.[5]

In this communication we present an easy and straightforward method for growing 2D assemblies of Ag nanostructures characterized by a tunable in-plane optical anisotropy. Ag NPs are deposited by DC sputtering in an Ar plasma at room temperature onto bundled nanocolumnar SiO<sub>2</sub> thin films grown by glancing angle physical vapor deposition (GAPVD). In contrast with previously reported processes involving the grazing angle deposition of the metal[6], DC sputtering is performed at normal incidence. The topology of the Ag deposit changes from isolated spherical Ag nanoparticles with isotropic optical properties to strongly dichroic Ag nanostripes oriented along the bundling direction of the SiO<sub>2</sub> nanocolumns. A simple model is proposed in order to explain the significant effect of the width and shape of the bundled SiO<sub>2</sub> nanocolumns tips on the metal local atom flux arriving to them and on the final structure of the metal/oxide composites. This model also evidences that one of the most important factors driving the formation of the Ag nanostripes is the shadowing effects during metal deposition.

### References:

- [1] J. Homola, S. S. Yee, G. Gauglitz, *Sensors and Actuators B: Chemical* **54**, (1999),3
- [2] U. Kreibig, V. M., Eds., *Optical properties of metal clusters*, (1999).
- [3] T. Kitahara, A. Sugawara, H. Sano, G. Mizutani, *J. Appl. Phys.* **95**, (2004),5002
- [4] R. M. Bakker, H. K. Yuan, Z. T. Liu, V. P. Drachev, A. V. Kildishev *et al.*, *Appl. Phys. Lett.* **92**, (2008)
- [5] S. Camelio, D. Babonneau, D. Lantiat, L. Simonot, F. Pailloux, *Phys. Rev. B* **80**, (2009)
- [6] M. Suzuki, Y. Taga, *J. Appl. Phys.* **71**, (1992),2848

## Figures:

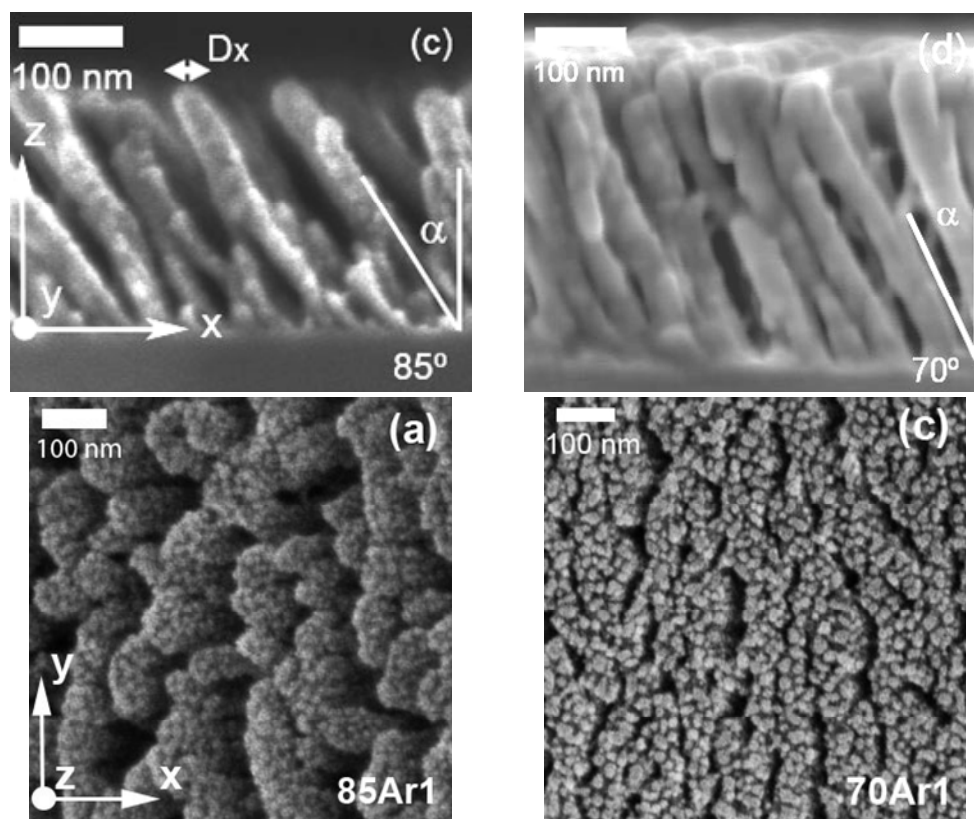


**Figure.** Top) Cross Sectional SEM micrographs of the SiO<sub>2</sub> columnar thin films grown at a 85° (left) and 70° (right) incidence angle.. Bottom) SEM plan-views micrographs of the SiO<sub>2</sub> surface after the deposition of silver for the thin films grown at a 85° (left) and 70° (right) incidence angle.

## Control of the aggregation state of Rhodamine 6G dye molecules adsorbed in porous columnar GAPVD thin films

Juan R. Sánchez-Valencia\*, Iwona Blaszczyk-Lezak, Juan P. Espinós, Agustín R. González-Elipe, and Angel Barranco

Instituto de Ciencia de Materiales de Sevilla (CSIC-Univ. Sevilla), c/Américo Vespucio 49, 41092, Sevilla, Spain.

\*corresponding author e-mail: jrsanchez@icmse.csic.es

### Abstract

Rhodamine 6G (Rh6G) is a well characterized fluorescent dye molecule widely used for a large variety of applications.[1] For the majority of them, the dye molecule has to be incorporated as guest into a solid host material. This feature has fostered the development of many new synthetic and processing methods[2-4]. The main interest of these composite materials relies on the high fluorescence emission of the dye molecule in the solid material. The luminescent emission is associated with the agglomeration state of the dye and can be modified by the interaction with the solid matrix. Thus, previous studies on the fluorescence behaviour of Rh6G molecules incorporated into host matrices show that they can appear in the form of isolated molecules or higher aggregates. Such aggregates are the so-called non fluorescent H dimer and the fluorescent J dimers. These different type of aggregates are characterized by well defined absorption/emission frequencies and fluorescence yields.[5]

In the present work, Rh6G dye molecules have been incorporated into transparent and porous thin films of different oxides prepared by evaporation at glancing angles (GAPVD).[6] Hybrid composite films were prepared by immersion of the thin film into a solution of the dye at a given pH. It is found that the amount of Rh6G molecules incorporated into the film is directly dependent on the pH of the solution and can be accounted for by a model based on the point of zero charge (PZC) concepts originally developed for colloidal oxides.[7] At low pHs, the dye molecules are incorporated in the film as monomers and dimers or higher aggregates are formed as the pH increases. Depending on the actual preparation and treatment conditions, they also exhibit high relative fluorescence efficiency. The thermal stability of the composite films has been also investigated by characterizing their optical behaviour after heating in an Ar atmosphere at increasing temperatures up to 275 °C. Heating induces a progressive loss of active dye molecules, a change in their agglomeration state and an increment in their relative fluorescence efficiency. The obtained luminescent hybrid composite thin films do not disperse the light and therefore can be used as optically active layers in optical structures or photonic devices.

### References:

- [1] P. D. Yang, G. Wirnsberger, H. C. Huang, S. R. Cordero, M. D. McGehee *et al.*, *Science* **287**, (2000),465
- [2] A. Barranco, P. Groening, *Langmuir* **22**, (2006),6719
- [3] J. Bujdak, N. Iyi, *The journal of physical chemistry. B* **109**, (2005),4608
- [4] F. del Monte, J. Mackenzie, D. Levy, *Langmuir* **16**, (2000),7377
- [5] V. Martinez, F. Arbeloa, J. Prieto, T. Lopez, I. Arbeloa, *The journal of physical chemistry. B* **108**, (2004),20030
- [6] K. Robbie, L. Friedrich, S. Dew, T. Smy, M. Brett, *Journal of vacuum science & technology. A. Vacuum, surfaces, and films* **13**, (1995),1032
- [7] J. R. Sanchez-Valencia, A. Borrás, A. Barranco, V. J. Rico, J. P. Espinos *et al.*, *Langmuir* **24**, (2008),9460

Figures:

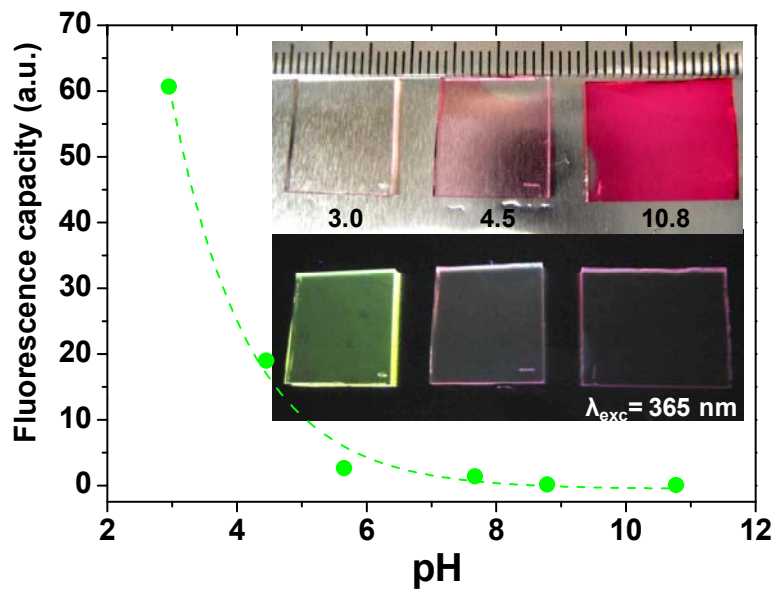


**Figure.** Representation of the fluorescence capacity as a function of the pH used for preparing the films. The inset shows images taken for actual films prepared at the indicated pHs that are being illuminated with an halogen lamp (top) and with a low energy fluorescent lamp ( $\lambda=365 \text{ nm}$ ) (bottom)

## Controlling the magnetization direction with hydrogen

*Benito Santos<sup>1</sup>, Arantzazu Mascaraque<sup>2</sup>, Andreas K. Schmid<sup>3</sup>, Juan de la Figuera<sup>1</sup>.*

*1. Instituto de Química-Física "Rocasolano", Madrid, Spain.*

*2. Universidad Complutense de Madrid, Madrid, Spain.*

*3. Lawrence Berkeley National Laboratory, Berkeley, CA, USA.*

[benitosantos001@gmail.com](mailto:benitosantos001@gmail.com)

The ability to control easy-axis of magnetization is an important topic. The magnetic anisotropy is due principally to competition of two interactions: the magnetic dipole contribution which favors an in-plane magnetization in thin films and the magneto-crystalline anisotropy. The latter, despite being usually smaller, is responsible for the modifications in the magnetic anisotropy. In some cases it can even turn the magnetization out of the plane of the films.

The experiments have been performed in a spin-polarized low-energy electron microscope (SPLEEM) with in-situ grown cobalt films. This technique allows to image the magnetization of surfaces and thin films with sub-micron resolution. The SPLEEM consists of a spin-polarized electron source as illumination source of a low-energy electron microscope. For a given electron spin direction, real-space images of the reflected electrons at low electron energies are acquired. Subtracting images taken with opposite spin-polarization, removes topographic features from the images providing pure magnetic contrast images of the magnetization component in the electron spin direction selected.

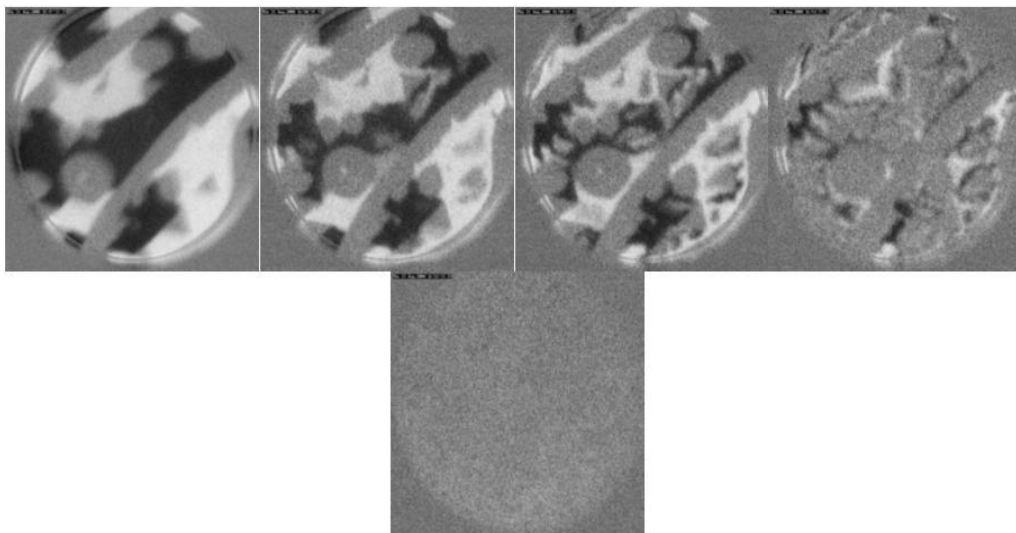
The growth of the cobalt thin layers on Ru(0001) is layer-by-layer up to 10 ML[1]. Films thicker than the first monolayer are relaxed to the Co bulk lattice spacing. The first Co layer shows an in-plane easy-axis of magnetization. On the other hand, the second Co layer presents an out-of-plane magnetization. More than 3 ML of Co on Ru(0001) shows again an in-plane magnetization. This consecutive spin reorientation transition has been attributed to a combination of strain and surface effects. Capping the Co layer with non-magnetic metals like Pd, produces additional spin reorientation transitions[2].

In this work we report the change observed in the magnetic anisotropy of the cobalt bilayer upon hydrogen adsorption. When molecular hydrogen is introduced in the chamber, a gradual change in the domains pattern can be observed. Domains start to breakup into smaller ones. As more hydrogen is dosed, the out-of-plane magnetization starts to disappear. When the hydrogen dose is around 0.4 L the out-of-plane magnetic signal vanished. Heating the films to 400 K, presumably desorbing the hydrogen from the surface, restores the magnetization out-of-the plane. To determine the cause of the spin reorientation, low energy electron diffraction intensity vs energy (LEED-IV) and low energy electron reflectivity data were taken. No structural changes were detected within the accuracy of these techniques. The results obtained so far suggest that hydrogen adsorption changes the magnetic anisotropy purely through an electronic effect, without significant changes in the strain of the films.

**References:**

- [1] El Gabaly F, Puerta JM, Klein C, Saa A, Schmid AK, McCarty KF, Cerda JI and de la Figuera J 2007 Structure and morphology of ultrathin Co/Ru(0001) films *New J Phys* 9 80
- [2] El Gabaly F, McCarty KF, Schmid AK, de la Figuera J, Muñoz MC, Szunyogh L, Weinberger P and Gallego S 2008 Noble metal capping effects on the spin-reorientation transitions of Co/Ru(0001) *New J Phys* 10 073024

**Figures:**



## **Mesoporous silica based materials and osteoprogenitor cells for bone tissue engineering**

Santos-Ruiz L<sup>1,3</sup>, Amat D<sup>1,3</sup>, Díaz-Cuenca A<sup>2</sup>, Becerra J<sup>3</sup>

1. CIBER-BBN; Dep. B. Celular, Genética y Fisiología; Fac. Ciencias; Campus de Teatinos; Málaga; Spain. [lsantos@uma.es](mailto:lsantos@uma.es)
2. Instituto de Ciencia de Materiales de Sevilla-CSIC: Americo Vespucio 49; Sevilla; Spain
3. Universidad de Málaga; Dep. B. Celular, Genética y Fisiología; Fac. Ciencias; Campus de Teatinos; Malaga; Spain

Biomaterials can help bone repair by serving as delivery systems for drug administration, or by providing a substrate where cells can be seeded to fabricate an engineered tissue. Materials in the ternary system SiO<sub>2</sub>-CaO-P<sub>2</sub>O<sub>5</sub> have demonstrated an excellent bioactivity. The present work explores the possible application of silica-based mesoporous materials to tissue engineering by evaluating the in vitro interaction of these materials with several cell types.

The biocompatibility of SBA-15 and HA-SBA-15 materials was evaluated in vitro using organ explant culture, standard 2D cell culture, and micromass (3D) cell culture. Rodent and human osteoblasts and adult MSC (mesenchymal stem cells) were used for these assays.

Mouse calvarium explants and 2D cultures of rat and human MSC proliferated normally in the presence of up to 100 ug/mL SBA-15 or HA-SBA-15. Spontaneous attachment of cells to the materials was observed. Micromass culture showed that rat and human MSC can be grown in three dimensions when cells use SBA-15 or HA-SBA-15 materials as scaffolds.

**CONCLUSIONS:** SBA-15 and HA-SBA-15 materials are biocompatible in vitro, and sustain MSC adhesion and proliferation, providing a suitable scaffold for three-dimensional culture. These data support further experimentation for adapting them to tissue engineering.

**Saturation, spectroscopy and time correlated studies of single-walled carbon nanotubes**

*S. M. Santos, J. Shaver, L. Cagnet, Ph. Tamarat, B. Lounis*  
CPMOH- Université Bordeaux 1, 351 cours de la libération 33405, Talence, France  
[s.santos@cpmoh.u-bordeaux1.fr](mailto:s.santos@cpmoh.u-bordeaux1.fr)

Singled-Walled Carbon Nanotubes (SWNTs) are a 1D model system that can be used to study exciton photophysics. High binding energies suggest that excitonic effects may dominate all aspects of the optical properties of carbon nanotubes [1]. Theoretical calculations predict 4 singlet states, one of which can radiatively recombine with the ground state (a bright state). Although progress has been made in the study of the excitonic states in SWNTs, there is still much to investigate. In particular, the dynamics and decay of various excitonic states (between dark and bright states) is still unclear as well as the environmental effects on the band edge structure [2].

We investigate individual SWNT optical properties through continuous wave and time resolved micro-photoluminescence (PL). This technique avoids complications due to inhomogeneous broadening in ensemble measurements. Our CW experiments focus on power dependence and saturation behavior of the lowest energy bright exciton state (Fig. 1). This is explained by multi-excitonic effects, namely Auger recombination and exciton-exciton annihilation [3]. Interestingly, at high excitation intensities, side-band peaks are observed (Fig.1. This side-band has been associated with a exciton-phonon coupling to a higher energy, finite angular momentum dark-state [4,5]. Our time resolved experiments were performed as a function of temperature and give insight to bright-dark state coupling at low temperatures. We observe a bi-exponential behavior with temperature dependant decay rates (Fig. 2) .

In summary, we have used different approaches to obtain information on the exciton dynamics in a 1D system through the optical properties of SWNTs.

**References:**

- [1] G. Dukovic *et al*, Nano Lett., **5** (2005), 2314-2318
- [2] M. S. Dresselhaus *et al*, Annu. Rev. Phys. Chem., **58** (2007) 719-747.
- [3] Heinz T.F. *et al*, Ultrafast Phenomena XV, **88** (2007), 683-685
- [4] Y. Murakami *et al*, Phy Rev B, **79** (2009), 195407
- [5] O.N. Torrens *et al*, Phys. Rev. Lett., **101** (2008), 157401

Figures:

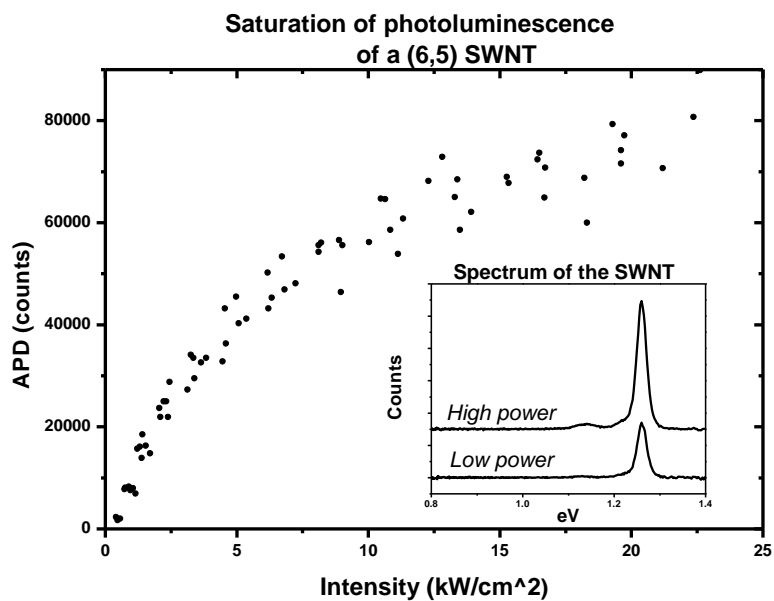


Fig 1: Saturation curve and spectrum of a SWNT

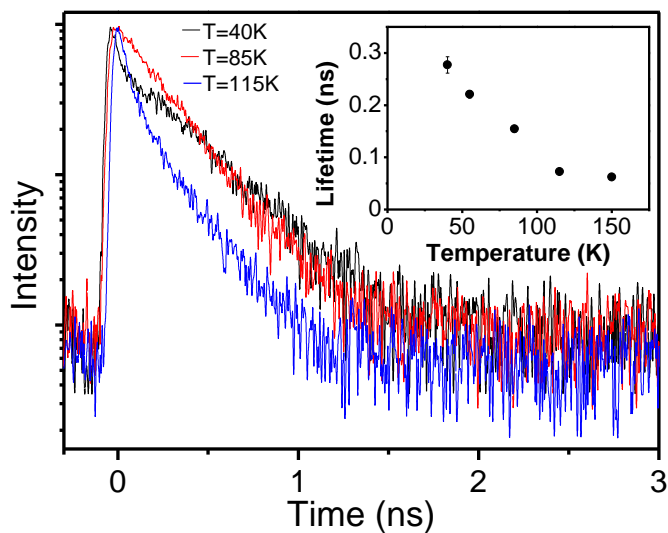


Fig.2: Normalized decay curves at different temperatures

**Time-evolution of the screening charge around a suddenly created point charge at a metal surface**

*V. M. Silkin,<sup>1,2,3</sup> A. K. Kazansky,<sup>2</sup> P. M. Echenique,<sup>1,2</sup> E. V. Chulkov<sup>1,2</sup>*

<sup>1</sup>*Depto. de Física de Materiales, Facultad de Química, Universidad del País Vasco, Apdo. 1072, 20080 San Sebastian, Basque Country, Spain*

<sup>2</sup>*Donostia International Physics Center (DIPC), P. de Manuel Lardizabal 4, 20018 San Sebastián, Basque Country, Spain*

<sup>3</sup>*IKERBASQUE, Basque Foundation for Science, 48011, Bilbao, Spain*

[waxslavs@sc.ehu.es](mailto:waxslavs@sc.ehu.es)

The space-time evolution of the dynamical screening charge density caused by a suddenly created point charge at the Cu(111) surface is investigated in the linear response approximation. Considering a finite-thickness slab as a model for the Cu(111) surface we investigate the confinement effects on dynamical screening as well. The results have been obtained on base of self-consistent evaluation of the energy-momentum dependent response function taking into account the realistic surface band structure of Cu(111).

At the initial stage, we observe fast long range charge density oscillations due to excitation of the surface plasmon modes. Then we observe the propagation of the shock wave of the electron-hole excitations along the slab with velocity determined by the Fermi velocity of bulk Cu. At longer times, we have identified the propagation along the two slab surfaces of much slower (with velocity  $\sim 0.3$  a.u., close to the Fermi velocity of the Cu(111) surface state) charge disturbance due to acoustic surface plasmon. A role of the energy band gap in the direction perpendicular to the surface on the establishing of the screening is also addressed.

## Carbon Nanotube Electron Windmills

M.Sledzinska, A. Barreiro, A.Bachtold  
CIN2, Campus UAB, 08193 Bellaterra

The miniaturization trend affects mechanical devices, which results in the transition from MEMS (microelectromechanical systems) to NEMS (nanoelectromechanical systems). This has motivated the researchers to look for new materials, which are suitable for these nanodevices. Due to their properties, such as favourable elastic modulus and tensile strength, high electric and thermal conductivity and low inter-shell friction, multi-wall carbon nanotubes may play an important role in constructing those systems.

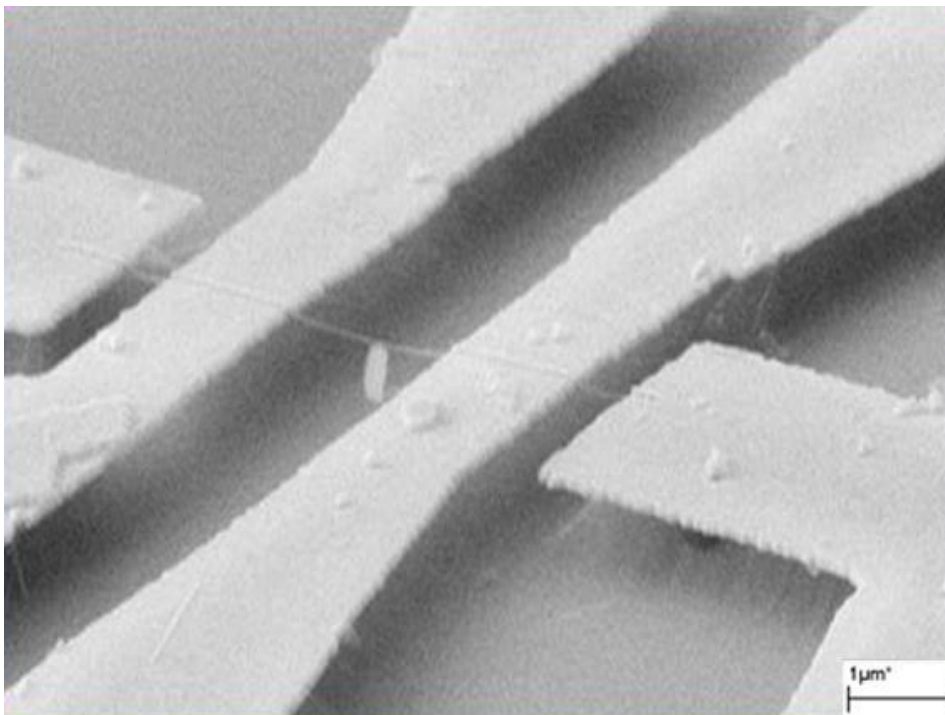
As for now the reported drive mechanisms for nanotube rotors and actuators were based on electric field and thermal gradient. Bailey, Amanatidis, and Lambert have proposed a new mechanism to drive a nanotube rotor, which is based upon the torque generated by a flux of electrons passing through a chiral tube [1].

We will present our progress in the fabrication of these nanotube windmills. Devices consist of a suspended multi-wall nanotube, contacted to two gold electrodes. A few outer shells are removed in between the electrodes, leaving the inner tube free to rotate. When passing a current through the devices electrons are forced to tunnel from the outer onto the inner shells. Due to angular momentum conservation, a tangential force is produced that causes the inner tube to rotate.

### References:

- [1] S.W.D. Bailey, I. Amanatidis, C.J. Lambert, PRL, **100**, 256802 (2008)

### Figures:



## **Multifunctional nanomechanical systems for multiplexed highly selective and sensitive biological detection**

*Javier Tamayo<sup>1</sup>, Priscila M. Kosaka<sup>1</sup>, Johann Mertens<sup>1</sup>, Oscar Ahumada<sup>2</sup>, Hien-Duy Tong<sup>3</sup>,  
Montserrat Calleja<sup>1</sup>*

*<sup>1</sup>Bionanomechanics Lab-Instituto de Microelectrónica de Madrid- CSIC, Isaac Newton 8  
(PTM), Tres Cantos 28760, Madrid, Spain*

*<sup>2</sup>Mecwins S.L., Santiago Grisolia , Tres Cantos 28760, Madrid , Spain*

*<sup>4</sup>Nanosens, Berkelkade 11, NL 7201 JE Zutphen, The Netherlands*

[jtamayo@imm.cnm.csic.es](mailto:jtamayo@imm.cnm.csic.es)

Prediction of risk factors and early diagnosis of disease are the best means to preserve health and to avoid costly and inefficient medical interventions after symptoms and disease have developed. Current platforms for analysis require large amount of sample, have many sample pre-treatment steps prone to human error, are relatively slow, suffer of low sensitivity for the detection of multiple malignancies, and often provide false positives and negatives. In addition, these instruments are bulky equipment that is frequently not available to clinics or point of care diagnosis. The goal of discovering new devices and new transduction concepts for biological detection remains of paramount importance. Nanotechnology based approaches are promising candidates for providing portable and low cost nanosensor devices, capable of analyzing tiny amounts of sample, and specifically disease markers from patients. Also, the advancement of new approaches that provide the needed robustness and reproducibility of the response, as well as a high degree of multiplexing, is needed. MEMS/NEMS devices are good candidates to attain this goal, but this approach needs the further development of advanced instrumentation which demands combined expertise in fabrication, design, engineering and modelling. We have found that a private – public partnership is especially suitable to attain the cited purposes. In this work, two spin-off companies Mecwins S.L. and Nanosens GmbH have collaborated with our group to develop an instrument with the capability for highly multiplexed detection (up to 128 sensors in parallel already demonstrated) together with an accurate control of the gas environment[1] and a biochip comprising 128 cantilevers in groups of 8 cantilevers for differential measurements.

The developed nanomechanical systems and transduction schemes and techniques have been tested and applied to solve problems in the field of biomedicine but also in other areas such as polymer science. The largest potential is in the detection of the hybridization of nucleic acids for early disease detection, including the early detection of cancer based on downregulation or overexpression of genes. Also, the detection of harmful pathogens by nanomechanical systems is in need of a cost-effective and rapid technique, as the one described here, for detecting pathogens in the early stages to avoid epidemics. The advantage of immunosensors based on nanomechanical sensors over traditional diagnosis systems such as Enzyme-Linked Immunosorbent Assay (ELISA) is that intact bacteria or viruses can be detected without need of secondary markers. More interestingly, nanomechanical sensors proposed provide unprecedented levels of sensitivity and specificity as we demonstrate in this work[1,2].

## References:

- [1] Mertens, J., Rogero, C., Calleja, M., Ramos, D., Martín-Gago, J.A., Briones, C. & Tamayo, J., *Nature Nanotechnology* **3** (2008) 301.  
 [2] D. Ramos, M. Arroyo-Hernandez, E. Gil Santos, H. Duy Tong, C. van Rijn, M. Calleja, J. Tamayo, *Analytical Chemistry* **81** (2009) 2274

## Figures:

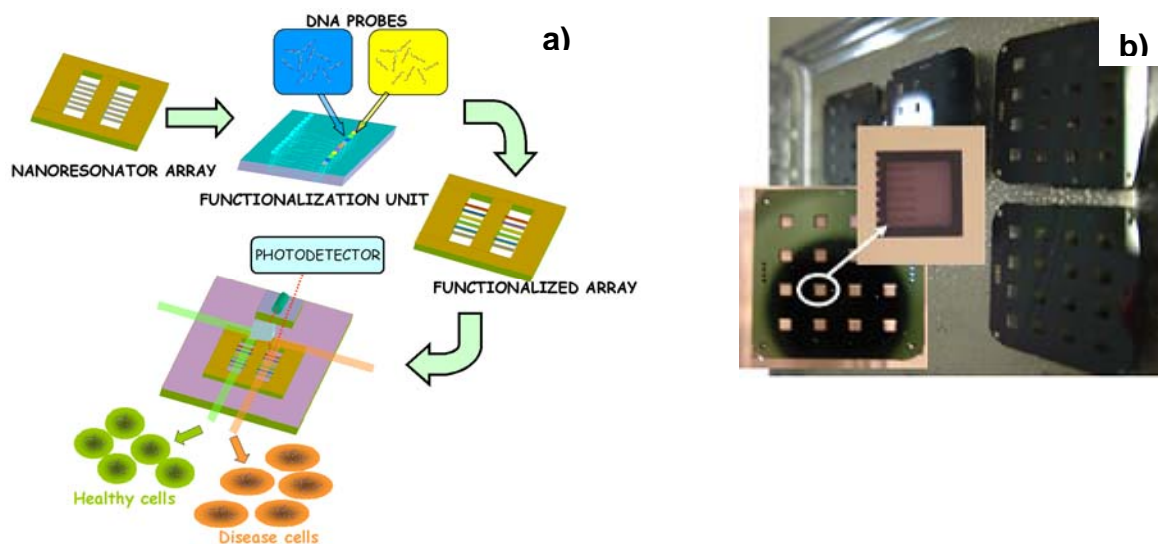


**Figure 1.** a) Conceptual drawing of the Mecwins chips and platform. The fabricated array consists of several separated rows of cantilevers. Each row of cantilevers is sensitized with the same combination of DNA probes by means of a microfluidics or microinjection techniques. The sensitised array is then inserted in the readout instrument composed of a scanning optical system for measuring the resonant frequency and mechanical deformations of each cantilever. 128 cantilevers have been detected simultaneously. In a possible application, the gene expressed content of disease and healthy cells is flowed over each row of cantilevers for comparison of the gene expression pattern and determination of genes responsible of disease. A picture of the actual chips manufactured by Nanosens is also shown in b).

**Gold nanoparticle-sod enzyme conjugates for therapeutic applications**

*Edurne Teiletxea Malda<sup>1</sup>, Luis Olangua<sup>1</sup>, Aaron C. Asensio<sup>2</sup>, Gurutze Arzamendi<sup>3</sup>, Luis M. Gandía<sup>3</sup>, Jose F. Moran<sup>2</sup>*

*<sup>1</sup>FideNa, Centro I+D en Electrónica y Comunicaciones Jerónimo de Ayanz, C/Tajonar s/n, 31006 Pamplona, Navarra, Spain*

*<sup>2</sup>Instituto de Agrobiotecnología, Universidad Pública de Navarra-CSIC-Gobierno de Navarra, Campus de Arrosadia s/n, 31006, Pamplona, Navarra, Spain*

*<sup>3</sup>Departamento de Química Aplicada, Universidad Pública de Navarra, Campus de Arrosadia s/n, 31006, Pamplona, Navarra, Spain  
[edurne.teiletxea@fiden.es](mailto:edurne.teiletxea@fiden.es)*

Design and development of devices based on enzyme immobilization onto gold nanoparticles is of great current interest in the field of bio-nanotechnology, mainly due to its potential applications in the fields of biosensors, disease diagnosis, and catalysis [1].

Gold nanoparticles (GNPs) are of specific importance due to their size-dependent catalytic, electrical and optical properties [2]. Thus, the very high surface-to-volume ratio leads to dramatic changes in their properties [3]. All nanoparticles syntheses involve the use of a size stabilizing agent, which associates with the surface of the particle providing charge, biocompatibility or solubility properties to keep the nanoparticles suspended, and thereby preventing their aggregation [4]. The physical properties strongly depend on the particle size, shape, interparticle distance and nature of the protecting organic shell [5].

Superoxide dismutase (SOD) is a metallo-enzyme that catalyzes the dismutation of superoxide radicals into hydrogen peroxide and oxygen [6]. Reactive oxygen species, such as superoxide radicals, are thought to underlie the pathogenesis of several diseases, such as familial amyotrophic lateral sclerosis, Parkinson's disease, Alzheimer's disease, Down's syndrome, cataract, cardiac myocytes and several neurological disorders. SOD enzymes have great physiological significance and therapeutic potential in the prevention of the oxidative damage from superoxide radicals [7].

In this work we describe the synthesis of gold nanoparticles, the production and purification of recombinant protein FeSOD, and the immobilization of the purified enzymes on the gold nanoparticles.

Monodispersed GNPs with an average diameter of 20 nm were synthesized by a wet reduction method. An aqueous solution of the gold precursor hydrogen tetrachloroauric acid (HAuCl<sub>4</sub>) was boiled during 1 h under vigorous stirring. Reductant solution, containing trisodium citrate and the stabilizer tannic acid was quickly added to the boiling solution of HAuCl<sub>4</sub> and heating is maintained for 15 min. Then the colloidal suspension of GNPs was cooled to room temperature, centrifuged and filtered [8]. The resulting nanoparticles were spherical and very uniform, with a narrow size distribution. The size distributions of the particles in the colloids were measured by Dynamic Light Scattering (DLS) and their shape was observed by Field-Emission Scanning Electron Microscopy (FE-SEM).

Recombinant FeSOD from cowpea (*Vigna unguiculata*) was over-expressed in *Escherichia coli* using self-induction system [9] [10]. Self-induction of the bacteria may take between 16-24 h with optimal results, after which period cells are harvest by centrifugation and either used or stored at  $-80^{\circ}\text{C}$ . FeSOD is over-expressed using plasmid pET28a(+), and the gene has been cloned at the *NdeI* site of this vector, which implies the synthesis of the protein with a 6(Hys)-tag [6]. Up to 50 mg of protein can be affinity purified from 1L of bacteria culture in a single chromatography step with a 5 mL NTA-Ni column (Amersham-Pharmacia).

GNPs were incubated at pH 7.5 and at room temperature with the lowest amount of SOD enzyme that maintain stable the GNPs. The excess of protein was eliminated by centrifugation, followed by washing in phosphate saline buffer [11]. Once the GNPs-protein conjugate was achieved, the GNP-enzyme conjugates were characterized in more detail using DLS. The difference between the bare GNPs and conjugate GNPs corresponded to a monolayer of adsorbed FeSOD. Secondly, the absorption spectral measurements have showed that the peak attributed to the Surface Plasmon Band of GNPs shifted to higher wavelengths corresponding to the adsorption of protein. And finally, gel electrophoreses has been used to confirm the conjugation of GNPs-FeSOD. The mobility of the conjugate differs from both the free protein and free GNP; the conjugates became more mobile in the electric field than the GNP itself. Those data indicated that superoxide dismutase protein binds to gold colloids nanoparticles.

### Acknowledgements

We gratefully acknowledge FideNa for its financial support under R&D contract to the Public University of Navarra OTRI 2008 807 022.

### References:

- [1] M-E Aubin-Tam and K Hamad-Schifferli, *Biomed Mater*, **3** (2008) 034001.
- [2] S. Chen, A.C. Templeton, R. W. Murray, *Langmuir* **16** (2000) 3543.
- [3] Angshurman Pal, Sunil Shah, Surekha Devi, *Colloids and Surfaces A: Physicochem. Eng. Aspects*, **302** (2007) 51.
- [4] Daizy Philip, *Spectrochimica Acta Part A*, **71** (2008) 80. [5] Brust, M., Kiely, C.J. *Colloids surf. A. Physicochem. Eng. Asp*, **202** (2002) 17.
- [6] Halliwell B, Gutteridge JMC, *Free radicals in biology and medicine*. 4rd edition. Oxford University Press. Oxford (2007)
- [7] Noor et al., *Medical Science Monitor* **8** (2002), RA210
- [8] Jianhui Liao, Ning Gu, *Colloids and Surfaces A : Physicochem. Eng. Aspects* **223** (2003) 177.
- [9] Studier, F. W, *Protein Expression and Purification*, **41**(2005), 207.
- [10] Urarte E, Auzmendi I, Rol S, Ariz I, Aparicio-Tejo PM, Arredondo-Peter R, Moran JF *Methods in Enzymology* **436** (2008), 411.
- [11] D Pissuwan, CH Cortie, SM Valenzuela, MB Cortie, *Gold Bulletin* **40/2** (2007), 121.

## Depth Profiling Analysis of Metallic Nanolayers on Polymer Films for Microelectronics Applications by Secondary Ion Mass Spectrometry

*Helena Téllez, José M. Vadillo, J. Javier Laserna*

*University of Málaga, Department of Analytical Chemistry, 29071, Málaga, Spain*

[htellez@uma.es](mailto:htellez@uma.es); [laserna@uma.es](mailto:laserna@uma.es)

The characterization of solids, surfaces and thin films has represented a great challenge in many fields and it has been faced by several disciplines, such as Material Science, Solid State Physics or Analytical Chemistry, among others. Furthermore, most of the developments achieved in nanotechnology have been inevitably linked to the availability of characterization techniques allowing a deep knowledge of the chemical composition, morphology and interfacial chemistry of multilayered samples in the sub-micron scale. In this context, secondary ion mass spectrometry (SIMS) has been consolidated as one of the most powerful techniques due to its outstanding capabilities in terms of sensitivity, specificity and spatial resolution, both lateral and in-depth resolutions.

The in-depth analysis of nanometric metallic layers deposited over thin polymeric films by secondary ion mass spectrometry (SIMS) is presented in this work. These metallized polymer films are used in the capacitor industry, offering a great number of advantages over other types of film capacitors, such as paper-foil or plastic films, mainly derived from their customized size and improved technical performance. The capacitors are made of a thin polymer film acting as the dielectric material, typically biaxially oriented polypropylene films (BO-PP) or polyethylene terephthalate (PET), with thicknesses ranging between 5 and 15  $\mu\text{m}$ . These polymer films are metallized by physical vapour deposition (PVD) with nanometric metallic layers composed of pure Al, pure Zn or a dual- metallization Zn/Al. The thickness of the metallic layer ranges between 5 to 100 nm. The metallized film capacitors are susceptible to modifications in the metal/polymer interface structure and composition which may strongly decrease their functionality [1].

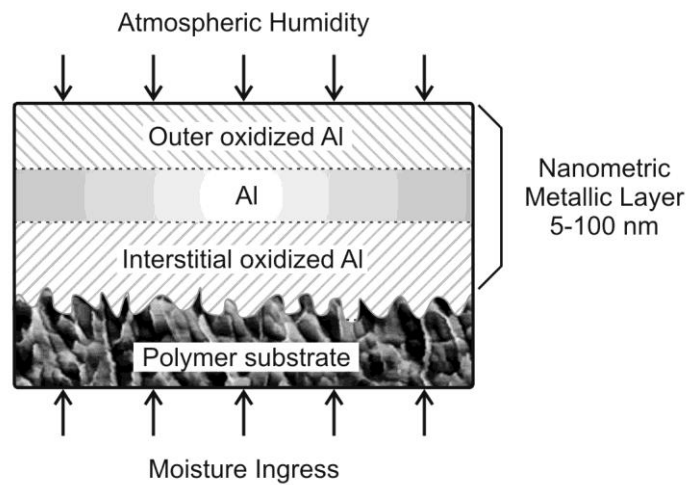
Dynamic SIMS (d-SIMS) depth profiling provides layer-by-layer analysis of the metallized film with subnanometric resolution and complete atomic/molecular information generated by the analysis of the fragments emitted during the sputtering process. Furthermore, the secondary ion yield is very sensitive to modifications in the oxidation state of the elements present in the specimen, representing an excellent alternative to monitor possible oxidation processes along the multimaterial structure. However, several experimental considerations must be taken into account due to the presence of isobaric interferences coming from the different matrices ( $^{27}\text{Al}^+ / ^{43}\text{AlO}^+$  from the metallized layer and  $^{27}\text{C}_2\text{H}_3^+ / ^{43}\text{C}_3\text{H}_7^+$  from the polymer film) and the different electrical behaviour of the involved layers. The development of an energy-resolved depth profiling method has allowed the discrimination of these isobaric species according to the different kinetic energy distribution of the secondary ions from the involved matrixes [2].

SIMS has provided important results about the origin of the morphological and chemical degradation of metallized polymer films, relating the surface and interstitial chemistry modifications with severe failures in the capacitors performance. Although the polymer film is a hydrophobic material, it exhibits significant permeability to moisture and oxygen, allowing the oxidation from both sides of the vapour-deposited metallic layer. The presence of the diverse oxidized species related to the main constituents of the metallization layer has been identified in degraded samples. The in-depth analysis of these altered regions shows high contents of oxides and hydroxyl species ( $\text{AlO}^+$  and  $\text{AlOH}^+$ ). The presence of interstitial moisture and demetallization processes have been also related to the capacitance losses during capacitor testing and service life [3,4].

**References:**

- [1] Brown R. W. IEEE T. Device Mat. Re. **6** (2006) 326.
- [2] Téllez H., Vadillo J. M., Laserna J. J., Rapid Commun. Mass Spectrom, **23** (2009) 2357.
- [3] Téllez H., Vadillo J. M., Laserna J. J., Rapid Commun. Mass Spectrom. **24** (2010) 463.
- [4] Téllez H., Vadillo J. M., Laserna J. J., J. Anal. At. Spectrom. DOI: 10.1039/b922705a.

**Figures:**



## Quantifying many-particle Coulomb correlation through the super-poissonian noise of electron current in resonant structures

*F. L. Traversa<sup>1</sup>, E. Buccafurri<sup>2</sup>, X. Oriols<sup>1</sup>*

*1 Departament d'Enginyeria Electrònica, Universitat Autònoma de Barcelona 08193 Bellaterra SPAIN*

*2 INL-INSA-Lyon, 7 av. Jean Capelle, 69621 Lyon, Villeurbanne Cedex, France*

[fabiolorenzo.traversa@uab.es](mailto:fabiolorenzo.traversa@uab.es)

Electron transport in mesoscopic systems has been understood mainly from a single-particle description. In principle interacting many-electron systems are well assessed through many-body Schrödinger equation, but its solution is a very hard problem even in the case of few electrons correlated by coulomb interaction. In any case the quantum many-body effects can impact dramatically macroscopic measurement. The first emergency was in 1911 when K. Onnes astonished the word by discovering the super-conductivity. Since then, numerous techniques have been developed to simulate quantum correlations, and many models have been sought for to explain the transport properties of many-body systems.

Here we focus on how the many-body Coulomb interaction might affect noise in resonant structures. Specifically, the correlation between an electron trapped in the resonant state during a dwell time  $\tau_d$  and the ones remaining in the cathode has been investigated. The reason why this correlation occurs is because of the potential energy perturbation on the other electrons due to the trapped electron. As an example of resonant structure, we considered a double barrier resonant tunneling diode (RTD) [1], [2]. As depicted in figure 1, an electron tunneling into the well from the cathode raises the potential energy of the well by an amount of  $e/C_{eq}$ , where  $e$  is the electron charge and  $C_{eq}$  the structure capacitance. As a consequence, the density of state in the well is shifted upwards by the same amount. This can affect the noise in two different ways: if the resonant energy is over the conduction band edge of the cathode, the raised density of state is accessible to electrons staying in the tail of the cathode occupation factor. Therefore the majority of the electrons in the cathode results blocked approximately for a dwell time  $\tau_d$ . This suppresses the randomization of the injection and consequently augments the sub-poissonian noise already present in the limit of partition noise only [2]. Conversely if the resonant energy is under the conduction band edge of the cathode, the raised density of state is accessible to electrons staying near the maximum of the cathode occupation factor. Therefore the majority of the electrons in the cathode can tunnel in the well. Thus the Coulomb interaction tries to regroup the electrons providing an enhancement of the randomization of the injection and consequently gives a super-poissonian noise.

To quantitatively analyze this pure quantum many-body effect we employed two different approaches. The first is based on an algorithm recently developed by Oriols [3]. This provides a way to compute many-particle trajectories within the Bohm's picture, from single-particle time dependent Schrödinger equation with time dependent potential energy that account for correlations. By means of this powerful algorithm, and the generalization of Ramo-Shockley theorem to compute the current [4], and the very inclusion of Coulomb interaction in the many-particle Hamiltonian beyond the mean field [5], we were able to correctly simulate the current and noise in the RTD.

The second approach is based on a completely analytical model of the RTD proposed in [6]. This model was improved by including scattering [7] in a consistent way with the Breit-Wigner formulation [8]. Accordingly with the formalism proposed in [9] based on sequential tunneling and accounting for the coulomb interaction within a Hartree approximation, we were able to derive a general formula for the Fano factor

$$\gamma = 1 - 2 \frac{(\Lambda_Q - \Lambda_C + \Gamma' - \Gamma_R)(\Lambda_Q + \Gamma_R)}{(\Lambda_Q + \Gamma')^2} \quad (1)$$

where  $\Lambda_Q$  and  $\Lambda_C$  are the quantum and Coulomb interaction energies respectively and read as a generalization of the interaction energy proposed in [2].  $\Gamma'$  is the reduced total width of the resonant level and  $\Gamma_R$  the width associated to the right barrier.

As shown in figure 2 the analytical model of DC current is in excellent agreement with the quantum Monte Carlo simulation and the Fano factor reproduces correctly the sub-poissonian and super-poissonian noise regime [1], [2]. Comparing both approaches, due to the excellent agreement, it is shown that the analytical one is capable to perfectly catch and quantify quantum many-particle effects that emerge in the super-poissonian noise regime. Furthermore the variation of the pick height, compared with that of other relevant relative quantities (see figure 3), is in general one or more orders of magnitude larger. It makes this feature extremely important in order to extract parameters from measurement carrying many-body information.

In conclusion we analyzed quantum many-body interaction in the transport and noise of resonant structures by means of two different approaches: quantum Monte Carlo simulation and an analytical model. This result has two merits. On the one hand it shows that the analytical approach is able to capture relevant many-particle information (such many-particle density of states) not easily accessible from other DC transport. On the other hand it furnishes a way to predict quantitatively these effects and is useful for the design of resonant structure.

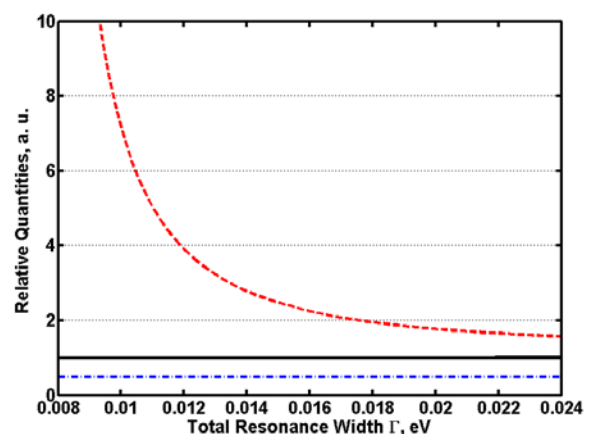
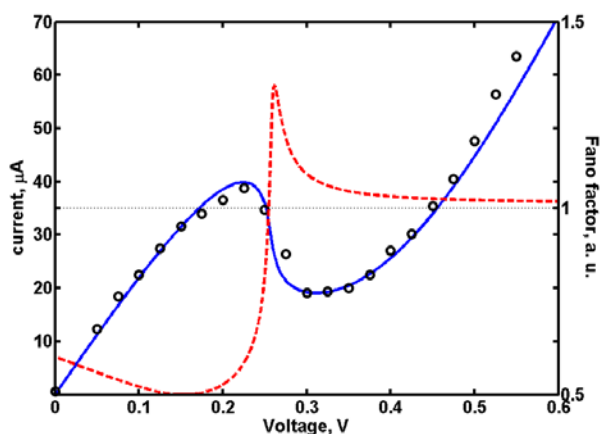
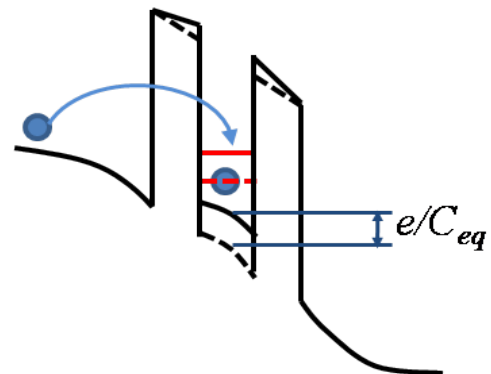
## References:

- [1] G. Iannaccone et al., Phys. Rev. Lett. **80** (1998) 1054
- [2] Ya. M. Blanter, M. Büttiker, Phys. Rev. B **59** (1999) 10217
- [3] X. Oriols, Phys. Rev. Lett. **98** (2007) 066803.
- [4] A. Alarcón, X. Oriols, J. Stat. Mech. **01** (2009) 01051
- [5] G. Albareda, J. Suñé, X. Oriols, Phys. Rev. B **79** (2009) 075315
- [6] E. Buccafurri et al., Phys. Status Solidi C **6** (2009) 1408-1411
- [7] E. Buccafurri, F. L. Traversa, X. Oriols, *to be published*
- [8] M. Büttiker, IBM J. of Res. Develop. **32** (1988) 63,
- [9] G. Iannaccone, M. Macucci, B. Pellegrini, Phys. Rev. B **55** (1997) 4539

**Figure 1 (top right):** Potential energy for a RTD without (dashed line) and within (solid line) an electron in the well. Red lines are the correspondent resonant states.

**Figure 2 (bottom left):** Quantum Monte Carlo simulation of DC current (symbols), analytical model (solid blue line) and Fano factor (1) (dashed red line).

**Figure 3 (bottom right):** Fano factor maxima locus (dashed red line); Fano factor minima locus (dashed dot blue line); relative pick current magnitude curve (black solid line).



## Tayloring of morphology, dimensions and magnetic properties of $\alpha$ -MnO<sub>2</sub> nanoparticles by the change of reaction parameters

*Polona Umek<sup>1</sup>, Alexandre Gloter<sup>2</sup>, Marko Jagodič<sup>3</sup>, Zvonko Jagličić<sup>3,4</sup>, and Denis Arčon<sup>1,5</sup>*  
*Jožef Stefan Institute, Jamova cesta 39, Ljubljana, Slovenia*  
[polona.umek@ijs.si](mailto:polona.umek@ijs.si)

We have controlled the diameter and length of MnO<sub>2</sub> nanorods through the selective regulation of the reaction temperature, reaction time and concentration of KMnO<sub>4</sub> in the reaction mixture. MnO<sub>2</sub> nanorods have been synthesized with high yields (figure 1a) by the reduction of KMnO<sub>4</sub> in the acidic environment under hydrothermal conditions. According to the XRD all the present materials have commonly crystallized with  $\alpha$ -MnO<sub>2</sub>-type structure.

It has been found out that a concentration of KMnO<sub>4</sub> in the reaction mixture has the highest impact on the diameter and length of  $\alpha$ -MnO<sub>2</sub> nanorods mainly due to the increased pressure in the reaction vessel. When the number of mmols of KMnO<sub>4</sub> has been increased from 1.6 to 6 mmols the average diameter decreased from 35 to 20 nm while the range of nanorods lengths has also been reduced significantly. The length of nanorods on the other hand can also be successfully regulated with the reaction time. MnO<sub>2</sub> is not stable in the acidic environment and it is further reduced to Mn<sup>2+</sup>. With prolongation of reaction time from 6 to 24 h the average length was reduced from approximately 2 to 1  $\mu$ m.

Recently we have found out that the presence of Fe<sup>3+</sup>(aq) ions in the reaction mixture triggers the growth of  $\alpha$ -MnO<sub>2</sub> nanotubes (figure 2) [1] instead of nanorods. Here we show that the concentration of Fe<sup>3+</sup>(aq) ions in the reaction mixture has affected the transition temperature in  $\alpha$ -MnO<sub>2</sub> nanotubes (figure 1b). With the increased concentration the transition temperature increased from 14.4 to 16.4 K (figure 2). At the same time also the Pauli-like temperature independent contribution to the magnetic susceptibility increased. The results show that Fe<sup>3+</sup> ions have an intrinsic effect on the electronic structure of  $\alpha$ -MnO<sub>2</sub> nanotubes.

### References:

[1] Umek P, Gloter A, Pregelj M, Dominko R, Jagodič M, Jagličić , Zimina A, Brzhezinskaya M, Potočnik A, Filipić C, Levstik A, and Arčon D; *J. Phys. Chem C*, 113 (2009), 14798–14803.

### Figures:

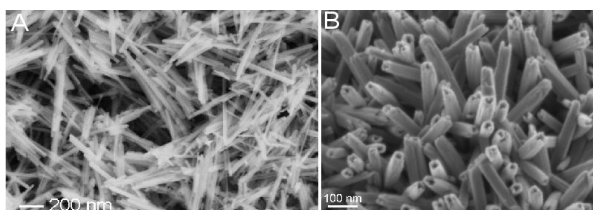


Figure 1. FE-SEM images of  $\alpha$ -MnO<sub>2</sub> (a) nanorods and (b) nanotubes.

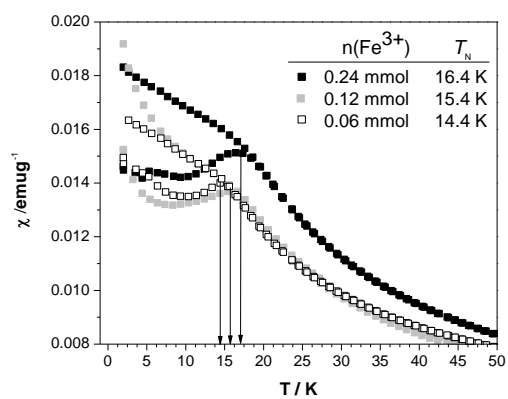


Figure 2. Temperature dependence magnetic susceptibility,  $\chi$ , for  $\alpha$ -MnO<sub>2</sub> nanotubes doped with different amount of Fe<sup>3+</sup>.

## **In-depth Characterization of Nanolayered Structures in III-V Semiconductors by Secondary Ion Mass Spectrometry (SIMS)**

*José Miguel Vadillo, Helena Téllez, J. Javier Laserna*

*University of Málaga, Department of Analytical Chemistry, 29071, Málaga, Spain*

[jmvadillo@uma.es](mailto:jmvadillo@uma.es); [laserna@uma.es](mailto:laserna@uma.es)

The progressive structural and functional complexity in modern microelectronic devices represents the driving force to improve or develop analytical techniques for the characterization of surfaces, interfaces and thin films [1]. On the other hand, most of those microelectronic devices are layered materials in which the chemical composition for major constituents, trace elements, dopants and impurities might vary within the sample thickness. Moreover, a wide variety of factors could affect the microstructure and interstitial chemistry of such devices due to the nanometric thicknesses involved and the different nature of the constituent beds, making the analysis especially challenging. Therefore, the information provided by the characterization techniques must be accurate and reliable in order to provide a depth understanding about the materials quality and the impact of the individual processing steps during device manufacturing. Nowadays, the most important developments in microelectronics are focused on physics and technology of semiconductors, depending mainly on two families of materials: the group IV elements and the III-V compounds [2].

Several surface analysis techniques are commonly used in this field - such as X-ray photoelectron spectroscopy (XPS), Auger electron spectroscopy (AES), Rutherford backscattering spectroscopy (RBS), atomic force microscopy (AFM), scanning electron microscopy (SEM), energy-dispersive X-ray spectroscopy (EDX), etc- providing complementary insights of the sample chemical composition and morphology. However, SIMS is considered the reference technique for both in-depth elemental/molecular distributions and chemical mapping of microelectronics/semiconductor devices due to its capability for detecting all elements with excellent sensitivity (up to sub-part per million) and sub-nanometric depth resolution [3-5].

Nowadays, some of the most important developments in microelectronics are focused on physics and technology of semiconductors, depending mainly on two families of materials: the group IV elements and the III-V compounds. In this communication, the application of SIMS depth profiling to the analysis of triple junction solar cells and the investigation of metallic diffusion in High Electron Mobility Transistors (HEMTs) is shown [6,7]. These samples represent a great challenge due to their multilayered structure, the reduced thickness of many of them, the different inter-diffusion and migration processes that may occur during the fabrication, and the large range of concentrations where the main constituents may be present.

**References:**

- [1] Alford T. L., Feldman L. C., Mayer J. W. (2007) Fundamentals of nanoscale film analysis. Springer, Germany.
- [2] Ruterana P., Albrecht M., Neugebauer J. (2003) Nitride semiconductors. Handbook on materials and devices. Wiley-VHC.
- [3] Magee C. W., Frost M. R., Int J Mass Spectrom Ion Process, 143 (1995)
- [4] Tsukamoto K., Yoshikawa S., Toujou F., Morita H., Appl Surf Sci., 203 (2003).
- [5] Lloyd K. G., O'Keefe D. P. Appl Surf Sci, 231 (2004)
- [6] Téllez H., Vadillo J. M., Laserna J. J., Anal Bional Chem. (2010d) DOI: 10.1007/s00216-010-3482-5
- [7] Téllez H., Vadillo J. M., Rodríguez E., Sánchez J. M., Laserna J. J., Surf Interf Anal. (submitted)

**Figures:**

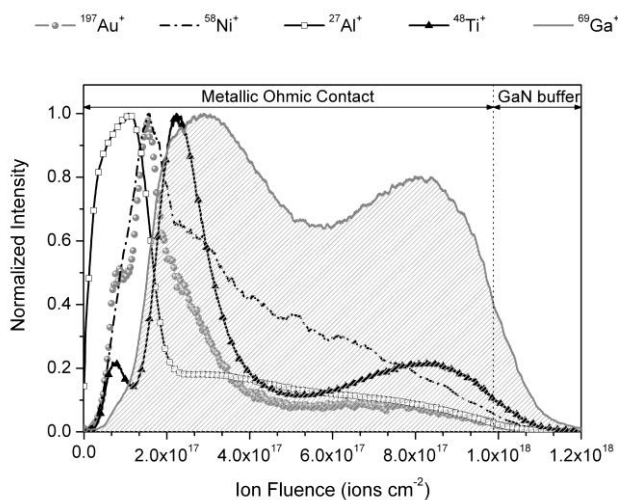


Figure 1. Positive SIMS depth profile of an annealed ohmic contact

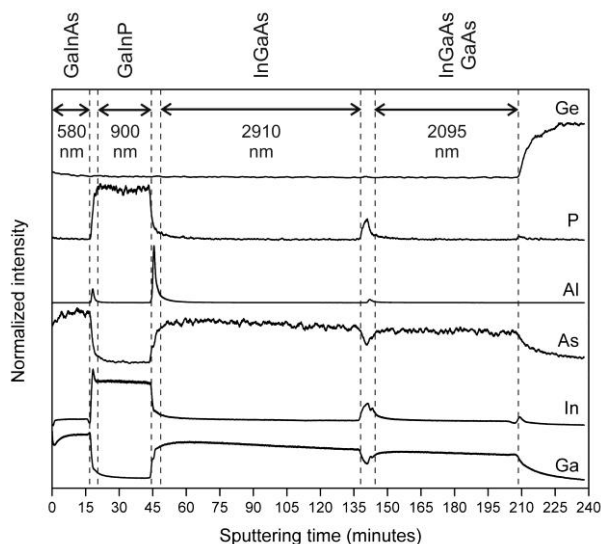


Figure 2. In-depth analysis of a triple junction solar cell. The top, middle and bottom subcells are clearly identified, as well as the outer AlGaAs contact layer.

## Nanoparticle Electrofluidization

*J M Valverde, M A S Quintanilla, M J Espin, A Castellanos*

*Dept. of Electronics and Electromagnetism, Faculty of Physics, University of Seville, Avda Reina Mercedes s/n, Seville, Spain*

[jmillan@us.es](mailto:jmillan@us.es)

Processing and handling of granular materials in fluidized beds is widespread in industry because of their multiple advantages such as enhanced gas-solid contact and improved flowability. In a typical fluidized bed the granular material rests on a horizontal porous plate through which gas is pumped to the bed. Fluidization of functionalized nanoparticles, providing extremely high gas-solid contact efficiency, has become one of the most promising techniques for emerging industrial applications [1]. Unfortunately, most nanopowders cannot be uniformly fluidized, thus hampering the efficiency of industry processes relying on gas-solid contact efficiency. Usually, nanoparticle powders are characterized by the existence of large and hard agglomerates that impede homogeneous expansion when the powder bed is subjected to a gas flow. This is the case, for example, of unsieved silica nanopowder. Because of contact and tribo charging mechanisms, nanoparticle agglomerates naturally accumulate sufficient electrostatic charge to be appreciably excited by electric fields of strength on the order of 1 kV/cm [2]. In our work, a direct visualization technique has been developed to automatically track nanoparticle agglomerate trajectories when excited by an externally applied field (see video clip below). This technique enables us to measure nanoparticle agglomerate properties such as their size, charge, and fractal dimension. Moreover, it is shown that the application of either a cross-flow or a co-flow alternating electric field is useful to enhance fluidization of this system by forcing the oscillation of nanoparticle agglomerates, which homogenizes the flow and enhances the gas-solid contact efficiency. The most effective technique to assist fluidization is shown to consist of application of a nonuniform alternating electric field, which is weak in the vicinity of the free surface but strong close to the bottom of the bed (see figure below). Due to the wide size distribution of the nanoparticle agglomerates, especially in the case of unsieved samples ranging from tens of microns to millimetres, the conventional nanoparticle fluidized bed is highly stratified, with the larger agglomerates sinking to the bottom of the bed and the smaller agglomerates almost free floating in the free surface. These smaller agglomerates are easily elutriated if the gas flow is increased to mobilize the larger agglomerates, resulting in poor bed expansion and inhomogeneous fluidization. The alternating nonuniform field agitates strongly the larger agglomerates while has almost no effect on the smaller agglomerates, thus enhancing fluidization and at the same time avoiding excessive elutriation.

### References:

- [1] J. M. Valverde, A. Castellanos, 2007. Fluidization, bubbling and jamming of nanoparticle agglomerates. *Chem. Eng. Sci.* 62: 6947--6956.
- [2] M.J. Espin, J.M. Valverde, M.A.S. Quintanilla, A. Castellanos, 2009. Electromechanics of fluidized beds of nanoparticles. *Phys. Rev. E* 79, 011304.



**Video clip: Fluidized bed of silica nanoparticle agglomerates excited by an externally applied alternating electric field (click twice on it for visualization)**

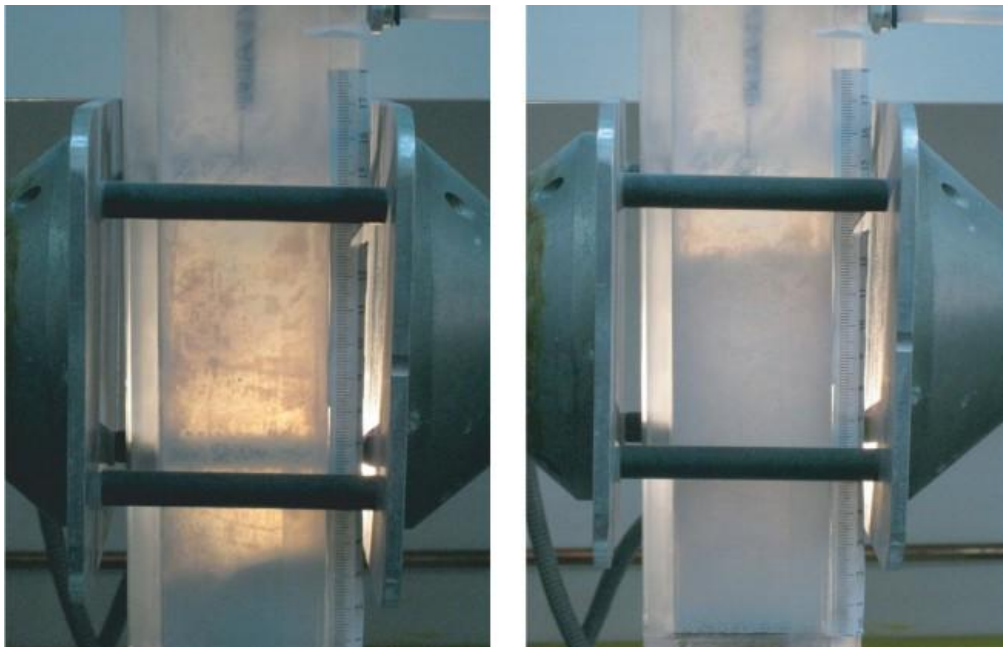


**Figure: Fluidized bed of silica nanoparticle agglomerates before (left) and after (right) being excited by an alternating nonuniform electric field**

## Supramolecular Architectures Formed by Hierarchical Self-Assembled PTM radicals

*Francisco Vera,<sup>a</sup> Marta Mas-Torrent,<sup>a</sup> Concepció Rovira,<sup>a</sup> Jaume Veciana,<sup>a</sup> Yanfei Shen,<sup>b</sup> Takashi Nakanishi<sup>b</sup>*

*<sup>a</sup>Institut de Ciència de Materials de Barcelona (CSIC), Campus Universitari de Bellaterra, 08193, Barcelona, Spain; <sup>b</sup>Max Planck Institute of Interfaces and Colloids, 14424, Potsdam, Germany.*

*fvera@icmab.es*

The use of weak intermolecular forces can give rise to supramolecular architectures various morphologies and properties with potential applications in chemistry, materials science and nanotechnology.<sup>1</sup> Nowadays, the molecular self-assembly is a well-known field where many research efforts have been made,<sup>2</sup> but the self-organization of nano- and mesoscopic objects or systems from discrete molecules is not very predictable.

Polychlorotriphenylmethyl (PTM) radicals can be included in the molecular skeleton of the molecules in order to give different properties to the self-organized system. PTM radicals present a magnetic dipole moment and electrochemical activity, and the functionalization of these molecules have permitted to use these radicals to prepare new molecular materials that show specific properties, like in molecular switches in solution<sup>3a</sup> and on surface<sup>3b</sup>, ONL systems,<sup>4</sup> porous magnets<sup>5</sup> and systems that shows intramolecular electronic transference phenomena.<sup>6</sup>

In previous works, PTM derivatives were covalently anchored to different surfaces by formation of self-assembled monolayers (SAMs).<sup>3b,7</sup> Another approach that has been employed is the study of the physisorption of a PTM-radical derivatives on HOPG. The functionalization of these PTMs consists in some attached alkyloxy chains (three, or two chains in metha or ortho positions) that dramatically changes the thermal properties of the molecules. Thus, compounds **1** and **2** are solid at room temperature, but **3** shows a liquid-like behaviour, as POM and DSC studies reveal. Some of those radicals organize on HOPG forming lamellar structures.<sup>8</sup>

The AFM studies of **1** and **2** on graphite shows this very well ordered structure (Figure 2), due to the fact that they have two clearly distinct regions that interact very differently between themselves (interactions between the PTM heads and between the aliphatic chains). This prompted us to study, following the work of T. Nakanishi *et al.*<sup>9</sup> with C<sub>60</sub>, the formation of hierarchically organized supramolecular architectures using different solvents to precipitate the PTM radical. This investigation opened the possibility to study the multifunctional PTM-derivative molecules (Figure 1) as potential building blocks for preparing supramolecular materials with unique morphologies.

Indeed, we have found micro-objects with compounds **1** and **2** from a large variety of solvents, obtaining different sized objects between 2 and 40 micrometres, like desert-roses, particles, plates and fibers, as shown in a SEM image (Figure 3). The formation of hierarchically assembled PTM-micro-objects is an important step in the field of molecular magnetism because of they can present promising magnetic interactions between radicals compared with the non-structured bulk (as seen in EPR studies).

### References:

- [1] K. Sada, M. Takeuchi, N. Fujita, M. Numata, S. Shinkai, *Chem. Soc. Rev.*, **36** (2007) 514.  
 [2] J.-M. Lehn, *Angew. Chem. Int. Ed. Engl.*, **27**, (1988) 89.  
 [3] a) I. Ratera, D. Ruiz-Molina, J. Vidal-Gancedo, K. Wurst, N. Daro, J. F. Létard, C. Rovira, J. Veciana, *Angew. Chem. Int. Ed.*, **40** (2001) 919; b) N. Crivillers, M. Mas-Torrent, S. Perruchas, N. Roques, J. Vidal-Gancedo, J. Veciana, C. Rovira, L. Basabe-Desmonts, B. Jan Ravoo, M. Crego-Calama, D. N. Reinhoudt, *Angew. Chem. Int. Ed.*, **46** (2007) 2215.  
 [4] I. Ratera, S. Marcen, S. Montant, D. Ruiz-Molina, C. Rovira, J. Veciana, J.-F. Létard, E. Freysz, *Chem. Phys. Lett.*, **363** (2002) 245.  
 [5] D. Maspoch, D. Ruiz-Molina, K. Wurst, N. Domingo, M. Cavallini, F. Biscarini, J. Tejada, C. Rovira, J. Veciana, *Nat. Mater.*, **2** (2003) 190.  
 [6] J. Bonvoisin, J. P. Launay, C. Rovira, J. Veciana, *Angew. Chem. Int. Ed. Engl.*, **33** (1994) 2106.  
 [7] N. Crivillers, M. Mas-Torrent, J. Vidal-Gancedo, J. Veciana, C. Rovira, *J. Am. Chem. Soc.*, **130** (2008) 5499.  
 [8] N. Crivillers, S. Furukawa, A. Minoia, A. Ver Heyen, M. Mas-Torrent, C. Sporer, M. Linares, A. Volodin, C. Van Haesendonk, M. Van der Auweraer, R. Lazzaroni, S. De Feyter, J. Veciana, C. Rovira, *J. Am. Chem. Soc.*, **131** (2009) 6246.  
 [9] a) T. Nakanishi, K. Ariga, T. Michinobu, K. Yoshida, H. Takahashi, T. Teranishi, H. Möhwald, D. G. Kurth, *Small*, **12** (2007) 2019; b) T. Nakanishi, Y. Shen, J. Wang, H. Li, P. Fernandes, K. Yoshida, S. Yagai, M. Takeuchi, K. Ariga, D. G. Kurth, H. Möhwald, *J. Mater. Chem.*, **20** (2010) 1253.

### Figures:

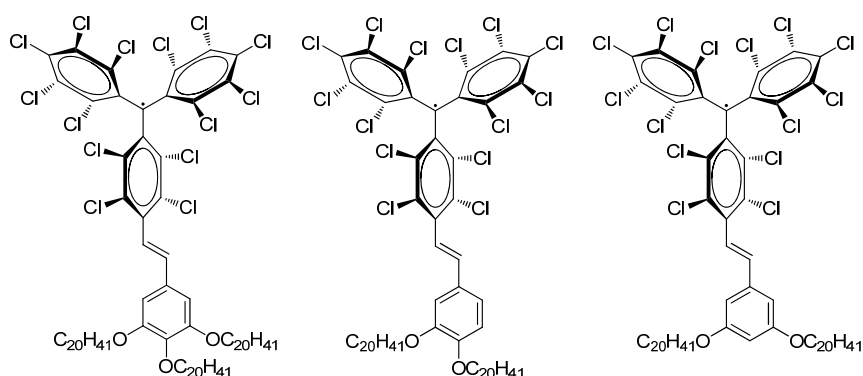


Figure 1. Molecules **1**, **2**, and **3**, PTM derivatives.

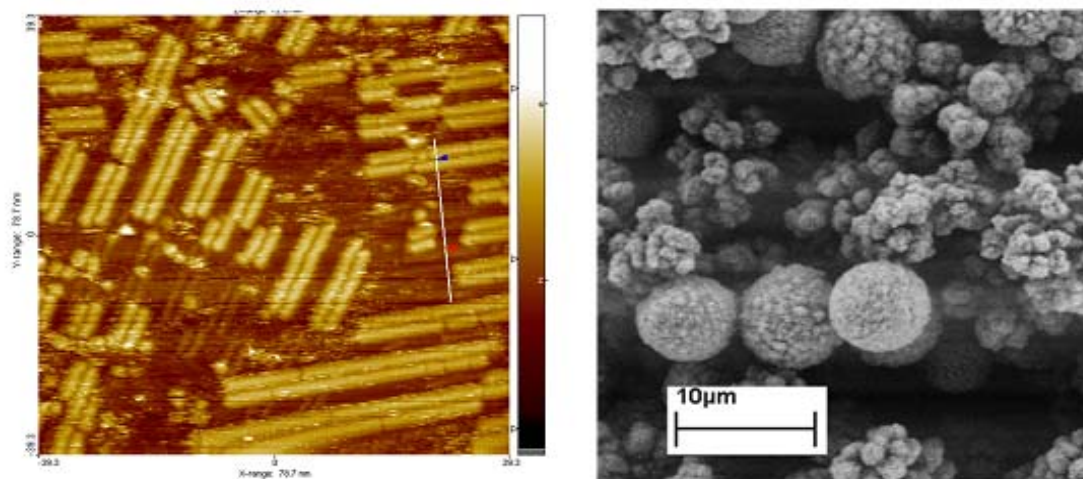


Figure 2. AFM image of **1** on HOPG. Figure 3. SEM image of **1** from a iPrOH solution.

## Solid supports for Dendrimers. Preparation and Bio-Applications.

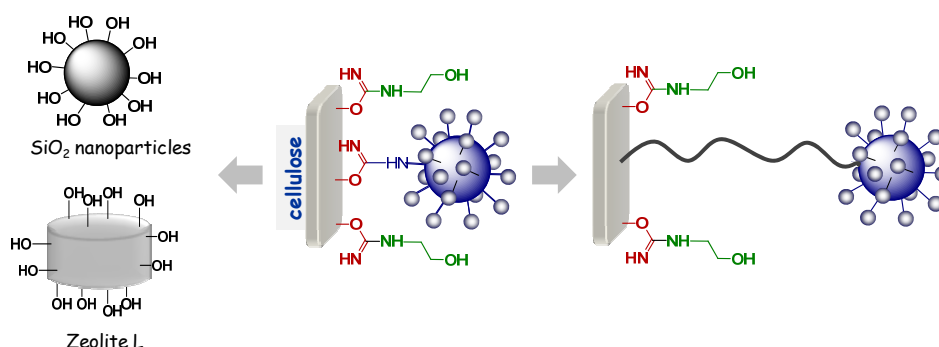
Vida, Y.,<sup>1</sup> Ruiz-Sanchez, A.J.,<sup>1</sup> Montañez, M.I.,<sup>2</sup> Mayorga, C.,<sup>2</sup> Blanca, M.,<sup>2</sup> Suau, R.,<sup>1</sup> De Cola, L.,<sup>3</sup> Perez-Inestrosa, E.<sup>1</sup>

<sup>1</sup>Department of Organic Chemistry. Faculty of Sciences. University of Málaga, Campus Teatinos s/n, 29071, Malaga, Spain

<sup>2</sup>Fundación IMABIS, Hospital Carlos Haya, Malaga, Spain

<sup>3</sup>Physikalisches Institut, University of Münster, Mendelstrasse, D-48149 Münster, Germany  
[yolvida@uma.es](mailto:yolvida@uma.es)

$\beta$ -lactam antibiotics (BL) are the most frequently drugs involved in allergic reactions. IgE recognition is produced after the opening of the BL ring by different macromolecules, usually serum or cell bound proteins to form hapten-carrier conjugates. Conjugation of BL to a macromolecular carrier has been used as a tool for the *in vitro* test for diagnosing. RAST is a blood test used to determine what a person is allergic to, based on the amount of IgE reacting specifically with suspected or known allergens.<sup>1</sup> Classical conjugation of HSA (Human Serum Albumin) with penicillin has been proposed as hapten-carrier structure for the assays, despite of as a protein, HSA is chemically complicate to work. PLL (poly-L-Lysine) is a versatile homopolymer, however they use as carrier in the *in vitro* assays lacks of reproducibility due to differences in the degree of polymerization and subsequent functionalization. We use dendrimeric nanostructures in the formation of the hapten-carrier conjugate in order to solve these problems with successful approach. We use the PAMAM penicilloylated derivatives as hapten-carrier for *in vitro* testing, using cellulose-disk as solid support.<sup>2,3</sup> The results of the RAST were really successful. Nevertheless, the internal side of the dendrimeric structure is not accessible to IgE, because of steric hindrance. We developed a new methodology to covalently bind the dendrimer to the solid support using spacers between both. We used desymmetrized polyethylene glycol chains of different length to control the distance between the dendrimer and the solid support.<sup>4</sup> On the other hand, the shift from cellulose (fibrous and rough surface, with holes that can host the dendrimer) to nano/microstructure transparent surfaces as zeolites or silica nanoparticles seems to be an important improvement in our system. The presence of a flat and highly functionalized substrate compared with cellulose will allow a high coverage with the penicilloylated PAMAM dendrimers.



### References:

- [1] Blanca, M., Mayorga, C., Sanchez, F., Vega, J. M., Fernandez, J., Juarez, C., Suau, R., Perez-Inestrosa, E. *Allergy* **1991**, *46*, 632.
- [2] Montañez, M. I., Perez-Inestrosa, E., Suau, R., Mayorga, C., Torres, M. J., Blanca, M., *Biomacromolecules* **2008**, *9*, 1461.
- [3] Perez-Inestrosa, E., Suau, R., Blanca, M., Montañez, M. I., Mayorga, C., Torres, M. J. **2003**, PATENT: P200302737.
- [4] Sánchez-Ruiz, A. J., Vida, Y., Suau, R., Perez-Inestrosa, E. *Tetrahedron* **2008**, *69*, 11661.

## A collagen-targeted rhBMP-2 improves bone formation in vivo

Arrabal PM, Visser R, Becerra J, Cifuentes M

CIBER-BBN. Department of Cell Biology, Genetics and Physiology. Faculty of Science,  
University of Málaga, Spain. [visser@uma.es](mailto:visser@uma.es)

Since BMPs are the only growth factors with known osteoinductive activity, their use as therapeutic agents in order to enhance bone repair is being widely studied. The search for alternatives to autologous bone grafting led to the approval by the FDA of an absorbable collagen carrier combined with rhBMP-2 for the treatment of certain bone diseases and fractures. One of the main problems of this method is the low natural binding-affinity of rhBMP-2 to collagen carriers. This obliges to the use of high amounts of rhBMP-2 in clinical assays, which can lead to the appearance of undesired side effects.

Our goal was the production of a modified rhBMP-2 with only an additional collagen-binding decapeptide (CBD) derived from the von Willebrand factor. We examined the collagen-binding properties of the fusion protein (rhBMP2-CBD) and evaluated its ability to induce ectopic bone formation *in vivo* when implanted in combination with absorbable collagen sponges.

The results showed not only that our rhBMP2-CBD had an increased affinity to collagen, but also that this binding was stable during a prolonged period of time. *In vivo* experiments demonstrated that this rhBMP2-CBD maintained its osteoinductive activity, being capable of inducing new bone formation at lower concentrations than native rhBMP-2.

These results indicate that the combination of our fusion protein with absorbable collagen may be a suitable and safer alternative to rhBMP-2 for bone repair purposes.

*This work has been granted by: Ministerio de Educación y Ciencia (BIO2006-03599); Junta de Andalucía, Consejería de Salud (TCRM 0012/2006); Junta de Andalucía, Consejería de Innovación, Ciencia y Empresa (PO7-CVI-2781); Red de Terapia Celular, Instituto de Salud Carlos III (RD06/0010/0014)*

## Supramolecular Assemblies of Carbon Nanohorns and Porphyrin for Photovoltaic Devices

*María Vizuete,<sup>†</sup> María José Gómez-Escalonilla,<sup>†</sup> José Luis G. Fierro,<sup>‡</sup> Atula S. D. Sandanayaka,<sup>§</sup> Taku Hasobe,<sup>§,£</sup> Masako Yudasaka,<sup>□</sup> Sumio Iijima,<sup>€</sup> Osamu Ito,<sup>£,\*</sup> and Fernando Langa<sup>†,\*</sup>*

<sup>†</sup>*Instituto de Nanociencia, Nanotecnología y Materiales Moleculares (INAMOL), Universidad de Castilla-La Mancha, 45071 Toledo, Spain;*

<sup>‡</sup>*Instituto de Catálisis y Petroleoquímica, CSIC, Madrid, Spain;*

<sup>§</sup>*School of Materials Science, Japan Advanced Institute of Science and Technology, Asahidai, Nomi, 923-1292, Japan;*

<sup>£</sup>*PRESTO, Japan Science and Technology Agency (JST), 4-1-8 Honcho, Kawaguchi, Saitama, 332-0012, Japan;*

<sup>□</sup>*Nanotube Research Center, National Institute of Advanced Industrial and Technology, Higashi, Tsukuba, Ibaraki 305-8565, Japan;*

<sup>€</sup>*Department of Physics, Meijo University, Shiogamaguchi, Tenpaku-ku, Nagoya 468-8502, Japan;*

<sup>£</sup>*NIMS (Tsukuba) & IMRAM, Tohoku University (Sendai), Japan*

Contact e-mail: [María.Vizuete@uclm.es](mailto:María.Vizuete@uclm.es)

Carbon Nanohorns <sup>[1]</sup> (CNHs) represent a new type of nanostructured carbon-based material. One of the merits of CNHs different from other carbonaceous materials is a high purity due to the absence of any metal nano-particles. Thus, CNHs have attracted a great deal of attention in several fields as optoelectronic applications. <sup>[2]</sup>

Combination of covalent and non-covalent functionalization of CNHs is particularly promising for building donor–acceptor nanohybrids. Among various non-covalent methodologies reported, self-assembly by using an ammonium ion-crown ether interaction is regarded as one of the most powerful methods. Porphyrin / Fullerene based donor–acceptor supramolecular systems involving crown ether-ammonium interactions have been prepared for probing photo-induced electron processes. This concept has been extended to build porphyrin / SWCNT donor–acceptor nanohybrids, and occurrence of photo-induced charge separation processes is clearly demonstrated. <sup>[3]</sup>

Herein, we describe a supramolecular assemble of CNH covalently bonded with amino groups via spacer (sp) (CNH-sp-NH<sub>3</sub><sup>+</sup>), which is included in crown-ether appending porphyrin (Crown-ZnP). Nanohybrid CNH-sp-NH<sub>3</sub><sup>+</sup> and the supramolecular assemble CNH-sp-NH<sub>3</sub><sup>+</sup>;Crown-ZnP were characterized by means of several techniques as HR-TEM, TGA, XPS, Raman, FT-IR and UV-vis spectroscopies. Photoinduced electron-transfer processes of the nanohybrids are confirmed on combining the time-resolved absorption and fluorescence measurements, in addition to the accumulation of viologen cation radical in solution with steady-light illumination. The efficiency of this system in photovoltaic solar cells is shown.

### References:

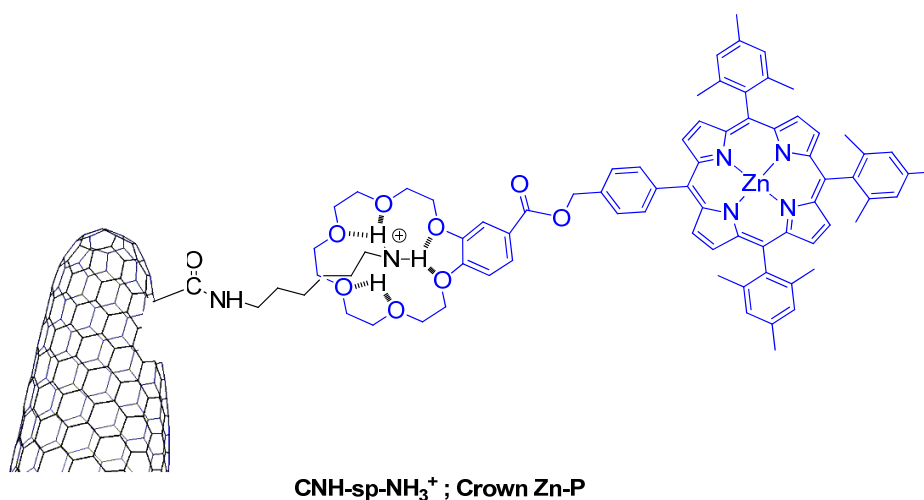
[1] Iijima, S.; Yudasaka, M.; Yamada, R.; Bandow, S.; Suenaga, K.; Kokai, F.; Takahashi, K. *Chem. Phys. Lett.* , 309 (1999) ,165.

[2] (a) Iijima, S. *Physica B*, 23 (2002), 1. (b) Fan, J.; Yudasaka, M.; Kasuya, Y.; Kasuya, D.; Iijima, S. *Chem. Phys. Lett.*, 397 (2004), 5. (c) Murata, K.; Hashimoto, A.; Yudasaka, M.;

Kasuya, D.; Kaneko, K.; Iijima, S. *Adv. Mater.* 16 (2004), 1520. (d) Murakami, H.; Ajima, K.; Miyawaki, J.; Yudasaka, M.; Iijima, S.; Shiba, K. *Mol. Pharm.* 1 (2004), 399. (e) Sandanayaka, A. S. D.; Pagona, G.; Tagmatarchis, N.; Yudasaka, M.; Iijima, S.; Araki, Y.; Ito, O. *J. Mater. Chem.* 17 (2007), 2540. (f) Cioffi, C.; Campidelli, S.; Sooambar, C.; Marcaccio, M.; Marcolongo, G.; Meneghetti, M. S.; Paolucci, D.; Paolucci, F.; Ehli, C.; Rahman, A.; G. M.; Sgobba, V.; Guldi, D. M.; Prato, M. *J. Am. Chem. Soc.* 129 (2007), 3938. (g) Sandanayaka, A. S. D.; Ito, O.; Tanaka, T.; Isobe, H.; Nakamura, E.; Yudasaka, M.; Iijima, S. *New J. Chem.* 33 (2009), 2261.

[3] D'Souza, F.; Ito, O. *Chem. Commun.* (2009), 4913.

### Figures:



## A New Paradigm for Cell Architecture: Celloidosomes<sup>®</sup>

Manuel Marquez<sup>1,2,3</sup>, Samantha M. Marquez<sup>1</sup>, Tommy Angelini<sup>2</sup>, Sergio Martinez<sup>3</sup>, Tony Garcia<sup>3</sup>

(1) YNANO LLC, (2) Harvard University and (3) Arizona State University, USA  
[Manuel.Marquez@YNano.com](mailto:Manuel.Marquez@YNano.com)

The cornerstone of this research project lies in the ability to design and fabricate 3D organized cell structures we call Celloidosomes<sup>®</sup>. The methodology employed to obtain core-shell structures from colloids (Colloidosomes) [1] has been used to design three dimensional cellular architectures (Celloidosomes<sup>®</sup>) [2]. The Celloidosomes<sup>®</sup> is, by definition, a “living capsule” with a biomembrane (tissue) shell and a unique core that acts as container or reservoir. We present some of the new research and opportunities that arises by precisely controlling fluid flow and mixing using microfluidic devices. We describe studies to elucidate mechanisms of droplets and bubbles formation and use these to create Celloidosome’s structures. We focus on showing the potential of this emerging and enabling technology to design complex systems as reactors and templates in chemistry, materials science and bioengineering [3]. One of the examples is a revolutionary Cell Architecture process for the design & fabrication of core/shell multicellular structures based on a “bottom-up strategy”.. By definition, these systems are ideal-models for the design of Bio-Microreactors, Artificial Microglands and could be used as independent units for 3D, scaffold-less Tissue Engineering. Our process is based on cells-self-assembly on Liquid-Liquid, Liquid-Gel, and/or Liquid-Gas interfaces. The Celloidosomes<sup>®</sup> could be considered part of the new Synthetic Biology research field. We have developed several key strategies to drive & organize living cells (yeast, fibroblast, etc) to the surface of a Gel, Liquid or Gas (Bubble) buy controlling the cells and templates surfaces a) using LbL polyelectrolyte decoration, b) selective gelation using CaCO<sub>3</sub> nanoparticles–Cells composites, c) Hydrophobic deposition, etc. The ability to control the chemistry and physics of the interface at the nanoscale level, allow us to tune, drive and direct assembly of cells into Celloidosomes<sup>®</sup> by gels, liquid or bubbles templates using capillary microfluidics. One of the most important contributions of this proof of concept is that the Celloidosomes<sup>®</sup> are potential model structures, which serve as a tool for the future design and control of Stem Cell Fate: stem cell behavior and cellular differentiation [4,5]

### References:

- 1) A. D. Dinsmore, M. Marquez, A. R. Bausch and D. A. Weitz, "Colloidosomes: Self-Assembly of Selectively-Permeable Capsules Composed of Colloidal Particles", *Science*, 298, 1006-1009 (2002)
- 2) a) M. Marquez, S. M. Marquez, and A. A. Garcia, “Celloidosomes, Viroidosomes, Vesciodosomes, Lipoidosomes, and Method for Their Manufacture”, *US Provisional Patent* 61/165,989. b) S. M. Marquez, M. Marquez, and A. A. Garcia, “Artificial Micro-Glands” *US Provisional Patent* 61/275,666. c) S. M. Marquez, M. Marquez, and A. A. Garcia, “Anisotropic micro-scale biosupraparticles”, *US Provisional Patent* 61/260,824 d) Celloidosomes<sup>®</sup>. US Patent and Trade Office, Reg. No. 3,738,109 . EU Trade Mark filed (2009).
- 3) Rhutesh K. Shah, Ho Cheung Shum, Amy C. Rowat, Daeyeon Lee, Jeremy J. Agresti, Andrew S. Utada, Liang-Yin Chu, Jin-Woong Kim, Alberto Fernandez-Nieves, Carlos J. Martinez, and David A. Weitz, "Designer emulsions using microfluidics", *Materials Today* **11**, 18-27 (2008).
- 4) Robert Langer, et al, “Bioinspired Materials for Controlling Stem Cell Fate”, *Accounts of Chemical Research*, August 24, 2009.
- 5) Odorico, J. S.; Kaufman, D. S.; Thomson, J. A. Multilineage differentiation from human embryonic stem cell lines. *Stem Cells* , 19, 193–204.(2001).

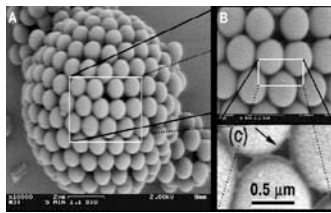
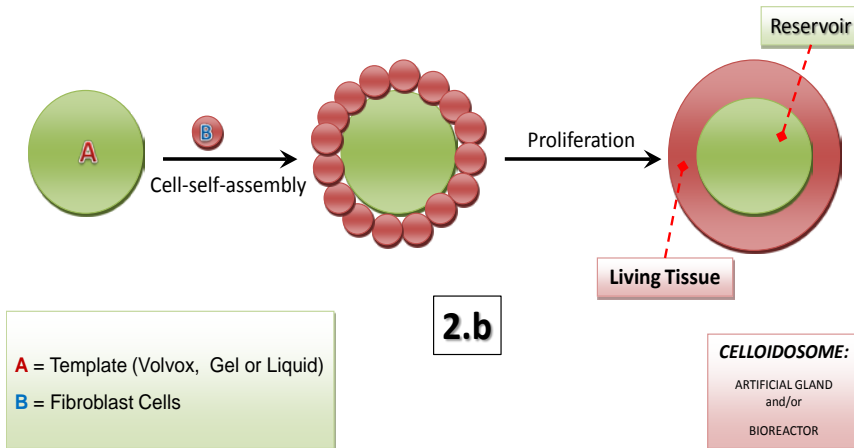
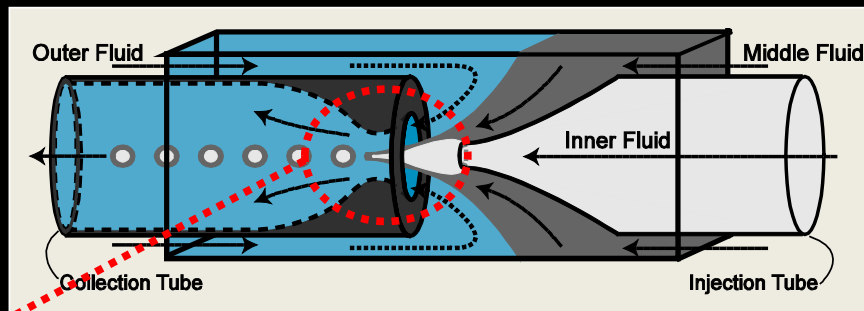


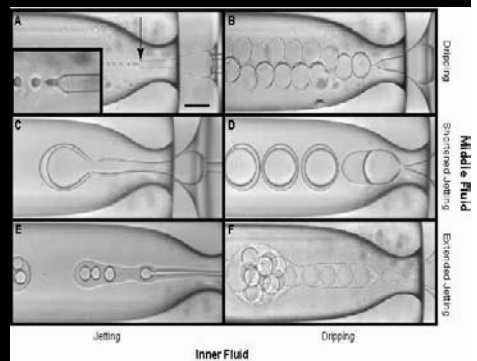
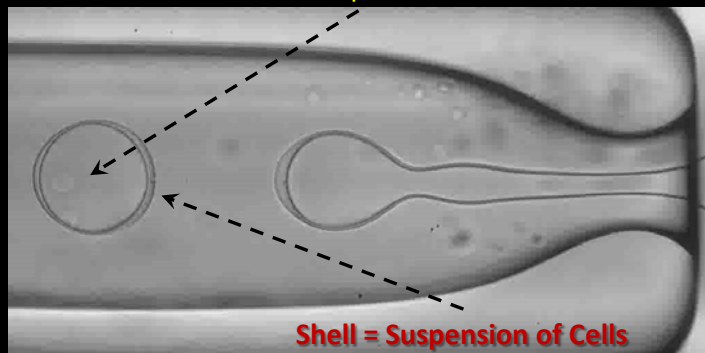
**Figure 2:** (1.a) SEM image of a dried, 10 micrometer diameter Colloidosome composed of 900 nm diameter polystyrene spheres. The Colloids have been assembled on a droplet's surface. (1.b) By analogy, a Celloidosomes, is the self-assembly of living-cells on a template's surface.



## Core/Shell Droplet Formation



Core = Liquid or Gel



science • industry • society

# IMAGINENANO

Bringing together  
Nanoscience and Nanotechnology

April 11-14, 2011 - Bilbao Exhibition Centre (Spain)

[www.imagenano.com](http://www.imagenano.com)

ImagineNano will comprise 5 parallel international conferences, a huge industrial exhibition and a social event where everyone can meet and greet Nanotechnology side by side

Science



- Graphene 2011
- nanoBio&Med 2011
- Nanolberian 2011
- TNA Energy  
Trends in NanoApplications
- PPM 2011  
Photonics/Plasmonics/Magneto-Optics

Society



industry

